

**Quantum control of binary and many-body interactions
in ultracold molecular gases**

by

Felipe Herrera

B.Sc. Chemistry, Universidad de Chile, 2007

A THESIS SUBMITTED IN PARTIAL FULFILLMENT
OF THE REQUIREMENTS FOR THE DEGREE OF

Doctor of Philosophy

in

THE FACULTY OF GRADUATE STUDIES

(Chemistry)

The University of British Columbia

(Vancouver)

June 2012

© Felipe Herrera, 2012

Abstract

Ultracold molecules are expected to find applications in cold chemistry, quantum phases, precision measurements and quantum information. In this thesis three novel applications of cold molecules are studied.

First the thesis presents a general method for coherent control of collisions between non-identical particles. It is shown that by preparing two alkali-metal atoms in a superposition of hyperfine states, the elastic-to-inelastic cross section ratio can be manipulated at ultracold temperatures by tuning laser parameters in the presence of a magnetic field. The static field is needed to induce quantum interference between scattering states. Extensions of this scheme for ultracold molecular reactive scattering are discussed.

Second, the thesis describes rotational excitons and polarons in molecular ensembles trapped in optical lattices. Rotational excitons can be manipulated using static electric and magnetic fields. For a one-dimensional molecular array with substitutional impurities any localized exciton state can be delocalized by applying a suitable electric field. The electric field induces correlations between diagonal and off-diagonal disorder. It is also shown that the translational motion of polar molecules in an optical lattice can lead to phonons. The lattice dynamics and the phonon spectrum depend on the strength and orientation of a static electric field. An array of polar molecules in an optical lattice can be described by generalized polaron model with tunable parameters including diagonal and off-diagonal exciton-phonon interactions. It is shown that in a strong electric field the system is described by a generalized Holstein model, and at weak electric fields by the Su-Schrieffer-Heeger (SSH) model. The possibility of observing a sharp polaron transition in the SSH model using polar alkali-metal dimers is discussed.

Finally, the thesis presents a method to generate entanglement of polar molecules using strong off-resonant laser pulses. Bipartite entanglement between alkali-metal dimers separated by hundreds of nanometers can be generated. Maximally entangled states can be prepared by tuning the pulse intensity and duration. A scheme is proposed to observe the violation of Bells inequality based on molecular orientation correlation measurements. It is shown that using a combination of microwave and off-resonant optical pulses, arbitrary tripartite and many-particle states can be prepared.

Preface

Part of the material in Chapter 4 has been published in Ref. (I) (see list below). This research project was identified by Roman Krems and designed by the author. The author developed the theoretical analysis and performed the numerical calculations. The results were analyzed by the author under supervision of Roman Krems. The author wrote the manuscript in collaboration with Roman Krems.

Part of the material in Chapters 3 and 5 have been published in Refs. (II) and (III). The research project that lead to the publication in Ref. (II) was identified and designed by Roman Krems. The author developed the theoretical analysis and performed the numerical calculations. The manuscript was written by Roman Krems in collaboration with Marina Litinskaya and the author.

The research project that lead to the publication in Ref. (III) was identified and designed by the author and Roman Krems. The author developed the theoretical analysis and Jesus Pérez-Ríos performed the numerical calculations. Roman Krems analyzed the results and wrote the manuscript in collaboration with Jesus Pérez-Ríos and author.

Part of the material in Chapter 6 has been published in Ref (IV). The research project was identified and designed by the author. The theoretical analysis and the numerical calculations were performed by the author. The manuscript was written by the author in collaboration with Roman Krems.

The following is a list of publications containing some of the results presented in this dissertation:

- (I) F. Herrera, *Magnetic field-induced interference of scattering states in ultra-cold collisions*, Phys. Rev. A 78, 054702, **2008**
- (II) F. Herrera, M. Litinskaya, R.V. Krems, *Tunable disorder in a crystal of cold polar molecules*, Phys.Rev. A 82, 033428, **2010**
- (III) J. Pérez-Ríos, F. Herrera, R.V. Krems, *External field control of collective spin excitations in an optical lattice of $^2\Sigma$ molecules*, New. J. Phys., 12, 103007, **2010**
- (IV) F. Herrera and R.V. Krems, *Tunable Holstein model with cold polar molecules*, Phys. Rev. A 84, 051401(R) **2011**

Table of Contents

Abstract	ii
Preface	iv
Table of Contents	vi
List of Tables	xi
List of Figures	xii
Acknowledgments	xvi
1 Introduction	1
1.1 Cold collisions and controlled chemistry	1
1.2 Tunable condensed-matter phenomena	4
1.3 Entanglement and quantum information	8
1.4 Thesis overview	10
2 Diatomic molecules at cold temperatures	12
2.1 Chapter overview	12
2.2 Rovibrational structure of diatomic molecules	13
2.3 Hyperfine structure of closed-shell molecules	16
2.4 Diatomic molecules in static electric and magnetic fields	21
2.4.1 Closed-shell molecules in static electric fields	21
2.4.2 Closed-shell molecules in static magnetic fields	23
2.4.3 Open-shell molecules in static magnetic fields	26
2.5 Diatomic molecules in far-detuned optical fields	28

2.5.1	Dynamical Stark shift of molecular states	28
2.5.2	Polarizability of diatomic molecules at optical frequencies	32
2.6	Electric dipole-dipole interaction	34
2.6.1	Closed-shell molecules without nuclear spin	34
2.6.2	Closed-shell molecules with hyperfine structure	37
2.6.3	Open-shell molecules without nuclear spin	40
2.7	Optical trapping of diatomic molecules	41
2.7.1	Dipole traps	42
2.7.2	One-dimensional optical lattice	43
2.7.3	Higher-dimensional optical lattices	45
2.7.4	Rotational Raman couplings in optical traps	48
3	Engineering molecular interactions with external fields	55
3.1	Chapter overview	55
3.2	Dipole-dipole interaction in external fields	56
3.3	Closed-shell molecules in electric fields	57
3.3.1	Strength and anisotropy of the dipole-dipole interaction	58
3.4	Open-shell molecules in combined electric and magnetic fields	61
3.4.1	Rotational level structure of $^2\Sigma$ molecules	63
3.4.2	Field-induced electron spin exchange between $^2\Sigma$ molecules	65
3.4.3	Control of molecular spin entanglement with external fields	67
3.5	Closed-shell molecules in strong off-resonant optical fields	69
3.5.1	Rotational structure in strong off-resonant optical fields	70
3.5.2	Dipolar interactions in DC electric and strong off-resonant fields	73
4	Towards coherent control of bimolecular scattering	78
4.1	Chapter overview	78
4.2	The principle of coherent control	79
4.3	Coherent control of collisions	80
4.4	Field induced interference of scattering channels	84
4.5	Control of ultracold atomic scattering	85
4.5.1	Alkali-metal atoms in 2S states	86

4.5.2	Coherent control of elastic vs inelastic scattering	89
5	Molecular crystals with cold polar molecules	97
5.1	Chapter overview	97
5.2	Interacting polar molecules in optical lattices	98
5.2.1	Hamiltonian in second-quantized form	98
5.2.2	Heitler-London and two-level approximations	101
5.2.3	Rotational excitons in molecular arrays	105
5.2.4	Excitons in molecules with hyperfine structure	115
5.3	Controlling exciton transport with external fields	124
5.3.1	Electric field control of exciton-impurity scattering	125
5.3.2	Field-induced delocalization of excitons in a disordered array	129
5.4	Suggested applications	135
6	Tunable polaron phenomena with polar molecules	137
6.1	Chapter overview	137
6.2	Polaron models in condensed matter	138
6.2.1	Fröhlich model	139
6.2.2	Holstein model	141
6.2.3	Su-Schrieffer-Heeger model	144
6.3	Polarons with cold molecules in optical lattices	147
6.3.1	Molecular Lattice Hamiltonian	148
6.3.2	Lattice Dynamics	150
6.3.3	External field control of phonon dynamics	154
6.3.4	Typical parameters for alkali dimers in optical lattices	159
6.3.5	Frequency of lattice vibrations in a finite array	160
6.3.6	Phonon spectrum of an infinite array	163
6.3.7	Exciton-phonon interaction	164
6.4	Polaron regimes in static electric fields	169
6.4.1	Strong fields: Holstein regime	171
6.4.2	Weak fields: SSH regime	176
7	Entanglement of cold molecules using off-resonant light	183
7.1	Chapter overview	183

7.2	Molecular alignment with adiabatic pulses	184
7.2.1	Single molecule alignment	184
7.2.2	Adiabatic vs non-adiabatic alignment	185
7.3	Dipolar interactions in strong off-resonant fields	187
7.4	Entanglement of polar molecules in the absence of DC fields	189
7.4.1	Time-evolution of two-molecule states	189
7.4.2	Molecular parameters for alkali-metal dimers	192
7.4.3	Entanglement length scale	192
7.4.4	Dynamical entanglement generation	193
7.4.5	Pulse shape effects	194
7.4.6	Field-free entanglement in optical lattices	198
7.5	Entanglement in combined DC fields and optical pulses	200
7.5.1	Novel couplings induced by the DC electric field	200
7.5.2	Spatial bounds for entanglement generation	204
7.6	Quantification of entanglement using cold molecules	208
7.6.1	Orientation correlation for entangled molecules	208
7.6.2	Violation of Bell’s inequalities in optical lattices	210
7.6.3	Tripartite and many-particle entanglement	215
8	Conclusion	219
8.1	Overall conclusions of the dissertation	219
8.2	Contributions of the dissertation	220
8.2.1	Cold collisions and controlled chemistry	220
8.2.2	Tunable condensed-matter phenomena	221
8.2.3	Quantum entanglement and quantum information	224
8.3	Future research directions	225
8.3.1	Nonlinear quantum optics in the microwave domain	225
8.3.2	Quantum computation with cold homonuclear molecules	226
8.3.3	Coherent control of ultracold molecular reactions	227
	Bibliography	229
A	Effective Hamiltonian for a molecule in a far-off resonant field	252

B	Dipole-dipole interaction in spherical tensor form	257
C	Hyperfine structure of closed-shell diatomic molecules	262
C.1	Fully coupled basis: $\mathbf{I} = \mathbf{I}_1 + \mathbf{I}_2$ and $\mathbf{N} + \mathbf{I} = \mathbf{F}$	263
C.2	Spin coupled basis: $\mathbf{I} = \mathbf{I}_1 + \mathbf{I}_2$	268
D	Hamiltonian for an ensemble of interacting molecules	270
D.1	Single-particle energies	271
D.2	Two-body interaction	271
D.3	Transformation to exciton operators	274
D.4	Many-level model Hamiltonian	276
E	Simple methods for the polaron problem	279
E.1	Fröhlich polaron	279
E.2	Holstein polaron	281
E.3	SSH polaron	284
E.4	Exciton-phonon coupling constant $M(\mathbf{k}, \mathbf{q})$	285
F	Bell's inequality for angular and time correlations	288
F.1	Proof of Bell's inequality	288
F.2	Equivalence between spin orientations and rotational evolution . .	290

List of Tables

Table 2.1	Hyperfine molecular constants for some alkali-metal dimers. . .	18
Table 2.2	Static polarizabilities of heteronuclear alkali-metal dimers . . .	33
Table 2.3	Tensor light shift of the lowest nine rotational states $ N, M\rangle$. . .	49
Table 6.1	Equilibrium geometry of an array of interacting molecules. . .	157
Table 6.2	Electric field at which $dE/B_e = 1$ selected closed-shell polar molecules.	179
Table 7.1	Typical alignment laser intensity I_0 for selected polar alkali-metal dimers.	193

List of Figures

Figure 2.1	Zero-field-splitting of the $N = 0$ rotational state for $^{41}\text{K}^{87}\text{Rb}$ molecules.	20
Figure 2.2	Stark effect on $^1\Sigma$ molecules.	22
Figure 2.3	Zeeman spectra for a $^{41}\text{K}^{87}\text{Rb}$ molecule in $N = 0$ and $N = 1$ rotational states	25
Figure 2.4	Rotational levels of a $^2\Sigma$ molecule in the presence of a magnetic field.	27
Figure 2.5	Illustration of a two-dimensional optical lattice potential for polar molecules	47
Figure 2.6	Tensor light shifts of rotational states $ (N), M\rangle$ as a function of the DC electric field.	51
Figure 2.7	Rotational levels in a DC electric field along $\hat{\mathbf{Z}}$ and an $\hat{\mathbf{X}}$ -polarized CW far-detuned laser.	52
Figure 3.1	Dipole-dipole energies J_{12} , V_{12}^{eg} , V_{12}^{gg} , and V_{12}^e as functions of the DC electric field strength.	60
Figure 3.2	Dipole-dipole energies D_{12} and U_{12} as functions of the DC electric field strength.	61
Figure 3.3	Dipole-dipole energies J_{12} , V_{12}^{eg} , V_{12}^{gg} , and V_{12}^e as functions of the orientation of the DC electric field.	62
Figure 3.4	Zeeman spectra of a $^2\Sigma$ molecule in the presence of a weak DC electric field	64
Figure 3.5	Exchange coupling constant J_{12} for SrF molecules in combined electric and magnetic fields.	66
Figure 3.6	Rotational energies in the presence of a CW far-detuned laser.	71

Figure 3.7	Wavefunctions of the ground and first excited rotational states in the presence of a CW far-detuned laser.	72
Figure 3.8	Energy of the two lowest rotational states in the presence of a DC electric field and a CW far-detuned laser.	74
Figure 3.9	Exchange constant J_{12} in the presence of a DC electric field and a CW far-detuned laser.	75
Figure 3.10	Energy shift D_{12} in the presence of a DC electric field and a CW far-detuned laser.	76
Figure 4.1	Zeeman effect for ^7Li and ^{133}Cs atoms in the ground electronic state.	87
Figure 4.2	Energy difference between hyperfine states of ^7Li and ^{133}Cs atoms as a function of an applied magnetic field.	90
Figure 4.3	Cross sections for collisions between ^7Li and ^{133}Cs atoms as a function of the magnetic field.	93
Figure 4.4	Interference cross section as a function of magnetic field for collisions between ^7Li and ^{133}Cs atoms.	95
Figure 4.5	Control map for elastic to inelastic cross section ratio for collisions between ^7Li and ^{133}Cs atoms.	96
Figure 5.1	Schematic illustration of the transitions induced by the dipole-dipole interaction.	103
Figure 5.2	Exciton spectrum for a finite array of LiCs molecules	107
Figure 5.3	Lowest exciton eigenstates for a finite array of LiCs molecules	109
Figure 5.4	Stark effect on rotational excitons.	113
Figure 5.5	Electric dipole transitions between hyperfine states at weak magnetic fields.	116
Figure 5.6	Hyperfine Raman couplings induced by an off-resonant trapping laser at weak magnetic fields.	119
Figure 5.7	Electric dipole transitions between hyperfine states at high magnetic fields.	121
Figure 5.8	Schematic illustration of a crystal with tunable impurities . . .	125

Figure 5.9	Electric field control of the exciton-impurity scattering cross section.	127
Figure 5.10	Spectrum and eigenstates of a 1D exciton in a disordered lattice.	132
Figure 5.11	Electric field induced delocalization of a one-dimensional exciton in disordered lattice.	134
Figure 6.1	Polaron dispersion for the SSH model in the non-adiabatic regime.	146
Figure 6.2	Potential energy for two molecules in an optical lattice interacting repulsively.	156
Figure 6.3	Potential energy for two molecules in an optical lattice interacting attractively.	158
Figure 6.4	Energy ratio $\rho = (U_g/a_L^3)/V_0$ for LiCs molecules.	159
Figure 6.5	Normal mode frequencies for a 1D array of 10 polar molecules as a function of the ratio $\rho = (U_g/a_L^3)/V_0$	162
Figure 6.6	Phonon spectrum of an infinite 1D array of polar molecules as a function of the ratio $\rho = (U_g/a_L^3)/V_0$	163
Figure 6.7	Ratio $ D_{12}/J_{12} $ as a function of the DC electric field strength.	172
Figure 6.8	Polaron ground state energy shift ΔE_g for an array of LiCs molecules, as a function of the exciton-phonon coupling strength.	173
Figure 6.9	Size dependence of the polaron shift ΔE_g for a 1D array of LiCs molecules.	175
Figure 6.10	Polaron phase diagram in the SSH model for selected alkali-metal dimers.	177
Figure 6.11	Level scheme for parity-preserving Raman couplings via the intermediate rovibrational states.	180
Figure 6.12	Polaron phase diagram for KRb and RbCs molecules in the presence of near resonant laser fields.	181
Figure 7.1	Single molecule alignment for adiabatic and non-adiabatic pulses.	186
Figure 7.2	Rotational wavepacket revivals for a non-adiabatic pulse. . . .	187
Figure 7.3	Two-molecule level scheme for interaction greater than the single-molecule transition energy	189

Figure 7.4	Entanglement length R_e as a function of the laser intensity . . .	194
Figure 7.5	Dynamical entanglement generation with a moderately strong pulse.	195
Figure 7.6	Entanglement generation with strong pulses of different duration.	196
Figure 7.7	Entanglement generation with strong pulses of different peak intensity.	197
Figure 7.8	Entanglement generation for polar molecules in optical lattices.	199
Figure 7.9	Interaction energy A_{12} in the presence of a DC electric field and a CW far-detuned laser.	201
Figure 7.10	Interaction energy B_{12} in the presence of a DC electric field and a CW far-detuned laser.	202
Figure 7.11	Interaction energies A_{12} and B_{12} as a function of the DC field strength.	203
Figure 7.12	Entanglement length R_e as a function of the laser intensity for weak DC electric fields.	205
Figure 7.13	Entanglement generation in combined AC and weak DC electric fields.	207
Figure 7.14	Entanglement generation in combined AC and moderate DC electric fields.	208
Figure 7.15	Violation of Bell's inequality for molecular orientation correlations.	213

Acknowledgments

“I give you praise, Father, Lord of heaven and earth, for although you have hidden these things from the wise and the learned you have revealed them to the childlike.” (Luke 10, 21)

Throughout these years of graduate studies I have enjoyed the support and encouragement from my wife Maria Victoria Carrasco. To her this dissertation is dedicated as a modest recognition of the sacrifices she has made and also to congratulate her professional accomplishments in a foreign land. I am also grateful for the permanent encouragement and prayers from my parents, Leonor and José, my dear aunt Lizarda, my grandfather Antonio, and my parents-in-law María and José.

I am most grateful to my supervisor Roman Krems for his generosity and encouragement during my graduate studies. After having the possibility to study in virtually any school in the world, I realize now that joining his group has been one of the best decisions I have ever made. It is my hope that I can develop such ingenuity and perseverance when approaching a physical problem. I have definitely been influenced by his person in ways that go far beyond the scientific practice.

It has been a privilege to collaborate over these years with Marina Litinskaya, Kirk Madison, Mona Berciu, Jesus Pérez Ríos, Guido Pupillo, Peter Zoller and Sabre Kais. I am grateful for what I have learned from all of them. I am most grateful to Peter Zoller and Sabre Kais for their hospitality during my research visits to their groups. Special thanks to Peter Zoller for important words of encouragement in the early stages of my studies.

Finally, I want to acknowledge financial support from the Department of Chemistry through the Gladys Stella Laird Fellowship and from the University of British Columbia through the Four Year Fellowship.

To my brother Pablo Herrera Urbina

Chapter 1

Introduction

This thesis is a theoretical contribution to the field of cold molecules. The roots of this field are intimately related to the spectacular developments of laser cooling and trapping of alkali-metal atoms over the last two decades. The preparation of molecular gases at cold [1–11] and ultracold [12–21] temperatures is expected to find important applications in the study of cold chemistry, dipolar quantum phases, precision measurements, tests of fundamental symmetries and quantum information processing [22–25]. The work presented in this thesis is an attempt to advance the knowledge and scope of the field by introducing concepts from other disciplines of physical chemistry and physics. In particular, an attempt is made to suggest applications of cold polar molecules using notions of coherent control, excitonic phenomena and quantum entanglement. In an effort to stimulate experimental work along the lines of this thesis, the complexity of the suggested systems has been kept to the minimum. The contributions made in this work have been categorized into three distinct areas in which the specific research questions and goals of this thesis are contextualized below.

1.1 Cold collisions and controlled chemistry

Collisions in atomic and molecular gases at very low temperatures are qualitatively different compared with thermal samples. In thermal gases and high energy beams, the translational motion of a particle can be described quantum mechanically as a

plane wave propagating in a well-defined direction. For many purposes, this plane wave description of the translational motion can be replaced by the classical notion of a point particle following a well-defined trajectory in phase space. As the temperature is lowered, the plane wave character of the particle motion loses relevance in favor of a spherical wave description. The direction of propagation of the spherical matter wave is not well-defined. The probability density for a particle to have a given orientation in space is determined by spherical harmonic wavefunctions $Y_{l,m}(\theta, \phi)$, the same as the electron distribution in atomic and molecular orbitals. It is common to refer as the *ultracold* regime to the temperature limit in which a single spherical harmonic, or partial wave, describes the motion of a particle. This can be loosely defined as temperatures below 1 millikelvin [25]. This regime is also referred to as the *s-wave* regime, since collisions are described by the motion of a single partial wave with $l = 0$ for identical bosons or non-identical particles, and $l = 1$ (*p-wave*) regime for identical fermions [23]. Collisions in the *cold* temperature regime involve the contribution of a relatively small number of partial waves. This is valid for temperatures approximately up to 1 Kelvin. The crossover from the cold to the ultracold regime is determined by the mass of the particles and the strength of their long-range interaction.

Long-range interactions between molecules are dominated in first and second order of perturbation theory by the dipole-dipole interaction. The dipole-dipole interaction between polar molecules depends on the intermolecular distance as $1/R^3$ and is proportional to the product of dipole moments of the molecules. For atoms and homonuclear molecules the dipole-dipole interaction to second order in perturbation theory corresponds to the familiar van der Waals interaction, which depends on the distance as $1/R^6$ and is proportional to the product of the polarizabilities of the interacting particles. The expectation value of the dipole-dipole interaction between two polar molecules in an *s-wave* collision is zero for a three-dimensional collision. However, if ultracold collision occurs in the presence of an external DC electric field or the molecular motion is restricted to only one or two dimensions, the collisional dynamics can vary significantly with respect to the field-free three-dimensional case.

The study of ultracold molecules in the presence of static fields has found direct application in current molecular cooling and trapping experiments. Elastic colli-

sions determine the rate of evaporative cooling and inelastic collisions are associated with losses in electrostatic traps. Approximate theories for collisions between polar molecules in static electric fields have been developed [26–29]. These theories aim to find relations between the collision cross section and parameters such as the collision energy and the DC field strength, that are valid regardless of the molecular species. These relations are referred to as universal scaling. Although approximate models provide insight into the nature of collision dynamics at low temperatures, rigorous molecular scattering calculations in the presence of external fields are essential in order to understand the mechanisms for external field control of collisions at cold and ultracold temperatures [30–34].

The rapid development of optical trapping techniques has motivated the study of collisions between ultracold atoms and molecules in confined geometries. Neutral particles can be confined into quasi one-dimensional and two-dimensional traps using optical forces [35, 36]. The energy dependence of cross sections for atomic and molecular collisions in confined geometries is different from a bulk gas sample [37–40]. Therefore, the spatial confinement introduces an additional degree of control for inelastic collisions and chemical reactions at ultracold temperatures [41, 42]. Inelastic collisions are suppressed with respect to elastic scattering in confined geometries, which increases the stability of ultracold molecular gases [39, 42]. Moreover, it has recently been experimentally demonstrated that the chemical reaction $\text{KRb} + \text{KRb} \rightarrow \text{K}_2 + \text{Rb}_2$ at ultracold temperatures can be suppressed several orders of magnitude by confining the molecules to a quasi-2D geometry in the presence of a static electric field oriented perpendicular to the trap plane [43].

Controlling atomic and molecular collisions using static fields and restricted geometries may provide valuable insight into the nature of state resolved chemical reactions in the limit where quantum effects are dominant. In this quantum limit of chemical reactivity yet another proven method of control may find direct applications in the study of cold and ultracold molecular gases. Coherent control of molecular dynamics has been successfully demonstrated for a number of unimolecular processes such as photodissociation, but schemes for coherent control of bimolecular processes have yet to be realized [44, 45]. In order to control the outcome of a collision between non-identical particles, the proposed schemes

require the preparation of fragile molecular superposition states that involve correlations between internal and translational degrees of freedom. These restrictive conditions make coherent control of collisions practical for identical particles only. It is therefore necessary to extend the principles of coherent control to collisions between non-identical particles without the restrictions imposed by current schemes. In this thesis I pursue such goal by combining elements from original coherent control schemes and control methods developed for ultracold gases. It is believed that the coherent interaction between matter waves required by coherent control can be best achieved at cold and ultracold temperatures. Understanding the role of quantum coherence in chemical reactivity remains an important open question in physical chemistry, and the research presented in this thesis constitutes an initial step in that direction.

1.2 Tunable condensed-matter phenomena

The realization of Bose-Einstein condensates (BEC) and degenerate Fermi gases has been one of the milestones in the study of quantum mechanics at temperatures near the absolute zero [46–50]. Most of this progress has been done using alkali metal atoms. The relatively simple internal structure of atoms allows them to be cooled efficiently using laser forces [51–53]. For atoms it is possible to characterize the collisional properties using a single parameter at ultracold temperatures: the s -wave scattering length [54, 55]. The interaction of the atomic magnetic dipole moment of an atom with an external magnetic field is the basis of several schemes to control the motion of single atoms [56], as well as collisions between trapped atoms [57]. The importance of external field control in a dilute atomic gas can be best described by considering the mean field description of an atomic BEC. In this limit, the dynamics of an ensemble of identical atoms is determined by the single particle Schrödinger equation $i\hbar\partial_t\Psi(\mathbf{r},t) = \hat{H}_{\text{NL}}\Psi(\mathbf{r},t)$, where the nonlinear Hamiltonian

$$\hat{H}_{\text{NL}} = -\frac{\hbar^2}{2m}\nabla^2 + V_{\text{trap}}(\mathbf{r},t) + g|\Psi(\mathbf{r},t)|^2 \quad (1.1)$$

accounts for an average contact interaction between atoms in the ensemble. The collisional interaction between atoms leads to the nonlinearity in Eq. (1.1), and the parameter $g = 4\pi\hbar^2 a/m$ is proportional to the s -wave scattering length a . The state

of the system also depends on the trapping potential $V_{\text{trap}}(\mathbf{r}, t)$, which results from the interaction between atoms and electromagnetic fields. If the energies g and $V_{\text{trap}}(\mathbf{r}, t)$ can be tuned using external fields, the wavefunction of the system $\Psi(\mathbf{r}, t)$, and therefore the observable properties, can be manipulated experimentally. It has been widely demonstrated that this is possible using magnetic fields to tune the scattering length via Feshbach resonances [57] and controlling the degree of confinement of the gas using optical fields [58].

Ultracold molecular gases offer additional possibilities to the study of quantum states of matter due to their rich internal structure. Diatomic molecules are most commonly used in experiments [25]. Heteronuclear diatomic molecules are particularly important because the permanent dipole moment can lead to a strong dipole-dipole interaction between molecules, which completely modifies the behaviour of a molecular quantum gas in comparison with atoms. For example, in the limit of dilute or weakly interacting dipolar gases, the non-linear Hamiltonian \hat{H}_{NL} in Eq. (1.1) needs to be supplemented by the non-local potential

$$V = \int d\mathbf{r}' V_{\text{dd}}(\mathbf{r}, \mathbf{r}') |\Psi(\mathbf{r}', t)|^2,$$

arising from the dipole-dipole interaction between molecules $V_{\text{dd}}(\mathbf{r}, \mathbf{r}')$. The relative strength of the dipole-dipole interaction compared with the s -wave scattering parameter g determines the stability of a dipolar gas and its collapse dynamics [59–64]. Dipolar Bose-Einstein condensates have been produced using chromium atoms [65, 66], which have a large magnetic dipole moment. In the near future, it is expected that similar results will be obtained using polar molecules with electric dipole moment, which offer a larger degree of external field control than atoms. The non-linearity introduced by the dipole-dipole interaction in a molecular gas results in the emergence of collective properties such as solitons and vortices in confined gases [67–71]. Dipolar Fermi gases with molecules have been less studied than their bosonic gases. It is believed that a strong dipole-dipole interaction between fermions can lead to new regimes of superconductivity involving anisotropic pairing [49, 50, 72–76], which differ significantly from electrons in metals.

The study of dipolar quantum gases in confined geometries has been motivated by the development of optical lattices [36, 77–79]. It is now technologically possi-

ble to produce an optical lattice for atoms and molecules with a periodic trapping potential having arbitrary geometry and dimensionality. Using cold bosonic atoms in optical lattices, it was demonstrated that a phase transition from a superfluid (BEC) to an insulator can be induced by increasing the strength of the lattice potential [80, 81]. Since then, the study of condensed-matter phenomena in optical lattices using cold atoms and molecules has become an important research direction during the last decade [82, 83]. Molecular gases with strong dipole-dipole interactions trapped in an optical lattice give rise to novel quantum phases that are difficult to achieve using dipolar atoms (magnetic dipole) or weakly interacting molecules. The strong dipole-dipole interaction introduces quantum correlations between molecules that cannot be taken into account using a mean field treatment as in Eq. (1.1). Most importantly, the properties of these strongly correlated quantum phases can be tuned using electromagnetic fields to modify the internal states of the molecules and the confining potential. The Hubbard Hamiltonian provides a basic model that describes the physics of interacting quantum gases in optical lattices. In its simplest form, the Hubbard Hamiltonian can be written as [84]

$$\hat{H} = \frac{U}{2} \sum_i \hat{n}_i (\hat{n}_i - 1) - t \sum_{\langle i,j \rangle} \hat{a}_i^\dagger \hat{a}_j, \quad (1.2)$$

where \hat{a}_i^\dagger and \hat{a}_i are creation and annihilation operators for particle i , $\hat{n}_i = \hat{a}_i^\dagger \hat{a}_i$ is the particle number operator and $\langle i, j \rangle$ denotes nearest-neighbours. The first term represents the site energy U , which is determined by the collisional properties of the particles. The second term represents hopping of particles between lattice sites. The hopping amplitude t is determined by the trapping potential. If the lattice potential is deep enough, particle hopping is suppressed and the ground state of the system is a Mott-insulator with a finite number of particles per lattice site [82]. An extension of the simple model in Eq. (1.2) is required to describe strongly correlated phases of dipolar particles in optical lattices [64, 85, 86]. Bosonic and fermionic polar molecules in confined geometries offer exciting possibilities for the creation of exotic strongly-correlated quantum phases [87–95]. It has been shown that the interaction potential between polar molecules in a quasi-2D geometry can be engineered using a DC electric field and a microwave field tuned near resonance

with a rovibrational transition [90]. This work illustrates the great advantages of manipulating the internal states of polar molecules with external fields, in order to engineer many-body Hamiltonians in a way that is not possible using conventional solids.

The insulator phase is one of the simplest examples of quantum phases that can be achieved with molecules in an optical lattice. Here the hopping of molecules between lattices is suppressed by a strong confining potential. The dynamics of molecules in a single site is independent from other sites. A one-dimensional optical lattice, for example, can be described as a periodic array of quasi-2D traps where the strong confinement is along the direction of periodicity [79]. The dipole-dipole interaction between polar molecules in such two-dimensional trap can be made repulsive using a DC electric field that orients the dipole moment of the molecules parallel to each other. If the thermal energy of the ensemble is smaller than the dipole-dipole interaction energy, then the system is predicted to self-assemble into a molecular crystal with a well-defined lattice structure [96]. Repulsive interactions between the molecules and tight transverse confinement are required to preserve the stability of the molecular aggregate. As for any aggregate of molecules interacting via dipole-dipole forces in which charge transfer between sites does not occur, two-dimensional dipolar crystals at ultracold temperatures are characterized by the presence of Frenkel excitons and lattice phonons [97–100]. Polaron phenomena has been predicted to occur in a system of atoms moving on top of a self-assembled dipolar crystal [96], where atoms interact with the molecular lattice, and the associated displacement of the molecules from their equilibrium positions lead to atom-phonon coupling, in analogy with electron-phonon coupling in solids. More recently, two-dimensional polarons have been recently observed in ultracold spin-polarized Fermi gases [101], where a single spin-up impurity interacts with an environment of spin-down atoms.

For an ensemble of polar molecules, the hopping particles corresponds to Frenkel excitons. These are collective rotational excitations (rotational excitons) distributed coherently throughout the molecular array. Lattice phonons arise from the motion of the molecules in the many-particle interaction potential that determines the equilibrium geometry of the array. The coupling of excitons with phonons is due to the dependence of the dipole-dipole interaction energy on the center-of-mass distance

between coupled molecules. The size-enhanced coupling of excitons with electromagnetic radiation has been exploited to propose self-assembled dipolar crystals as a quantum memory for quantum information processing [102, 103]. This work might have important applications in the design of hybrid quantum devices involving molecular gases and solid state qubits [104]. Self-assembled dipolar crystals are less suitable for quantum simulation of condensed-matter phenomena occurring in molecular solids and aggregates at room temperature. The reasons for this are the restrictive conditions imposed on the aligning DC electric field and the confining potential, as well as the extremely low temperatures required to achieve the 2D insulator phase. It is therefore necessary to design a controllable quantum system that can be used to simulate exciton, polaron and polariton phenomena that occur in condensed media at room temperature. In this thesis I pursue such goal by considering an ensemble of polar molecules trapped in a three-dimensional optical lattice with a single molecule per lattice site. The development of technology based on excitonic and polaritonic phenomena not only has found important applications in optical communication and clean energy devices [105–108], but has provided a significant motivation for fundamental studies of open quantum dynamics [109–116]. It is expected that an advancement of similar magnitude can be achieved in the field of cold and ultracold polar molecules. The work in this thesis constitutes an initial step in that direction.

1.3 Entanglement and quantum information

Polar molecules at ultracold temperatures have become attractive candidates for the physical implementation of a quantum computer. This is due to a number of properties unique to polar molecules that are competitive with condensed-matter architectures [25, 117]. The rich internal structure of molecules includes hyperfine, rotational and vibrational states. The rotational degrees of freedom of polar molecules constitute a natural choice to encode quantum information. The radiative lifetime of rotational states exceeds typical experimental timescales [118, 119] and the rotational states of polar molecules can be manipulated using DC and AC electric fields. The availability of several long-lived and field-sensitive states for encoding information is a feature shared with other implementations using neutral

atoms and ions [120–124], as it is an important requirement for the efficient realization of single-qubit gates [125]. Polar molecules in the presence of a static electric field interact with each other via dipole-dipole forces. The long-range character of the electric dipole-dipole interaction makes the coupling between molecules strong for separation distances of a few hundred nanometers. The strong interaction between remote molecular qubits makes it possible to engineer fast logic gates using an ensemble of trapped polar molecules.

The prototype example for the implementation of quantum information processing using ultracold molecules consists of an ensemble of polar molecules trapped in individual sites of a one-dimensional optical lattice [126]. Variations of this original scheme have also been proposed [127–130]. Here molecules are confined in individual microtraps created by weak off-resonant laser fields. A static electric field is used to induce dipole moments on the molecules. Qubits are encoded into two rotational states of each molecule. Each qubit should be addressed individually in order to perform single-qubit rotations spectroscopically. Large separation between molecules favors single-qubit addressability but decreases the speed of two-qubit gates. This problem can be solved by imposing an electric field gradient along the lattice axis in order to distinguish the qubit transition frequency at different sites, for lattices with relatively small site separation. Two-qubit gates are performed spectroscopically by exploiting the state-dependent dipole-dipole force between neighbouring qubits. In this implementation, the dipole-dipole interaction between qubits is “always on”, which adds unnecessary complexity to the system. In order to couple a single pair of qubits, unwanted couplings need to be effectively removed using a number of specifically designed electromagnetic pulses as it is done in NMR-based quantum computing implementations [125, 131–133]. The biggest advantage of using individually trapped polar molecules for quantum information processing is that decoherence in the system is relatively easy to suppress. Qualitatively different approaches aim towards the integration of ensembles of cold molecules with solid-state architectures such as superconducting qubits [102–104], yet other schemes consider encoding quantum information using the large number of internal states of isolated molecules [134–136]. Each type of implementation using polar molecules has its unique advantages and drawbacks, and at this point none of them has been realized experimentally.

The experimental realization of long-lived polar molecules trapped in single sites of an optical lattice opens exciting possibilities for the study of entanglement and quantum information processing using arrays of cold and ultracold molecules [137, 138]. Entanglement is a major ingredient in most quantum computation algorithms. The role of bipartite and many-particle entanglement in arrays of field-dressed polar molecules has only recently been addressed in the literature [139–141]. Most of the proposed schemes for quantum information processing with polar molecules involve the use of a static electric field to manipulate the rotational states of molecules. Although the field strengths required are not prohibitively large for practical use, it would be desirable to avoid the decoherence introduced by electric field noise. It is therefore important to engineer a system in which molecules, not necessarily polar, are trapped individually in a weak optical trap and can be pair-wise entangled in a controlled manner in the absence of static electric or magnetic fields. Most importantly, the separation between sites should be large enough to allow for spectroscopic resolution of single molecules. Such system would motivate not only the development of novel schemes for quantum information processing, but would also bring the study of entanglement-related phenomena at the heart of quantum mechanics to the molecular realm. In this thesis I pursue such goal by considering the interaction between polar diatomic molecules and strong off-resonant laser pulses. The work in this thesis constitutes the first steps towards the development of a general entanglement protocol that uses optically trapped ensembles of heteronuclear diatomic molecules as well as polar and non-polar polyatomic molecules.

1.4 Thesis overview

The body of this thesis is divided in two parts. The first part is composed of chapters 2 and 3, which contain general background information relevant for the work presented here and also original results that are used in later chapters. The second part of the thesis contains original research results related to each of the three goals described in this introduction. Chapter 4 is about coherent control of collisions, Chapters 5 and 6 are about tunable condensed-matter phenomena with po-

lar molecules, and Chapter 7 is about entanglement generation in cold molecular ensembles. The conclusions of the dissertation are provided in Chapter 8, and supplementary information is provided in the appendices.

Chapter 2

Diatomic molecules at cold temperatures

2.1 Chapter overview

This chapter provides the background information necessary for a basic understanding of the physical processes that are relevant for experiments that use optically trapped molecules to explore physics and chemistry at ultracold temperatures. Section 2.2 is a short review of the quantum mechanical description of rovibrational structure of diatomic molecules. In Section 2.3, the hyperfine structure of rotational levels in closed-shell molecules is discussed. Section 2.4 provides a basic description of the Stark and Zeeman effects in closed-shell and open-shell molecules without orbital electronic angular momentum. In Section 2.5 the interaction of a single molecule with far-detuned AC optical fields is described, and the electric dipole-dipole interaction between polar molecules is discussed in Section 2.6. Finally, a general description of optical trapping of molecules and the theory of molecules in optical lattices is provided in Section 2.7.

2.2 Rovibrational structure of diatomic molecules

In a coordinate system that moves with the center of mass of a diatomic molecule, the total Hamiltonian $\hat{\mathcal{H}}_T = \hat{\mathcal{H}}_{\text{el}} + \hat{\mathcal{H}}_{\text{nuc}}$ that describes the electronic and nuclear motion, in the absence of external electric or magnetic fields, can be written as [142]

$$\hat{\mathcal{H}}_{\text{el}} = -\frac{\hbar}{2m} \sum_i \nabla_i^2 - \frac{\hbar}{2M_N} \sum_{i,j} \nabla_i \cdot \nabla_j + \frac{1}{4\pi\epsilon_0} \sum_{i<j} \frac{e^2}{R_{ij}} - \frac{1}{4\pi\epsilon_0} \sum_{i<j} \frac{Z_\alpha e^2}{R_{i\alpha}} + \mathcal{H}(\mathbf{S}_i, \mathbf{I}_\alpha) \quad (2.1)$$

and

$$\hat{\mathcal{H}}_{\text{nuc}} = -\frac{\hbar}{2\mu} \nabla_R^2 + \frac{1}{4\pi\epsilon_0} \frac{Z_\alpha Z_\beta e^2}{R}, \quad (2.2)$$

where \mathbf{R}_i denotes electronic coordinates, \mathbf{R}_α nuclear coordinates, m is the electron mass, $M_N = M_1 + M_2$ is the total nuclear mass, and $\mu = M_1 M_2 / (M_1 + M_2)$ is the reduced nuclear mass. The first term in Eq. (2.1) is the electronic kinetic energy operator. The second term is a mass polarization term that is strongly suppressed by the factor $1/M_N$. The third term is the electronic coulomb repulsion. The last two terms denote the relativistic interactions that depend on the electronic spins \mathbf{S}_i and the nuclear spins \mathbf{I}_α . The nuclear Hamiltonian in Eq. (2.1) is a sum of the kinetic energy of the nuclei and their coulomb repulsion. By transforming from a rotating coordinate system with z axis is along the internuclear axis (molecule-fixed frame) into the laboratory coordinate system (space-fixed frame), the nuclear Hamiltonian can be written as

$$\hat{\mathcal{H}}_{\text{nuc}} = -\frac{\hbar}{2\mu R^2} \frac{\partial}{\partial R} \left(R^2 \frac{\partial}{\partial R} \right) + \frac{\hbar^2}{2\mu R^2} \mathbf{R}^2 + \frac{1}{4\pi\epsilon_0} \frac{Z_\alpha Z_\beta e^2}{R}, \quad (2.3)$$

where \mathbf{R} is the angular momentum operator of the rotating coordinate system and R is the internuclear distance.

The electronic kinetic energy operator can also be written in angular coordinates in order to separate the contribution of the orbital and spin angular momentum of the electrons. Let us denote the total electronic angular momentum operator by $\mathbf{P} = \mathbf{L} + \mathbf{S}$, where $\mathbf{L} = \sum_i \mathbf{l}_i$ and $\mathbf{S} = \sum_i \mathbf{s}_i$ are the total orbital and spin electronic angular momentum, respectively. It can be shown that the nuclear Hamiltonian for

molecules with electronic and spin angular momenta can be written as [142]

$$\hat{\mathcal{H}}_{\text{nuc}} = -\frac{\hbar^2}{2\mu R^2} \frac{\partial}{\partial R} \left(R^2 \frac{\partial}{\partial R} \right) + \frac{\hbar^2}{2\mu R^2} (\mathbf{J} - \mathbf{L} - \mathbf{S})^2 + V_c(R) \quad (2.4)$$

where $V_c(R) = (1/4\pi\epsilon_0) \sum_{\alpha,\beta} Z_\alpha Z_\beta e^2/R$ is the coulomb interaction between the nuclei, and \mathbf{J} is defined as the total angular momentum excluding nuclear spin.

In the usual Born-Oppenheimer approximation to the solution of the total molecular Hamiltonian $\hat{\mathcal{H}}_T$, the nuclear kinetic energy $\hat{T}_N = -(\hbar/2\mu)\nabla_R^2$ is treated as a small perturbation to the electronic Hamiltonian, due to the smallness of the mass ratio m/μ . The zero-th order wavefunctions are then written as the product of electronic and nuclear states $|\Psi_T^0\rangle = |\psi_e^0(\mathbf{r}, R)\rangle |\phi_{vr}^0(\mathbf{R})\rangle$, and the electronic eigenvalue problem $\hat{\mathcal{H}}_{\text{el}} |\psi_e^0(\mathbf{r}, R)\rangle = E_e(R) |\psi_e^0(\mathbf{r}, R)\rangle$ is solved for a fixed nuclear configuration. The electronic energy $E_e(R)$ thus depends on the internuclear distance R and the complete set of quantum numbers that characterize the state $|\psi_e^0(\mathbf{r}, R)\rangle$. The energy $E_e(R)$ can be included in the nuclear Hamiltonian $\hat{\mathcal{H}}_{\text{nuc}}$ as an additional potential energy term, i.e., $V_{\text{nuc}}(R) = E_e(R) + V_c(R)$. The electronic wavefunction is also an eigenstate of the operators \hat{L}_z and \hat{S}_z , with eigenvalues $\hbar\Lambda$ and $\hbar\Sigma$, respectively.

The complete set of orthonormal electronic states $|\psi_e^n(\mathbf{r}, R)\rangle$ can be used to construct a solution to the total Hamiltonian $\hat{\mathcal{H}}_{\text{el}} + \hat{\mathcal{H}}_{\text{nuc}}$ as a linear combination of Born-Oppenheimer product states,

$$|\Psi_T\rangle = \sum_n a_n |\psi_e^n(\mathbf{r}, R)\rangle |\phi_{vr}^n(R, \theta, \phi)\rangle. \quad (2.5)$$

After substituting this expression in the Schrödinger equation we obtain the secular equation

$$a_n \{V_{\text{nuc}}^n(R) - E\} |\phi_{vr}^n\rangle + \sum_{n'} a_{n'} C_{n,n'} |\phi_{vr}^{n'}\rangle = 0, \quad (2.6)$$

where E is the total energy of the molecule, and $C_{n,n'} |\phi_{vr}^{n'}\rangle = \langle \psi_e^n | \hat{T}_N | \psi_e^{n'} \rangle |\phi_{vr}^{n'}\rangle$ are the non-adiabatic coupling functions. In the adiabatic approximation, only the diagonal terms $C_{n,n'} = \delta_{n,n'} C_n$ are retained in Eq. (2.6). By using Eq. (2.4), it can be shown that the nuclear wavefunctions associated with each electronic state $|\psi_e^n\rangle$

thus satisfy the equation

$$\left\{ -\frac{\hbar^2}{2\mu R^2} \frac{\partial}{\partial R} \left(R^2 \frac{\partial}{\partial R} \right) + \frac{\hbar^2}{2\mu R^2} \mathbf{J}^2 - \frac{\hbar^2}{2\mu R^2} (2\Omega_n \hat{f}_z - \Omega_n^2) + E_e^n(R) + \frac{1}{4\pi\epsilon_0} \sum_{\alpha,\beta} \frac{Z_\alpha Z_\beta e^2}{R} + A_n(R) \right\} |\phi_{vr}^n(R, \theta, \phi)\rangle = 0, \quad (2.7)$$

where $\Omega_n = \Lambda_n + \Sigma_n$ is the projection of the total electronic angular momentum \mathbf{P} along the internuclear axis, and A_n is a small adiabatic correction to the nuclear potential energy associated with the electronic state $|\psi_e^n\rangle$.

The nuclear Schrödinger equation in Eq. (2.7) can be solved by separating the radial and the angular terms, which leads to the rotational wave equation

$$\left\{ \frac{\hbar^2}{2\mu R^2} \mathbf{J}^2 - \frac{\hbar^2}{2\mu R^2} (2\Omega \hat{f}_z - \Omega^2) \right\} |J\Omega M\rangle = E_{\text{rot}}(R) |J\Omega M\rangle, \quad (2.8)$$

with eigenvalue $E_{\text{rot}}(R) = (\hbar^2/2\mu R^2) [J(J+1) - \Omega^2]$. The rotational energy $E_{\text{rot}}(R)$ then enters into the vibrational wave equation as a centrifugal correction, which can be neglected for the lowest vibrational states [142]. The rotational wavefunction $|J\Omega M\rangle$ is given by

$$|J\Omega M\rangle = \left[\frac{2J+1}{4\pi} \right]^{1/2} \mathcal{D}_{M,\Omega}^{(J)}(\phi, \theta, \chi)^*, \quad (2.9)$$

where $\mathcal{D}_{M,\Omega}^{(J)}$ is an element of the Wigner rotation matrix [143], and (ϕ, θ, χ) are the Euler angles of the transformation between the space-fixed and the molecule-fixed frames. The total molecular wavefunction can be written as

$$|\Psi\rangle_T = |n, \Lambda\rangle |v(J)\rangle |S, \Sigma\rangle |J\Omega M\rangle, \quad (2.10)$$

where $|\Psi_e\rangle = |n, \Lambda\rangle$ is the electronic wavefunction, $|v(J)\rangle$ is the vibrational wavefunction, which may depend on the rotational energy, and $|S, \Sigma\rangle$ is the electronic spin state. This choice of Hamiltonian and wavefunctions is known conventionally as the Hund's coupling case (a) [142]. It is the choice for the molecular species considered in this Thesis. In particular, we consider alkali metal dimers such as LiCs,

in their electronic and vibrational ground states. The ground electronic states of alkali dimers have no unpaired electrons. In this case $\Lambda = 0 = \Sigma$, and the rotational wavefunction in Eq. (2.9) reduces to

$$|JM\rangle = \left[\frac{2J+1}{4\pi} \right]^{1/2} \mathcal{D}_{M,0}^{(J)} = Y_{J,M}(\theta, \phi), \quad (2.11)$$

where $Y_{J,M}(\theta, \phi)$ is the spherical harmonic of rank J and component M [143]. In this work, we focus our discussion on the rotational states of the electronic and vibrational ground state. For the ground vibrational state, we can neglect the variation of the rotational moment of inertial of the molecule with the vibrational motion. This is the rigid rotor approximation, for which Eq. (2.8) can be written as

$$\hat{H}_{\text{rot}}|J\Omega M\rangle = B_e [J(J+1) - \Omega^2] |J\Omega M\rangle, \quad (2.12)$$

where $B_e = \hbar^2/2\mu R_e^2$ is the rotational constant and R_e is the equilibrium internuclear distance. Typically $B_e/h \sim 10$ GHz for the molecules we consider in this work.

The rovibrational Hamiltonian in Eq. 2.7 can be used to obtain the leading contributions to the rotational energies, but ignores hyperfine effects due to the interaction between electronic, rotational, and nuclear angular momenta. Using perturbation theory, it is possible to derive effective Hamiltonians that take into account such effects [142, 143]. In practice, the appropriate effective Hamiltonian and its corresponding eigenstates are used depending on the physical situation of interest. In this Thesis we consider molecules composed of alkali metal and alkali-earth atoms. The nuclear magnetic moments of these atoms can lead to hyperfine splittings of the rotational levels that are typically smaller than the rotational constant B_e .

2.3 Hyperfine structure of closed-shell molecules

In recent experiments, ultracold molecules have been prepared by magneto-association of ultracold atoms near a Feshbach resonance [15, 18–21]. The atomic samples are initially prepared in specific hyperfine states $|f m_f\rangle$, where $\mathbf{f} = \mathbf{j} + \mathbf{i}$ is the total

angular momentum of the atom, $\mathbf{j} = \mathbf{l} + \mathbf{s}$ is the total electronic angular momentum, and \mathbf{i} is the nuclear spin angular momentum. The position and width of Feshbach resonances depend on the states of the colliding partners. Let m_{f_1} and m_{f_2} denote the projections of atoms 1 and 2 along the quantization axis. The total projection $M_F = m_{f_1} + m_{f_2}$ is a conserved quantity in the magneto-association process. The magneto-association of atoms produces weakly bound molecular states that are best described by atomic quantum numbers. Additional laser-assisted population transfer steps are needed to produce molecules in deeply bound states. Molecules are formed in hyperfine states $|(F), M_F\rangle$ by preserving the total projection M_F . Here $\mathbf{F} = \mathbf{J} + \mathbf{I}$, as in the atomic case, but now $\mathbf{J} = \mathbf{N} + \mathbf{S}$ and $\mathbf{I} = \mathbf{I}_1 + \mathbf{I}_2$. \mathbf{N} is the rotational angular momentum, \mathbf{S} is the electronic spin angular momentum, and \mathbf{I} is the vector sum of the nuclear spin angular momenta of the constituent atoms. The notation (F) indicates that the F quantum number is not conserved in the presence of an external field. In later chapters, we discuss interactions between heteronuclear alkali-metal dimers in the presence of static electric fields. In this thesis we consider alkali atoms with large nuclear spin $I \geq 3/2$. Although the hyperfine interactions in alkali dimers cause small splittings on the order of tens of kHz in the rotational lines [142], these splittings are comparable with the light-shifts induced by the optical trapping fields and dipole-dipole interaction energy between molecules at optical lattice separations. It is therefore necessary to understand the hyperfine structure of alkali-metal dimers, first in the absence of external fields, and then in the presence of weak and strong magnetic fields.

The Hamiltonian for a molecule in the absence of external fields, including hyperfine structure can be written as $\hat{H} = \hat{H}_R + \hat{H}_{\text{HF}}$, where $\hat{H}_R = B_e \mathbf{N}^2$ and \hat{H}_F is the hyperfine Hamiltonian. \hat{H}_F can be written as the sum of the following terms [142]

$$\hat{H}_Q = -eT^{(2)}(\vec{\nabla}E_1) \cdot T^{(2)}(Q_1) - eT^{(2)}(\vec{\nabla}E_2) \cdot T^{(2)}(Q_2), \quad (2.13a)$$

$$\hat{H}_{\text{SR}} = c_1 \mathbf{N} \cdot \mathbf{I}_1 + c_2 \mathbf{N} \cdot \mathbf{I}_2 \quad (2.13b)$$

$$\hat{H}_T = c_3 \mathbf{I}_1 \cdot \hat{T}^{(2)} \cdot \mathbf{I}_2 \quad (2.13c)$$

$$\hat{H}_{\text{SC}} = c_4 \mathbf{I}_1 \cdot \mathbf{I}_2. \quad (2.13d)$$

	$^7\text{Li}^{133}\text{Cs}$	$^{87}\text{Rb}^{133}\text{Cs}$	$^{87}\text{Rb}_2$	$^{40}\text{K}^{87}\text{Rb}$	$^{41}\text{K}^{87}\text{Rb}$
B_e (GHz)	5.636	0.504		1.114	1.096
I_1	3/2	3/2	3/2	4	3/2
I_2	7/2	7/2	3/2	3/2	3/2
$(eQq)_1$ (kHz)	18.5	-872	-1188	306	-298
$(eQq)_2$ (kHz)	188	51	-1188	-1520	-1520
c_1 (Hz)	32	98.4	209	-24	10
c_2 (Hz)	3014	194.1	209	420	413
c_3 (Hz)	140	192.4	346	-48.2	21
c_4 (Hz)	1610	17345.4	25021	-2030.4	896
g_r	0.0106	0.0062	0.0093	0.0140	0.0138
g_1	2.171	1.834	1.834	-0.324	0.143
g_2	0.738	0.738	1.834	1.834	1.834

Table 2.1: Predicted molecular constants including hyperfine structure for some alkali-metal dimers. The notation is defined in Eqs. (2.13). Data taken from Refs.[144–146].

The electric quadrupole interaction \hat{H}_Q described the interaction between the quadrupole moment of each nuclei Q_i with the gradient of the electric field $\vec{\nabla}E_i$ generated by the electrons. The nuclear spin-rotation coupling \hat{H}_{SR} represents the coupling between the nuclear magnetic moments of each nuclei with the magnetic field generated by the rotation of the molecule. The tensor spin-spin coupling \hat{H}_T describes the magnetic dipole-dipole interaction between nuclear spins, and the scalar spin-spin interaction \hat{H}_{SC} describes the coupling between nuclear spins mediated by the electron density. We have neglected terms depending on the electronic spin \mathbf{S} because we restrict the discussion to closed-shell molecules with zero electronic angular momentum ($^1\Sigma$ states).

In Table 2.1 we reproduce literature values of the molecular constants defined in Eqs. (2.13) for selected alkali-metal dimers [144–146]. For closed-shell $^1\Sigma$ states, the hyperfine splittings of the rotational lines are largely due to the nuclear quadrupole moments of the atoms. The electric quadrupole constant (eqQ) is at least two orders of magnitude larger than rest of the hyperfine constants for most alkali-metal dimers. The electric quadrupole interaction can in principle couple

different rotational states of the molecules. However, the rotational splitting is several orders of magnitude larger than the quadrupole constant so N can be considered a good quantum number. In the absence of external fields, the quantum numbers (F, M_F) are conserved. In Appendix C we derive the matrix elements for each term in Eq. (2.13) using three different basis sets. For weak external fields, it is more convenient to use the fully coupled basis $|(NI)FM_F\rangle$ [142]. The matrix elements of the quadrupole operator \hat{H}_Q in this basis can be written as

$$\begin{aligned} & \langle (NI)FM_F | \hat{H}_Q | (NI')FM_F \rangle \\ &= (-1)^{F+I+I_1+I_2} (2N+1) [(2I+1)(2I'+1)]^{1/2} \left\{ \begin{matrix} I' & N & F \\ N & I & 2 \end{matrix} \right\} \quad (2.14) \\ & \quad \times \begin{pmatrix} N & 2 & N \\ 0 & 0 & 0 \end{pmatrix} \left[\frac{(eqQ)_1}{4} G_1(I, I', I_1, I_2) + \frac{(eqQ)_2}{4} G_2(I, I', I_1, I_2) \right], \end{aligned}$$

where G_1 and G_2 are functions of the nuclear spin angular momenta. The $3j$ -symbol in the second line of Eq. (2.15) imposes the selection rule $\Delta N = 0$ for $N \neq 0$, i.e., there is no quadrupole interaction in the rotational ground level. The same selection rule applies to the tensor spin-spin interaction \hat{H}_T (see Appendix C) because it has the same tensorial form as the quadrupole interaction [142].

In Appendix C it is shown that the matrix elements of the nuclear spin-rotation operator \hat{H}_{SR} are given by

$$\begin{aligned} & \langle (NI)FM_F | \hat{H}_{SR} | (NI')FM_F \rangle \\ &= (-1)^{F+N+I+I_1+I_2+1} [N(2N+1)(N+1)(2I+1)(2I'+1)]^{1/2} \\ & \quad \times \left\{ \begin{matrix} I' & N & F \\ N & I & 1 \end{matrix} \right\} \left[(-1)^{I'} \left\{ \begin{matrix} I_1 & I' & I_2 \\ I & I_1 & 1 \end{matrix} \right\} c_1 + (-1)^I \left\{ \begin{matrix} I_2 & I' & I_1 \\ I & I_2 & 1 \end{matrix} \right\} c_2 \right], \quad (2.15) \end{aligned}$$

which vanish for $N = 0$. The zero-field-splitting (ZFS) of the rotational ground level is therefore due to the scalar spin-spin coupling \hat{H}_{SC} [142]. The matrix representation of \hat{H}_{SC} is diagonal in the fully-coupled basis, with elements given by

$$\langle (NI)FM_F | \hat{H}_{SC} | (NI)FM_F \rangle = \frac{c_4}{2} [I(I+1) - I_1(I_1+1) - I_2(I_2+1)]. \quad (2.16)$$

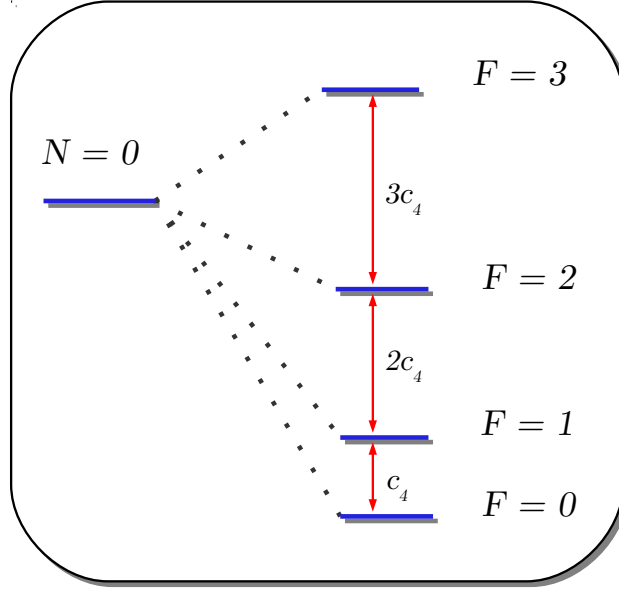


Figure 2.1: Zero-field-splitting of the $N = 0$ rotational state for $^{41}\text{K}^{87}\text{Rb}$ ($I_{\text{K}} = I_{\text{Rb}} = 3/2$). The scalar nuclear spin coupling constant is $c_4 = 896$ Hz. N and F are the rotational angular momentum and total angular momentum quantum numbers, respectively.

The ZFS of the ground rotational state ($N = 0$) is thus on the order of $0.1 - 10$ kHz for alkali-metal dimers. This is a small perturbation to the rotational energy, but is comparable to the depth of a typical far-detuned optical trap. The values of the atomic nuclear spins are given in Table 2.1. For $^7\text{Li}^{133}\text{Cs}$ molecules, the molecular spin states are $I = 2, 3, 4, 5$. The rotational ground state $N = 0$ has $(2I_1 + 1)(2I_2 + 1) = 32$ hyperfine states. In the absence of magnetic fields these states are ordered into five levels characterized by the total angular momentum $F = I$. Each hyperfine level is $(2F + 1)$ -fold degenerate. In $^{41}\text{K}^{87}\text{Rb}$ molecules, both nuclei have the same spin. The possible spin states are $I = 0, 1, 2, 3$. The zero-field splitting between hyperfine states in the $N = 0$ level follow the interval rule $E_F - E_{F-1} = c_4 F$. This is illustrated in Fig. 2.1.

The hyperfine structure of rotational excited states is more complex than the ground state. The number of hyperfine states increase significantly with N and all

the terms in Eq. (2.13) contribute to the ZFS of the levels. For ${}^7\text{Li}^{133}\text{Cs}$ molecules, the first rotational excited level $N = 1$ has $32 \times (2N + 1) = 96$ hyperfine states. These states are ordered into 12 hyperfine levels in the absence of magnetic fields, characterized by $F = I + N \dots, |I - N|$. The quadrupole interaction couples hyperfine states $|(NI)FM_F\rangle$ with the same value of F but different total nuclear spins I . Therefore, an accurate evaluation of the hyperfine spectrum for the $N = 0$ and $N = 1$ rotational levels requires in principle the diagonalization of a matrix of dimension $\mathcal{D} = 128 \times 128$. This matrix can be divided into sub-blocks associated with the quantum numbers (N, F, M_F) , which can be diagonalized independently. As explained below, an external electric or magnetic field introduces couplings between different sub-blocks.

2.4 Diatomic molecules in static electric and magnetic fields

2.4.1 Closed-shell molecules in static electric fields

A polar diatomic molecule has an asymmetric charge distribution due to the difference between the nuclear charges Z_1 and Z_2 . The electric dipole moment of the molecule is the position-weighted sum over nuclear and electronic charges. The electric dipole moment lies along the internuclear axis (molecule-fixed z axis), and rotates with the molecule. The dipole moment interacts with an applied DC electric field \mathbf{E} , and tends to align along the field direction. The space-fixed coordinate system can be chosen such that the electric field lies along the Z axis, i.e., $\mathbf{E} = E_Z \hat{\mathbf{Z}}$. The interaction is then represented by the Stark Hamiltonian

$$\hat{H}_{\text{dc}} = -\mathbf{d} \cdot \mathbf{E} = -d_0 E_Z \cos \theta = -d_0 E_Z \mathcal{D}_{0,0}^{(1)}(\theta)^*, \quad (2.17)$$

where $d_0 = |\langle v | \mu(R) | v \rangle|$ is the vibrationally-averaged permanent dipole moment, and θ is the angle between the electric field and the internuclear axis. In this work we consider alkali-metal dimers whose ground electronic state has zero orbital and spin angular momentum. In spectroscopic notation this is a $X^1\Sigma$ electronic state. We use the rotational basis defined in Eq. (2.11) with $\mathbf{J} = \mathbf{N}$ to write the matrix

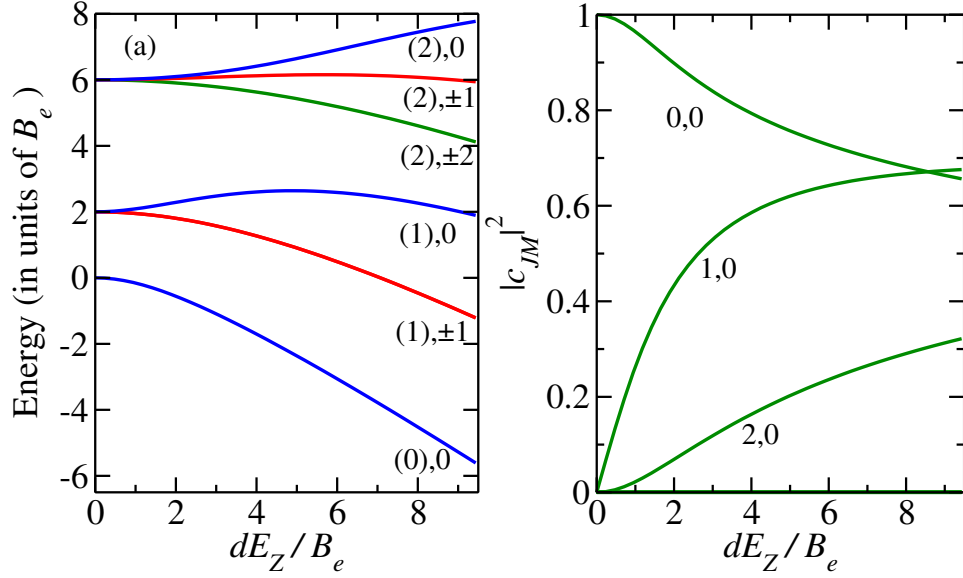


Figure 2.2: Stark effect on $^1\Sigma$ molecules: (a) energies of the field-dressed states $|(N)M\rangle$ in units of B_e , as a function of the electric field strength parameter $d_0 E_Z / B_e$; (b) Mixing coefficients $|c_{NM}|^2$ of the field-dressed ground state $|(0)0\rangle = \sum_N c_{N0} |N0\rangle$, as a function of the ratio $d_0 E_Z / B_e$. d_0 is the permanent dipole moment, E_Z the field strength, and B_e the rotational constant.

elements of the operator in Eq. (2.17) as

$$\langle NM_N | \hat{H}_{dc} | N' M'_N \rangle = -d_0 E_Z \langle NM_N | \mathcal{D}_{0,0}^{(1)} | N' M'_N \rangle, \quad (2.18)$$

where

$$\begin{aligned} \langle NM_N | \mathcal{D}_{0,0}^{(1)} | N' M'_N \rangle &= (-1)^M [(2N+1)(2N'+1)]^{1/2} \\ &\times \begin{pmatrix} N & 1 & N' \\ 0 & 0 & 0 \end{pmatrix} \begin{pmatrix} N & 1 & N' \\ -M_N & 0 & M'_N \end{pmatrix}. \end{aligned} \quad (2.19)$$

From the symmetry properties of the $3j$ -symbols in Eq. (2.18), it can be shown that the matrix element vanishes unless $N - N' = \pm 1$, and $M_N = M'_N$. The eigenstates of the Stark Hamiltonian are therefore superpositions of rotational states $|NM_N\rangle$ with different parity $p_J = (-1)^N$ and the same value of the angular mo-

momentum projection M_N along the electric field axis. The DC Stark eigenstates are denoted here as $|(N)M_N\rangle$, where (N) labels the quantum number to which the state corresponds when the electric field is turned-off adiabatically. In Figure 2.2(a) we show the energies of the lowest field-dressed $|(N)M\rangle$ of the rigid rotor Hamiltonian in a DC electric field $\hat{H} = B_e \mathbf{N}^2 - d_0 E_0 \cos \theta$. The electric field splits the field-free rotational state $|N = 1, M_N\rangle$ in two degenerate lower states with $|M_N| = 1$, and a higher state with $M_N = 0$. The first four field-dressed rotational states $\{|(0)0\rangle, |(1)0\rangle, |(1)\pm 1\rangle\}$ form the subspace of interest in this work. Figure 2.2(b) shows the mixing probabilities $|c_{J,M}|^2$ of each field-free rotational state $|J, 0\rangle$ for the ground field-dressed state $|(0)0\rangle = \sum_N c_{N,0} |N, 0\rangle$. The strength of the electric field is parametrized by the dimensionless parameter $\lambda = d_0 E_0 / B_e$. For $\lambda > 2$ the contribution of the field-free state $|2, 0\rangle$ on the field-dressed ground state $|(0)0\rangle$ cannot be neglected.

2.4.2 Closed-shell molecules in static magnetic fields

An atomic nucleus with non-zero spin I has an associated magnetic moment $\vec{\mu} = g\mu_N \mathbf{I}$, where g is the nuclear g-factor and μ_N is the nuclear magneton. Each atomic nucleus in a molecule interacts independently with an applied magnetic field \mathbf{B} . The interaction is represented by

$$\hat{H}_B = -\vec{\mu}_1 \cdot \mathbf{B} - \vec{\mu}_2 \cdot \mathbf{B} \equiv -g_1 \mu_N \mathbf{I}_1 \cdot \mathbf{B} - g_2 \mu_N \mathbf{I}_2 \cdot \mathbf{B}. \quad (2.20)$$

In addition to the nuclear spin magnetic moments, the rotational motion of the molecule generates a magnetic moment $\vec{\mu}_R = g_R \mu_N \mathbf{N}$. As shown in Table 2.1, the rotational g-factor is at least two orders of magnitude smaller than the nuclear g-factors. We can therefore ignore the interaction of the rotational magnetic moment with the magnetic field. If we assume the magnetic field to be $\mathbf{B} = B_Z \hat{\mathbf{Z}}$, the matrix

elements of \hat{H}_B can be written in the fully coupled basis as (see Appendix C)

$$\begin{aligned}
& \langle (NI)FM_F | \hat{H}_B | (NI')F'M_F \rangle \\
&= (-1)^{1+N+I_1+I_2+I'-M_F} [(2F+1)(2F'+1)(2I+1)(2I'+1)]^{1/2} \\
&\quad \times \begin{Bmatrix} I' & F' & N \\ F & I & 1 \end{Bmatrix} \begin{pmatrix} F & 1 & F' \\ -M_F & 0 & M_F \end{pmatrix} \\
&\quad \times \left(g_1 \mu_N B_Z (-1)^{I'} \begin{Bmatrix} I_1 & I' & I_2 \\ I & I_1 & 1 \end{Bmatrix} [I_1(I_1+1)(2I_1+1)]^{1/2} \right. \\
&\quad \left. + g_2 \mu_N B_Z (-1)^I \begin{Bmatrix} I_2 & I' & I_1 \\ I & I_2 & 1 \end{Bmatrix} [I_2(I_2+1)(2I_2+1)]^{1/2} \right). \quad (2.21)
\end{aligned}$$

The magnetic field therefore couples hyperfine states according to the selection rules $\Delta M_F = 0$ and $|\Delta F| = 0, 1$. For magnetic fields such that $g\mu_N B_Z$ is larger than the hyperfine splitting, there is a strong mixing of F angular momentum states for each hyperfine level. In this regime, the fully coupled basis $|(NI)FM_F\rangle$ is no longer the best choice to describe the spin degrees of freedom of the molecule. The spin coupled basis $|NM_N\rangle|IM_I\rangle$ is a common choice to describe hyperfine interactions in the presence of intermediate magnetic fields [142]. In this regime, the rotational motion is said to be uncoupled from the nuclear spin. The rotational angular momentum N and the total projection $M_F = M_N + M_I$ are good quantum numbers. The matrix elements of the Zeeman Hamiltonian \hat{H}_B in the spin uncoupled basis can be written as

$$\begin{aligned}
& \langle NM_N IM_I | \hat{H}_B | NM_N I' M_I \rangle = \\
&= (-1)^{I+I_1+I_2-M_I} [(2I+1)(2I'+1)]^{1/2} \begin{pmatrix} I & 1 & I' \\ -M_I & 0 & M_I \end{pmatrix} \\
&\quad \times \left[g_1 \mu_N B_Z (-1)^{I'} [I_1(I_1+1)(2I_1+1)]^{1/2} \begin{Bmatrix} I_1 & I' & I_2 \\ I & I_1 & 1 \end{Bmatrix} \right. \\
&\quad \left. + g_2 \mu_N B_Z (-1)^I [I_2(I_2+1)(2I_2+1)]^{1/2} \begin{Bmatrix} I_2 & I' & I_1 \\ I & I_2 & 1 \end{Bmatrix} \right]. \quad (2.22)
\end{aligned}$$

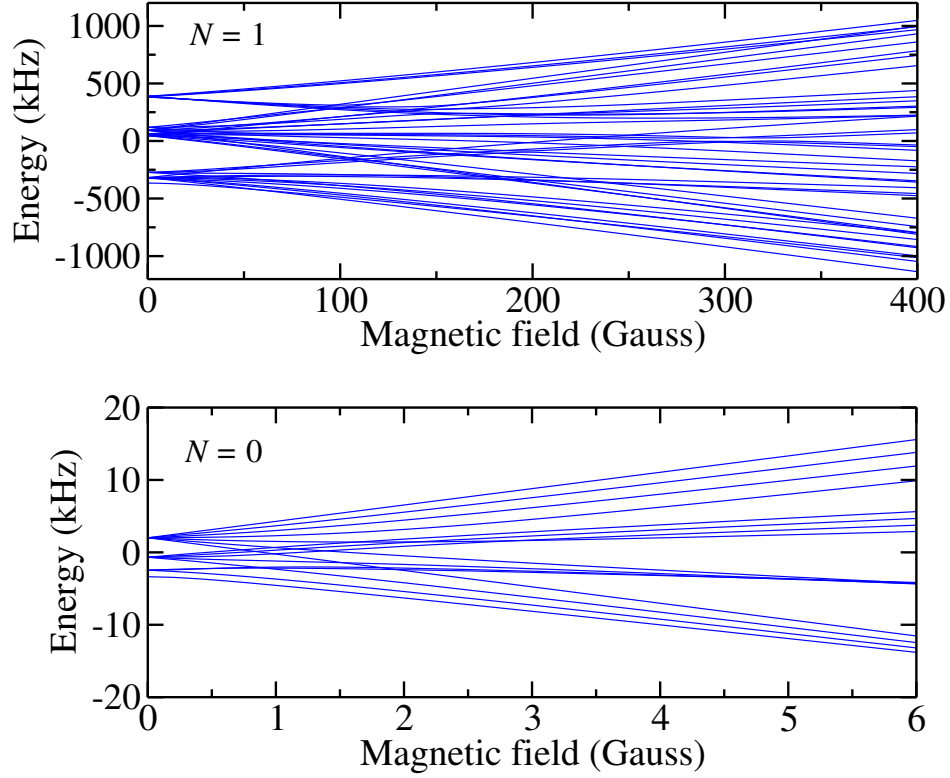


Figure 2.3: Zeeman spectra for a $^{41}\text{K}^{87}\text{Rb}$ molecule in $N = 0$ and $N = 1$ rotational states of the ground electronic and vibrational state. The energy is measured with respect to $E_N = B_e N(N + 1)$.

Another useful basis set can be used to describe the nuclear degrees of freedom. In the fully decoupled basis $|NM_N\rangle|I_1M_{I_1}\rangle|I_2M_{I_2}\rangle$ the Zeeman Hamiltonian is diagonal, which is useful for assigning quantum numbers to the molecular levels at high magnetic fields [142]. The matrix elements of \hat{H}_B in this basis are given by

$$\langle NM_N|\langle I_1M_{I_1}|\langle I_2M_{I_2}|\hat{H}_B|NM_N\rangle|I_1M_{I_1}\rangle|I_2M_{I_2}\rangle = -g_1\mu_N B_Z M_{I_1} - g_2\mu_N B_Z M_{I_2}. \quad (2.23)$$

The hyperfine structure for each rotational level is obtained by diagonalizing the total molecular Hamiltonian in the presence of a static magnetic field

$$\hat{H} = \hat{H}_R + \hat{H}_{\text{HF}} + \hat{H}_B.$$

In Figure 2.3 we show the Zeeman energies of the hyperfine levels in states $N = 0$ and $N = 1$ for $^{41}\text{K}^{87}\text{Rb}$ molecules. For clarity, we only show the magnetic sub-levels with $|M_F| = 1$. Molecular states with the same total projection M_F and different values of F interact in the presence of a magnetic field, leading to the level repulsion observed in Fig. 2.3. These avoided crossings occur at relatively weak magnetic fields $B_Z \sim 10$ Gauss for most heteronuclear alkali-metal dimers in the $N = 0$ state. For the $N = 1$ state, the avoided crossings occur at larger fields because the hyperfine splittings are larger.

2.4.3 Open-shell molecules in static magnetic fields

Let us consider polar molecules with one unpaired electron in the ground electronic state denoted $X^2\Sigma$, such as SrF and CaF. If the nuclear magnetic moments are neglected, the effective Hamiltonian used to describe the field-free spectral lines of $^2\Sigma$ molecules in the vibrational state $|v\rangle$ is [142, 143]

$$\hat{H} = B_v \mathbf{N}^2 + \gamma_v \mathbf{N} \cdot \mathbf{S} = B_v \mathbf{N}^2 + \gamma_v \hat{N}_z \hat{S}_z + \frac{\gamma_v}{2} (\hat{N}_- \hat{S}_+ + \hat{N}_+ \hat{S}_-) \quad (2.24)$$

where \mathbf{S} is the electron spin angular momentum, $\mathbf{N} = \mathbf{J} - \mathbf{S}$, is the rotational angular momentum of the nuclei, and $\hat{N}_\pm = \hat{N}_x \pm i\hat{N}_y$ are the raising and lowering operators (an analogous definition holds for \hat{S}_\pm). $\gamma_v \ll B_v$ is the constant for the electronic spin-rotation interaction. The uncoupled basis set $|NM_N\rangle|SM_S\rangle$ is chosen to represent the Hamiltonian in Eq. (2.24). The first two terms of the Hamiltonian are diagonal in this basis, with matrix elements given by

$$\langle NM_N | \langle SM_S | \hat{H} | NM_N \rangle | SM_S \rangle = B_v N(N+1) + \gamma_v M_N M_S. \quad (2.25)$$

The last term in Eq. (2.24) is non-diagonal in the chosen basis set. It mixes spin projections and rotational angular momentum projections for rotational states with $N \geq 1$, but does not couple states with a different value of N . The off-diagonal matrix elements of the Hamiltonian are [143]

$$\begin{aligned} \langle NM_N - 1 | \langle SM_S + 1 | \hat{H} | NM_N \rangle | SM_S \rangle &= \frac{\gamma_v}{2} [N(N+1) - M_N(M_N - 1)]^{1/2} \\ &\times [S(S+1) - M_S(M_S + 1)]^{1/2} \end{aligned} \quad (2.26)$$

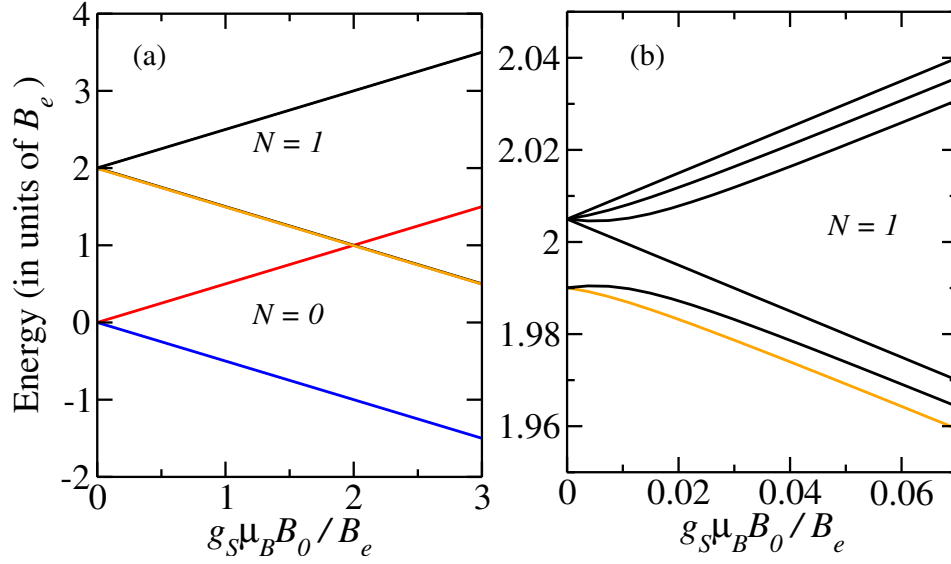


Figure 2.4: Rotational levels of a $X^2\Sigma$ molecule in the presence of a magnetic field with strength B_0 : (a) First two rotational manifolds $N=0$ and $N=1$ showing a level crossing for $g_S \mu_B B_0 / B_e \approx 2$; (b) $N=1$ excited states for weak magnetic fields. The spin rotation constant is $\gamma = 0.01 B_e$. Energy is in units of the rotational constant B_e . μ_B is the Bohr magneton and $g_S = 2.0$ is the electron g-factor.

$$\begin{aligned} \langle NM_N + 1 | \langle SM_S - 1 | \hat{H} | NM_N \rangle | SM_S \rangle &= \frac{\gamma_v}{2} [N(N+1) - M_N(M_N+1)]^{1/2} \\ &\times [S(S+1) - M_S(M_S-1)]^{1/2} \quad (2.27) \end{aligned}$$

The unpaired electron of the $^2\Sigma$ molecule has a magnetic moment $\vec{\mu}_m = g_S \mu_B \mathbf{S}$, where μ_B is the Bohr magneton, and $g_S \approx 2.00$ is the corresponding spin g-factor. The magnetic moment interacts with an applied magnetic field \mathbf{B} . The interaction is represented by the Zeeman Hamiltonian $\hat{H}_B = g_S \mu_B \mathbf{S} \cdot \mathbf{B}$. This Hamiltonian is diagonal in the basis $|NM_N\rangle |SM_S\rangle$ for a magnetic field directed along the space-fixed Z axis, with matrix elements $\langle NM_N | \langle SM_S | \hat{H}_B | NM_N \rangle | SM_S \rangle = g_S \mu_B M_S$. The states $|NM_N\rangle |1/2, M_S = \pm 1/2\rangle$ are therefore split into doublets in the presence of a magnetic field, with an energy separation that scales linearly with the field strength B_Z for values of the field strength satisfying $\gamma \ll g_S \mu_B B_Z \ll 2B_e$. In Figure 2.4 we show the rotational levels of a $^2\Sigma$ molecule in the presence of a magnetic field with

strength B_Z . We choose the electronic spin-rotation constant $\gamma = 0.01B_e$, which is representative of experimentally relevant molecules such as SrF [147].

2.5 Diatomic molecules in far-detuned optical fields

In this section we review the theory of the interaction of a molecule with a classical electromagnetic field with a frequency ω far-detuned from any molecular transition. The analysis presented in this section forms the basis for the description of molecular alignment in high-intensity optical fields, as well as optical trapping of molecules with field of lower intensity.

2.5.1 Dynamical Stark shift of molecular states

Let us consider a general Hamiltonian for a diatomic molecule in the center of mass frame given by $\hat{H}_{\text{mol}} = \hat{T}_N(R) + \hat{H}_{\text{el}}(\{\mathbf{r}_i\}, R)$, where $\hat{T}_N(R)$ is the Hamiltonian describing the nuclear motion (vibrational and rotational), and \hat{H}_{el} describes the kinetic and coulomb potential energy of the electrons, with coordinates \mathbf{r}_i with respect to the center of mass of the molecule. The electronic Hamiltonian depends on the internuclear separation R through the attractive electron-nucleus and repulsive nucleus-nucleus coulomb interaction.

In the Born-Oppenheimer approximation, the total molecular wavefunction, neglecting spin, can be written as $|e(R)\rangle|v(R); r(\theta, \phi)\rangle$, where $|e(R)\rangle$ is the electronic wavefunction that depends parametrically on the internuclear distance R , and $|v(R); r(\theta, \phi)\rangle$ is the rovibrational wavefunction. The wavefunctions satisfy the eigenvalue equation $\hat{H}_{\text{mol}}|e \ v \ r\rangle = E_{evr}|e \ v \ r\rangle$. Since we want to describe the interaction of a molecule with a monochromatic electromagnetic wave, the starting point is the time-dependent Schrödinger equation

$$i\hbar \frac{d}{dt} |\Psi(t)\rangle = (\hat{H}_{\text{mol}} + \hat{V}(t)) |\Psi(t)\rangle, \quad (2.28)$$

where $\hat{V}(t) = -\mathbf{d} \cdot \mathbf{E}(\mathbf{r}, t)$ is the light-matter interaction energy in the dipole approximation. In a semi-classical approximation, the components of electromagnetic field $\mathbf{E}(\mathbf{r}, t)$ can be treated as time-dependent complex numbers. The solution of Eq. 2.28 can be written in the most general way in terms of a complete basis of

eigenstates as

$$|\Psi(t)\rangle = \sum_e \sum_v \sum_r C_{evr}(t) |e \ v \ r\rangle e^{-iE_{evr}t/\hbar}, \quad (2.29)$$

which can be inserted in Eq. 2.28 to obtain a set of coupled differential equations for the time-dependent complex coefficients $C_{evr}(t)$. This system of equations can in principle be solved provided we know the solution $|\Psi(t_0)\rangle$ at the initial time t_0 . Suppose that at the initial time $t_0 = 0$ the system is described by a rotational wavepacket in a particular vibronic state $|\Psi(0)\rangle = \sum_r C_r |e_i v_i r\rangle$, and we are interested in the time-evolution of this wavepacket under the influence of an AC electric field far-detuned from any molecular resonance. In Appendix A it is shown that the light-matter interaction in far off-resonant conditions can be described by the effective Schrödinger equation

$$i\hbar \frac{d}{dt} C_r(t) = \sum_{r'} C_{r'}(t) \langle r | \hat{H}_{AC} | r' \rangle e^{\frac{i}{\hbar}(E_r - E_{r'})t}, \quad (2.30)$$

where we have omitted the vibrational and electronic indexes (e_i, v_i) for simplicity. The effective rotational Hamiltonian \hat{H}_{AC} in Eq. (2.30) is given by (see Appendix A)

$$\hat{H}_{AC} = - \sum_{ev} \frac{\langle e_i v_i | \mathbf{E}(\mathbf{r}) \cdot \mathbf{d} | ev \rangle \langle ev | \mathbf{d} \cdot \mathbf{E}^*(\mathbf{r}) | e_i v_i \rangle}{E_{ev} - E_{e_i v_i} - \hbar\omega} + \frac{\langle e_i v_i | \mathbf{E}^*(\mathbf{r}) \cdot \mathbf{d} | ev \rangle \langle ev | \mathbf{d} \cdot \mathbf{E}(\mathbf{r}) | e_i v_i \rangle}{E_{ev} - E_{e_i v_i} + \hbar\omega} \quad (2.31)$$

The matrix elements in Eq. 2.31 are evaluated in the space-fixed frame, since observable quantities such as $|C_r(t)|^2$ must refer to the laboratory frame. Due to the rotation of the molecule-fixed frame with respect to the laboratory frame according to the angular coordinates (θ, ϕ, χ) [143], the transformation of the matrix elements in Eq. (2.31) from the molecule-fixed to the space-fixed frame introduces elements of the rotation matrices $\hat{R}(\theta, \phi, \chi)$ that couple different rotational states. Equation (2.31) can be written as

$$\hat{H}_{AC} = - \sum_p \sum_{p'} E_p(\mathbf{r}) \hat{\alpha}_{p,p'} E_{p'}^*(\mathbf{r}), \quad (2.32)$$

where we have expanded the electric field vectors in space-fixed spherical basis $\mathbf{E}(\mathbf{r}) = \sum_q E_q(\mathbf{r}) \hat{\mathbf{e}}_q^*$ ¹. The general form of the polarizability operator $\hat{\alpha}_{q,q'}$ is given by

$$\hat{\alpha}_{p,p'} = \sum_{ev} \frac{\langle e_i v_i | \hat{d}_p^\dagger | ev \rangle \langle ev | \hat{d}_{p'} | e_i v_i \rangle}{E_{ev} - E_{e_i v_i} - \hbar\omega} + \frac{\langle e_i v_i | \hat{d}_{p'} | ev \rangle \langle ev | \hat{d}_p^\dagger | e_i v_i \rangle}{E_{ev} - E_{e_i v_i} + \hbar\omega} \quad (2.33)$$

$$= (-1)^{-p} \hat{\alpha}_{-p,p'} \quad (2.34)$$

where the components of the dipole operators in the spherical basis refer to the space-fixed frame. In Eq. (2.34) the definition $\hat{d}_p^\dagger = (-1)^{-p} \hat{d}_{-p}$ has been used to redefine the polarizability operator as $\alpha_{-p,p}$ in agreement with the standard notation [148]. The polarizability components in the spherical basis satisfy $\alpha_{-p,p'}^* = (-1)^{p-p'} \alpha_{-p',p}$.

The polarizability tensor $\hat{\alpha}_{p,p'}$ couples different rotational states of the molecule due to the dependence of the space-fixed dipole operators \hat{d}_p on the molecule-fixed operators \hat{d}_q through the transformation

$$\hat{d}_p = \sum_q \mathcal{D}_{pq}^{(1)}(\theta, \phi, \chi)^* \hat{d}_q, \quad (2.35)$$

where $\mathcal{D}_{pq}^{(1)}(\theta, \phi, \chi)^*$ is the pq element of the inverse rotation matrix of rank one [142, 143]. Using Eq. (2.35) and its hermitian conjugate, Eq. (2.32) can thus be rewritten as [149]

$$\hat{H}_{AC} = - \sum_{p,p'} (-1)^{-p} \left[\sum_{q,q'} \alpha_{-q,q'} \mathcal{D}_{-p-q}^{(1)}(\Omega)^* \mathcal{D}_{p'q'}^{(1)}(\Omega)^* \right] E_p(\mathbf{r}) E_{p'}^*(\mathbf{r}), \quad (2.36)$$

where the spherical components of the polarizability tensor $\alpha_{-q,q'}$ in the molecule-fixed frame are defined in analogy with Eq. (2.34). Equation (2.36) can be further simplified using the Clebsch-Gordan series [142, 143] to give

$$\hat{H}_{AC} = - \sum_{p,p'} \sum_j \begin{pmatrix} 1 & 1 & j \\ p & p' & k \end{pmatrix} \alpha_k(j) \mathcal{D}_{kk'}^{(j)}(\Omega) (-1)^{-p} E_p(\mathbf{r}) E_{p'}^*(\mathbf{r}), \quad (2.37)$$

¹The alternative definition $\mathbf{E}(\mathbf{r}) = \sum_q E_q(\mathbf{r}) \hat{\mathbf{e}}_q$ gives the same expression for \hat{H}_{AC}

where

$$\alpha_{k'}(j) = (2j+1) \sum_{qq'} \alpha_{-q,q'} \begin{pmatrix} 1 & 1 & j \\ -q & q' & k' \end{pmatrix} \quad (2.38)$$

gives the irreducible component of the polarizability tensor of order j in terms of its components in the spherical basis $\alpha_{-q,q'}$. The frequency-dependent polarizability components $\alpha_{-q,q'}$ are numerical parameters evaluated in the molecule-fixed frame. The Wigner matrix elements $\mathcal{D}_{kk'}^{(j)}(\Omega)$ are the operators acting on the rotational states $|r\rangle$. The off-diagonal elements of the \hat{H}_{AC} correspond to rotational Raman transitions and the diagonal elements correspond to the AC Stark shift of the rotational states. For an arbitrary molecule interacting with an electromagnetic plane wave linearly polarized along the space-fixed Z axis ($E_p = \delta_{p,0}E_0/2$), the light-matter Hamiltonian in Eq. (2.36) gives

$$\hat{H}_{AC} = -\frac{|E_0|^2}{4} \left\{ \frac{1}{3}(\alpha_{0,0} - \alpha_{1,-1} - \alpha_{-1,1})\mathcal{D}_{0,0}^{(0)} + \frac{1}{3}(2\alpha_{0,0} + \alpha_{1,-1} + \alpha_{-1,1})\mathcal{D}_{0,0}^{(2)} \right\}. \quad (2.39)$$

For diatomic molecules, the only non-zero elements of the polarizability tensor in cartesian coordinates are $\alpha_{\perp} \equiv \alpha_{xx} = \alpha_{yy}$ and $\alpha_{zz} \equiv \alpha_{\parallel}$. In the spherical basis these correspond to $\alpha_{-11} = \alpha_{1-1} = \alpha_{\perp}$ and $\alpha_{0,0} = \alpha_{\parallel}$. Using these definitions and the expressions for the Wigner functions [143] we can write Eq. (2.39) as

$$\hat{H}_{AC} = -\frac{|E_0|^2}{4} \left\{ \frac{1}{3}(\alpha_{\parallel} + 2\alpha_{\perp}) + \frac{2}{3}(\alpha_{\parallel} - \alpha_{\perp})C_{2,0}(\theta) \right\}. \quad (2.40)$$

The modified spherical harmonic $C_{L,M}$ is defined by [143]

$$C_{L,M}(\theta, \phi) = \sqrt{\frac{4\pi}{2L+1}} Y_{L,M}(\theta, \phi). \quad (2.41)$$

Equation (2.40) has been used to describe the alignment of polar and non-polar molecules with intense off-resonant pulses [149, 150]. Intense light fields induce coherences between rotational states via the tensor part of the polarizability operator, which is proportional to the functions $C_{L,M}(\theta, \phi)$. The creation of rotational wavepackets localizes the rotational motion in angular space, similarly to the alignment induced by electrostatic fields, but the effect is much stronger with high-

intensity laser pulses. The simple expression in Eq. (2.40) for diatomic molecules can also be derived from simple energetic arguments [151]. However, having a general expression as in Eq. (2.36) can be useful to describe the interaction of a generic polyatomic molecule with a laser field of arbitrary helicity, as is the case in optical traps. The elements of the dynamic polarizability tensor in the molecular frame $\alpha_{q,q'}$ can be independently obtained from electronic structure calculations, or relations between different tensor elements can be deduced by measuring the light shift of a given rotational state, as Eq. (2.40) suggests.

2.5.2 Polarizability of diatomic molecules at optical frequencies

Due to the cylindrical symmetry of a diatomic molecule, the molecule-fixed coordinate system can be chosen such that the polarizability tensor has only three non-vanishing components: $\alpha_{xx} = \alpha_{yy} \neq \alpha_{zz}$. In the spherical basis, the non-vanishing components are $\alpha_{0,0} \neq \alpha_{1,-1} = \alpha_{-1,1}$, which enter in the light-matter interaction Hamiltonian in Eq. (2.40), for example. Let us consider a molecule with Born-Oppenheimer states $|n\Lambda\rangle|v(J)\rangle|J\Lambda M\rangle$. The wavefunction $|n\Lambda\rangle$ corresponds to an electronic state with energy E_n and electronic angular momentum \mathbf{L} , with projection $\hbar\Lambda$ along the internuclear axis. The rovibrational wavefunction $|v(J)\rangle|J\Lambda M_J\rangle$ corresponds to the vibrational state $v(J)$, which may include rotation-vibration coupling, and the rotational state described by the total rotational angular momentum $\mathbf{J} = \mathbf{R} + \mathbf{L}$, and projection $\hbar M_J$ along the space-fixed Z axis. The rotational dependence of the polarizability has been separated from the vibronic contribution in Eq. (2.36) due to large detuning of the optical fields from rotational transitions. The electronic and vibrational contributions to the polarizability components $\alpha_{0,0}$ and $\alpha_{1,-1} + \alpha_{-1,1}$ in the molecule-fixed frame are thus given by the summations [151–153]

$$\alpha_{0,0}^{n_i v_i} = \sum_n \sum_{\Lambda} \sum_{v(J)} \frac{2(E_{n\Lambda v} - E_{n_i \Lambda_i v_i})}{(E_{n\Lambda v} - E_{n_i \Lambda_i v_i})^2 - (\hbar\omega)^2} |\langle n\Lambda v | \hat{\mathbf{d}}_0 | n_i \Lambda_i v_i \rangle|^2, \quad (2.42)$$

	Cs ₂	Rb ₂	LiCs	LiRb	RbCs	KRb
α_{\parallel}	1012.2	789.7	597.0	524.3	904.0	748.7
α_{\perp}	509.0	405.5	262.5	246.5	492.3	382.9

Table 2.2: Static polarizabilities of heteronuclear alkali-metal dimers in $X^1\Sigma$ electronic states evaluated at the equilibrium intermolecular distance R_e . Values are in atomic units. Data taken from Ref. [154]

and

$$\begin{aligned}
\alpha_{1,-1}^{n_i v_i} + \alpha_{-1,1}^{n_i v_i} = & - \sum_n \sum_{\Lambda} \sum_{v(J)} \frac{2(E_{n\Lambda v} - E_{n_i \Lambda_i v_i})}{(E_{n\Lambda v} - E_{n_i \Lambda_i v_i})^2 - (\hbar\omega)^2} |\langle n\Lambda v | \hat{\mathbf{d}}_{-1} | n_i \Lambda_i v_i \rangle|^2 \\
& - \sum_n \sum_{\Lambda} \sum_{v(J)} \frac{2(E_{n\Lambda v} - E_{n_i \Lambda_i v_i})}{(E_{n\Lambda v} - E_{n_i \Lambda_i v_i})^2 - (\hbar\omega)^2} |\langle n\Lambda v | \hat{\mathbf{d}}_1 | n_i \Lambda_i v_i \rangle|^2.
\end{aligned} \tag{2.43}$$

For closed-shell molecules, which are the main focus of this work, $\Lambda_i = 0$ (Σ states). Therefore, Eqs. (2.42) and (2.43) show that the α_{\parallel} is associated with $n_i\Sigma \rightarrow n'\Sigma$ electronic transitions, and α_{\perp} with $n_i\Sigma \rightarrow n'\Pi$ electronic transitions. Since alkali metal dimers have $^1\Sigma$ electronic ground states, it is essential to have a good knowledge of the excited electronic states (Σ and Π) in order to estimate the molecular polarizability of a given rovibronic state. The static and dynamic polarizabilities of most alkali metal dimers are available in the literature [152–154]. Table 2.2 shows the predicted values for the static polarizabilities $\alpha_{\parallel}(\omega = 0)$ and $\alpha_{\perp}(\omega = 0)$ for a few alkali-metal dimers. The wavelengths of the trapping lasers used in recent molecular trapping experiments with alkali-metal dimers are close to $\lambda_L \approx 1100$ nm, which is far-detuned from the lowest energy electronic transition $X^1\Sigma \rightarrow a^3\Sigma$. The dynamic polarizabilities at these wavelengths is only a few times larger than the static values [152, 155].

2.6 Electric dipole-dipole interaction

2.6.1 Closed-shell molecules without nuclear spin

Let us neglect the hyperfine structure of rotational levels arising from interaction involving the nuclear spins. The rotational structure of $^1\Sigma$ molecules in their vibrational ground state can thus be described using the rigid rotor Hamiltonian

$$H_R = B_e \mathbf{N}^2, \quad (2.44)$$

with eigenstates given by spherical harmonics $|NM_N\rangle \equiv Y_{N,M_N}(\theta, \phi)$, and eigenvalues $E(N) = B_e N(N+1)$. The angular coordinates defined in a space-fixed frame.

We consider a pair of interacting diatomic molecules, denoted by A and B . Let \mathbf{R}_{AB} be the vector that joins the centers of mass of the molecules. In the gas phase, the vector \mathbf{R}_{AB} rotates freely in space, which is described the orbital angular momentum l , and the projection m_l along the space-fixed Z axis. In order to describe a molecular scattering process, the translational wavefunction of the collision complex is expanded in the basis $|l, m\rangle$, where $l = 0, 1, \dots, \infty$. These basis states are known as partial waves. The basis set for the combined states of two $^1\Sigma$ molecules in gas phase is thus given by the products $|N_A M_{N_A}\rangle |N_B M_{N_B}\rangle |lm_l\rangle$. However, when the translational motion of the molecules is constrained by external forces, for example as in an ordered array of microtraps, there is no relative rotation of molecules. In this case the vector \mathbf{R}_{AB} can be considered fixed in space. In this case, the basis set for the combined space of two molecules is given by $|N_A M_{N_A}\rangle |N_B M_{N_B}\rangle$. This basis describes molecules in the absence of external fields.

The electrostatic interaction energy between two neutral polar molecules can be described using classical electrodynamics by a multipole expansion of the form [156]

$$V_{AB}(R) = \frac{C_3}{R_{AB}^3} + \frac{C_5}{R_{AB}^5} + \dots \quad (2.45)$$

where C_n is a quantity that describes the interaction between the multipole moments of the molecular charge distributions. In a quantum mechanical description, these coefficients become operators acting on the internal states of the molecules.

The lowest order in this expansion corresponds to the dipole-dipole interaction. If we denote the dipole moments of molecules A and B as \mathbf{d}_A and \mathbf{d}_B , the interaction potential \hat{V}_{AB} can be written as

$$\hat{V}_{dd}(\mathbf{R}) = \left(\frac{1}{4\pi\epsilon_0} \right) \frac{1}{R_{AB}^3} \{ \mathbf{d}_A \cdot \mathbf{d}_B - 3(\mathbf{d}_A \cdot \hat{\mathbf{R}}_{AB})(\mathbf{d}_B \cdot \hat{\mathbf{R}}_{AB}) \}, \quad (2.46)$$

where $R_{AB} = |\mathbf{R}_{AB}|$ and $\hat{\mathbf{R}} = \mathbf{R}/R_{AB}$. It is convenient to rewrite the scalar products in Eq. (2.46) in terms of irreducible spherical tensors $\hat{T}_p^{(k)}$ and use angular momentum algebra to evaluate the matrix elements of \hat{V}_{dd} in the basis of eigenstates of the operators \mathbf{N}^2 and \hat{N}_Z . We derive this transformation in detail in Appendix B using standard angular momentum algebra [142, 143]. The resulting expression for the interaction is

$$\hat{V}_{dd}(\mathbf{R}_{AB}) = -\sqrt{\frac{6\pi}{5}} \left(\frac{2}{R_{AB}^3} \right) \sum_{p=-2}^2 (-1)^{-p} Y_{2,-p}(\theta_{R_{AB}}, \phi_{R_{AB}}) \hat{T}_p^{(2)}(\mathbf{d}_A, \mathbf{d}_B) \quad (2.47)$$

The dipole-dipole operator is thus given by the sum of five terms associated with the space-fixed projection p of the rank-two tensor $T_p^{(2)}(\mathbf{d}_A, \mathbf{d}_B)$. Each term is multiplied by an orientational factor given by components of the spherical harmonic of rank-two $Y_{2,-p}(\theta_{R_{AB}}, \phi_{R_{AB}})$. The angular coordinates $(\theta_{R_{AB}}, \phi_{R_{AB}})$ describe the orientation of the vector \mathbf{R}_{AB} in a space-fixed coordinate system. The matrix elements of this operator in the uncoupled basis $|N_A M_{N_A}\rangle |N_B M_{N_B}\rangle$ are given by (see Appendix B)

$$\begin{aligned} \langle N_A M_{N_A} | \langle N_B M_{N_B} | \hat{V}_{dd}(R, \theta_R) | N'_A M'_{N_A} \rangle | N'_B M'_{N_B} \rangle &= - \left(\frac{d_A d_B}{R^3} \right) (-1)^{-M_{N_A} - M_{N_B}} \\ &\times [(2N_A + 1)(2N'_A + 1)(2N_B + 1)(2N'_B + 1)]^{1/2} \begin{pmatrix} N_A & 1 & N'_A \\ 0 & 0 & 0 \end{pmatrix} \begin{pmatrix} N_B & 1 & N'_B \\ 0 & 0 & 0 \end{pmatrix} \\ &\times \left\{ \frac{3\sqrt{5}}{2} e^{-i2\phi} \sin^2 \theta \times D_2 + \frac{3\sqrt{5}}{2} e^{i2\phi_R} \sin^2 \theta \times D_{-2} + \sqrt{\frac{15}{2}} (3 \cos^2 \theta - 1) \times D_0 \right. \\ &\left. - 3\sqrt{5} \sin \theta \cos \theta e^{-i\phi} \times D_1 + 3\sqrt{5} \sin \theta \cos \theta e^{i\phi} \times D_{-1} \right\}, \end{aligned} \quad (2.48)$$

where D_p are constants that carry information about the selection rules for the total angular momentum projection $M_{N_A} + M_{N_B}$, as explained in Appendix B. Therefore, the selection rules depend on the orientation of the intermolecular axis with respect to the space-fixed frame. For example, for $\theta = \pi/2$, only terms proportional to D_2 , D_{-2} and D_0 contribute to the interaction between two $^1\Sigma$ molecules. The corresponding selection rules are

$$\begin{aligned}\Delta N_A &= \pm 1 \text{ and } \Delta N_B = \pm 1 \\ \Delta(M_{N_A} + M_{N_B}) &= 0, \pm 2.\end{aligned}\tag{2.49}$$

In the absence of a DC electric field, and when two molecules are too far apart for the dipole-dipole interaction to be significant, there is no preferred coordinate system for the definition of the angles that specify the rotational states $|N, M_N\rangle \equiv Y_{N, M_N}(\theta, \phi)$. Normally, we can define a space-fixed coordinate system with the single molecule at the origin, so that the states $|N, M_N\rangle$ are eigenstates of \hat{N}_z with eigenvalue M_N . Since the $2N + 1$ degenerate states associated to a particular level have equal probability of being populated, one averages all the single molecule observables, such as the transition dipole moments, over the three equivalent spatial directions in order to make observable predictions. When the dipole-dipole interaction between two molecules is considered, the energy of the system is characterized by the projection of the dipole moments on the intermolecular axis, so that the energy of the two-particle state is a minimum when the dipole moments are aligned with respect to this axis. Therefore, we can choose a coordinate system in which the z axis corresponds to the intermolecular axis, and define the angular coordinates of the tensor operators and wavefunctions in this coordinate system. If the molecules are constrained to localized regions in space, as in a crystalline array, we can use this coordinate system to be the space-fixed frame. However, if the intermolecular axis is allowed to rotate in space, as in a molecular collision event, we need to refer the spherical tensors to the space-fixed frame using rotation matrices, and calculate observable quantities, such as the cross section, by integrating over all possible rotation angles weighed with the appropriate angular probability density associated with the quantized rotation of the intermolecular axis.

As an illustrative example, let us consider the states $|g\rangle = |N=0, M_N=0\rangle$ and $|e\rangle = |N=1, M_N=0\rangle$ and define the matrix element

$$J_{AB}^{(0,0)} \equiv \langle e_A | \langle g_B | \hat{V}_{dd}(\mathbf{R}_{AB}) | g_A \rangle | e_B \rangle,$$

where the upper index is defined as $(M_{N_A} + M_{N_B}, M'_{N_A} + M'_{N_B})$. Following the above argument, we chose a space-fixed coordinate system in which \vec{R}_{AB} points along the Z axis. From these definitions follows that $\theta = 0$ in Eq. (2.47). The angle ϕ is irrelevant (set to zero for convenience). The only non-vanishing contribution to the interaction is thus the term $\sqrt{\frac{15}{2}}(3\cos^2\theta - 1) \times D_0$. After evaluating the numerical constant D_0 as explained in Appendix B we find that

$$J_{AB}^{(0,0)} = -6\sqrt{\frac{15}{2}} \frac{d_A d_B}{R_{AB}^3} \begin{pmatrix} 1 & 1 & 2 \\ 0 & 0 & 0 \end{pmatrix} \begin{pmatrix} 1 & 1 & 0 \\ 0 & 0 & 0 \end{pmatrix}^4 = -\frac{2}{3} \frac{d_A d_B}{R_{AB}^3}. \quad (2.50)$$

2.6.2 Closed-shell molecules with hyperfine structure

For the $^1\Sigma$ polar molecules considered in this thesis, the atomic nuclei have a relatively large spin angular momentum $I \geq 3/2$ (see Table 2.1). The hyperfine splittings vary from a few kHz for $N=0$ up to hundreds of kHz for $N=1$ rotational levels. These energy scales are comparable with the dipole-dipole interaction energy $U_{dd} = d^2/R_{12}^3$ for molecules separated by a few hundred nanometers, as well as the light-shift induced by the trapping laser fields. Moreover, techniques have been developed to prepare polar molecules in a specific hyperfine state of the ground rotational manifold $N=0$ [157]. It therefore is important to understand the dependence of the electric dipole-dipole interaction on the nuclear degrees of freedom of the molecules.

Weak magnetic fields

In the presence of a magnetic field small enough that hyperfine states with different total projection are only weakly admixed, the coupling scheme defined by $\mathbf{F} = \mathbf{N} + \mathbf{I}$ and $\mathbf{I} = \mathbf{I}_1 + \mathbf{I}_2$ is preferred to describe the coupling of angular momenta in a molecule [142]. The corresponding basis functions are the fully-coupled states

$|(NI)FM_F\rangle$. For simplicity, let us restrict the dipole-dipole tensor operator in Eq. (2.47) to the component $p = 0$

$$\hat{V}_{dd} = -\frac{\sqrt{6}}{2R_{AB}^3} (3\cos^2\theta - 1) T_0^2(\mathbf{d}_A, \mathbf{d}_B). \quad (2.51)$$

In Appendix C it is shown that the matrix elements of Eq. (2.51) in the two-molecule basis $|(N_A I_A)F_A M_{F_A}\rangle |(N_B I_B)F_B M_{F_B}\rangle$ are given by the expression

$$\begin{aligned} & \langle (N_A I_A)F_A M_{F_A} | \langle (N_B I_B)F_B M_{F_B} | \hat{V}_{dd} | (N'_A I'_A)F'_A M'_{F_A} \rangle | (N'_B I'_B)F'_B M'_{F_B} \rangle = \delta_{I_A, I'_A} \delta_{I_B, I'_B} \\ & \times -\left(\frac{d_A d_B}{R_{AB}^3}\right) \sqrt{\frac{15}{2}} (3\cos^2\theta - 1) (-1)^{-M_A - M_B} [(2N_A + 1)(2N_B + 1)]^{1/2} \\ & \times [(2N'_A + 1)(2N'_B + 1)]^{1/2} \begin{pmatrix} N_A & 1 & N'_A \\ 0 & 0 & 0 \end{pmatrix} \begin{pmatrix} N_B & 1 & N'_B \\ 0 & 0 & 0 \end{pmatrix} \\ & \times (-1)^{F'_A + F'_B + F_A + F_B + N_A + N_B} [(2F_A + 1)(2F_B + 1)(2F'_A + 1)(2F'_B + 1)]^{1/2} \\ & \times \begin{Bmatrix} N'_A & F'_A & I_A \\ F_A & N_A & 1 \end{Bmatrix} \begin{Bmatrix} N'_B & F'_B & I_B \\ F_B & N_B & 1 \end{Bmatrix} \times D_0^F. \end{aligned} \quad (2.52)$$

The first two lines in Eq. (2.52) are identical to the expression for the dipole-dipole matrix element in Eq. (2.48) without including nuclear spin. The remaining result from the coupling of rotational and nuclear angular momenta. The numerical constant D_0^F is identical to the expression for D_0 in Eq. (2.48) but with the rotational quantum numbers (N, M_N) replaced by the total angular momentum quantum numbers (F, M_F) (see Appendix B). Using the methods in Appendix C, it is straightforward to evaluate matrix elements of other tensor components of the dipole-dipole operator $p \neq 0$.

From expression for the matrix elements in Eq. (2.52) the selection rules for the $p = 0$ component of the dipole-dipole interaction operator are

$$\begin{aligned} \Delta F_A &= 0, \pm 1 \quad \text{and} \quad \Delta F_B = 0, \pm 1 \\ \Delta N_A &= \pm 1 \quad \text{and} \quad \Delta N_B = \pm 1 \\ \Delta I_A &= 0 \quad \text{and} \quad \Delta I_B = 0 \end{aligned} \quad (2.53)$$

$$\Delta(M_{F_A} + M_{F_B}) = 0. \quad (2.54)$$

The $\Delta F = 0$ selection rule applies to states with $F > 0$. The dipole-dipole interaction does not couple the hyperfine states of molecules within the same rotational manifold, but can mix the hyperfine states in different rotational levels. The selection rule for the angular momentum projections in Eq. (2.54) is valid for the $p = 0$ component of the dipole-dipole operator. When other components of the dipole-dipole tensor are included a more general selection rule applies which depends on the orientation of the intermolecular vector $\hat{\mathbf{R}}_{AB}$ with respect to the space-fixed Z axis.

Let us consider the states $|g\rangle = |(N = 0, I = 1)F = 1, M_F = 0\rangle$ and $|e\rangle = |(N = 1, I = 1)F = 0, M_F = 0\rangle$. The exchange matrix element $J_{AB} = \langle e_A | \langle g_B | \hat{V}_{dd} | g_A \rangle | e_B \rangle$ can be evaluated for $\theta = 0$ in Eq. (2.52) as

$$J_{AB}^{(0,0)} = -2 \frac{d_A d_B}{R_{AB}^3} \times \left\{ \begin{array}{ccc} 0 & 1 & 1 \\ 0 & 1 & 1 \end{array} \right\}^2 = -\frac{2}{9} \frac{d_A d_B}{R_{AB}^3}, \quad (2.55)$$

which is three times smaller than the analogous result for molecules without nuclear spin in Eq. (2.50).

Intermediate magnetic fields

The rotational motion is decoupled from the nuclear degrees of freedom for magnetic fields strong enough to mix hyperfine states with different values of F . The preferred coupling scheme in this case is defined by $\mathbf{I} = \mathbf{I}_1 + \mathbf{I}_2$ and the associated spin-coupled basis states are $|NM_N\rangle |IM_I\rangle$. The electric dipole-dipole interaction operator \hat{V}_{dd} in Eq. (2.51) only couples to the rotational degrees of freedom of the molecule. The matrix elements of the $p = 0$ component of the interaction operator in the spin-coupled basis are therefore given by

$$\begin{aligned} & \langle N_A M_{N_A} | \langle I_A M_{I_A} | \langle N_B M_{N_B} | \langle I_B M_{I_B} | \hat{V}_{dd} | N'_A M'_{N_A} \rangle | I'_A M'_{I_A} \rangle | N'_B M'_{N_B} \rangle | I'_B M'_{I_B} \rangle \\ &= \delta_{I_A, I'_A} \delta_{I_B, I'_B} \delta_{M_{I_A}, M'_{I_A}} \delta_{M_{I_B}, M'_{I_B}} \langle N_A M_{N_A} | \langle N_B M_{N_B} | \hat{V}_{dd} | N'_A M'_{N_A} \rangle | N'_B M'_{N_B} \rangle, \end{aligned}$$

where the matrix element over rotational states is given by Eq. (2.48). Contrary to the case of weak or zero magnetic fields, the nuclear spins do not influence

the strength of the dipole-dipole interaction between polar molecules for relatively large magnetic fields.

The crossover from the weak field to the intermediate field regime can be loosely defined by the position of the avoided crossings in the hyperfine Zeeman spectra in Fig. 2.3. In the absence of external fields, a molecular state has a well-defined value of the total angular momentum F . In this limit the fully coupled basis diagonalizes the molecular Hamiltonian. As the magnetic field increases, coupling between hyperfine states with different values of F makes the fully-coupled basis less meaningful, particularly near an avoided crossing [145, 146]. For $^{41}\text{K}^{87}\text{Rb}$ molecules, these avoided crossings occur at magnetic fields of a few Gauss for the $N = 0$ and $N = 1$ rotational levels.

2.6.3 Open-shell molecules without nuclear spin

Let us consider polar molecules with $^2\Sigma$ ground electronic states. The unpaired electron spins of two $^2\Sigma$ molecules separated by a distance R_{AB} interact weakly through a magnetic dipole-dipole interaction that scales as $\sim \alpha^2/R_{AB}^3$, where $\alpha \approx 1/137$ is the fine structure constant. The magnitude of the electric dipole-dipole interaction between polar molecules is much larger than the magnetic spin dipole-dipole interaction. Therefore, the interaction between two open-shell polar molecules is dominated by the electric dipole-dipole interaction between states with the same spin projection. For instance, consider a rovibrational state of a $^2\Sigma$ molecule described in the uncoupled basis

$$|nNM_N\rangle|S, M_S\rangle,$$

where n describes the electronic and vibrational motion, N is the magnitude of the total angular momentum excluding the electron spin, S is the magnitude of the electron spin angular momentum, and (M_N, M_S) are the projections of the corresponding angular momenta on a space-fixed quantization axis. In this basis, the matrix elements of the dipole dipole operator in Eq. (2.47) are simply given by

$$\begin{aligned} & \langle N_A M_{N_A} S_A M_{S_A} | \langle N_B M_{N_B} S_B M_{S_B} | \hat{V}_{dd} | N'_A M'_{N_A} S'_A M'_{S_A} \rangle | N'_B M'_{N_B} S'_B M'_{S_B} \rangle \\ &= \delta_{M_{S_A}, M'_{S_A}} \delta_{M_{S_B}, M'_{S_B}} \langle N_A M_{N_A} | \langle N_B M_{N_B} | \hat{V}_{dd} | N'_A M'_{N_A} \rangle | N'_B M'_{N_B} \rangle. \end{aligned} \quad (2.56)$$

The matrix element in the rotational basis is given by Eq. (2.48). In other words, if the electronic spin is decoupled from the rotational motion of the molecule, the dipole-dipole interaction is identical to the case of closed-shell molecules, provided the electronic spin projections are conserved for the interacting molecules. In Chapter 3 we describe a scheme that can be used to induce spin-changing electric dipole-dipole interaction between $^2\Sigma$ molecules in superimposed static electric and magnetic fields.

2.7 Optical trapping of diatomic molecules

The interaction of a ground state molecule with an optical field can be considered to be conservative if the detuning of the light field from any transition between molecular states is much larger than the linewidth Γ of the states [79]. In other words, the population of the excited states is small and the effects of spontaneous emission in the dynamics of a ground state molecule interacting with a laser can be neglected. In current experiments with cold molecules, laser beams whose frequencies are far from any vibronic resonance are used to trap slow molecules using a light-induced force derived from a spatially dependent AC Stark shift. The degree of confinement for the molecular motion depends on the intensity profile of the optical trapping lasers. Dipole traps [35] create a three-dimensional confinement for a molecular or atomic ensemble and have been used to study collisions at cold and ultracold temperatures [158]. Superimposing several retro-reflecting laser beams results in a periodic trapping potential in one, two, or three dimensions known as optical lattices [36, 79]. Ultracold atomic and molecular gases in optical lattices have been studied in the context of quantum simulation of condensed matter phenomena [80, 82, 90, 96], quantum information processing [103, 117, 126], precision measurements [159], and ultracold collisions in confined geometries [37, 39]. Most experimental groups work with alkali-metal atoms in optical lattices. After the preparation of the first ultracold molecules in the rovibrational ground state [15, 18–21], it has become technologically possible to trap homonuclear and heteronuclear molecules in optical lattices [20, 137].

The starting point for the description of the light-induced potentials is Eq. (2.32)

$$\hat{H}_{AC} = - \sum_p \sum_{p'} \hat{\alpha}_{p,p'} E_p(\mathbf{r}) E_{p'}^*(\mathbf{r}), \quad (2.57)$$

where $\epsilon_p(\mathbf{r})$ is the p component of the positive frequency electric field vector in the spherical basis and $\hat{\alpha}_{p,p'}$ is an element of the polarizability tensor evaluated in the space-fixed frame. The space-fixed molecular polarizability can be written in terms of the molecule-fixed polarizability elements, as it was done in Eq. (2.36).

2.7.1 Dipole traps

A dipole trap for molecules can be created with a single Gaussian laser beam with wavelength λ_L far-detuned from an vibronic resonance [35]. The intensity distribution of a Gaussian laser propagating along the x axis is given by

$$I(r, x) = I_0 \left(\frac{w_0}{w(x)} \right)^2 e^{-2r^2/w^2(x)}, \quad (2.58)$$

where $w(x) = w_0 \sqrt{1 + (x/x_R)^2}$ is radius at which the intensity decreases by $1/e^2$ from its value I_0 at the center of the beam. The distance x is measured from the position of the minimum radius w_0 , known as the beam waist. The peak intensity is given by $I_0 = 2P/\pi w_0^2$, where P is the total power of the laser. The Rayleigh length $x_R = \pi w_0^2/\lambda_L$ and the beam waist w_0 provide an estimate of the longitudinal and transverse dimensions of the trapped molecular cloud, respectively. The dimensions of the dipole trap can be on the order of a few millimeters [35]. If the laser beam is linearly polarized along the z axis, then the optical dipole potential for a diatomic molecule is given by the diagonal elements of the Hamiltonian

$$\hat{H}_{AC} = -|E(x, r)|^2 \left\{ \frac{1}{3}(\alpha_{\parallel} + 2\alpha_{\perp}) + \frac{2}{3}(\alpha_{\parallel} - \alpha_{\perp})C_{2,0}(\theta) \right\} \quad (2.59)$$

where $E(x, r)$ is the electric field amplitude of the laser beam, α_{\parallel} is the molecular polarizability along the internuclear axis, α_{\perp} is the polarizability perpendicular to the internuclear axis, and $C_{L,M}$ a modified spherical harmonic. For $^1\Sigma$ molecules in the ground vibronic state $|X^1\Sigma, v=0\rangle$, Eq. (2.59) couples different rotational

states $|NM_N\rangle$, with matrix elements

$$\begin{aligned}
\langle NM_N|H_{AC}|N'M'_N\rangle &= \\
&= -|E(x, r)|^2 \left\{ \alpha_{sc} \delta_{N,N'} \delta_{M_N, M'_N} + \alpha_{ten} (-1)^{-M_N} [(2N' + 1)(2N + 1)]^{1/2} \right. \\
&\quad \times \begin{pmatrix} N & 2 & N' \\ 0 & 0 & 0 \end{pmatrix} \begin{pmatrix} N & 2 & N' \\ -M_N & 0 & M'_N \end{pmatrix} \left. \right\}, \tag{2.60}
\end{aligned}$$

where we have defined the scalar and tensor polarizabilities as $\alpha_{sc} = \frac{1}{3}(\alpha_{\parallel} + 2\alpha_{\perp})$ and $\alpha_{ten} = \frac{2}{3}(\alpha_{\parallel} - \alpha_{\perp})$ [154, 160]. The selection rules for rotational couplings from Eq. (2.60) are $\Delta M_N = 0$, $\Delta N = 2, 4, \dots$, and $\Delta N = 0$ for $N \neq 0$. The second 3- j symbol contains the dependence on the angular momentum projection M_N , which leads to the so-called tensor shifts. The optical dipole potentials are thus obtained from the diagonalization of \hat{H}_{AC} in a truncated basis of rotational states in the ground vibronic state.

In general the trapping laser will induce coherences between rotational states of the same parity, which induces alignment of the molecule along the laser field polarization. If the off-diagonal elements in Eq. 2.60 are smaller than the energy difference between the coupled rotational states $\Delta = E(N + 2k) - E(N)$, then the rotational Raman coupling can be neglected. This is the case for alkali metal dimers such as LiCs and LiRb in dipole traps and optical lattice traps with laser intensities on the order a few mW/cm².

2.7.2 One-dimensional optical lattice

Two identical counter-propagating laser beams create an interference pattern with a sinusoidal intensity profile, with period $a_L = \lambda_L/2$. Along the axis $r = 0$ of a single Gaussian beam given by Eq. (2.58), the electric field can be approximated by a plane wave $\mathbf{E}(x, t) = E_0 \cos(k_L x - \omega_L t) \hat{\mathbf{e}}$, with amplitude E_0 at the beam waist w_0 , and polarization vector $\hat{\mathbf{e}}$. The total field \mathbf{E}_T at the center of the beam waist is the sum of the counter-propagating waves, i.e.,

$$\begin{aligned}
\mathbf{E}_T &= E_0 [\cos(k_L x - \omega_L t) + \cos(-k_L x - \omega_L t)] \hat{\mathbf{e}} \\
&= 2E_0 \cos(k_L x) \cos(\omega_L t) \hat{\mathbf{e}}. \tag{2.61}
\end{aligned}$$

The time-averaged intensity is $I(x) \propto \langle E_T^2(x, t) \rangle = 2|E_0|^2 \cos^2(k_L x)$. Due to the angular momentum dependence of the AC Stark shift, the periodic potential is slightly different for different rotational states $|N, M_N\rangle$. From Eq. (2.59) the light-induced potentials for the first two rotational states $J = 0$ and $J = 1$ with $M = 0$ are

$$|N = 0, M_N = 0\rangle \rightarrow V(x) = -|E_0|^2 \alpha_{\text{sc}} \cos^2(k_L x), \quad (2.62)$$

$$|N = 1, M_N = 0\rangle \rightarrow V(x) = -|E_0|^2 \left(\alpha_{\text{sc}} + \frac{2}{5} \alpha_{\text{ten}} \right) \cos^2(k_L x). \quad (2.63)$$

Therefore, the optical potentials experienced by the rotational states $|0, 0\rangle$ and $|1, 0\rangle$ have intensity minima at the same position, but the trap depth for the ground state is smaller. Equations (2.62) and (2.63) are examples of optical lattice potentials. Molecules in a given rotational state are strongly confined near the minima of the periodic potential. The lattice period is $a_L = \lambda_L/2$. The equations above describe the potential along the axial direction of two counter-propagating Gaussian beams. In this direction the confinement is twice as large compared with a single beam due to constructive interference. Along the radial direction the confinement is weaker, which has been used to study collisional dynamics in quasi-2D geometries [37, 39].

The trapping frequency along the axial direction of the optical lattice can be obtained by expanding the lattice potential near one of the minima. We can shift the potential $V(x)$ by one lattice period using $V_0 \cos^2(k_L x) = V_0 - V_0 \sin^2(k_L x)$, and expand for $k_L x \ll 1$ to get $V(x) \approx V_0 k_L^2 x^2 \equiv (1/2)m\omega_0^2 x^2$, where m is the molecular mass. The harmonic oscillator frequency ω_0 , or trapping frequency, is then

$$\omega_0 = \frac{2}{\hbar} \sqrt{V_0 E_R} \quad (2.64)$$

where $E_R = \hbar^2 k_L^2 / 2m$ is the recoil energy, which is usually used as the energy scale in experiments [79]. The energy $\hbar\omega_0$ gives the energy splitting between the lowest motional states of the optical lattice potential. For sufficiently deep lattices, the anharmonicity of the spectrum can be neglected [37, 79].

2.7.3 Higher-dimensional optical lattices

More complex lattice geometries can be produced by superimposing several laser beams. For a lattice with dimensionality d , the number of beams required is at least $d + 1$, in order to stabilize the relative phases between the laser beams [36]. Two-dimensional lattices have been created using three [78] and four laser beams [77], and three-dimensional lattices using four or six laser beams [36]. One possible realization of a two-dimensional lattice consists of two pairs of counterpropagating beams with equal amplitudes and zero relative phase form the standing waves $\mathbf{E}_1(\mathbf{r}, t) = 2E_0 \cos(\mathbf{k}_1 \cdot \mathbf{r}) \cos(\omega_1 t) \hat{\mathbf{e}}_1$ and $\mathbf{E}_2(\mathbf{r}, t) = 2E_0 \cos(\mathbf{k}_2 \cdot \mathbf{r}) \cos(\omega_2 t) \hat{\mathbf{e}}_2$. The standing waves propagate along the directions \mathbf{k}_1 and \mathbf{k}_2 . The polarization vectors are $\hat{\mathbf{e}}_1$ and $\hat{\mathbf{e}}_2$. The total electric field in the region of space where the standing waves are superposed is $\mathbf{E}_T = \mathbf{E}_1 + \mathbf{E}_2$. According to Eq. (2.32) the interaction of a polarizable particle with the electric field $\mathbf{E}_T(\mathbf{r}, t)$ can be represented by the light-induced potential $U(\mathbf{r}, t)$ given by

$$U(\mathbf{r}, t) = 4|E_0|\bar{\alpha} \left\{ \cos^2(\mathbf{k}_1 \cdot \mathbf{r}) \cos^2(\omega_1 t) + \cos^2(\mathbf{k}_2 \cdot \mathbf{r}) \cos^2(\omega_2 t) + \cos(\mathbf{k}_1 \cdot \mathbf{r}) \cos(\mathbf{k}_2 \cdot \mathbf{r}) \cos(\omega_1 t) \cos(\omega_2 t) \hat{\mathbf{e}}_1 \cdot \hat{\mathbf{e}}_2 \right\}, \quad (2.65)$$

where $\bar{\alpha}$ is a scalar parameter that describes the polarizability of the particle. Equation (2.65) shows that for a particle with scalar polarizability the time-average light-induced potential $U(\mathbf{r}) = \langle U(\mathbf{r}, t) \rangle_t$ is separable in the directions \mathbf{k}_1 and \mathbf{k}_2 if the polarizations of the corresponding standing waves are orthogonal. For simplicity the frequencies ω_1 and ω_2 can be chosen to be identical, but if the polarization of the standing waves are not perfectly orthogonal, then a frequency mismatch makes the time-average of the cross term in Eq. (2.65) vanish. In many cases, the polarizability of atoms in low angular momentum states can be considered as a scalar quantity. The same is valid for a molecule trapped in the rovibrational ground state $N = 0$ (see Eq. (2.62)).

It is possible to obtain expressions for an optical lattice potential for an arbitrary electromagnetic field $\mathbf{E}_T(\mathbf{r}, t)$. As explained in Section 3.5 and Appendix A, when the positive frequency component of the field at position \mathbf{r} can be expanded in spherical basis as $\mathbf{E}^{(+)}(\mathbf{r}) = \sum_p E_p(\mathbf{r}) \hat{\mathbf{e}}_p^*$, the light-matter interaction Hamiltonian \hat{H}_{AC} is given by Eq. (2.32). The optical lattice potential \hat{H}_{AC} can be written in

terms of molecular-frame polarizabilities using Eqs. 2.37 and 2.38. Let us consider a two-dimensional optical lattice created by superimposing two standing waves with equal amplitude E_0 and wavenumber $k_L = 2\pi/\omega_L$, propagating in orthogonal directions: one standing wave propagates along the x axis with linear polarization $\hat{\mathbf{y}}$ and the other propagates along the y axis with linear polarization $\hat{\mathbf{x}}$. If there is no phase difference between the field amplitude of the two waves, the positive frequency component of the total electric field can be written as

$$\begin{aligned}\mathbf{E}_L^{(+)} &= E_0 \{ \cos(k_L y) \hat{\mathbf{x}} + \cos(k_L x) \hat{\mathbf{y}} \} \\ &= -\frac{E_0}{\sqrt{2}} \{ [\cos(k_L y) + i \cos(k_L x)] \hat{\mathbf{e}}_1^* + [-\cos(k_L y) + i \cos(k_L x)] \hat{\mathbf{e}}_{-1}^* \},\end{aligned}$$

i.e., the optical lattice is composed of right-circular E_1 and left-circular E_{-1} polarizations. According to Eq. (2.32) the light-induced potential is given by

$$\hat{H}_{AC} = \hat{\alpha}_{-1,1} E_1 E_1^* + \hat{\alpha}_{1,-1} E_{-1} E_{-1}^* + \hat{\alpha}_{11} E_{-1} E_1^* + \hat{\alpha}_{-1-1} E_1 E_{-1}^*, \quad (2.66)$$

which expressed in terms of molecular-frame irreducible polarizabilities $\alpha(j)$ reads

$$\begin{aligned}\hat{H}_{AC} &= \left[2\alpha(0) \begin{pmatrix} 1 & 1 & 0 \\ 1 & -1 & 0 \end{pmatrix} \mathcal{D}_{0,0}^{(0)} + 2\alpha(2) \begin{pmatrix} 1 & 1 & 2 \\ 1 & -1 & 0 \end{pmatrix} \mathcal{D}_{0,0}^{(2)} \right] |E_1|^2 \\ &\quad + \alpha(2) \begin{pmatrix} 1 & 1 & 2 \\ 1 & 1 & -2 \end{pmatrix} \left[\mathcal{D}_{2,0}^{(2)} (E_1 E_{-1}^*) + \mathcal{D}_{-2,0}^{(2)} (E_{-1} E_1^*) \right]. \quad (2.67)\end{aligned}$$

The light-matter interaction Hamiltonian written in this form has a direct physical interpretation. The first line of Eq. (2.67) is proportional to the field amplitudes $E_1 E_1^* = E_{-1} E_{-1}^*$ which according to their definition in Appendix A correspond to virtual absorption and emission of photons with the same polarization, imparting no net angular momentum to the molecular states. Terms of this type are proportional to the Wigner functions $\mathcal{D}_{0,0}^{(j)}$. The second line in Eq. (2.67) contains the product of field amplitudes $E_1 E_{-1}^*$ (and its complex conjugate), which represents absorption of a right-circularly polarized photon and emission of a left-circularly polarized photon, imparting a net angular momentum $p - p' = 2$ to the molecu-

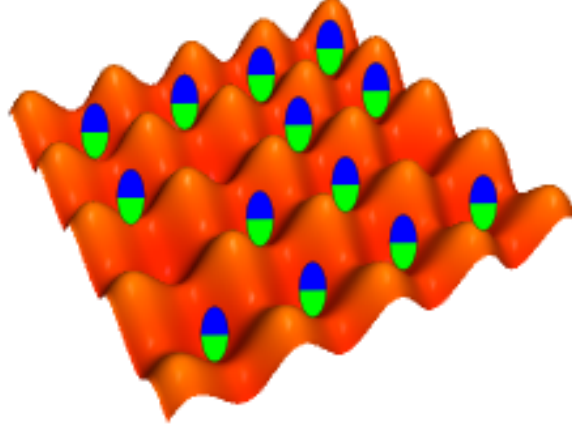


Figure 2.5: Illustration of a two-dimensional optical lattice potential for polar molecules.

lar states. This angular momentum transfer is represented by the Wigner function $\mathcal{D}_{2,0}^{(2)}$.

The two-dimensional optical lattice potential in Eq. (2.67) can be written in a form that makes explicit its dependence on the direction of propagation of the laser beams as

$$\begin{aligned}
 \hat{H}_{AC} = & |E_0|^2 \cos^2(k_L x) \left(\frac{\alpha(0)}{\sqrt{3}} \mathcal{D}_{0,0}^{(0)} + \frac{\alpha(2)}{\sqrt{5}} \left[\mathcal{D}_{-2,0}^{(2)} + \frac{2}{\sqrt{6}} \mathcal{D}_{0,0}^{(2)} + \mathcal{D}_{2,0}^{(2)} \right] \right) \\
 & + |E_0|^2 \cos^2(k_L y) \left(\frac{2\alpha(0)}{\sqrt{3}} \mathcal{D}_{0,0}^{(0)} - \frac{\alpha(2)}{\sqrt{5}} \left[\mathcal{D}_{-2,0}^{(2)} - \frac{2}{\sqrt{6}} \mathcal{D}_{0,0}^{(2)} + \mathcal{D}_{2,0}^{(2)} \right] \right) \\
 & + |E_0|^2 \cos(k_L x) \cos(k_L y) \frac{\alpha(2)}{\sqrt{5}} i \left(\mathcal{D}_{2,0}^{(2)} - \mathcal{D}_{-2,0}^{(2)} \right). \quad (2.68)
 \end{aligned}$$

Therefore, the light shift potential for a superposition of two standing waves propagating in orthogonal directions, with orthogonal polarizations in the XY plane, is given by a sum of the contributions of each independent beam plus a cross term that makes the potential non-separable for rotational states with $N \geq 1$. In Figure 2.5 a separable two-dimensional optical lattice potential is illustrated.

The periodic potential \hat{H}_{AC} in Eq. (2.68) contains terms proportional to $\hat{C}_{2,q}$. In the rotational angular momentum basis $|N, M\rangle$, the corresponding matrix elements

are given by

$$\begin{aligned} \langle NM_N | \hat{C}_{2,q} | N' M'_N \rangle &= \\ &= (-1)^{M_N} [(2N' + 1)(2N + 1)]^{\frac{1}{2}} \begin{pmatrix} N & 2 & N' \\ 0 & 0 & 0 \end{pmatrix} \begin{pmatrix} N & 2 & N' \\ -M_N & q & M'_N \end{pmatrix}. \end{aligned} \quad (2.69)$$

The term proportional to $C_{2,0}$ was analyzed earlier when discussing dipole traps. This term contributes to the state-dependent AC Stark shift of the rotational levels and also couples rotational states of the same parity and projection M_N . This is the only term that has non-zero matrix diagonal elements for the field-free state $|N = 0, M_N = 0\rangle$. The term proportional to $C_{2,\pm 2}$ has selection rules $\Delta N = \pm 2$, $\Delta N = 0$ for $N \neq 0$, and $\Delta M_N = \pm 2$. As we pointed out before, the optical lattice intensity is usually not strong enough to mix rotational states with different values of N . However, the operator $\hat{C}_{2,\pm 2}$ induces Raman couplings between states with different projections M_N within a given rotational angular momentum manifold for $N \geq 1$. In section 2.7.4 we analyze these Raman couplings in detail, since they have been previously neglected in the recent literature [41, 94, 161].

The effective optical lattice potential for any laser beam configuration can be obtained by diagonalizing the light-shift operator \hat{H}_{AC} in the basis of field-free rotational states $|N, M\rangle$. If an additional DC electric field is present, the light-shift operator must be diagonalized in the field-dressed basis $|(N), M\rangle$ in order to obtain the corresponding optical lattice potential for each field-dressed state, as discussed below.

2.7.4 Rotational Raman couplings in optical traps

Linearly polarized far-detuned optical fields

Let us rewrite the Hamiltonian in Eq. (2.59) for the interaction of a molecule with a 1D optical lattice with linear polarization along the space-fixed \hat{Z} axis. Neglecting the state-independent AC Stark shift and in units of the rotational constant B_e , the

molecular Hamiltonian is given by

$$\begin{aligned}\hat{H} &= \hat{H}_R + \hat{H}_{AC} \\ &= \hat{N}^2 - \frac{2}{3}\Omega_I \mathcal{D}_{0,0}^{(2)}(\boldsymbol{\theta}) \cos^2(k_L x),\end{aligned}\quad (2.70)$$

where

$$\Omega_I = \frac{|E_L|^2(\alpha_{\parallel} - \alpha_{\perp})}{B_e}$$

is a parameter that characterizes the strength of the light-matter interaction. The intensity of laser beam along the propagation axis is $I_L = |E_L|^2/2\epsilon_0 c$. Since we assume that $\Omega_I \ll 1$, we can neglect Raman couplings of the form $N \leftrightarrow N+2$. The tensor light shifts Δ_{N,M_N} of the rotational state $|NM_N\rangle$ are given by the diagonal matrix elements of $\mathcal{D}_{0,0}^{(2)}$. Table 2.3 presents the tensor shifts for the rotational states with $N \leq 2$, evaluated using Eq. (2.70). The shifts do not depend on the sign of M_N , as a consequence of the cylindrical symmetry of the Hamiltonian. In the absence of additional electric fields, the state $|1,0\rangle$ is the lowest rotational excited state.

(N, M_N)	(0,0)	(1,0)	(1,1)	(2,0)	(2,1)	(2,2)
$\Delta_{N,M_N}/\Omega_I$	0	-4/15	2/15	-4/21	-2/21	4/21

Table 2.3: Tensor light shift $\Delta_{N,M}$ for the rotational state $|N, M_N\rangle$ in units of $\Omega_I = |E_0|^2 \Delta\alpha/B_e$.

Collinear DC electric and linearly polarized optical trap

Let us consider a polar molecule in its vibrational ground state, under the influence of a DC electric field and a CW far-detuned optical field. If the laser polarization is collinear with the direction of the DC electric field, which is chosen as the space-fixed $\hat{\mathbf{Z}}$ axis, the dimensionless molecular Hamiltonian can thus be written as

$$\begin{aligned}\hat{H} &= \hat{H}_R + \hat{H}_{DC} + \hat{H}_{AC} \\ &= \hat{N}^2 - \lambda \mathcal{D}_{0,0}^{(1)} - \frac{2}{3}\Omega_I \mathcal{D}_{0,0}^{(2)} \cos^2(k_L x),\end{aligned}\quad (2.71)$$

where $\lambda = dE_Z/B_e$ parametrizes the strength of the DC electric field. E_Z is the magnitude of the DC electric field and d is the permanent dipole moment of the molecule. The rotational spectrum is dominated by the first two terms in Eq. (2.71) for $\Omega_I \ll 1$. The matrix elements of the spherical tensor $\mathcal{D}_{0,0}^{(1)}$ in the basis of field-free rotational states $|NM_N\rangle$ are given in Eq. (2.18).

The total shift of the rotational levels in the presence of superimposed AC and DC electric fields can be obtained by diagonalizing Eq. (2.71). Let us consider the situation in which the AC electric field from the optical trap is much weaker than the DC electric field, i.e., $\Omega_I \ll \lambda \sim 1$. This experimentally relevant case was originally analyzed in Ref. [153]. The contribution of the optical field to the total Stark shift can be obtained by subtracting the DC Stark shift from the eigenvalues of the total Hamiltonian in Eq. (2.71). In Fig. (2.6) we plot the tensor light shift $\Delta_{(N),M}$ for the state $|(N),M\rangle$, where the quantum number in parenthesis (N) is not strictly conserved in the presence of the DC field. Panel (a) shows that the tensor light shifts of different field-dressed states become equal at certain values of the field strength $\lambda = dE_Z/B_e$. For the states considered, these so-called “magic spots” occur at non-perturbative DC electric fields ($\lambda > 1$). In the limit $\lambda \rightarrow 0$, the light shifts approach their field-free values given in Table 2.3. In precision experiments, it might be useful to use a DC electric field to make the tensor light shifts of two rotational states identical since the states would experience the same trapping potential in an optical trap. However, most of the applications in this thesis consider the DC electric field as a free parameter. Therefore, we assume the most general case where molecules in different internal states experience slightly different trapping potentials.

Perpendicular DC electric and linearly polarized optical trap

Let us consider a configuration in which the polarization of the far-detuned optical field is linear, but orthogonal to the direction of an applied DC electric field. This is the most natural configuration in 2D and 3D optical lattices [36]. The quantization axis for the rotational angular momentum can be chosen to be the direction of the DC electric field, which is the space-fixed $\hat{\mathbf{Z}}$ axis for convenience. The polarization vector of the electromagnetic field can be chosen to lie along the $\hat{\mathbf{X}}$ axis. For a laser

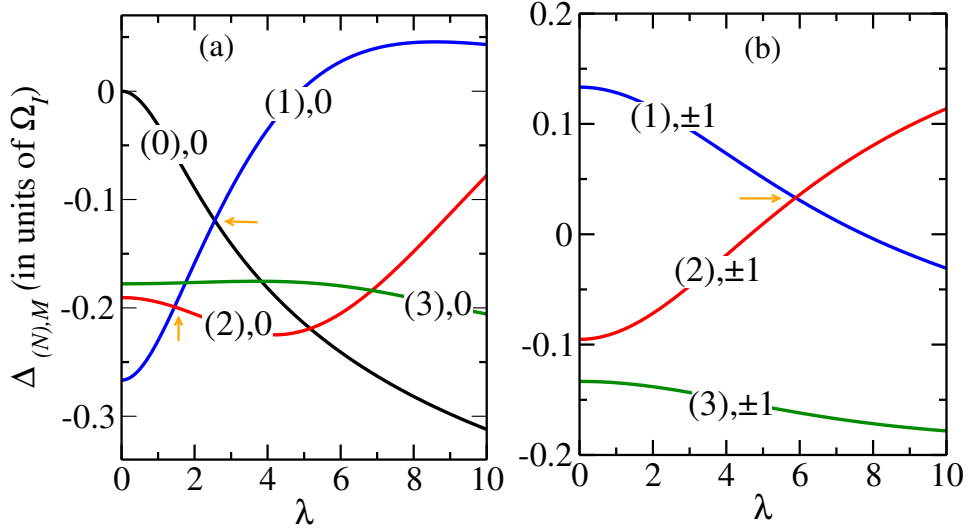


Figure 2.6: Tensor light shifts $\Delta_{(N),M}$ of rotational states $|(N),M\rangle$ as a function of the DC electric field parameter $\lambda = dE_Z/B_e$: (a) Lowest four states with $M = 0$; (b) Lowest six states with $|M| = 1$. Points where the shifts are equal for two different states are marked by arrows. The tensor shifts are given in units of $\Omega_I = |E_0|^2 \Delta\alpha/B_e$. The curves correspond to collinear AC and DC electric fields, with $\Omega_I \ll 1$.

beam propagating along the $\hat{\mathbf{Y}}$ axis, the positive frequency component $\mathbf{E}^{(+)}(\mathbf{r})$ of the AC electric field vector is given by

$$\mathbf{E}^{(+)}(\mathbf{r}) = E_0 \cos(k_L y) \hat{\mathbf{X}} = \frac{E_0}{\sqrt{2}} \cos(k_L y) (\hat{\mathbf{e}}_{-1} - \hat{\mathbf{e}}_1),$$

where E_0 is the field amplitude, and $\hat{\mathbf{e}}_{\pm 1}$ are components of the spherical basis with positive and negative helicity [143]. The effective Hamiltonian for the interaction of the molecule with the off-resonant electromagnetic wave is thus given by

$$\hat{H}_{AC} = -\frac{|E_0|^2}{2} [\hat{\alpha}_{1,1} + \hat{\alpha}_{-1,-1} - (\hat{\alpha}_{1,-1} + \hat{\alpha}_{-1,1})] \cos^2(k_L y), \quad (2.72)$$

where $\hat{\alpha}_{p,p'}$ is a component of the electric polarizability tensor in the space-fixed coordinate system. The total molecular Hamiltonian including the interaction with

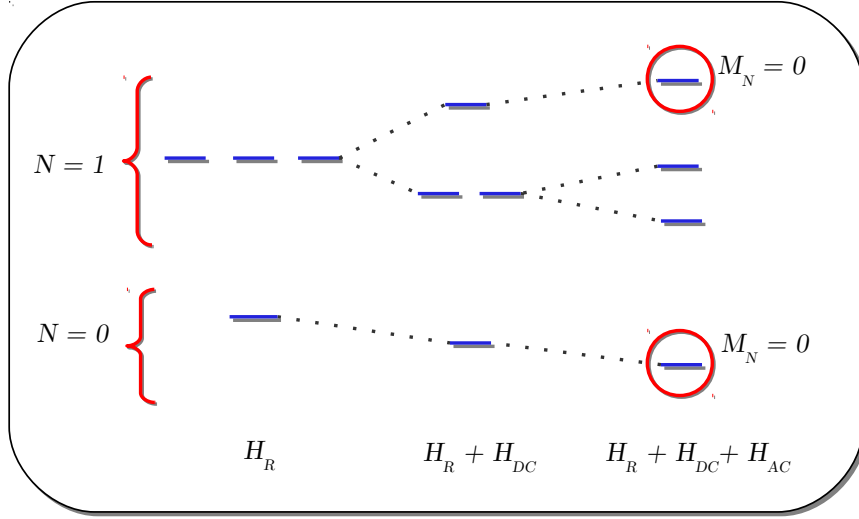


Figure 2.7: Energy level diagram showing the lowest four rotational states in the presence of a DC electric field along the Z axis and an weak off-resonant optical field with polarization not collinear with the DC field. In red-circles the states with $M_N = 0$ projection along the Z axis are shown.

the laser beam in (2.72) can be written as

$$\begin{aligned}\hat{H} &= \hat{H}_R + \hat{H}_{DC} + \hat{H}_{AC} \\ &= \hat{N}^2 - \lambda \hat{C}_{1,0} - \frac{1}{6} \Omega_I \left\{ \sqrt{6} \hat{C}_{2,-2} - 2 \hat{C}_{2,0} + \sqrt{6} \hat{C}_{2,2} \right\} \cos^2(k_L y). \quad (2.73)\end{aligned}$$

where we have neglected the state-independent AC Stark shift.

In the basis of field-free rotational states $|N, M_n\rangle$, the term \hat{H}_{AC} is not diagonal for any value of Ω_I . This is contrary to the case of collinear fields, where for $\Omega_I \ll 1$ the off-diagonal elements of \hat{H}_{AC} could be ignored. In general, the term proportional to $\hat{C}_{2,\pm 2}$ couples different M_N states within the same rotational level

for $N \geq 1$. As an example, let us write the Hamiltonian \hat{H} in the field-free rotational subspace $\mathcal{S} = \{|0, 0\rangle, |1, M\rangle\}$ in the block diagonal form

$$\hat{H} = \begin{pmatrix} 0 & -\lambda & 0 & 0 \\ -\lambda & 2(1 + \frac{1}{15}\Omega_I) & 0 & 0 \\ 0 & 0 & 2(1 - \frac{1}{30}\Omega_I) & \frac{1}{5}\Omega_I \\ 0 & 0 & \frac{1}{5}\Omega_I & 2(1 - \frac{1}{30}\Omega_I) \end{pmatrix}.$$

The rotational states $|1, 1\rangle$ and $|1, -1\rangle$ are degenerate for all values of the DC electric field. Therefore, for all finite values of Ω_I the Raman coupling

$$\langle 1, -1 | H | 1, 1 \rangle = \frac{1}{5}\Omega_I$$

mixes these angular momentum states. These couplings should be present in the limit $\Omega \ll 1$, which is relevant in optical trapping experiments. The first rotational excited state of the molecule for $\Omega_I > \lambda$ corresponds to the antisymmetric combination $|e\rangle = 1/\sqrt{2}\{|1, 1\rangle - |1, -1\rangle\}$. The energy level scheme for the lowest four rotational states of a generic polar molecule is illustrated in Fig. 2.7. For any value of N , the AC field orthogonal to the DC field splits the rotational sublevels $|(N), M\rangle$ and $|(N), -M\rangle$, which are otherwise degenerate for any value of λ . This splitting is proportional to Ω_I , and could be easily verified spectroscopically in an optical trap using circularly polarized microwave radiation.

For the applications discussed in this thesis, we consider rotational states with angular momentum projection $M_N = 0$. These states are isolated from other rotational states for a weak DC electric field with $\lambda > 0.1$, regardless of the polarization of the laser beams that make the optical trap. This is illustrated in Fig. (2.7) for the first two rotational levels $N = 0$ and $N = 1$.

Although we have derived the light-matter Hamiltonian in Eq. (2.73) for perpendicular DC and AC fields, the conclusions are also valid for any field configuration that is not collinear. Many 2D and 3D optical lattices are obtained by superimposing multiple laser beams with orthogonal polarizations. Standing waves with parallel polarizations are avoided in atom trapping experiments due to the presence of time-dependent interference terms in the lattice potential that cancel for orthogonal polarizations [79].

For some applications it might be necessary to eliminate the coupling between the sublevels $|(N), M\rangle$ and $|(N), -M\rangle$ for $M \neq 0$ that result from Raman couplings in a non-collinear configuration of multiple electric fields, as in a 3D optical lattice in the presence of a DC electric field. In this case, an additional preparation step is necessary before applying the optical lattice lasers: with molecules in a dipole trap with polarization collinear with an applied DC electric field, a strong near-resonant CW microwave field with circular polarization can be used to shift a specific rotational sublevel $|(N), M\rangle$ out of resonance with $|(N), -M\rangle$. In order to achieve this, the CW microwave field can be tuned near resonance with the transition $|(N), M\rangle \rightarrow |(N \pm 1), M \pm 1\rangle$, before ramping up the intensity of the optical lattice lasers. As long as the AC Stark shift induced by the microwave field is larger than the depth of the lattice potential, the rotational state of interest $|(N), M\rangle$ can be considered isolated from other rotational states. This approach was recently proposed in Ref. [94].

In later chapters we analyze coherent collective phenomena that occur in a Mott-insulator phase of polar molecules. We assume the molecules are trapped in a three-dimensional optical lattice with one molecule per lattice site, with no tunneling of molecules between sites. We impose this restriction in order to avoid collisional decoherence and losses. Although we consider a three-dimensional optical lattice, an ensemble of two-dimensional molecular arrays can be generated, for example, if the separation between molecules in two adjacent layers is larger than the separation between molecules within a layer. Similarly, ensembles of one-dimensional molecular arrays can be produced.

Chapter 3

Engineering molecular interactions with external fields

3.1 Chapter overview

In this chapter a detailed discussion is given on the influence of external fields on the dipole-dipole interaction between polar molecules. In Section 3.2 a procedure is outlined for the numerical evaluation of the dipole-dipole interaction in the presence of dressing fields. Section 3.3 then focuses on the dependence of the interaction energy between closed-shell $^1\Sigma$ polar molecules on the strength and orientation of an applied static electric field. In Section 3.3 an analogous study is done for open-shell $^2\Sigma$ polar molecules in combined static electric and magnetic fields, including a scheme for generating two-particle entangled molecular electron spins. In Section 3.5 the interaction between closed-shell polar molecules is described in the presence of a far off-resonant optical field.

The results in this chapter set the stage for the work presented later on the interaction between molecules in optical lattices. Therefore, the analysis is restricted to the case of fixed intermolecular distances. Collisional interactions are not considered here.

3.2 Dipole-dipole interaction in external fields

Let us consider two identical polar molecules denoted 1 and 2 separated by the distance R_{12} . We can write the Hamiltonian representing the molecules as

$$\mathcal{H} = \hat{H}_1 + \hat{H}_2 + \hat{V}_{12}. \quad (3.1)$$

where \hat{H} represents the energy of a single-molecule and \hat{V}_{12} is the dipole-dipole interaction operator. The dipole-dipole energy can be expressed in units of

$$U_{dd} = \left[\frac{1}{4\pi\epsilon_0} \right] \frac{d_1 d_2}{R_{12}^3}, \quad (3.2)$$

where d is the molecular permanent dipole moment. The factor in square brackets is needed to express this energy in S.I. units. Throughout this Thesis we use atomic units ($4\pi\epsilon_0 = 1$). The single-molecule Hamiltonian \hat{H}_i describes the rovibrational structure of the molecule as well as the interaction with a time-independent external field. The dipole-dipole energy U_{dd} is typically small compared to the energy scales that define \hat{H} . It is a common practice to evaluate the interaction matrix elements $\langle \phi_1 | \langle \psi_2 | \hat{V}_{12} | \phi'_1 \rangle | \psi'_2 \rangle$ in the basis of eigenstates of \hat{H}_1 and \hat{H}_2 in order to describe the interaction between molecules. The effective interaction potential depends on the applied external fields via the field-dressed single-particle states $\{|\phi\rangle\}$.

A straightforward numerical procedure can be used to evaluate the matrix elements of the dipole-dipole interaction in the basis of field-dressed states. After specifying the single-molecule Hamiltonian \hat{H} (for identical molecules $\hat{H}_1 = \hat{H}_2 = \hat{H}$), we chose a convenient basis \mathcal{U}_1 to construct the matrix of \hat{H} . This matrix is diagonalized using standard algebraic routines. The eigenvectors of \hat{H} can be written as linear combinations of the states from the basis \mathcal{U}_1 . The basis of single-molecule eigenvectors \mathcal{V}_1 can be used to build the two-molecule basis $\mathcal{V}_{12} = \mathcal{V}_1 \otimes \mathcal{V}_1$. The matrix elements of the interaction operator \hat{V}_{12} in the basis \mathcal{V}_{12} are then given by linear combinations of matrix elements of \hat{V}_{12} in the two-molecule basis $\mathcal{U}_{12} = \mathcal{U}_1 \otimes \mathcal{U}_1$. Therefore, if we know the matrix of \hat{V}_{12} in the basis \mathcal{U}_{12} and the eigenvectors of \hat{H} in the basis \mathcal{U}_1 , we can evaluate matrix elements of \hat{V}_{12} in the two-molecule basis \mathcal{V}_{12} . Since we are interested in molecular interactions in the presence of external fields, we write the single molecule Hamil-

tonian as $\hat{H} = \hat{H}_M + \hat{H}_F$, where \hat{H}_F contains the interaction of the molecule with the external field. In the simplest cases we chose \mathcal{U}_1 to be the basis of eigenstates of the field-free molecular Hamiltonian \hat{H}_M . The matrix elements of \hat{H}_M in the basis \mathcal{U}_1 have analytical form but the matrix elements of \hat{H}_F in the same basis can be obtained analytically only in the perturbative regime $\hat{H}_F \ll \hat{H}_M$.

3.3 Closed-shell molecules in electric fields

As the first illustration of this procedure we consider the interaction between two closed-shell polar molecules in $^1\Sigma$ electronic states. An external DC electric field interacts with the electric dipole moment of the molecule (see Section 2.4). The dimensionless single-molecule Hamiltonian is

$$\hat{H} = \hat{H}_R + \hat{H}_{DC} = \hat{N}^2 - \lambda \mathcal{D}_{0,0}^{(1)} \quad (3.3)$$

where $\lambda = dE_Z/B_e$. E_Z is the magnitude of the DC electric field and d is the permanent dipole moment. The field-free single molecule basis \mathcal{U}_1 consists of all the angular momentum states $|N, M_N\rangle$ up to a given value of N_{\max} . The two-molecule basis \mathcal{U}_2 is constructed from the product states $|N_1, M_{N_1}\rangle |N_2, M_{N_2}\rangle$, and the dipole-dipole matrix \hat{V}_{dd} is evaluated in this basis using the results in Appendix B. The eigenvectors of the Stark Hamiltonian in Eq. (3.3) can be easily obtained as in Section 2.4. Let us consider for example the field-dressed eigenstates states $|g\rangle = |(0), 0\rangle$ and $|e\rangle = |(1), 0\rangle$ which can be written for $\lambda < 1$ as

$$|g\rangle = a|0, 0\rangle + b|1, 0\rangle \quad \text{and} \quad |e\rangle = -b|0, 0\rangle + a|1, 0\rangle, \quad (3.4)$$

where $a \gg b \sim E_Z^2$ and $|a|^2 + |b|^2 \approx 1$, as can be easily derived using second-order perturbation theory [142]. In order to evaluate the dipole-dipole matrix element $\langle e_1 | \langle g_2 | \hat{V}_{dd} | g_1 \rangle | e_2 \rangle$, we use Eq. (3.4) and the results in Appendix B to obtain

$$\begin{aligned} \langle e_1 | \langle g_2 | \hat{V}_{dd} | g_1 \rangle | e_2 \rangle &= a^4 \langle 10 | \langle 00 | \hat{V}_{dd} | 00 \rangle | 10 \rangle + b^4 \langle 00 | \langle 10 | \hat{V}_{dd} | 10 \rangle | 00 \rangle \\ &\quad - a^2 b^2 \langle 10 | \langle 10 | \hat{V}_{dd} | 00 \rangle | 00 \rangle - a^2 b^2 \langle 00 | \langle 00 | \hat{V}_{dd} | 10 \rangle | 10 \rangle \\ &= (a^2 - b^2)^2 \langle 10 | \langle 00 | \hat{V}_{dd} | 00 \rangle | 10 \rangle \\ &\approx a^4 J_{12}^{(0,0)}, \end{aligned} \quad (3.5)$$

where $J_{12}^{(0,0)} = \langle 10 | \langle 00 | \hat{V}_{dd} | 00 \rangle | 10 \rangle = \langle 10 | \langle 10 | \hat{V}_{dd} | 00 \rangle | 00 \rangle$ is the field-free exchange interaction constant (See Section 2.6), which gives rise to the exchange of rotational excitations between molecules. Equation (3.5) shows that the interaction that exchanges rotational excitations between two molecules is smaller in the presence of a DC field compared with the field-free case. In this example we have only used the reduced subset $\{|g_1\rangle|e_2\rangle, |e_1\rangle|g_2\rangle\}$ from the two-molecule field-dressed basis $\mathcal{V}_2 = \mathcal{V}_1 \otimes \mathcal{V}_1$. The evaluation of field-dressed interaction matrix elements between other states is analogous.

The numerical value of the field-dressed matrix elements depend on the dimensionality of the field-free basis \mathcal{U}_1 . Convergence tests can be made to ensure that the value of the desired matrix element does not depend on the value of N_{\max} . In this Thesis we mainly deal with transitions within the rotational subspace $\mathcal{S}_1 = \{|N=0, M_N=0\rangle, |N=1, M_N=0, \pm 1\rangle\}$. Convergence of the dipole-dipole matrix elements to less than 1% of their value is achieved for $N_{\max} = 4$.

For $N_{\max} = 4$ the dimension of the single-molecule basis \mathcal{U}_1 is $\mathcal{D}_1 = \sum_{N=0}^{N_{\max}} (2N+1) = 25$. The two-molecule basis \mathcal{U}_2 has dimension $\mathcal{D}_2 = 625$, and the dipole-dipole matrix \hat{V}_{dd} has dimension $(\mathcal{D}_2)^2$. From the large number of dipole-dipole matrix elements, we chose those involving states within the subspace \mathcal{S}_1 . We focus our attention to the matrix elements of the form: $V_{12}^{eg} = \langle e_1 | \langle g_2 | \hat{V}_{dd} | e_1 \rangle | g_2 \rangle$, $V_{12}^{gg} = \langle g_1 | \langle g_2 | \hat{V}_{dd} | g_1 \rangle | g_2 \rangle$, $J_{12} = \langle e_1 | \langle g_2 | \hat{V}_{dd} | g_1 \rangle | e_2 \rangle = \langle e_1 | \langle e_2 | \hat{V}_{dd} | g_1 \rangle | g_2 \rangle$, and $V_{12}^{ee'} = \langle e_1 | \langle e'_2 | \hat{V}_{dd} | e_1 \rangle | e'_2 \rangle$. The state $|g\rangle$ is the field-dressed rovibrational ground state, and the states $|e\rangle$ and $|e'\rangle$ represent the sublevels associated with the field-free rotational level $N=1$. A more detailed discussion of the processes associated with each of these matrix elements is given in Chapter 5.

3.3.1 Strength and anisotropy of the dipole-dipole interaction

Dependence on the electric field strength

Figure 3.1 presents the dipole-dipole energies J_{12} , V_{12}^{eg} , V_{12}^{gg} , and V_{12}^e as functions of the DC electric field strength $\lambda = dE_Z/B_e$. The energy is plotted in units of $U_{dd} \equiv d^2/R_{12}^3$ so that the curves are valid for any $^1\Sigma$ polar molecule. The two-particle states are characterized by the total angular momentum projection along

the electric field axis $M = M_{N_1} + M_{N_2}$. Because the ground state has projection $M_N = 0$, the three values of the total projection M shown in the Fig. 3.1 correspond to the possible projections of the excited state $M_N = -1, 0, 1$. The curves in Fig. (3.1) correspond to DC electric field perpendicular to the vector \mathbf{R}_{12} that joins the centers of mass of the molecules. In panels (a) and (b) it is shown that the dipole energies depend on the absolute value of the total projection $|M|$. The dipole exchange constant J_{12} has opposite sign for states with $M = 0$ and $|M| = 1$ independent of the value of λ , but V_{12}^{eg} has the same sign for large values of λ . Only the exchange constant J_{12} does not vanish at zero electric fields, because it depends on the transition dipole moment between $|g\rangle$ and $|e\rangle$. The rest of the matrix elements depend on the permanent dipole moments of the states $|g\rangle$ and $|e\rangle$, which vanish in the absence of electric fields. The energy V_{12}^{ee} is an order of magnitude smaller than the rest of the matrix elements considered for any value of λ . Later in this Thesis (see Chapters 5-6) we use the parameters $D_{12} = V_{12}^{eg} - V_{12}^{gg}$, $U_{12} = V_{12}^{ee} + V_{12}^{gg} - 2V_{12}^{eg}$, and J_{12} in order to describe collective effects in an ensemble of interacting polar molecules. Figure 3.2 shows the dipole energies D_{12} and U_{12} as a function of the field strength parameter λ , for a DC electric field perpendicular to the intermolecular axis. The curves are obtained for $|e\rangle = |(1), 0\rangle$.

Dependence on the electric field orientation

The dipole-dipole interaction operator \hat{V}_{dd} is anisotropic due to its dependence on the orientation of the intermolecular axis with respect to the space-fixed Z axis. In Chapter 2 we showed that \hat{V}_{dd} can be written as

$$\hat{V}_{dd}(\mathbf{R}_{12}) = -2(6\pi/5)^{1/2} R_{12}^{-3} \sum_{p=-2}^2 (-1)^{-p} Y_{2,-p}(\theta_{R_{12}}, \phi_{R_{12}}) \hat{T}_p^{(2)}(\mathbf{d}_1, \mathbf{d}_2), \quad (3.6)$$

where $Y_{2,-p}(\theta_{R_{12}}, \phi_{R_{12}})$ is a spherical harmonic that depends on the orientation of \mathbf{R}_{12} with respect to the DC electric field direction (Z -axis). Let us consider the matrix element

$$J_{12}^{(0,1)} = \langle (1), 1 | \langle (0), 0 | \hat{V}_{dd} | (0), 0 \rangle | (1), 0 \rangle.$$

The dipole-dipole operator in this case couples two-molecule states with total projections $M = 0$ and $M = 1$. The only term that can induce this coupling in Eq. (3.6)

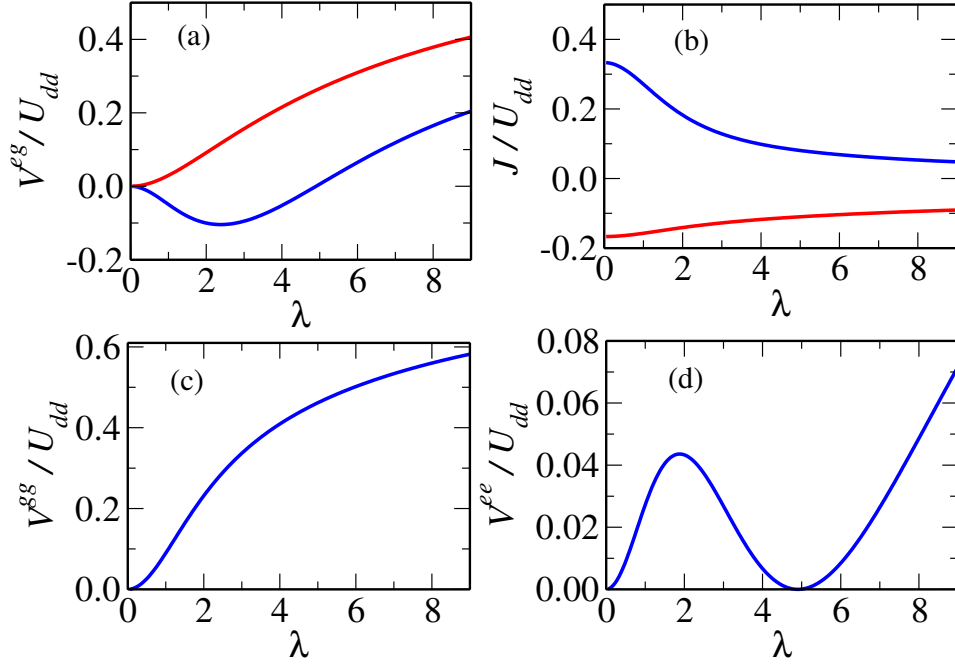


Figure 3.1: Dipole-dipole energies as a function of the field strength parameter $\lambda = dE_Z/B_e$. The rovibrational ground state is $|g\rangle = |(0), 0\rangle$. (a) $V_{12}^{eg} = \langle e_1 | \langle g_2 | \hat{V}_{dd} | e_1 \rangle | g_2 \rangle$ for $|e\rangle = |(1), 0\rangle$ (blue curve) and $|e\rangle = |(1), |1\rangle$ (red curve). (b) $J_{12} = \langle e_1 | \langle g_2 | \hat{V}_{dd} | g_1 \rangle | e_2 \rangle$ for $|e\rangle = |(1), 0\rangle$ (blue curve) and $|e\rangle = |(1), |1\rangle$ (red curve). (c) V_{12}^{gg} for $|e\rangle = |(1), 0\rangle$. (d) V_{12}^{ee} for $|e\rangle = |(1), 0\rangle$. The electric field is perpendicular to the intermolecular axis. Energy in units of $U_{dd} = d^2/a_L^3$, where d is the dipole moment and a_L is the lattice constant.

is $p = 1$, with an angular dependence $Y_{2,-1} \propto \cos \theta \sin \theta$. Therefore, the coupling constant $J_{12}^{(0,1)}$ vanishes for $\theta = 0$ and $\theta = \pi/2$ and has a maximum at $\theta = \pi/4$. Matrix elements such as $J_{12}^{(-1,1)} = \langle (1), -1 | \langle (0), 0 | \hat{V}_{dd} | (0), 0 \rangle | (1), 1 \rangle$ that couple two-molecule states with $\Delta M = \pm 2$ are given by tensor components with $p = \pm 2$ in Eq. (3.6), which have the angular dependence $Y_{2,\pm 2} \propto \sin^2 \theta$. These terms vanish for $\theta = 0$ and have a maximum at $\theta = \pi/2$. The most common type of matrix element used in Thesis couples two-molecule states with $\Delta M = 0$ which have the angular dependence $Y_{2,0} \propto (3 \cos^2 \theta - 1)$. These matrix elements change sign at $\theta = \cos^{-1}(1/\sqrt{3})$ from attractive (negative sign) to repulsive (positive sign) as the

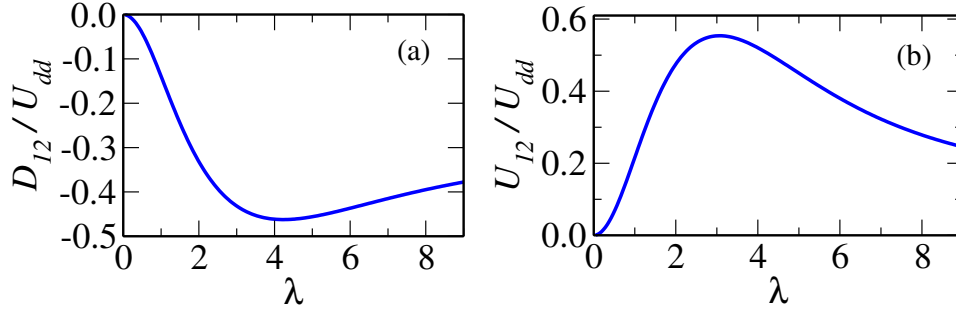


Figure 3.2: Dipole-dipole energies D_{12} and U_{12} as a function of the field strength parameter $\lambda = dE_Z/B_e$ are shown in panels (a) and (b), respectively. The states $|g\rangle = |(0),0\rangle$ and $|e\rangle = |(1),0\rangle$ are used. The electric field is perpendicular to the intermolecular axis. Energy in units of $U_{dd} = d^2/a_L^3$.

angle θ is varied from 0 to $\pi/2$. The angular dependence of selected dipole-dipole matrix elements is shown in Fig. 3.3.

3.4 Open-shell molecules in combined electric and magnetic fields

Ultracold $^2\Sigma$ molecules can be produced by photoassociation of ultracold alkali metal atoms with ultracold alkaline earth [162] or closed shell Yb atoms [17, 163], buffer gas loading [1, 164] or direct laser cooling [165], as was recently demonstrated for the molecule SrF [147]. The presence of the unpaired electron in a $^2\Sigma$ molecule allows for new applications of ultracold molecules exploiting weak couplings of the electron spin with the rotational angular momentum of the molecule [25, 87]. In particular, the electron spin of $^2\Sigma$ molecules can be used for encoding quantum information as in other spin-1/2 particles [125] and for quantum simulation of many-body spin dynamics [87]. In order to realize these applications, it is necessary to develop techniques for entangling the spin degrees of freedom and controlled preparation of many-body spin-dependent states of ultracold molecules. Micheli and coworkers showed that the electric dipole-dipole interaction between $^2\Sigma$ molecules on an optical lattice leads to spin-dependent binary interactions whose parameters can be tuned by a combination of dc electric and

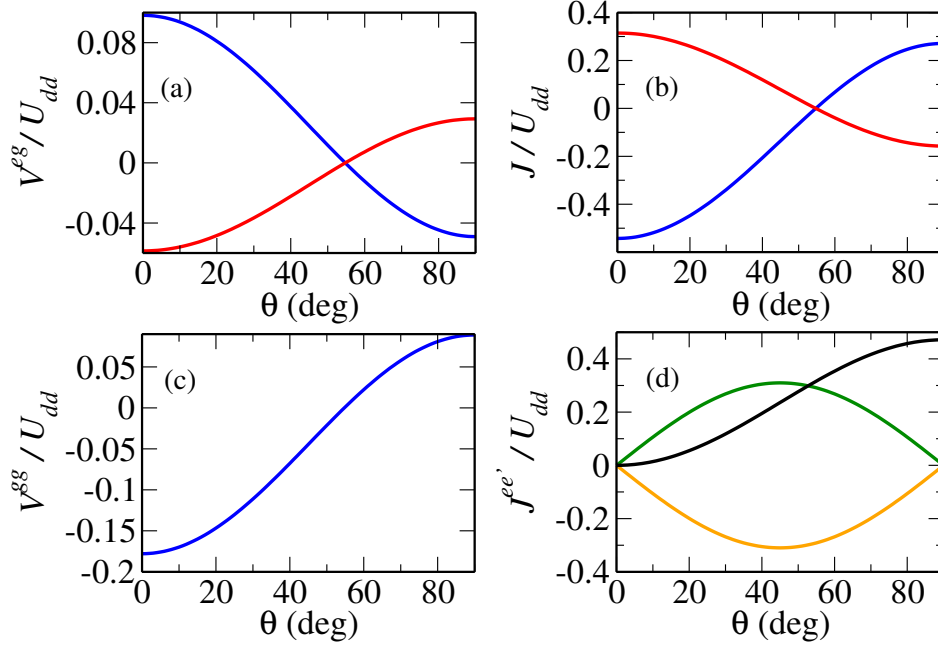


Figure 3.3: Dipole-dipole energies as a function of the angle θ between the intermolecular axis and the DC electric field. The rovibrational ground state is $|g\rangle = |(0), 0\rangle$. (a) $V_{12}^{eg} = \langle e_1 | \langle g_2 | \hat{V}_{dd} | e_1 \rangle | g_2 \rangle$ for $|e\rangle = |(1), 0\rangle$ (blue curve) and $|e\rangle = |(1), 1\rangle$ (red curve). (b) $J_{12} = \langle e_1 | \langle g_2 | \hat{V}_{dd} | g_1 \rangle | e_2 \rangle$ for $|e\rangle = |(1), 0\rangle$ (blue curve) and $|e\rangle = |(1), 1\rangle$ (red curve). (c) V_{12}^{gg} for $|e\rangle = |(1), 0\rangle$. (d) $J_{12}^{ee'}$ for $|e\rangle = |(1), 0\rangle$ and $|e'\rangle = |(1), 1\rangle$ (green line), $|e\rangle = |(1), 0\rangle$ and $|e'\rangle = |(1), -1\rangle$ (orange line), $|e\rangle = |(1), 1\rangle$ and $|e'\rangle = |(1), -1\rangle$ (black line). The DC field strength is $\lambda = 1$. Energy in units of $U_{dd} = d^2/a_L^3$.

microwave fields [87]. This section explores the possibility of tuning the binary interaction between $^2\Sigma$ molecules using superimposed electric and magnetic fields.

As an illustrative example, SrF molecules are used for the calculations in this section. This molecule has a relatively large dipole moment, a relatively small rotational constant and a very weak spin-rotation interaction by comparison with other $^2\Sigma$ molecules [166]. The effects studied here should be more pronounced, making the experiments easier, in an ensemble of molecules with a larger dipole moment and a larger spin-rotation interaction constant. The experimental work on the creation of ultracold $^2\Sigma$ molecules other than SrF is currently underway in

several laboratories [1, 147, 165, 167]. Molecules in the $^3\Sigma$ electronic state exhibit similar energy level structure at certain combinations of electric and magnetic fields [34, 168], which significantly widens the range of molecules that can be used for the interaction scheme proposed in this section.

3.4.1 Rotational level structure of $^2\Sigma$ molecules

The Hamiltonian for a single $^2\Sigma$ molecule in the presence of superimposed electric and magnetic fields can be written in the rigid-rotor approximation as (See Section 2.4)

$$\hat{H} = B_e \hat{N}^2 + \gamma_{\text{SR}} \mathbf{S} \cdot \mathbf{N} - \mathbf{E} \cdot \mathbf{d} + 2\mu_B \mathbf{B} \cdot \mathbf{S}, \quad (3.7)$$

where the first term determines the ro-vibrational structure of the molecule, γ_{SR} is the constant of the spin-rotation interaction between the rotational angular momentum \mathbf{N} and the spin angular momentum \mathbf{S} of the molecule, \mathbf{E} and \mathbf{B} are the vectors of the electric and magnetic fields, \mathbf{d} is the dipole moment of the molecule and μ_B is the Bohr magneton. We assume that both \mathbf{E} and \mathbf{B} are directed along the quantization axis Z . We consider molecules in the vibrational ground state $v = 0$. It is convenient to use the basis of direct products of the rotational $|NM_N\rangle$ and spin $|SM_S\rangle$ wave functions to evaluate the eigenvectors and eigenvalues of Hamiltonian in Eq. (3.7). Here, M_N and M_S denote the projections of \mathbf{N} and \mathbf{S} , respectively, on the Z axis. The diagonalization of this Hamiltonian gives the energy levels of the molecule in superimposed electric and magnetic fields, shown in Fig. 3.4 for a generic molecule. The energy is shown in units of B_e . As in Section 2.4 we use the spin-rotation parameter is $\gamma = \gamma_{\text{SR}}/B_e$, the magnetic field parameter $\mu = 2\mu_B B_Z/B_e$, and the electric field parameter $\lambda = dE_Z/B_e$ to define a dimensionless Hamiltonian. We neglect the hyperfine structure of the molecule. This is a good approximation for the magnetic fields considered in this Section.

At zero electric field, the rotational angular momentum quantum number N is conserved. For the ground rotational state $N = 0$, the spin-rotation interaction vanishes (See Section 2.4) and two lowest energy levels of the molecule in a weak magnetic field correspond to the projections $M_S = -1/2$ and $M_S = +1/2$ of the electron spin angular momentum \mathbf{S} along the magnetic field axis. The state with $M_S = -1/2$ (state α in Fig. 3.4) is the absolute ground state of the molecule at

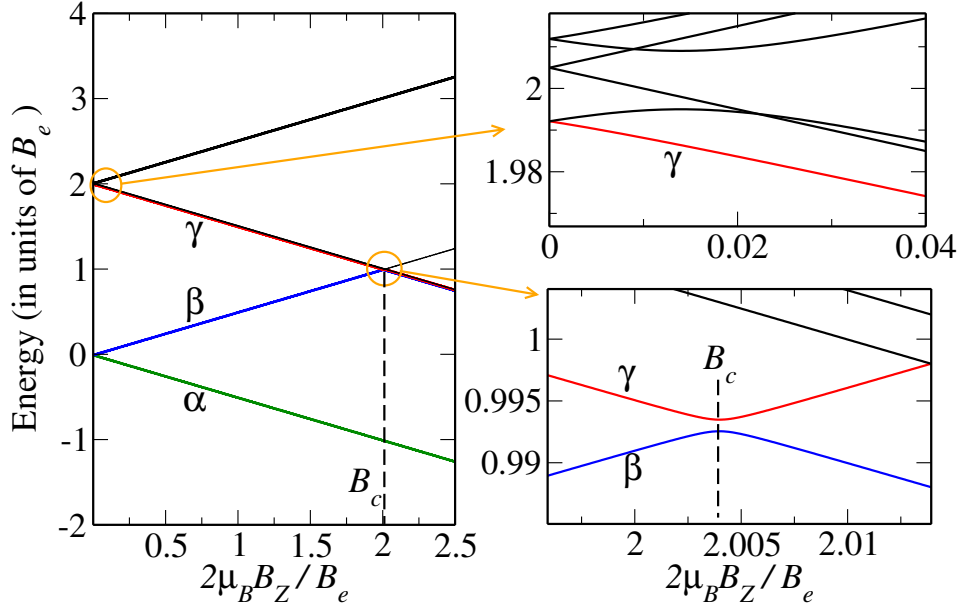


Figure 3.4: Zeeman spectra of a $^2\Sigma$ molecule in the presence of a weak DC electric field. States β and γ are degenerate at the magnetic field value B_c in the absence of electric fields. A weak DC field $\lambda = dE_Z/B_e \ll 1$ couples these states leading to an avoided crossing. The value of B_c varies with the electric field strength. The electric and magnetic fields are collinear. The parameters $\gamma_{SR}/B_e = 0.1$ and $\lambda = 0.2$ are used. The energy is in units of B_e .

all magnitudes of the magnetic field. The state with $M_S = +1/2$ (state β in Fig. 3.4) becomes degenerate with a high-field-seeking Zeeman state (state γ in Fig. 3.4) of the $N = 1$ manifold at some value of a magnetic field (denoted B_c in Fig. 3.4). This degeneracy occurs for $\mu = 2\mu_B B_Z/B_e = 2$. States β and γ have different parity $p = (-1)^N$. The $\mathbf{E} \cdot \mathbf{d}$ interaction is the only term in Hamiltonian (3.7) that couples states of different parity. Therefore, the crossing between states β and γ is real in the absence of an electric field and becomes avoided in the presence of electric fields. In the next Section, it is shown that the avoided crossing depicted in Fig. 3.4 can be exploited for inducing and controlling spin exchange between two distant molecules.

3.4.2 Field-induced electron spin exchange between $^2\Sigma$ molecules

Using the notation from Fig. 3.4 the ground and first excited states of the molecule are $|\alpha\rangle$ and $|\beta\rangle$, where the eigenstates α and β are in general given by the superposition

$$|\phi\rangle = \sum_{NM_N} \sum_{M_S} C_{NM_N M_S}^\phi |NM_N\rangle |SM_S\rangle, \quad (3.8)$$

where $\phi = \alpha, \beta$. For weak magnetic fields in the absence of electric fields Eq. (3.8) reduces to $|\alpha\rangle = |0,0\rangle|-\rangle$ and $|\beta\rangle = |0,0\rangle|+\rangle$ (omitting S and $|M_S|$ for simplicity). According to the discussion in Section 2.6 the matrix element of the dipole-dipole interaction $V_{12}^{\alpha\alpha} = \langle\alpha_1|\langle\alpha_2|\hat{V}_{dd}|\alpha_1\rangle|\alpha_2\rangle$, $V_{12}^{\beta\beta} = \langle\beta_1|\langle\beta_2|\hat{V}_{dd}|\beta_1\rangle|\beta_2\rangle$, and $V_{12}^{\alpha\beta} = \langle\alpha_1|\langle\beta_2|\hat{V}_{dd}|\alpha_1\rangle|\beta_2\rangle$ are spin-allowed but vanish due to parity selection rule. The exchange interaction matrix element $J_{12} = \langle\alpha_1|\langle\beta_2|\hat{V}_{dd}|\beta_1\rangle|\alpha_2\rangle$ is forbidden both by spin and parity selection rules.

In the presence of a weak DC electric field ($\lambda = dE_Z/B_e < 1$) and a magnetic field below the avoided crossing in Fig. 3.4 ($B_Z \ll B_c$), the states $|\alpha\rangle$ and $|\beta\rangle$ can be written as

$$|\alpha\rangle = a|0,0\rangle|\downarrow\rangle + b|1,0\rangle|\downarrow\rangle + c|1,-1\rangle|\uparrow\rangle \quad (3.9)$$

$$|\beta\rangle = a|1,0\rangle|\uparrow\rangle - b|0,0\rangle|\uparrow\rangle + c|1,1\rangle|\downarrow\rangle \quad (3.10)$$

where $a \gg b \gg c$ (ignoring contributions from $N = 2$ states). The terms proportional to c are present due to second-order couplings via the spin-rotation term $\gamma_{SR}\mathbf{S} \cdot \mathbf{N}$ in Eq. (3.7). In this regime, the exchange coupling constant J_{12} is given by

$$J_{12} = c^2 \{ a^2 \langle 00 | \langle 10 | \hat{V}_{dd} | 11 \rangle | 00 \rangle \langle \downarrow\downarrow | \downarrow\downarrow \rangle + b^2 \langle 1-1 | \langle 00 | \hat{V}_{dd} | 00 \rangle | 1-1 \rangle \langle \uparrow\uparrow | \uparrow\uparrow \rangle \}. \quad (3.11)$$

We have considered dipole-dipole transitions between states with no net change in rotational angular momentum projection $M = M_{N_1} + M_{N_2} = 0$. The relative weight of each of the non-zero matrix elements in Eq. (3.11) depends on the coupling between the states of different parity, but the overall magnitude of J_{12} depends on c^2 , i.e., on the amount of mixing between rotational levels in the $N = 1$ manifold induced by the spin-rotation interaction.

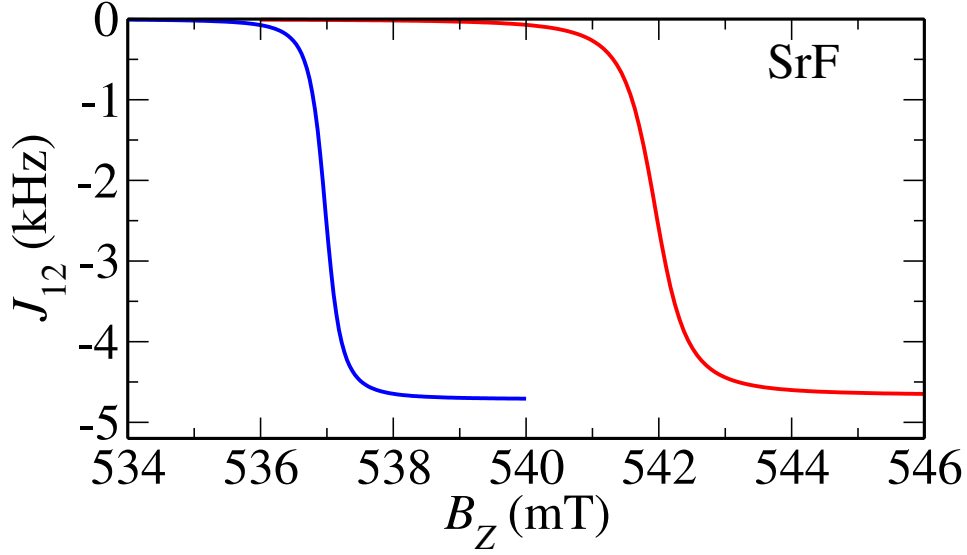


Figure 3.5: Spin exchange coupling $J_{12} = \langle \alpha_1 | \langle \beta_2 | \hat{V}_{dd} | \beta_1 \rangle | \alpha_2 \rangle$ for two SrF molecules as a function of the magnetic field near the avoided crossing B_c between states β and γ in Fig. 3.4. The molecules are separated by 400 nm in the presence of a DC electric field of 1 kV/cm (blue line) and 2 kV/cm (red line). The rotational constant of SrF is 0.251 cm^{-1} , the spin-rotation interaction constant γ_{SR} is $2.49 \times 10^{-3} \text{ cm}^{-1}$ and the dipole moment is 3.47 Debye.

For magnetic fields far below the avoided crossing in Fig. 3.4 ($B_Z \ll B_c$) the value of c is very small and J_{12} is negligible. As the avoided crossing is approached from below $B_Z \approx B_c$ the states $|0,0\rangle|\uparrow\rangle$ and $|1,1\rangle|\downarrow\rangle$ become closer in energy, and in the presence of a DC electric field the second order coupling between these states mix them strongly. The enhanced contribution of the field-free states $|1,-1\rangle$ and $|1,1\rangle$ in the eigenstates in Eq. (3.10) increases the value of J_{12} . In this regime, the states $|\alpha\rangle$ and $|\beta\rangle$ do not have a well defined spin projection M_S , but as long as $B_Z < B_c$ in these rotational states the unpaired electrons can be considered to have opposite spins. As the magnetic field is slowly ramped up above the avoided crossing between the states β and γ in Fig. 3.4 ($B_Z > B_c$) a state transfer occurs between states with opposite spins. The first excited state in this regime is given by Eq. (3.10) with $c \gg b \gg a$. The magnitude of J_{12} above the avoided crossing

achieves its maximum value. This is shown in Fig. 3.5 for SrF molecules separated by 400 nm. The inflection point of each curve indicates the position of the avoided crossing B_c for at the chosen electric field. The magnitude of J_{12} for SrF is a few times smaller than the couplings between rotational states in $^1\Sigma$ molecules with comparable dipole moments (see Section 3.3). For example, for LiCs molecules ($d = 5.5$ Debye) separated by 400 nm in a DC field of 1 kV/cm perpendicular to the intermolecular axis, we have $J_{12} = 23$ kHz for the states $|g\rangle = |(0), 0\rangle$ and $|e\rangle = |(1), 0\rangle$. This should be compared with the value $|J_{12}| = 4.7$ kHz from Fig. 3.5 at $E_Z = 1$ kV/cm. The coupling for LiCs molecules is approximately a factor of 2 larger than the scaled value $J_{\text{LiCs}} = J_{\text{SrF}} \times (d_{\text{LiCs}}^2/d_{\text{SrF}}^2) = 12$ kHz obtained simply by taking into account the difference in the dipole moments between the two molecules. Figure 3.5 shows that as the electric field is increased, the range of magnetic fields $B < B_c$ for which $J_{12} \neq 0$ increases. The value of J_{12} past the avoided crossing $B > B_c$ depends weakly on the electric field as it mostly depends on the magnitude of the spin-rotation constant γ_{SR} .

3.4.3 Control of molecular spin entanglement with external fields

Entangled eigenstates for interacting molecules

The Hamiltonian for a pair of interacting molecules is given by Eq. (3.1). Using the two particle basis $\mathcal{V}_2 = \{|g_1 g_2\rangle, |g_1, e_2\rangle, |e_1 g_2\rangle, |e_1, e_2\rangle\}$ this Hamiltonian can be written in matrix form as

$$\mathcal{H} = \begin{pmatrix} 2\varepsilon_g + V_{12}^{gg} & 0 & 0 & 0 \\ 0 & \varepsilon_g + \varepsilon_e + V_{12}^{eg} & J_{12} & 0 \\ 0 & J_{12} & \varepsilon_g + \varepsilon_e + V_{12}^{eg} & 0 \\ 0 & 0 & 0 & 2\varepsilon_e + V_{12}^{ee} \end{pmatrix}, \quad (3.12)$$

where the states $|g\rangle$ and $|e\rangle$ represent rovibrational states of polar molecules in the presence of static electric and magnetic fields. We have assumed that the dipole-dipole interaction is a small perturbation to the rotational spectra, i.e., $\varepsilon_e - \varepsilon_g \gg \max\{V_{12}, J_{12}\}$. In this case the eigenstates of the two-molecule Hamiltonian \mathcal{H}

are given by

$$\begin{aligned}
& |g_1 g_2\rangle \\
& \frac{1}{\sqrt{2}} \{ |g_1 e_2\rangle - |e_1 g_2\rangle \} \equiv |\Psi_-\rangle \\
& \frac{1}{\sqrt{2}} \{ |g_1 e_2\rangle + |e_1 g_2\rangle \} \equiv |\Psi_+\rangle \\
& |e_1 e_2\rangle
\end{aligned} \tag{3.13}$$

The two-molecule eigenstates $|\Psi_-\rangle$ and $|\Psi_+\rangle$ are not separable into a product of the form $|\phi_1\rangle|\phi_2\rangle$, where $|\phi\rangle$ is a single-molecule eigenstate. This is a necessary condition for entanglement between two molecules [169]. Although a rigorous definition of entanglement and its consequences are outside the scope of this thesis, non-separability of composite states is adopted as an operational definition of entanglement. If the exchange coupling constant J_{12} vanishes, all the eigenstates of the two-molecule Hamiltonian \mathcal{H} would be separable, and there would be no entanglement of distant molecules.

An electromagnetic field $\mathbf{E}(t)$ with frequency $\omega \approx \varepsilon_e - \varepsilon_g$ can be used to induce transitions between the states in Eq. (3.13). Assuming the molecules are identical, the dipole moment for the transition to the one-excitation manifold from the absolute ground state is

$$\begin{aligned}
\langle \Psi_{\pm} | \hat{\mathbf{d}}_1 + \hat{\mathbf{d}}_2 | g_1 g_2 \rangle &= \frac{1}{\sqrt{2}} \{ \langle g_1 e_2 | \hat{\mathbf{d}}_1 + \hat{\mathbf{d}}_2 | g_1 g_2 \rangle \pm \langle e_1 g_2 | \hat{\mathbf{d}}_1 + \hat{\mathbf{d}}_2 | g_1 g_2 \rangle \} \\
&= \frac{1}{\sqrt{2}} \{ \langle e_2 | \hat{\mathbf{d}}_2 | g_2 \rangle \pm \langle e_1 | \hat{\mathbf{d}}_1 | g_1 \rangle \} \\
&= \begin{cases} \sqrt{2} \langle e | \hat{\mathbf{d}} | g \rangle & \text{for } |\Psi_+\rangle \\ 0 & \text{for } |\Psi_-\rangle \end{cases} .
\end{aligned} \tag{3.14}$$

A similar result holds for the transition dipole moment $\langle e_1 e_2 | \hat{\mathbf{d}}_1 + \hat{\mathbf{d}}_2 | \Psi_{\pm} \rangle$. The dipole-allowed transition $|g_1 g_2\rangle \rightarrow |\Psi_+\rangle$ is enhanced by a factor of $\sqrt{2}$ because the transition dipole moments of the interacting molecules are in phase. The state $|\Psi_+\rangle$ is known as superradiant. The transition to the $|\Psi_-\rangle$ state is forbidden because the transition dipoles of the molecules cancel each other.

Dynamic generation of entangled non-interacting spins

The electric and magnetic field dependence of the exchange coupling constant J_{12} illustrated in Fig. 3.5 suggests an interesting possibility of creating an entangled two-molecule states of *non-interacting* molecular electron spins. Starting from a pair of $^2\Sigma$ polar molecules in the rovibrational ground state $|\alpha\rangle$, this can be achieved by the following procedure:

- (a) Apply an electric field to couple the molecular states of different parity.
- (b) Tune the magnetic field adiabatically to a value $B_Z > B_c$ (see Fig. 3.4), where J_{12} is a maximum for the $\alpha \rightarrow \beta$ transition.
- (c) Apply a weak monochromatic electromagnetic field resonant with the transition frequency $\omega_{\beta\alpha} = (\varepsilon_\beta - \varepsilon_\alpha)/\hbar$ to create entangled state $|\Psi_+^\beta\rangle$.
- (d) Sweep the magnetic field to a value $B_Z \ll B_c$ and turn off the electric field.

If carried out faster than the inherent time scale of the excitation exchange dynamics, step (d) above must project the two-molecule wave function $|\Psi_+^\beta\rangle$ on the state

$$|\Psi\rangle = \frac{1}{\sqrt{2}} \{a|\uparrow\rangle_1|\downarrow\rangle_2 + b|\downarrow\rangle_1|\uparrow\rangle_2\} \quad (3.15)$$

where $|\uparrow\rangle = |N=0, M_N=0\rangle|S=1/2, M_S=1/2\rangle$ and $|\downarrow\rangle = |N=0, M_N=0\rangle|S=1/2, M_S=-1/2\rangle$. The variation of the magnetic field in step (d) must be generally faster than \hbar/J_{12} to preserve the state $|\Psi_+^\beta\rangle$, but slow enough to preclude the non-adiabatic transitions to molecular state γ . This can be achieved because the splitting of the molecular states β and γ at the avoided crossing in Fig. 3.4 is much greater than J_{12} . We have confirmed that the magnetic field can be detuned to a value $B \ll B_0$ without changing the magnitudes of the coefficients a and b by time-dependent calculations.

3.5 Closed-shell molecules in strong off-resonant optical fields

The basic description of the interaction of diatomic molecules with far off-resonant optical fields is reviewed in Chapter 2. An intense off-resonant AC electric field

shifts the rovibrational energy levels of the molecule, and induces alignment of the molecular axis along the axis of polarization of the field. The degree of alignment depends on the polarizability of the molecule and the intensity of the field. In the presence of the field, the rotational states of a diatomic molecule $|\Psi\rangle$ are given by superpositions of angular momentum states $|NM_N\rangle$ of the same parity. The expectation value of the dipole moment in the field-dressed rotational states $\langle\Psi|\vec{\mu}|\Psi\rangle$ therefore vanishes. From a classical point of view, this is a consequence of the oscillation of the electric field vector at optical frequencies. The electric dipole moment of the molecule follows the orientation of the electric field in space, therefore its time-averaged dipole moment vanishes.

The Hamiltonian for two interacting polar molecules in Eq. (3.12) depends on the matrix elements of the dipole-dipole interaction $V_{12}^{eg} = \langle e_1|\langle g_2|\hat{V}_{dd}|e_1\rangle|g_2\rangle$, $V_{12}^{gg} = \langle g_1|\langle g_2|\hat{V}_{dd}|g_1\rangle|g_2\rangle$, and $J_{12} = \langle g_1|\langle e_2|\hat{V}_{dd}|e_1\rangle|g_2\rangle$. In Appendix B it is shown that the parity of the rotational states in the two-molecule basis $|N_1M_{N_1}\rangle|N_2M_{N_2}\rangle$ determines the selection rules for these matrix elements. Both in free space and in the presence of a far off-resonant field, dipole-dipole couplings that are diagonal in the single-molecule basis, such as V_{12}^{eg} and V_{12}^{gg} , vanish by parity selection rule. The exchange coupling matrix element J_{12} is allowed by parity. In Section 3.3 it was shown that in the presence of a DC electric field the magnitudes of the energies $D_{12} = V_{12}^{eg} - V_{12}^{gg}$ and J_{12} can be tuned by changing the strength of the field and its orientation with respect to the intermolecular axis. The effect of an off-resonant AC electric field on the dipole-dipole interaction between molecules is analyzed in this Section.

3.5.1 Rotational structure in strong off-resonant optical fields

Closed-shell diatomic molecules without electronic angular momentum, in the presence of an electromagnetic plane wave with frequency far detuned from any vibronic transition and linear polarization along the space-fixed $\hat{\mathbf{Z}}$ axis, can be described by the effective dimensionless Hamiltonian (see Chapter 2)

$$\hat{H} = \hat{N}^2 - \frac{2}{3}\Omega_1\mathcal{D}_{0,0}^{(2)}(\theta), \quad (3.16)$$

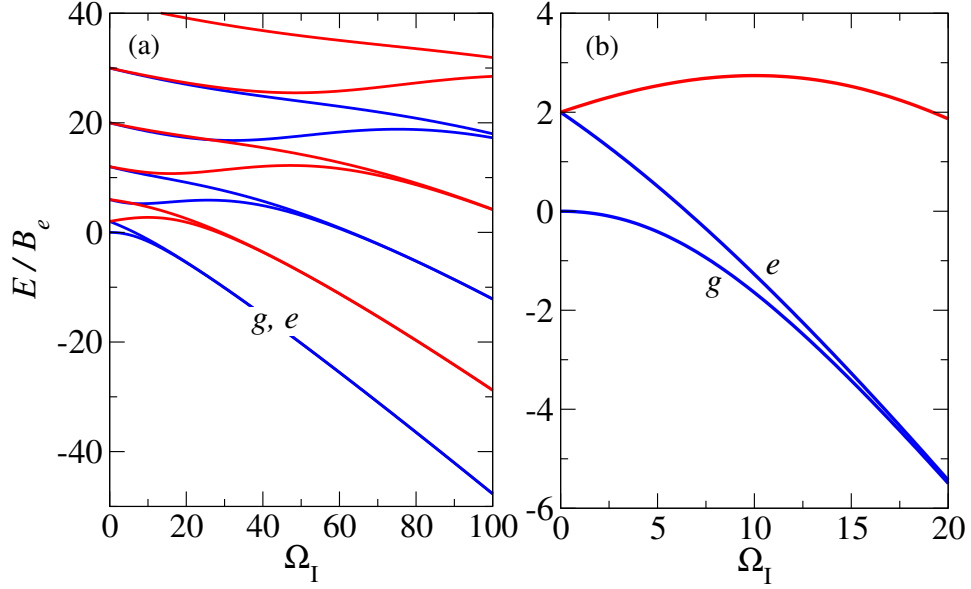


Figure 3.6: Dimensionless energy of the rotational states E/B_e of a molecule in the presence of a linearly-polarized CW far-detuned laser, as a function of the light-matter coupling strength $\Omega_I = \varepsilon^2 \Delta\alpha / 4B_e$: (a) Energies of the first six states with $M_N = 0$ (blue) and $|M_N| = 1$ (red); (b) Expanded view of the lowest two field-dressed states $|g\rangle = |(0), 0\rangle$ and $|e\rangle = |(1), 0\rangle$ for small values of Ω_I . B_e is the rotational constant, $\Delta\alpha$ is the polarizability anisotropy, and $\varepsilon^2 = I/2\varepsilon_0 c$, where I is the intensity of the laser.

where $\mathcal{D}_{0,0}^{(2)} = (3\cos^2\theta - 1)/2$ is an element of the rotation matrix of rank two, and

$$\Omega_I = \frac{\varepsilon^2(\alpha_{\parallel} - \alpha_{\perp})}{4B_e}$$

is a parameter that characterizes the strength of the light-matter interaction. We have neglected a state-independent AC Stark shift $\Delta_{ac} = (\varepsilon_0^2/4)(\alpha_{\parallel} - 2\alpha_{\perp})/3$ which only contributes to the overall phase of the eigenstates. The matrix elements of this Hamiltonian in the basis of eigenstates of \hat{N}^2 and \hat{N}_z are given in Section 2.5. The projection of the rotational angular momentum M_N is a conserved quantity. A far-detuned optical field with linear polarization along $\hat{\mathbf{Z}}$ therefore induces a state-dependent shift of the rotational levels, and also couples rotational states of the

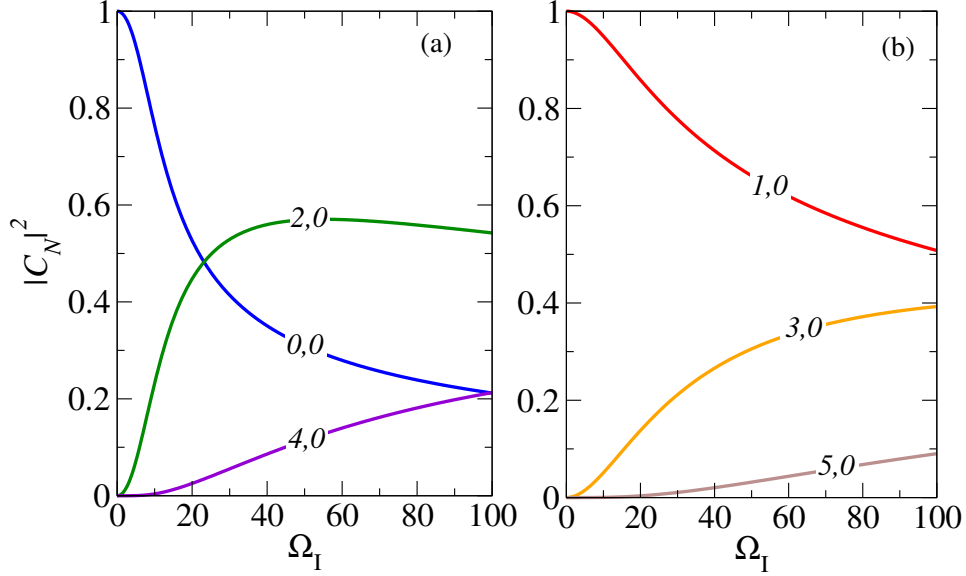


Figure 3.7: Probability amplitudes $|c_N|^2$ of each rotational state $|N, M\rangle$ in the field-dressed states $|\Psi_M\rangle = \sum_N c_N |N, M\rangle$, as a function of the light-matter coupling strength $\Omega_I = \varepsilon^2 \Delta \alpha / 4B_e$. Panels (a) and (b) correspond to the ground and first excited states, respectively, for which $M = 0$.

same parity and projection M_N . The light-matter Hamiltonian can be diagonalized independently for each value of M_N . In Figure 3.6 we show the lowest eigenvalues of the Hamiltonian in Eq. (3.16), in units of B_e , as a function of the interaction parameter Ω_I . The Hamiltonian is diagonalized by including rotational states with up to $N = 20$ in the basis. In the limit of very intense fields $\Omega_I \gg 1$, the energy spectrum consists of closely spaced doublets of states with opposite parity. The spectrum becomes harmonic in this limit, with an energy splitting proportional to $\sqrt{\Omega_I}$ between neighbouring doublets, as shown in panel (a) of Fig. 3.6. In panel (b) we show the lowest doublet corresponding to the rotational states $|N = 0, M_N = 0\rangle$ and $|N = 1, M_N = 0\rangle$ in the limit $\Omega_I \rightarrow 0$. The field-dressed states are given by superposition of the form $|\Psi_{M_N}\rangle = \sum_N c_N |N, M_N\rangle$. In Fig. 3.7 we present the prob-

ability amplitudes $|c_N|^2$ for the lowest field-dressed doublet states $|g\rangle$ and $|e\rangle$ as a function of Ω_I . Panel (a) shows the expansion coefficients for the field-dressed ground state $|g\rangle$. It is composed of field-free rotational states with even values of N and corresponds to the state $|N=0, M_N=0\rangle$ when the optical field is absent. For field intensities such that $\Omega_I \sim 10$, the occupation of the field-free ground state $N=0$ decreases by approximately 20%. The first excited field-dressed state $|e\rangle$ is shown in panel (b) of Fig. 3.7. It is composed of rotational states with odd values of N , and corresponds to the state $|N=1, M=0\rangle$ in the absence of the field.

The electric dipole transition matrix element between the ground and the first excited field-dressed state $\langle e|\hat{\mu}_Z|g\rangle$ is finite for all values of the parameter Ω_I , since it can be written as a linear combination of the transition matrix elements $\langle N \pm 1, M|\hat{\mu}_Z|N, M\rangle \neq 0$. The field-dressed states have no permanent dipole moments, i.e., $\langle \Psi|\hat{\mu}_Z|\Psi\rangle = 0$, because they have a well-defined parity.

3.5.2 Dipolar interactions in DC electric and strong off-resonant fields

Collinear DC electric and off-resonant optical fields

In Section 2.7 it was shown that the Hamiltonian for a polar molecule under the influence of a DC electric field and a CW far-detuned optical field, where the laser polarization is collinear with the direction of the DC electric field, can be written as

$$\hat{H} = \hat{N}^2 - \lambda \mathcal{D}_{0,0}^{(1)} - \frac{2}{3} \Omega_I \mathcal{D}_{0,0}^{(2)}, \quad (3.17)$$

where $\lambda = \mu_0 E_z / B_e$ parametrizes the strength of the DC electric field. In Section 2.7 the limit $\Omega_I \ll 1$ was considered, where the rotational spectrum is dominated by the DC Stark effect. The DC electric field couples states of opposite parity. In particular, it couples the closely spaced states of opposite parity that form each field-dressed doublet in Fig. 3.6. In the absence of DC electric fields, the splitting between the ground and the first excited rotational state (field-dressed doublet) is much smaller than B_e in the limit $\Omega_I \gg 1$. Therefore, a relatively weak DC field would strongly mix these states. The levels of the field-dressed doublets repel each other due to their interaction. In panel (a) of Figure 3.8 we show the energies of

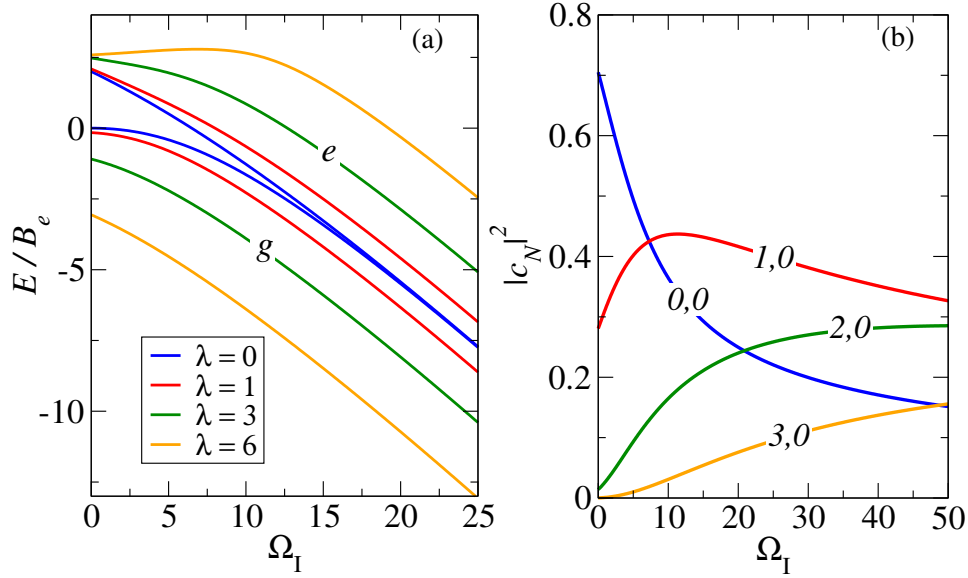


Figure 3.8: Rotational states in the presence of a DC electric field and a CW far-detuned laser: (a) Energy of the ground $|g\rangle$ and first excited $|e\rangle$ rotational states as a function of the laser intensity parameter Ω_I , for different values of the DC field strength parameter λ ; (b) Probability amplitude $|c_N|^2$ of the angular momentum state states $|NM\rangle$ in the field-dressed ground state $|g\rangle$, as a function of Ω_I for $\lambda = 3$.

the lowest two field-dressed states $|g\rangle$ and $|e\rangle$, as a function of the laser intensity parameter Ω_I , for different values of the DC field strength parameter λ . In panel (b) we show the probability amplitudes $|c_N|^2$ in the field-dressed ground state superposition $|g\rangle = \sum_N c_N |NM_N\rangle$, as a function of Ω_I for $\lambda = 3$. In the limit $\Omega_I \rightarrow 0$, the rotational ground state is primarily given by the superposition of the states $|0,0\rangle$ and $|1,0\rangle$.

Let us now consider the dipole-dipole interaction between two polar molecules in the presence of a DC electric field and CW far-detuned optical field. As discussed earlier in this Chapter, we use the eigenstates of the single-molecule Hamiltonian in Eq. (3.17) to define the states $|g\rangle$ and $|e\rangle$. We are interested in the dipole-dipole matrix elements D_{12} and J_{12} that are relevant in later Chapters for the description of collective rotational excitations in optical lattices. Figure 3.9 shows the exchange coupling constant $J_{12} = \langle g_1 | \langle e_2 | \hat{V}_{dd} | e_1 \rangle | g_2 \rangle$ as a function of the light-

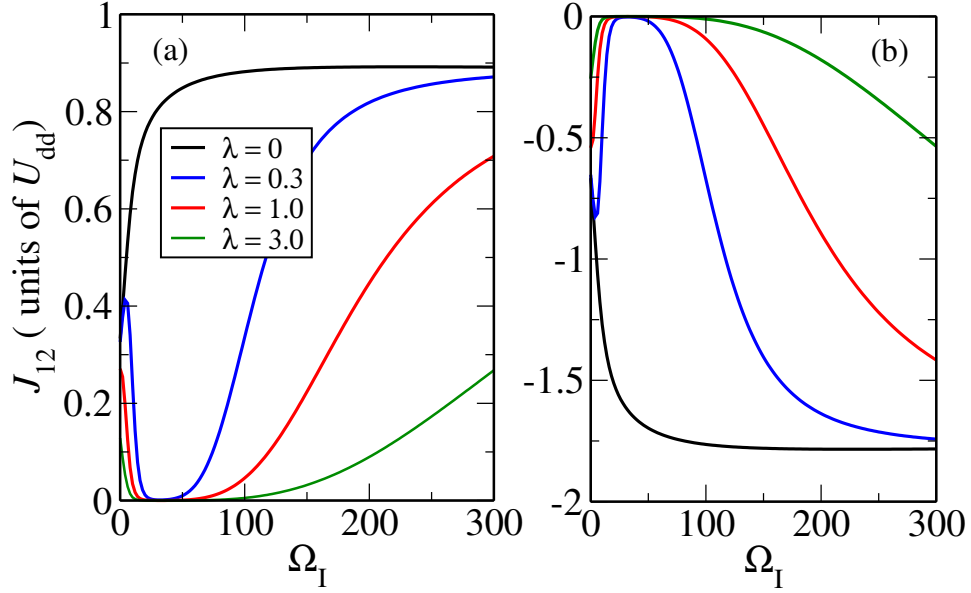


Figure 3.9: Exchange interaction $J_{12} = \langle g_1 | \langle e_2 | \hat{V}_{dd} | e_1 \rangle | g_2 \rangle$ between two molecules in their ground $|g\rangle$ and first excited $|e\rangle$ rotational states, in the presence of collinear DC electric with strength λB_e and CW far-detuned optical fields with strength $\Omega_I B_e$, where B_e is the rotational constant. Panels (a) and (b) correspond to a perpendicular and parallel orientation, respectively, of the intermolecular axis with respect to the field axis. The dipole-dipole energy is in units of $V_{dd} = d^2/R_{12}^3$, where d is the permanent dipole moment of the molecule and R_{12} is the intermolecular distance.

matter coupling strength Ω_I , for different values of the DC field strength parameter λ . $|g_i\rangle$ and $|e_i\rangle$ are the ground and first excited field-dressed rotational states of molecule i (see Fig. 3.8). The DC electric field and the laser field polarizations are collinear. Since the dipole-dipole interaction depends on the orientation of the intermolecular axis \mathbf{r}_{12} with respect to the Z axis, the field-dressed dipole-dipole matrix elements are plotted for \mathbf{r}_{12} perpendicular and parallel to the orientation of the fields in panels (a) and (b), respectively. The exchange constant J_{12} increases monotonically with Ω_I in the absence of DC electric fields, and is suppressed in the presence of a DC field as a function of Ω_I . This is shown in Figure 3.9. The resonant energy exchange between molecules in the lowest field-dressed doublet is

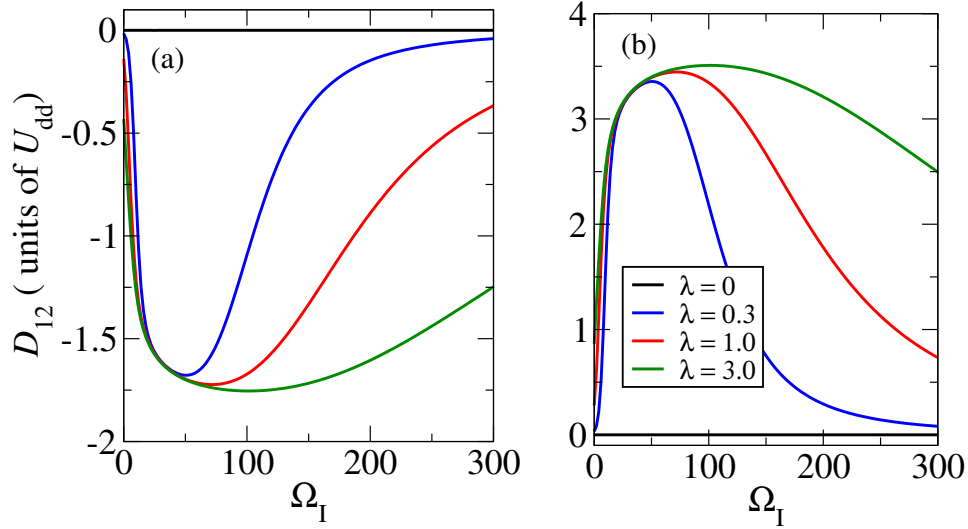


Figure 3.10: Energy shift $D_{12} = \langle e_1 | \langle g_2 | \hat{V}_{dd} | e_1 \rangle | g_2 \rangle - \langle g_1 | \langle g_2 | \hat{V}_{dd} | g_1 \rangle | g_2 \rangle$ for two molecules in their ground $|g\rangle$ and first excited $|e\rangle$ rotational states, in the presence of collinear DC electric with strength λB_e and CW far-detuned optical fields with strength $\Omega_I B_e$, where B_e is the rotational constant. Panels (a) and (b) correspond to a perpendicular and parallel orientation, respectively, of the intermolecular axis with respect to the field axis. The dipole-dipole energy is in units of $U_{dd} = d^2/R_{12}^3$, where d is the permanent dipole moment of the molecule and R_{12} is the intermolecular distance.

therefore suppressed in combined DC electric and far-detuned optical fields in the limit of strong fields $\Omega_I \gg 1$, and enhanced if the DC electric field is absent.

Figure 3.10 shows the value of the dipole-dipole shift of the rotational levels $D_{12} = \langle e_1 | \langle g_2 | \hat{V}_{dd} | e_1 \rangle | g_2 \rangle - \langle g_1 | \langle g_2 | \hat{V}_{dd} | g_1 \rangle | g_2 \rangle$ as a function of Ω_I , for different values of λ . Since $|g\rangle$ and $|e\rangle$ have well-defined parity in the absence of a DC electric field, the constant D_{12} vanishes for all values of Ω_I . A weak electric field ($\lambda \ll 1$) is sufficient to induce a permanent dipole moment in each state of the field-dressed doublet, which enhances the value of $|D_{12}|$. The constant D_{12} can be approximately three times larger than J_{12} for the parameters $\Omega_I = 0$ and $\lambda = 3$. For a CW off-resonant laser with $\Omega_I = 6$, and a DC field with $\lambda = 3$, the magnitudes of the couplings are $D_{12} = 1.0$ and $J_{12} = 0.03$, in units of $U_{dd} = d^2/R_{12}^3$, for the

fields perpendicular to the intermolecular axis. More generally, in combined DC and far-detuned AC electric fields perpendicular to the intermolecular axis, the ratio D_{12}/J_{12} is greater than 100 for $\Omega_{\text{I}} \geq 30$ and $\lambda \geq 0.1$. Curves analogous to those shown in Fig. 3.10 can be obtained for the related quantities V_{12}^{gg} and $U_{12} = V_{12}^{ee} + V_{12}^{gg} - 2V_{12}^{eg}$ defined in Section 3.3.

Chapter 4

Towards coherent control of bimolecular scattering

4.1 Chapter overview

This chapter presents a general scheme for the realization of coherent control of atomic and molecular collisions at cold and ultracold temperatures. The method relies on the interference between scattering states induced by a static field. In Section 4.2 the general principle of coherent control via pathway interference is reviewed. Section 4.3 describes earlier proposals to achieve control of bimolecular processes and mentions some difficulties inherent to these approaches. In Section 4.4 the mechanism of field-induced interference is explained, and in Section 4.5 the proposed scheme is applied to ultracold atomic scattering in the presence of magnetic fields. The controllability of a specific atomic collision process is analyzed. The chapter ends with comments on the applicability of the method to molecular scattering.

4.2 The principle of coherent control

In classical mechanics, interference is a general wave phenomena that results from the superposition principle. For two waves propagating through space, the total wave amplitude at a given position is the sum of the amplitudes of the two waves at that position. If the amplitudes of the two waves have the same magnitude and direction, the two waves interfere constructively and the total amplitude is the sum of the two individual waves. If the wave amplitudes have the same magnitude but oppose each other at the chosen position, they interfere destructively and the total amplitude vanishes at that point. For an observer that measures the square of the total wave amplitude at a specific point in space, there would be no signal from the waves that interfere destructively. This basic principle illustrates the potential use of interference to manipulate the outcome of a measurement. If the two opposing waves had not interfered at the point of measurement, the observer would record the individual signals for each wave. For constructively interfering waves, the measurement outcome is enhanced with respect to the case of non-interfering waves.

In quantum mechanics, the probability amplitude for a specific event behaves as the analogue of classical wave amplitudes. Let $|\Psi\rangle$ denote a general quantum state of a given system and $|\phi_n\rangle$ a specific state specified by the quantum number n . The probability amplitude for the system to be found in the state $|\phi_n\rangle$ after measurement is $A_n = \langle\phi_n|\Psi\rangle$. If the state of the system at a given moment of time can be described by the superposition

$$|\Psi\rangle = a|\psi_a\rangle + b|\psi_b\rangle, \quad (4.1)$$

then the probability of observing the state $|\phi_n\rangle$ at that moment of time $P_n = |A_n|^2$ can be written as

$$P_n = |a|^2 |\langle\phi_n|\psi_a\rangle|^2 + |b|^2 |\langle\phi_n|\psi_b\rangle|^2 + 2|a||b| |\langle\phi_n|\psi_a\rangle| |\langle\phi_n|\psi_b\rangle| \cos(\Delta\theta + \Delta\phi), \quad (4.2)$$

where the relative phases $\Delta\theta = \theta_b - \theta_a$ and $\Delta\phi = \phi_b - \phi_a$ are associated with the superposition coefficients $a = |a| e^{i\theta_a}$ and $b = |b| e^{i\theta_b}$, and the inner products $\langle\phi_n|\psi_a\rangle = |\langle\phi_n|\psi_a\rangle| e^{i\phi_a}$ and $\langle\phi_n|\psi_b\rangle = |\langle\phi_n|\psi_b\rangle| e^{i\phi_b}$.

The simple example discussed above illustrates one important feature of coherent control. Let us assume that the system is prepared in a superposition given by Eq. (4.1) and we want to control the measurement of the outcome state $|\phi_n\rangle$. If the transition amplitudes $\langle\phi_n|\psi_a\rangle$ and $\langle\phi_n|\psi_b\rangle$ do not vanish (the two pathways are allowed and indistinguishable) but one of them is much smaller than the other, the interference term in Eq. (4.2) becomes negligibly small, and the probability P_n is dominated by one of the satellites regardless of the magnitude of the coefficients a and b . Therefore, it is important for the observation of coherent control that the transition amplitudes of the interfering pathways are comparable.

It has to be noted that quantum interference alone does not imply controllability. In quantum beat spectroscopy, P_n corresponds to the probability of an atom or molecule to be in the ground state $|\psi_g\rangle$ after spontaneous emission of a photon from an excited state $|\psi_e\rangle$. Let us assume the particle is prepared in a superposition of excited eigenstates

$$|\Psi(t)\rangle = a|\psi_e^a\rangle e^{-iE_a t/\hbar} + b|\psi_e^b\rangle e^{-iE_b t/\hbar}, \quad (4.3)$$

and the outcome state is $|\phi_n\rangle = \hat{\mu}|\psi_g\rangle$, where $\hat{\mu}$ is the electric dipole operator. The probability $P_n = |\langle\psi_g|\hat{\mu}|\Psi\rangle|^2$ is proportional to the intensity of the radiation emitted by the particle at a given time. According to Eq. (4.2) the interference term is proportional to $\cos[(E_b - E_a)t/\hbar + \delta]$, where δ is the relative phase of the coefficients a and b (the transition amplitudes are assumed real). In this idealized case, external control over the relative phase δ does not guarantee control of the emission process because the interference term oscillates in time with a frequency $\omega_{ba} = (E_b - E_a)/\hbar$ so that the average signal over time as $t \rightarrow \infty$ does not exhibit any enhancement or suppression due to quantum interference. Coherent control is concerned with processes for which the interference term in Eq. (4.2) does not average to zero in the limit of long times.

4.3 Coherent control of collisions

Over the past two decades schemes for control of unimolecular processes via path-interference (frequency domain) and via wavepackets (time domain) have been successfully demonstrated experimentally [45]. In contrast, proposals for coherent

control of bimolecular processes have not been realized. Let us consider the general bimolecular scattering event

$$A + B \rightarrow \begin{cases} A + B \\ A + B^* \\ C + D \end{cases} \quad (4.4)$$

where the incoming particles S and B undergo elastic, inelastic or reactive scattering. Let us label the incoming and outgoing channels by the indices q and q' , respectively. The scattering events illustrated in Eq. (4.4) occur at the total energy E in the center of mass frame where each asymptotic state is characterized by the set of quantum numbers \mathbf{n} . The transition amplitude for the scattering events in Eq. (4.4) is given by

$$A_E(\mathbf{m}q'; \mathbf{n}q) = \langle E, q', \mathbf{m} | \hat{S} | E, q, \mathbf{n} \rangle \quad (4.5)$$

where \hat{S} is the scattering matrix [54, 170]. The scattering cross section σ_E is proportional to the scattering probability $P_E = |A_E|^2$. Following the basic prescription for coherent control outlined in Sec. 4.2, let us consider an incoming state in channel q given by the superposition of degenerate asymptotic states

$$|E, q\rangle = \sum_{\mathbf{n}} a_{\mathbf{n}} |E, q, \mathbf{n}\rangle. \quad (4.6)$$

The cross section for the scattering between two particles described by this superposition into the outgoing channel $|E, q, \mathbf{m}\rangle$ is thus

$$\begin{aligned} \sigma_E(q', \mathbf{m}; q) &\propto \sum_{\mathbf{n}} |a_{\mathbf{n}}|^2 |\langle E, q', \mathbf{m} | \hat{S} | E, q, \mathbf{n} \rangle|^2 \\ &+ \sum_{\mathbf{n}} \sum_{\mathbf{n}' \neq \mathbf{n}} a_{\mathbf{n}}^* a_{\mathbf{n}'} \langle E, q, \mathbf{n} | \hat{S} | E, q', \mathbf{m} \rangle \langle E, q', \mathbf{m} | \hat{S} | E, q, \mathbf{n}' \rangle. \end{aligned} \quad (4.7)$$

The total cross section into arrangement q is given by $\sigma_E(q'; q) = \sum_{\mathbf{m}} \sigma_E(q', \mathbf{m}; q)$. The cross section is composed of a sum of satellite and interference terms. The uncontrollable satellite terms represent the contributions of each individual incoming channel in the superposition 4.6, weighed by the probability $|a_{\mathbf{n}}|^2$ that the colliding particles have the set of quantum numbers \mathbf{n} . The interference terms can in prin-

ciple be controlled by manipulating the products $a_{\mathbf{n}}^* a_{\mathbf{n}'}$ at the step of preparation of the incoming superposition in Eq. (4.6). This scheme for coherent control of collisions was originally proposed in Ref. [171].

The incoming states $|E, q, \mathbf{n}\rangle$ in Eq. (4.6) describe the relative motion of the colliding particles in the center of mass frame at distances where the interaction between the particles is negligible compared to the internal and translational energies of the collision partners. In the laboratory frame, the state $|E, q, \mathbf{n}\rangle$ can be written as

$$|\psi_{\text{in}}^{\text{lab}}\rangle = |\phi_A\rangle|\phi_B\rangle e^{i\mathbf{k}^A \cdot \mathbf{r}_A} e^{i\mathbf{k}^B \cdot \mathbf{r}_B} = |\phi_A\rangle|\phi_B\rangle e^{i\mathbf{k} \cdot \mathbf{r}} e^{i\mathbf{K} \cdot \mathbf{R}} \equiv |E, q, \mathbf{n}\rangle |\mathbf{K}\rangle \quad (4.8)$$

where $|\phi\rangle$ denotes an internal state, $\mathbf{K} = \mathbf{k}^A + \mathbf{k}^B$ is the center of mass momentum and $\mathbf{k} = (m_B \mathbf{k}^A - m_A \mathbf{k}^B)/(m_A + m_B)$ the relative momentum. The relative position vector is $\mathbf{r} = \mathbf{r}_A - \mathbf{r}_B$ and the center of mass position vector is $\mathbf{R} = (m_A \mathbf{r}_A + m_B \mathbf{r}_B)/(m_A + m_B)$, where m_A and m_B are the masses of A and B, respectively. In the absence of external forces, the center of mass momentum \mathbf{K} of the collision pair is conserved in a scattering event. Scattering processes occurring with different center of mass momenta contribute independently to the measured signal. In a thermal gas where the distribution of center of mass momenta is broad, the average over the momenta of the particles can thus lead to vanishing signal for interference effects in the cross section.

Let us consider a specific form of the two-particle superposition in Eq. (4.6). The collision partners A and B can each be prepared in a superposition of internal states using standard optical techniques. The corresponding single particle states in the most general form are given by

$$|\psi\rangle_A = a_1 |\phi(1)\rangle_A e^{i\mathbf{k}_1^A \cdot \mathbf{r}_A} + a_2 |\phi(2)\rangle_A e^{i\mathbf{k}_2^A \cdot \mathbf{r}_A} \quad (4.9)$$

$$|\psi\rangle_B = b_1 |\phi(1)\rangle_B e^{i\mathbf{k}_1^B \cdot \mathbf{r}_B} + b_2 |\phi(2)\rangle_B e^{i\mathbf{k}_2^B \cdot \mathbf{r}_B}, \quad (4.10)$$

where a_i and b_i are complex coefficients. The wave functions $|\phi(i)\rangle_A$ and $|\phi(i)\rangle_B$ correspond to the internal states of the particles, where the index i labels the corresponding non-degenerate eigenvalues. The vectors \mathbf{k}_i^A , \mathbf{k}_i^B , \mathbf{r}_A and \mathbf{r}_B , are the wave vectors and position vectors in the laboratory frame associated with the i -th

internal state $|\phi(i)\rangle$ for particles A and B, respectively. The superpositions in Eqs. (4.9) and (4.10) involve a correlation between the internal and the translational degrees of freedom of each particle, i.e., the momentum of an atom or molecule in the laboratory frame depends on the internal state of the particle. The incoming asymptotic wave function is given by the product state

$$\begin{aligned} |\psi\rangle_{\text{inc}} &= |\psi\rangle_A |\psi\rangle_B \\ &= a_1 b_1 |\Gamma(11)\rangle e^{i\mathbf{k}_{11}\cdot\mathbf{r}+i\mathbf{K}_{11}\cdot\mathbf{R}} + a_1 b_2 |\Gamma(12)\rangle e^{i\mathbf{k}_{12}\cdot\mathbf{r}+i\mathbf{K}_{12}\cdot\mathbf{R}} \\ &\quad + a_2 b_1 |\Gamma(21)\rangle e^{i\mathbf{k}_{21}\cdot\mathbf{r}+i\mathbf{K}_{21}\cdot\mathbf{R}} + a_2 b_2 |\Gamma(22)\rangle e^{i\mathbf{k}_{22}\cdot\mathbf{r}+i\mathbf{K}_{22}\cdot\mathbf{R}}, \end{aligned} \quad (4.11)$$

where $|\Gamma(ij)\rangle = |\phi(i)\rangle_A |\phi(j)\rangle_B$, $\mathbf{K}_{ij} = \mathbf{k}_i^A + \mathbf{k}_j^B$, and $\mathbf{k}_{ij} = (m_B \mathbf{k}_i^A - m_A \mathbf{k}_j^B)/(m_A + m_B)$. The incident wavefunction in Eq. (4.11) generally consists of four independent terms having different center of mass momenta. It is possible for the terms proportional to $a_1 b_2$ and $a_2 b_1$ to interfere if the following conditions are satisfied:

$$\mathbf{K}_{12} = \mathbf{K}_{21} \quad (4.12)$$

$$\frac{\hbar^2 k_{12}^2}{2\mu} + E_A(1) + E_B(2) = \frac{\hbar^2 k_{21}^2}{2\mu} + E_A(2) + E_B(1), \quad (4.13)$$

where $\mu = m_A m_B / (m_A + m_B)$ is the reduced mass of the collision pair. $E_A(i)$ and $E_B(i)$ are the energies of the eigenstates $|\phi(i)\rangle_A$ and $|\phi(i)\rangle_B$. These conditions state that the two interfering terms should have the same center of mass momentum and the same energy in the center of mass frame, as required by Eq. (4.7). The terms proportional to $a_1 b_1$ and $a_2 b_2$ lead to uncontrollable satellite terms in the cross section.

The conditions for scattering interference in Eqs. (4.12) and (4.13) can be easily satisfied for collisions between identical particles. Since $E_A(i) = E_B(i)$ for identical particles, conservation of energy in the center of mass reduces to the condition $k_{12}^2 = k_{21}^2$ which is always satisfied.

Interference effects in collisions between non-identical particles is harder to achieve due to the necessary correlations between internal and translational degrees of freedom of the colliding partners. Equation 4.13 shows that interference between incoming scattering states can occur when $E_A(1) = E_A(2)$ and $E_B(1) =$

$E_B(2)$. This is true when particle A is in a single internal state and particle B is in a superposition of degenerate states, or when each particle is in a superposition of degenerate states. In Ref. [172] it was shown that the branching ratio between reactive and non-reactive scattering for $D + H_2$ can be controlled by preparing the molecule in a superposition of $(2J + 1)$ degenerate rotational sublevels $|JM_J\rangle$ and the atom is in the ground state. Control of atomic Penning ionization was also demonstrated numerically for $Ne^* + Ar$, where the Ne atom is prepared in a superposition of degenerate magnetic sublevels [173, 174]. Although these schemes for control of collisions between non-identical particles can be extended to bimolecular scattering, it would be desirable to have an alternative method in which atoms or molecules are prepared in a superposition of non-degenerate states, which could be easily prepared using a single near resonant electromagnetic pulse.

4.4 Field induced interference of scattering channels

In this section an alternative method is presented for coherent control of collisions between non-identical particles. The degeneracy condition in Eq. (4.13) can be written as

$$\frac{\hbar^2 k_{12}^2}{2\mu} + E_B(2) - E_B(1) = \frac{\hbar^2 k_{21}^2}{2\mu} + E_A(2) - E_A(1). \quad (4.14)$$

If the relative kinetic energies at each side of the equation are the same, i.e., $k_{12}^2 = k_{21}^2$, then the condition reduces to the equality of energy level splittings between the superposition states for both particles

$$E_B(2) - E_B(1) = E_A(2) - E_A(1). \quad (4.15)$$

This condition is easily satisfied for two identical particles if the superposition states are the same for both collision partners, but is generally not satisfied for non-identical particles. However, if the energies of the superposition states of one or both particles are sensitive to an external static field, it should be possible to shift the relevant energy splittings so that Eq. (4.15) is satisfied and the scattering channels $|\phi_A(1)\rangle|\phi_B(2)\rangle$ and $|\phi_A(2)\rangle|\phi_B(1)\rangle$ can interfere. This scheme is general for atomic and molecular scattering provided the chosen states of the coherent superposition can be shifted using static magnetic or electric fields and relative kinetic

energy and center of mass momenta are the same for the interfering scattering channels. Equality of momenta and relative kinetic energy is ensured for identical particles, and can be achieved for non-identical particles if the wave vector of a particle in different internal states is the same, i.e.

$$\mathbf{k}_1^A = \mathbf{k}_2^A = \mathbf{k}_A \quad \text{and} \quad \mathbf{k}_1^B = \mathbf{k}_2^B = \mathbf{k}_B. \quad (4.16)$$

Superposition of two internal states $|\phi(1)\rangle$ and $|\phi(2)\rangle$ with the same momentum can be prepared using a near resonant light pulse. If particle A, for example, is initially in the internal state $|\phi_A(1)\rangle$ with well-defined momentum $\hbar\mathbf{k}_A$, the momentum transfer from the light field during the light-matter interaction should be negligible in comparison with $\hbar\mathbf{k}_A$.

When the conditions in Eqs. (4.15) and (4.16) are satisfied, the incoming wave function in the limit of large interatomic distances can be rewritten as

$$|\psi_{\text{inc}}\rangle = \{a_1b_2|\Gamma(12)\rangle + a_2b_1|\Gamma(21)\rangle + a_1b_1|\Gamma(11)\rangle + a_2b_2|\Gamma(22)\rangle\} e^{i\mathbf{k}\cdot\mathbf{r} + i\mathbf{K}_{CM}\cdot\mathbf{R}_{CM}}. \quad (4.17)$$

Since Eq. (4.16) is satisfied, the incoming wavefunction is composed of four terms with the same relative and center of mass momenta. If an external field is used to shift the internal levels of particles A and B so that Eq. (4.15) is satisfied, then the first two channels become degenerate in the center of mass frame and can therefore interfere as described in Section 4.3. The main advantage of this coherent control scheme is its generality since it is always possible to choose field sensitive states in atoms and molecules for the required coherent superpositions. One possible drawback is that the degeneracy condition in Eq. (4.15) is satisfied only for a narrow range of field strengths. This disadvantage is also shared by field-induced Feshbach resonances in ultracold scattering where degeneracy between field-sensitive states is also required [57].

4.5 Control of ultracold atomic scattering

The production of cold and ultracold atoms and molecules has opened the possibility to study interactions between particles in a temperature regime where their translational energy is smaller than perturbations due to external fields [22, 24,

48, 175]. External fields shift the atomic or molecular energy levels by up to a few Kelvin, so control of gas-phase dynamics can be most easily achieved for translational energies near or less than one Kelvin. External control of collisions and chemical reactions has been a long sought-after goal in the fields of ultracold physics and chemistry [24]. Schemes for control using laser fields [162, 176] or static fields [177–180] have been developed. An alternative method is coherent control of collisions based on interference between scattering wave functions as discussed in previous sections.

4.5.1 Alkali-metal atoms in 2S states

Let us consider a specific example where the field-induced interference scheme can be demonstrated. Atomic scattering at ultracold temperatures has been widely studied both theoretically and experimentally [54]. The coherent control scheme described in Sec. 4.4 for ultracold atomic scattering can be used with an optically trapped mixture of ultracold alkali metal atoms. The ground electronic term of alkali atoms excluding the nuclear spin is $^2S_{1/2}$. The coupling of angular momenta $\mathbf{F} = \mathbf{S} + \mathbf{I}$ between the electron spin \mathbf{S} and the nuclear spin \mathbf{I} , results in the hyperfine splitting of the ground electronic level. The atomic states including hyperfine couplings in the absence of magnetic fields can be represented in the coupled basis $|FM_F\rangle$, where F is the total angular momentum and M_F its projection along the quantization axis. For a given value of the nuclear spin I , the total angular momentum takes the values $F = I + 1/2$ and $F = I - 1/2$. The Hamiltonian $\hat{H}_{\text{HF}} = \gamma \mathbf{S} \cdot \mathbf{I}$ describes the hyperfine splitting of the electronic state. The hyperfine coupling constant γ is on the order of 1 – 10 GHz for most alkali-metal atoms and is proportional to the zero-field splitting between the hyperfine states [181].

The interaction between the magnetic moment of the electron and the nucleus is described by the Hamiltonian $\hat{H}_B = 2\mu_B \mathbf{S} \cdot \mathbf{B} + g_I \mu_N \mathbf{I} \cdot \mathbf{B}$, where g_I denotes the nuclear g-factor, μ_B is the Bohr magneton and μ_N is the nuclear magneton. This Hamiltonian is best represented using the uncoupled basis $|SM_S\rangle|IM_I\rangle$, where M_S and M_I are the projections of the spin and nuclear angular momenta, respectively, along the direction of the magnetic field. The matrix elements of $\hat{H}_{\text{HF}} + \hat{H}_B$ in the coupled and uncoupled basis can be obtained using the methods described in Ap-

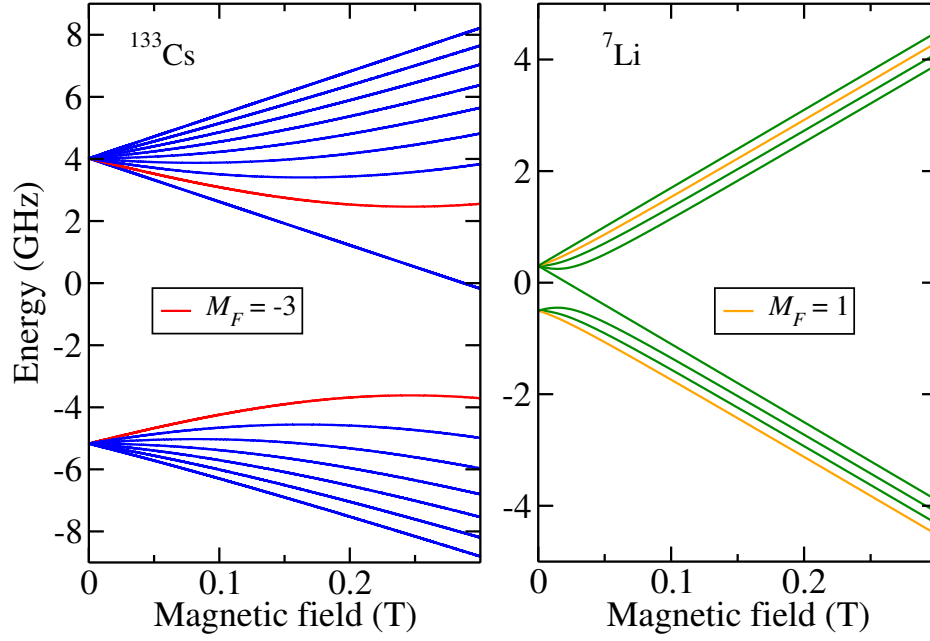


Figure 4.1: Zeeman effect for ^7Li and ^{133}Cs atoms in the ground electronic state. For each value of the total angular momentum projection M_F , there are two hyperfine states whose energies diverge in the strong field limit. The hyperfine levels with projection $M_F = -3$ for Cs and $M_F = 1$ for Li are used in the text. Data is taken from Ref. [178].

pendix C. In the presence of a weak magnetic field along the Z axis, each hyperfine level F splits into $(2F + 1)$ magnetic sublevels, as shown in Fig. 4.1 for ^7Li and ^{133}Cs atoms. The nuclear spin of ^7Li is $I = 3/2$ which results in the hyperfine levels $F = 1$ and $F = 2$ at zero magnetic fields. The zero-field splitting between these levels is 804 MHz. The nuclear spin of ^{133}Cs is $I = 7/2$, which results in the levels $F = 3$ and $F = 4$ separated in energy by approximately 9.2 GHz in the absence of magnetic fields. Ultracold mixtures of ^7Li and ^{133}Cs atoms in optical dipole traps have been produced and studied experimentally [182].

The total angular momentum projection $M_F = M_S + M_I$ is a good quantum number even in the presence of the magnetic field due to the cylindrical symmetry of the Hamiltonian $\hat{H}_{\text{HF}} + \hat{H}_{\text{B}}$. Two states with the same projection M_F that belong to different hyperfine manifolds F in the weak field limit can be used to prepare

the superposition of non-degenerate states with the same momentum

$$|\psi_{M_F}\rangle = a_1|\phi(1), M_F\rangle_A e^{i\mathbf{k}\cdot\mathbf{r}} + a_2|\phi(2), M_F\rangle_A e^{i\mathbf{k}\cdot\mathbf{r}}. \quad (4.18)$$

The preparation of such superposition state for each collision partner is a necessary step in the scheme for coherent control of scattering discussed in Sec. 4.3. The state in Eq. (4.18) can be prepared using the following procedure: (i) The population of the $F = I - \frac{1}{2}$ and the $F = I + \frac{1}{2}$ manifolds is optically pumped into one of the stretched states $|I - \frac{1}{2}, I - \frac{1}{2}\rangle$ [183]. (ii) A small magnetic field is applied to split the energy levels of the hyperfine states corresponding to the different projections M_F . (iii) The population is transferred from the stretched state $|I - \frac{1}{2}, I - \frac{1}{2}\rangle$ to a state $|I - \frac{1}{2}, M_F\rangle$ with a defined projection M_F via Rapid Adiabatic Passage [184]. (iv) A coherent superposition of states with the same projections $|I - \frac{1}{2}, M_F\rangle$ and $|I + \frac{1}{2}, M_F\rangle$ is produced using linearly polarized light, and the evolution of the Bloch vector can be controlled by changing laser parameters. After the preparation process, the magnitude of the net momentum transfer to the atoms is given by their hyperfine splitting. The momentum transfer is approximately a factor of 10^{-7} smaller than the atomic momenta for gas mixture with equilibrium temperature of $\sim 10 \mu\text{K}$ [182]. The equality of momenta in Eq. (4.16) for the internal states $|\phi(1), M_F\rangle$ and $|\phi(2), M_F\rangle$ is thus ensured.

When the two atomic species are independently prepared in a superposition of hyperfine states as in Eq. (4.18), the incoming scattering wavefunction can be written as in Eq. (4.17). The scattering state consists of four channels with different energies in the center of mass frame. The incoming channels have the same center of kinetic energy $\hbar^2\mathbf{k}/2\mu$, where μ is the reduced mass of the collision pair. As suggested in Sec. 4.4, a magnetic field can be used to shift the energies superposition states for both species to the point where the degeneracy condition (4.15) is satisfied. For any given pair of superposition states on each atom, it is possible to find a magnetic field at which the energy level splittings between the superposition states are degenerate. For ^7Li and ^{133}Cs atoms, the energy difference between the hyperfine states $|\phi(1), M_F\rangle$ and $|\phi(2), M_F\rangle$ for several values of M_F are shown in Fig. 4.2. For two specific projections M_F for Li and M'_F for Cs, the degeneracy between the incoming channels $|\Gamma(12)\rangle$ and $|\Gamma(21)\rangle$ in Eq. (4.17) is

achieved at the intersection point between the corresponding curves. The energy splittings that cross at the lowest value of the magnetic field correspond to states with projection $M_F = 1$ for ^7Li and $M'_F = -3$ for ^{133}Cs atoms at $B = 0.205187980$ Tesla.

The range of magnetic field values that induce interference between incoming scattering states depends on the range of energies at which condition (4.15) is satisfied. This energy range is centered at the intersection point between two curves in Fig. (4.2) and is given by the sum of the natural widths of the hyperfine states. The corresponding range of magnetic fields can be deduced from Fig. (4.2). For alkali metal atoms, the widths of the excited hyperfine levels are infinitesimal, so the range of magnetic fields that induce interference is extremely narrow. However, if electronic states are used instead of hyperfine states to create the required superpositions, this range of magnetic fields is significantly larger.

4.5.2 Coherent control of elastic vs inelastic scattering

Efficient sympathetic cooling of atoms and molecules in electromagnetic traps relies on a favourable ratio between elastic and inelastic collisional cross sections. While large elastic collision rates allows for rapid thermalization in a mixture of two species with different temperatures, inelastic collisions lead to loss of particles from the trap, as the kinetic energy released in inelastic processes usually exceeds the trapping energy. Therefore, it is desirable to have a large elastic to inelastic ratio in order for sympathetic cooling schemes to be practical.

In ultracold collisions, the kinetic energy of the collision pair $E_k = \hbar^2 k^2 / 2\mu$ is low enough to consider only S -wave scattering [23, 54]. The total cross section in the s -wave regime for scattering from the incoming state ψ_{inc} into the state $\Gamma(n')$ is given by

$$\sigma(n') = \frac{\pi}{k^2} |\langle \Gamma(n') | \hat{T} | \psi_{\text{inc}} \rangle|^2, \quad (4.19)$$

where k is the wave number of the incident channel $|\psi_{\text{inc}}\rangle$, and n' represents the set of quantum numbers that define the outgoing channel $|\Gamma(n')\rangle$. In elastic scattering the incoming and outgoing channels are identical, i.e., $\Gamma(n') = \psi_{\text{inc}}$. Inelastic processes correspond to a change in the internal state of the particle as a result of the collisional event, i.e., $\Gamma(n') \neq \psi_{\text{inc}}$. In conventional scattering theory, the incom-

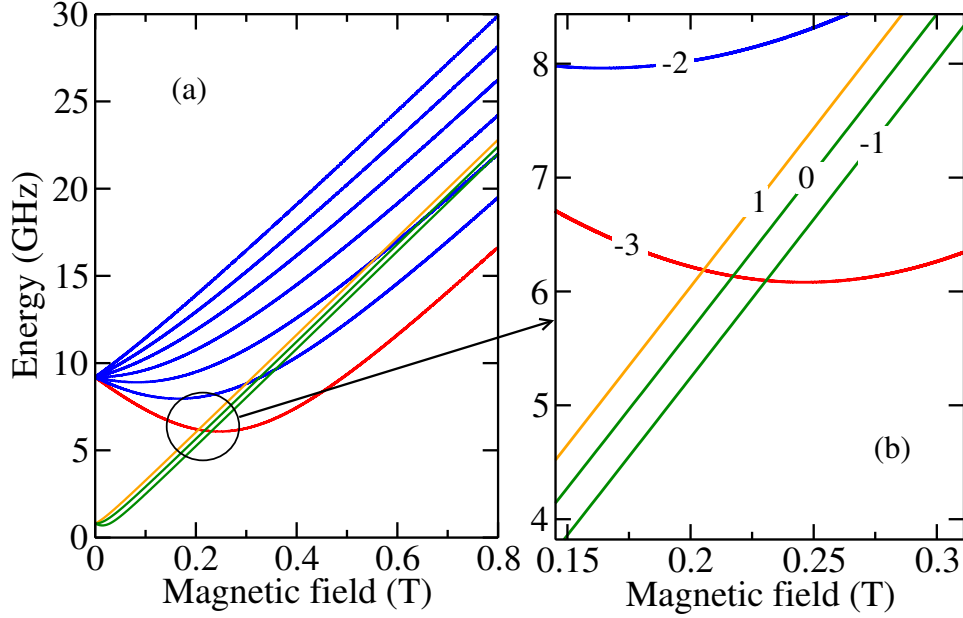


Figure 4.2: Energy difference between atomic Zeeman states with the same value of the total angular momentum projection M_F as a function an applied magnetic field. (a) Curves for ^7Li and ^{133}Cs are shown with the same color coding as in Fig. 4.1. (b) Expanded view of the encircled region showing the intersection point at $B = 0.20518798$ Tesla, where the incoming scattering channels $|\phi(1), M_F\rangle_{\text{Li}}|\phi(2), M'_F\rangle_{\text{Cs}}$ and $|\phi(2), M_F\rangle_{\text{Li}}|\phi(1), M'_F\rangle_{\text{Cs}}$ are degenerate for $M_F = 1$ and $M'_F = -3$.

ing wavefunction consists of a single channel $\psi_{\text{inc}} = \Gamma(n)$. Integral cross sections are measured over a range of kinetic energies in bulk experiments, or at a single collision energy in the collision of atomic and molecular beams.

The method for coherent control of collisions described in previous sections requires the incident scattering wave function to be a superposition of the form

$$|\psi_{\text{inc}}\rangle = \{a_1 b_2 |\Gamma(12)\rangle + a_2 b_1 |\Gamma(21)\rangle + a_1 b_1 |\Gamma(11)\rangle + a_2 b_2 |\Gamma(22)\rangle\} e^{i\mathbf{k}\cdot\mathbf{r} + i\mathbf{K}_{CM}\cdot\mathbf{R}_{CM}}. \quad (4.20)$$

In general, for non-identical particle the scattering superposition consists of incoming channels with different total energy. For the incident state in Eq. (4.20), the

total scattering cross section is determined by the sum,

$$\begin{aligned}\sigma(n') &= |C_{11}|^2 \sigma(n'|11) + |C_{22}|^2 \sigma(n'|22) + |C_{12}|^2 \sigma(n'|12) + |C_{21}|^2 \sigma(n'|21) + \\ &\quad + \sum_{ij} \sum_{nm \neq ij} C_{ij}^* C_{nm} \sigma(ij|nm)\end{aligned}\quad (4.21)$$

where

$$\sigma(n'|ij) = \frac{\pi}{k_{ij}^2} |\langle \Gamma(n') | \hat{T} | \Gamma(ij) \rangle|^2, \quad (4.22)$$

and

$$\sigma(ij|nm) = \frac{\pi}{k_{ij} k_{nm}} \langle \Gamma(ij) | \hat{T} | \Gamma(n') \rangle \langle \Gamma(n') | \hat{T} | \Gamma(nm) \rangle. \quad (4.23)$$

We have defined the amplitudes $C_{ij} = a_i b_j = |a_i b_j| e^{i(\theta_i + \theta_j)}$, involving the product of the single-particle preparation coefficients $a_i = |a_i| e^{i\theta_i}$ and $b_i = |b_i| e^{i\theta_i}$. The wavenumber of the incoming channel $\Gamma(ij)$ is $k_{ij} = \sqrt{2\mu[E - E_{ij}]}/\hbar$, where μ is the reduced mass of the collision complex and $E_{ij} = E_A(i) + E_B(j)$ is the channel internal energy.

The summation over crossed terms in Eq. (4.20) correspond to quantum interferences between incoming scattering states. The interference cross section $\sigma(ij|nm)$ in Eq. (4.23) vanishes if the incoming channels $\Gamma(ij)$ and $\Gamma(nm)$ are not degenerate. As discussed in Section 4.4, it is possible to use an external field to bring the channels $\Gamma(12)$ and $\Gamma(21)$ into degeneracy, so they can interfere. All the other crossed terms vanish because they violate energy conservation. In experiments where the cross sections are measured at a given total energy E , not all terms in Eq. (4.21) contribute simultaneously to the signal. If the cross section is measured at the total energy $E = \hbar k_{12}^2/2\mu + E_{12}$, the cross sections $\sigma_E(n'|11)$ and $\sigma_E(n'|22)$ vanish by energy conservation and Eq. (4.21) reduces to

$$\sigma_E(n') = |C_{12}|^2 \sigma_E(n'|12) + |C_{21}|^2 \sigma_E(n'|21) + [C_{12}^* C_{21} \sigma_E(12|21) + \text{c.c.}]. \quad (4.24)$$

The satellite cross section $\sigma_E(n'|21)$ and the interference cross section $\sigma_E(12|21) = |\sigma_E(12|21)| e^{i\delta(12|21)}$ have been included to account for the possibility of the channels $\Gamma(12)$ and $\Gamma(21)$ to be degenerate. If the degeneracy requirement is not satisfied, only the first term contributes to the energy resolved signal. By defining the real

variables $x = |C_{11}/C_{12}|$, $y = |C_{22}/C_{12}|$, $z = |C_{21}/C_{12}|$, as well as the relative phase $\phi_{12} = \arg\{C_{21}/C_{12}\}$, Eq. (4.24) can be written as

$$\sigma_E(n') = \frac{\sigma_E(n'|12) + z^2 \sigma_E(n'|21) + 2z |\sigma_E(12|21)| \cos[\phi_{12} + \delta_{(12|21)}]}{1 + r^2}, \quad (4.25)$$

where $r^2 = x^2 + y^2 + z^2$. The cross section thus depends on the amplitude parameter $S = z^2/(1 + r^2)$ and the relative phase ϕ_{12} . The control parameter $0 \leq S \leq 1$ is bounded from below when $|C_{21}|^2 = |a_2|^2 |b_1|^2 = 0$, i.e., if at least one of the colliding particles is not in a prepared in a coherent superposition of internal states, but in the single state $|\phi_A(1)\rangle$ for particle A or state $|\phi_B(2)\rangle$ for particle B. The amplitude parameter S is equal to unity when $|C_{21}|^2 = 1$. In this case none of the collision partners is prepared in a coherent superposition, but particle A is prepared in the $|\phi_A(2)\rangle$ and particle B in state $|\phi_B(1)\rangle$.

The total inelastic cross section at energy $E = \hbar k_{12}^2/2\mu + E_{12}$ is obtained from Eq. (4.24) by summing over all possible outgoing channels, i.e, $\sigma_E^{\text{in}} = \sum_{n'} \sigma_E(n')$. The elastic cross section σ_E^{el} is obtained by setting $\Gamma(n') = \Gamma(12)$ in Eq. 4.24. The ratio ρ between elastic and inelastic scattering at total energy E can thus be written as

$$\rho(S, \phi_{12}) \equiv \frac{\sigma^{\text{el}}}{\sigma^{\text{in}}} = \frac{\sigma^{\text{el}}(12) + z^2 \sigma^{\text{el}}(21) + 2z |\sigma^{\text{el}}(12|21)| \cos(\phi_{12} + \delta_{(12|21)}^{\text{el}})}{\sigma^{\text{in}}(12) + z^2 \sigma^{\text{in}}(21) + 2z |\sigma^{\text{in}}(12|21)| \cos(\phi_{12} + \delta_{(12|21)}^{\text{in}})}, \quad (4.26)$$

where $\sigma^{\text{in}}(ij) = \sum_{n'} (\pi/k_{ij}^2) \langle \Gamma(n') | \hat{T} | \Gamma(ij) \rangle$ and

$$\sigma^{\text{in}}(ij|ji) = (\pi/k_{ij} k_{ji}) \sum_{n'} \langle \Gamma(ij) | \hat{T} | \Gamma(n') \rangle \langle \Gamma(n') | \hat{T} | \Gamma(ji) \rangle.$$

Analogous definitions hold for the elastic cross sections by setting $\Gamma(n') = \Gamma(12)$. The material phases $\delta_{(12|21)}^{\text{el}} = \arg\{\sigma^{\text{el}}(12|21)\}$ and $\delta_{(12|21)}^{\text{in}} = \arg\{\sigma^{\text{in}}(12|21)\}$ are determined by the dynamical properties of the system.

In order to illustrate the coherent control scheme described here, let us consider the collision between ultracold ^7Li and ^{133}Cs atoms. In Fig. 4.2 it is shown that when the atoms are prepared in coherent superpositions of hyperfine states, degeneracy between specific scattering states can be induced in the presence of a mag-

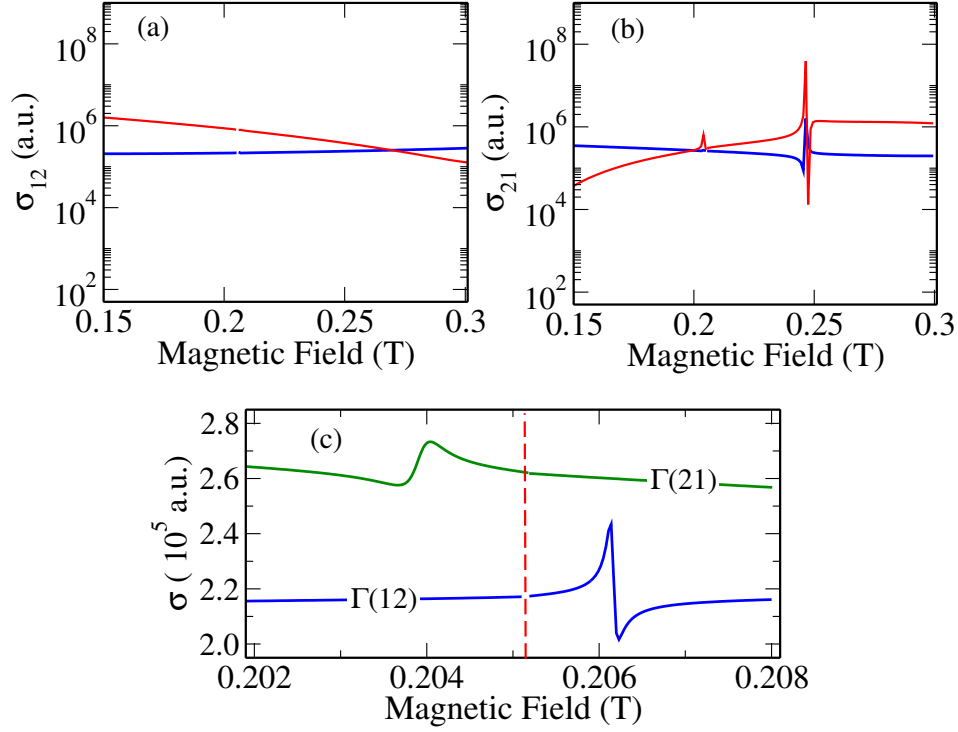


Figure 4.3: Elastic (blue line) and inelastic (red line) cross sections for collisions between ^7Li and ^{133}Cs atoms as a function of the magnetic field. (a) The incoming channel is $\Gamma(12) = |\phi_{\text{Li}}(1), M_F = 1\rangle |\phi_{\text{Cs}}(2), M'_F = -3\rangle$. (b) The incoming channel is $\Gamma(21) = |\phi_{\text{Li}}(2), M_F = 1\rangle |\phi_{\text{Cs}}(1), M'_F = -3\rangle$. (c) Elastic cross section for channels $\Gamma(12)$ and $\Gamma(21)$ near the point of degeneracy between the states at $B_{\text{deg}} = 0.20518798$ Tesla (shown with a dashed vertical line). The collision energy in each panel is 10^{-7} cm^{-1} . Cross sections are in atomic units.

netic field, at certain values of the field strength. As an example, the interference between incoming scattering states $\Gamma(12) = |\phi_{\text{Li}}(1), M_F = 1\rangle |\phi_{\text{Cs}}(2), M'_F = -3\rangle$ and $\Gamma(21) = |\phi_{\text{Li}}(2), M_F = 1\rangle |\phi_{\text{Cs}}(1), M'_F = -3\rangle$ is achieved at the magnetic field $B_{\text{deg}} = 0.20518798$ Tesla.

Elastic and inelastic cross sections $\sigma(ij)$ as well as interference cross sections $\sigma(ij|ji)$ can be obtained using the coupled-channel method [185]. A recently developed method for solving closed-channel equations for alkali-metal

atoms including the effect of magnetic fields is described in Ref. [178]. We use this method to evaluate the magnitude of the cross sections as a function of the magnetic field and the collision energy $\hbar k_{ij}^2/2\mu$. In Figure 4.3 the cross sections $\sigma(12)$ and $\sigma(21)$ for elastic and inelastic processes are shown as a function of the magnetic field for the fixed collision energy $E_k = 10^{-7} \text{ cm}^{-1}$. Panels (a) and (b) show the field-dependent elastic and inelastic cross sections for the incoming channels $\Gamma(12) = |\phi_{\text{Li}}(1), M_F = 1\rangle |\phi_{\text{Cs}}(2), M'_F = -3\rangle$ and $\Gamma(21) = |\phi_{\text{Li}}(2), M_F = 1\rangle |\phi_{\text{Cs}}(1), M'_F = -3\rangle$, respectively. Panel (c) is an expanded view of the elastic cross sections for both incoming channels near the region of degeneracy described earlier. In the region of magnetic fields shown in Fig. 4.3, a wide Feshbach resonance is present near $B = 0.245 \text{ T}$ for the incoming channel $|\Gamma(21)\rangle$ and smaller resonances occur near the magnetic field that induces degeneracy between the channels $|\Gamma(12)\rangle$ and $|\Gamma(21)\rangle$. However, as panel (c) shows, we are here interested in the region where the channels are energetically degenerate and there is no resonant structure in the cross section.

The ratio $\sigma^{\text{el}}/\sigma^{\text{in}}$ is of order unity near the magnetic field B_{deg} that induces degeneracy between the $\Gamma(12)$ and $\Gamma(21)$ channels, when the collision energy is 10^{-7} cm^{-1} . As the collision energy decreases, the inelastic cross section diverges according to the Wigner's threshold laws [23]. The magnitude of the interference cross section $\sigma^{\text{el}}(12|21) = (\pi/k_{12}k_{21}) \langle \Gamma(12) | \hat{T} | \Gamma(12) \rangle \langle \Gamma(12) | \hat{T} | \Gamma(21) \rangle$ is shown in Fig. 4.4 for magnetic fields approaching B_{deg} from below. Although one of the T -matrix elements involved in the definition of σ^{el} represents a transition between internal states upon collision, at the magnetic field B_{deg} these transition does not vary the kinetic energy in the center of mass frame. The diagonal matrix element $\langle \Gamma(12) | \hat{T} | \Gamma(12) \rangle$ can be considered independent of the collision energy and magnetic field in the range of variables considered here. For $B < B_{\text{deg}}$ the channel energy E_{21} is smaller than E_{12} . Therefore, in the limit of zero collision energy the transition matrix element $\langle \Gamma(12) | \hat{T} | \Gamma(21) \rangle$ vanishes, as the outgoing channel $\Gamma(12)$ is closed. If the collision energy is larger than the energy splitting $\Delta E = E_{12} - E_{21}$, the channel $\Gamma(12)$ is open and the interference cross section $\sigma^{\text{el}}(12|21)$ is finite. This is illustrated in Figure 4.4 for several collision energies. The magnitude of the interference cross section satisfies the Schwartz inequality $\sigma(12|21) \leq \sqrt{\sigma(12)\sigma(21)}$. The largest degree of controllability is

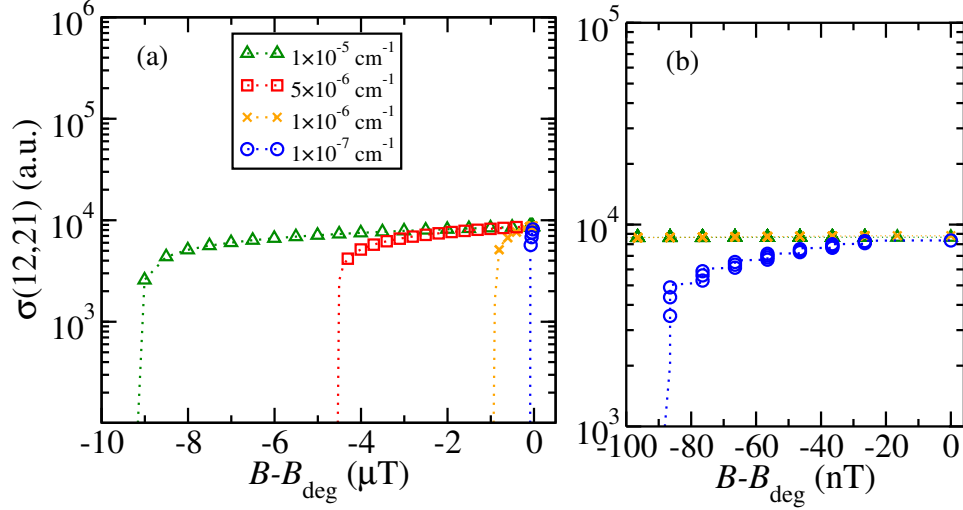


Figure 4.4: Magnitude of the elastic interference cross section $|\sigma^{\text{el}}(12|21)|$ as a function of magnetic field for collisions between ^7Li and ^{133}Cs atoms. Numerical data is shown for several collision energies. The magnetic field is shown with respect to the value B_{deg} where channel $\Gamma(12) = |\phi_{\text{Li}}(1), M_F = 1\rangle |\phi_{\text{Cs}}(2), M'_F = -3\rangle$ becomes degenerate with $\Gamma(21) = |\phi_{\text{Li}}(2), M_F = 1\rangle |\phi_{\text{Cs}}(1), M'_F = -3\rangle$.

achieved when the equality is satisfied. The curves in Fig. 4.4 converge to the value $\sigma^{\text{el}}(12|21) = 0.03\sqrt{\sigma^{\text{el}}(12)\sigma^{\text{el}}(21)}$ as the magnetic field approaches B_{deg} , which means that control is far from extensive for Li-Cs collisions.

In Figure 4.5 the control map for the elastic-to-inelastic ratio $\sigma^{\text{el}}/\sigma^{\text{in}}$ is shown as a function of the amplitude and phase parameters z and ϕ_{12} . The cross sections are calculated at the magnetic field $B = 0.205187980$ T and collision energy 10^{-5} cm^{-1} . The inelastic interference cross section satisfies $\sigma^{\text{in}}(12|21) = 0.30\sqrt{\sigma^{\text{in}}(12)\sigma^{\text{in}}(21)}$. When the atoms are not prepared in coherent superpositions ($z = 0$), the ratio ρ is approximately 2.7. This ratio can be increased only by a modest factor due to the small value of $|\sigma^{\text{el}}(12|21)|$.

In summary, this chapter presents a scheme to induce interference between scattering states in ultracold collisions using static magnetic fields. The scheme is based on the preparation of coherent superpositions of Zeeman states for each collision partner. The energy difference between Zeeman states forming the super-

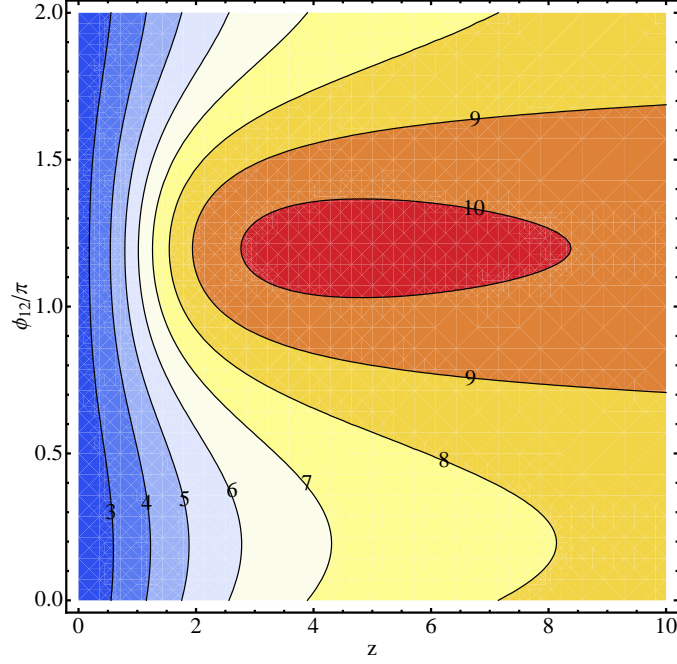


Figure 4.5: Control map for the ratio $\rho(z, \phi_{12}) = \sigma^{\text{el}}/\sigma^{\text{in}}$ between elastic and inelastic total cross sections for collisions between ^7Li and ^{133}Cs atoms, as a function of the amplitude and phase control parameters z and ϕ_{12} . The plot corresponds to the magnetic field $B_{\text{deg}} = 0.205187980$ Tesla, which induces interference between the incoming channels $\Gamma(12)$ and $\Gamma(21)$. The collision energy is 10^{-5} cm^{-1} .

positions is tuned by the magnetic field. For a certain value of the magnetic field, two incoming channels become degenerate, and the collision cross section includes an interference term that depends on the magnitudes and phases of the coefficients of the initial superpositions. The scheme we propose is general, and can be applied to collisions of ultracold molecules and molecules in beams. The energy levels of dipolar molecules can be shifted by dc electric fields, so electric fields can also be used to induce interference in collisions of polar molecules or in atom-molecule collisions. The possibility of using electric or magnetic fields makes the scheme more flexible and independent of the choice of the trapping method. This may be an advantage for future experimental realizations of the scheme.

Chapter 5

Molecular crystals with cold polar molecules

5.1 Chapter overview

Interacting polar molecules in individual sites of an optical lattice are gas-phase analogues of solid state molecular crystals. In this Chapter it is shown that using external field control of binary interactions leads to control of collective phenomena in an ensemble of polar molecules. In Section 5.2 the basic theory necessary to describe an ordered ensemble of interacting molecules is presented. In Section 5.2.3 I focus the discussion on the lowest-energy collective rotational excitations of the ensemble (rotational excitons), and discuss how an external DC electric field modifies the single exciton properties. In Section 5.3 I present the study of an ordered array of polar molecules with a small fraction of impurity molecules, in order to simulate a real impure solid at low temperatures, where the coupling to phonons is suppressed. In Section 5.3.1 it is shown that a DC electric field can be used to tune the energy level structure of the impurities so that scattering of a travelling exciton wave by the impurity is suppressed in a coherent way. In Section 5.3.2 it is shown that by choosing the appropriate field strength, a transition from localized to delocalized exciton states in an impure lattice can be achieved. Applications of this transport control scheme are suggested in Section 5.4.

5.2 Interacting polar molecules in optical lattices

Optical trapping of diatomic molecules was briefly discussed in Chapter 2. One important goal in the field of trapped molecules is the realization of quantum phases with ultracold polar molecules [80, 82, 96]. For example, the dipole-dipole interaction between polar molecules is predicted to induce novel features in the collective properties of dipolar molecular BEC [64]. Some of these features have already been observed using atoms with large magnetic dipole moments [65], but the significantly larger magnitude of electric dipolar interactions make molecules attractive candidates for the experimental study of dipolar quantum gases. Many of these applications require temperatures in the nanokelvin regime and large densities [25]. Optically trapped molecules can have temperatures in the microkelvin regime and higher [15, 18, 21], and molecular densities smaller than those required for quantum degeneracy. For such conditions, several research goals have been pursued theoretically and experimentally such as precision measurements and controlled chemistry [25]. These applications exploit the small degree of thermal noise at cold and ultracold temperatures to control single particle properties and two-particle interactions. In Chapter 3 it was shown that external fields can be used to modify the long-range dipole-dipole interaction between two distant molecules. Molecules were considered to be fixed in space, which can be realized experimentally by trapping molecules in individual sites of an optical lattice [20, 137]. If we assume the lattice is deep enough to suppress collision between molecules, it is possible to study the internal state dynamics of an ensemble of interacting polar molecules. This section describes the low-energy collective properties of such an ensemble using standard methods in condensed-matter theory [84, 99].

5.2.1 Hamiltonian in second-quantized form

Let us consider a lattice of N molecules fixed at the minima of an optical lattice potential. Let \mathbf{R}_i denote the position of the molecule i . The single molecule states are written as $|f_i\rangle$, where f denotes an internal state and i the position of the molecule in the lattice. The Hamiltonian for the many-body system is

$$\hat{\mathcal{H}} = \sum_i \hat{H}_i + \frac{1}{2} \sum_i \sum_{j \neq i} \hat{V}_{ij}, \quad (5.1)$$

where \hat{H}_i is the single-molecule Hamiltonian and \hat{V}_{ij} represents the interaction between molecules in different sites. The complete set of orthonormal states $|f_i\rangle$ satisfy the equation $\hat{H}_i|f_i\rangle = \epsilon_f|f_i\rangle$. We assume the overlap between molecular states at different sites vanishes, i.e., $\langle f_i|f_j\rangle \rightarrow 0$, but this restriction can be easily relaxed.

The eigenstates of the Hamiltonian in Eq. (5.1) can be written as $|\dots, \zeta_i, \dots\rangle$ where the set of N coordinates ζ_i define the single-particle eigenstates $|f_i\rangle$ for each molecule. For the case of molecules in the electronic and vibrational ground state, $|f\rangle$ are rotational states defined in terms of two angular coordinates $\zeta \equiv (\theta, \phi)$ (See Chapter 2). Alternatively, the eigenstates of the many-body Hamiltonian in Eq. (5.1) can be described by a set of N occupation numbers n_{if} , where $n_{if} = 1$ indicates that molecule i is in state f and $n_{if} = 0$ indicates that it is not. The occupation numbers for a given molecule satisfy the completeness relation $\sum_f n_{if} = 1$, which is analogous to $\sum_f |f_i\rangle\langle f_i| = \hat{1}$. In the occupation number representation the number operator \hat{n}_{if} is diagonal and satisfies $\hat{n}_{if}|\dots, n_{if}, \dots\rangle = n_{if}|\dots, n_{if}, \dots\rangle$, where $|\dots, n_{if}, \dots\rangle$ is the many-body wavefunction. The Hermitian number operator can be written in as a product

$$\hat{n}_{if} = \hat{b}_{if}^\dagger \hat{b}_{if},$$

where the non-Hermitian operators \hat{b}_{if}^\dagger and \hat{b}_{if} satisfy the equations

$$\hat{b}_{if}^\dagger |\dots, n_{if}, \dots\rangle = (1 - n_{if}) |\dots, n_{if} + 1, \dots\rangle \quad (5.2)$$

$$\hat{b}_{if} |\dots, n_{if}, \dots\rangle = n_{if} |\dots, n_{if} - 1, \dots\rangle. \quad (5.3)$$

From these equations it can be shown that the operators \hat{b}_{if}^\dagger and \hat{b}_{if} anticommute for the same (if) indices

$$\hat{b}_{if} \hat{b}_{if}^\dagger + \hat{b}_{if}^\dagger \hat{b}_{if} = 1, \quad (5.4)$$

and commute for different indices

$$\hat{b}_{if} \hat{b}_{je}^\dagger - \hat{b}_{je}^\dagger \hat{b}_{if} = 0 \quad (5.5)$$

The many-body Hamiltonian in Eq. (5.1) can be rewritten by introducing the field operator $\hat{\Psi}^\dagger(\zeta) = \sum_{if} |f_i(\zeta)\rangle \hat{b}_{if}^\dagger$ and its Hermitian conjugate [84, 99]. The Hamil-

tonian in Eq. (5.1) can be written in second-quantized form by integrating over the set of molecular coordinates $\{\zeta\}$ as

$$\begin{aligned}\hat{H} &= \int d\zeta \hat{\Psi}^\dagger(\zeta) \hat{\mathcal{H}}(\zeta) \hat{\Psi}(\zeta) \\ &= \sum_{i,f} \varepsilon_f \hat{b}_{if}^\dagger \hat{b}_{if} + \frac{1}{2} \sum_{i,j \neq i} \sum_{f,f'} \sum_{e,e'} \langle f e | V_{ij} | f' e' \rangle \hat{b}_{if}^\dagger \hat{b}_{je}^\dagger \hat{b}_{if'} \hat{b}_{je'}.\end{aligned}\quad (5.6)$$

Since the Hamiltonian does not commute with the number operator \hat{n}_{if}^\dagger , the eigenstates are given by linear combinations of states of the form $|\dots, n_{if}, \dots\rangle$. The number operator satisfies the completeness relation $\sum_f \hat{b}_{if}^\dagger \hat{b}_{if} = \hat{1}$ for each molecule. Summing over all molecules in the array we obtain the relation $\sum_{i,f} \hat{b}_{if}^\dagger \hat{b}_{if} = N$. The derivation of the Hamiltonian in Eq. (5.6) is a general result in condensed-matter theory [84] and can also describe an ultracold gas of free or trapped interacting atoms if the single-particle wavefunction $|f\rangle$ is also characterized by momentum $\hbar\mathbf{k}$ [82]. The Hamiltonian in Eq. (5.6) is completely defined by the single-particle spectrum ε_f and the matrix elements of the interaction operator

$$\langle f_i | \langle e_j | V_{ij} | f'_i \rangle | e'_j \rangle$$

in the basis of molecular states. Since this matrix has infinite dimensionality, in practice one needs to truncate the single molecule basis. Although Eq. (5.6) is defined in terms of the state creation operators \hat{b}_{if}^\dagger and its Hermitian conjugate, it is possible to write the Hamiltonian in a way that refers only to excited states. If we denote the ground state as $|g\rangle$ and the excited states by $|e\rangle$ (or $|f\rangle$), we can define the transition operator -also called exciton operator- as

$$\hat{B}_{if}^\dagger = \hat{b}_{if}^\dagger \hat{b}_{ig} \quad (5.7)$$

as a non-Hermitian product of state operators. This operator annihilates the ground state $|g\rangle$ and creates the excited state $|e\rangle$ in molecule i . This is an alternative notation for the familiar projector $|e_i\rangle\langle g_i|$. Using these operators, the contribution from the ground and the excited states to the Hamiltonian in Eq. (5.6) can be separated. The excited state contributions can be divided into terms containing different pow-

ers of the operators \hat{B}_{ie}^\dagger and \hat{B}_{ie} , as it is shown in Appendix D for molecules with an arbitrary number of excited states.

5.2.2 Heitler-London and two-level approximations

The simplest truncation scheme for the interaction term in Eq. (5.6) results from the assumption that each molecule consists of a ground state ($f = g$) and a single excited state ($f = e$). In this two-level approximation the completeness relation for each molecule reads

$$\hat{n}_{ig} + \hat{n}_{ie} = 1. \quad (5.8)$$

In Appendix D it is shown that when the number of independent interaction matrix elements in Eq. (5.6) is restricted to the set $\mathcal{V} = \{\langle gg|V_{ij}|gg\rangle, \langle e0|V_{ij}|00\rangle, \langle eg|V_{ij}|eg\rangle, \langle eg|V_{ij}|ge\rangle, \langle ee|V_{ij}|eg\rangle, \langle ee|V_{ij}|gg\rangle, \langle ee|V_{ij}|ee\rangle\}$, the resulting Hamiltonian can be written as $\hat{H} = V_g + \hat{H}_e$. The first term is a constant energy for fixed molecules given by (see Eq. (D.26) in Appendix D)

$$V_g = N\varepsilon_g + \frac{1}{2} \sum_{i,j \neq i} \langle gg|V_{ij}|gg\rangle, \quad (5.9)$$

where N is the number of molecules and ε_g is the energy of the ground state. The excited state Hamiltonian \hat{H}_e can be written as (see Eq. (D.27) in Appendix D)

$$\begin{aligned} \hat{H}_e = & \sum_i A_i (\hat{B}_{ie}^\dagger + \hat{B}_{ie}) + \sum_{i,j \neq i} C_{ij} (\hat{B}_{ie}^\dagger + \hat{B}_{ie}) \hat{B}_{je}^\dagger \hat{B}_{je} \\ & + \sum_i (\varepsilon_{eg} + D_i) \hat{B}_{ie}^\dagger \hat{B}_{ie} + \frac{1}{2} \sum_{i,j \neq i} J_{ij} (\hat{B}_{ie}^\dagger + \hat{B}_{ie}) (\hat{B}_{je}^\dagger + \hat{B}_{je}) \\ & + \frac{1}{2} \sum_{i,j \neq i} U_{ij} \hat{B}_{if}^\dagger \hat{B}_{if} \hat{B}_{jf}^\dagger \hat{B}_{jf}. \end{aligned} \quad (5.10)$$

Each term in this equation represents ultimately possible couplings between two-molecule states due to the pairwise interaction between molecules. These couplings lead to transitions in each molecule that are illustrated in Fig. 5.1. The first term in Eq. (5.10) represents the creation or annihilation of an excitation $|g_i\rangle \rightarrow |e_i\rangle$ in molecule i due to the interaction with molecule j in its ground state $|g_j\rangle$ (see

panel (a) in Fig. 5.1). The excitation amplitude A_i is given by

$$A_i = \sum_{j \neq i} \langle eg | V_{ij} | gg \rangle. \quad (5.11)$$

The second term in Eq. (5.10) is analogous to the previous term. It represents the creation or annihilation of an excitation $|g_i\rangle \rightarrow |e_i\rangle$ in molecule i due to its interaction with molecule j in its excited state $|e_j\rangle$ (see panel (b) in Fig. 5.1). The amplitude C_{ij} for this process is given by

$$C_{ij} = \langle ee | V_{ij} | eg \rangle - \langle eg | V_{ij} | gg \rangle. \quad (5.12)$$

The third term in Eq. (5.10) contains the site energies. This is the sum of the single-particle excitation energy $\varepsilon_{eg} = \varepsilon_e - \varepsilon_g$ and the energy shift D_i due to the interaction between molecule i in the excited state and molecule j in the ground state. This so called gas-condensed matter shift [99] is given by

$$D_i = \sum_{j \neq i} \{ \langle eg | V_{ij} | eg \rangle - \langle gg | V_{ij} | gg \rangle \}. \quad (5.13)$$

If the molecules in the ensemble are not identical, the single-molecule excitation energies become site dependent $\varepsilon_{eg} \rightarrow \varepsilon_{eg}(i)$.

The fourth term in Eq. (5.10) represents excitation exchange processes involving two or four molecules. By expanding the product $(\hat{B}_{ie}^\dagger + \hat{B}_{ie})(\hat{B}_{je}^\dagger + \hat{B}_{je})$ we obtain the terms $\hat{B}_{ie}^\dagger \hat{B}_{je}$ and $\hat{B}_{ie}^\dagger \hat{B}_{je}^\dagger$ as well as their Hermitian conjugates. The term $\hat{B}_{ie}^\dagger \hat{B}_{je}$ represents the annihilation of an excitation in molecule j and the creation of an excitation in molecule i (see panel (c) in Fig. 5.1). The Hermitian conjugate of this operator represents the transfer of an excitation from molecule i to j . The excitation hopping amplitude J_{ij} is given by

$$J_{ij} = \langle eg | V_{ij} | ge \rangle. \quad (5.14)$$

The operator $\hat{B}_{ie}^\dagger \hat{B}_{je}^\dagger$ represents the creation of two excitations in molecules i and j . The Hermitian conjugate represents the annihilation of these two excitations (see panel (d) in Fig. 5.1). The amplitude for this processes is also given by Eq. (5.14).

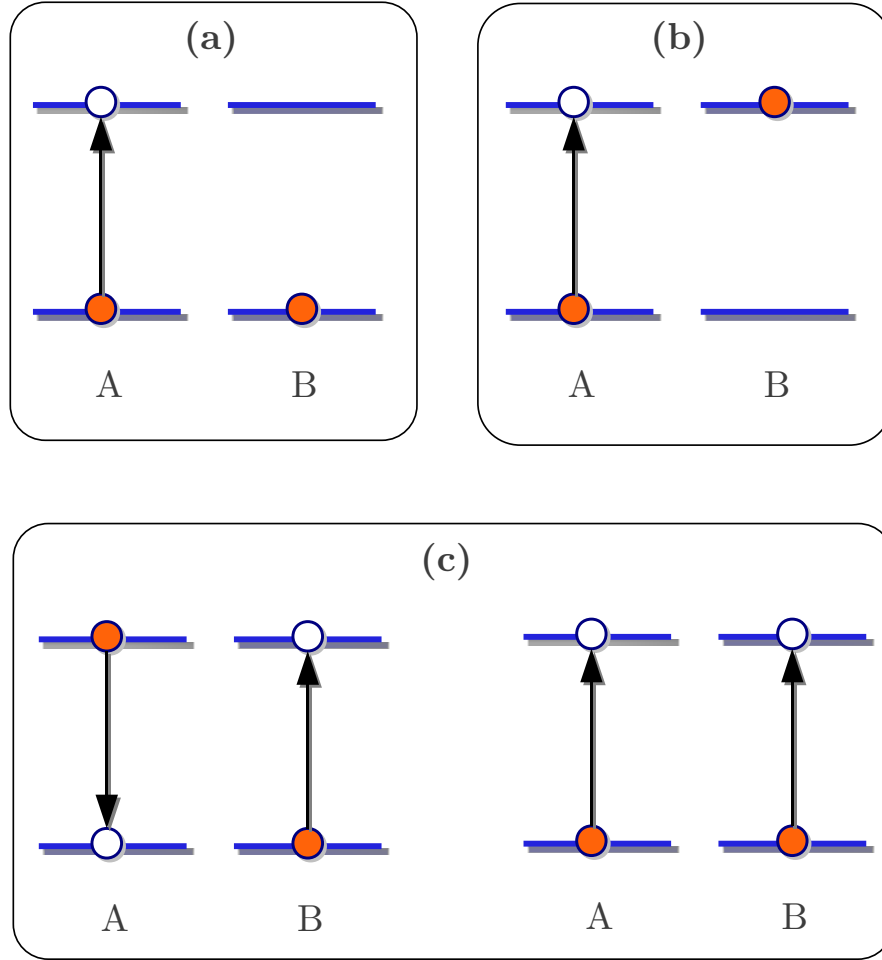


Figure 5.1: Schematic illustration of representative transitions induced by the dipole-dipole interaction between two-level molecules. Molecules A and B have two internal states.

The last term in Eq. (5.10) represents the electrostatic interaction between two excitations in different sites. The interaction energy U_{ij} can be written as

$$U_{ij} = \langle ee | V_{ij} | ee \rangle + \langle gg | V_{ij} | gg \rangle - 2\langle eg | V_{ij} | eg \rangle, \quad (5.15)$$

and can be either attractive or repulsive.

Up to this point the interaction operator \hat{V}_{ij} represents a general pairwise interaction. In this work, \hat{V}_{ij} is the dipole-dipole interaction between polar molecules (see Appendix B). This operator can be written in the form $\hat{V}_{ij} \approx \hat{d}_i \hat{d}_j$, where \hat{d} is the electric dipole operator. For single-particle states $|g\rangle$ and $|e\rangle$ with well-defined parity, the Hamiltonian parameters A_i , C_{ij} , D_i , and U_{ij} in Eq. (5.10) vanish because the associated dipole-dipole matrix elements are forbidden by parity. In this situation the excited state Hamiltonian \hat{H}_e simplifies to

$$\hat{H}_e = \sum_i \epsilon_{eg} \hat{B}_{ie}^\dagger \hat{B}_{ie} + \sum_{i,j \neq i} J_{ij} \hat{B}_{ie}^\dagger \hat{B}_{je} + \frac{1}{2} \sum_{i,j \neq i} J_{ij} (\hat{B}_{ie}^\dagger \hat{B}_{je}^\dagger + \hat{B}_{ie} \hat{B}_{je}). \quad (5.16)$$

The last term couples the absolute ground state of the ensemble $|g_1, \dots, g_i, \dots, g_N\rangle$ to states of the form $|g_1, \dots, e_i, e_j, \dots, g_N\rangle$ that belong to the two-excitation subspace \mathcal{S}_2 . For identical molecules, the states in \mathcal{S}_2 differ in energy from the absolute ground state by the amount $2\epsilon_{eg}$. If $\epsilon_{eg} \gg J_{ij}$ we can neglect the mixing between the ground state of the ensemble and states in \mathcal{S}_2 due to terms such as $\hat{B}_{ie}^\dagger \hat{B}_{ie}^\dagger$. If we are only interested in the ground state and states within the one-excitation subspace $\mathcal{S}_1 = \{|g_1, \dots, e_i, \dots, g_N\rangle : i = 1, \dots, N\}$ and the condition $J_{ij}/\epsilon_{eg} \ll 1$ is satisfied, we can neglect the last term in Eq. (5.16). The resulting Hamiltonian is referred to as the Heitler-London approximation [99], and is given by the quadratic form

$$\hat{H}_e = \sum_i (\epsilon_{eg} + D_i) \hat{B}_{ie}^\dagger \hat{B}_{ie} + \sum_{i,j \neq i} J_{ij} \hat{B}_{ie}^\dagger \hat{B}_{je}, \quad (5.17)$$

where we have included the energy shift D_i in the site energies for completeness. The Hamiltonian in the Heitler-London approximation commutes with the excitation number operator $\hat{N}_e = \sum_i \hat{B}_{ie}^\dagger \hat{B}_{ie}$, i.e., the total number of excitations is conserved. In the most general exciton Hamiltonian in Eq. (5.10) we include terms with odd powers of exciton operators (A_i and C_{ij} terms) that do not commute with \hat{N}_e . Even if the single-particle states do not have well-defined parity, these terms can be ignored if the condition $\epsilon_{eg} \gg \{A_i, C_{ij}\}$ is satisfied.

The Hamiltonian in Eq. (5.17) will be our working model to describe low-energy collective excitations in an ensemble of interacting molecules. The Hamiltonian is valid for a system of identical molecules coupled by the dipole-dipole

interaction. We restrict the discussion to the one-excitation subspace \mathcal{S}_1 which has the lowest excitation energies.

In Appendix D it is shown that the exciton Hamiltonian in the two-level approximation given by Eq. (5.10) can be written in terms of the Pauli spin matrices $\hat{\sigma}_i$. The transformation from exciton to spin operators results from a trivial redefinition of the energy reference.

5.2.3 Rotational excitons in molecular arrays

Interacting many-level polar molecules

After reviewing the formalism necessary to describe an ensemble of interacting molecules in the previous section, we now consider the possible experimental realization of a simple exciton model (see Eq. (5.17)) using polar molecules trapped in optical lattices. The many-body Hamiltonian was written earlier as $\hat{\mathcal{H}} = \sum_i \hat{H}_i + \frac{1}{2} \sum_i \sum_{j \neq i} \hat{V}_{ij}$, where \hat{H}_i describes a single molecule. We consider an optical lattice of $^1\Sigma$ polar molecules with one molecule in the rovibrational ground state per lattice site. If we ignore the AC Stark shift induced by the optical lattice laser beams, and consider molecules to be in the presence of a static DC electric field \mathbf{E} , we can write $\hat{H}_i = \sum_{l=1} B_e \hat{N}_l^2 - \vec{\mathbf{d}}_i \cdot \mathbf{E}$, where B_e is the rotational constant, $\vec{\mathbf{d}}_i$ is the electric dipole operator of molecule i . We ignore the hyperfine structure of the molecules. We assume that the tunneling of molecules to different lattice sites is entirely suppressed, which can be easily achieved by applying laser fields of sufficient power [79]. We consider lattice sites separated by 400 nm so the interaction between the molecules is entirely determined by the long-range dipole-dipole interaction potential.

In the absence of interactions $V_{ij} = 0$, the lowest excited states of the ensemble would be those of the individual molecules. For molecules prepared in the rovibrational ground state of the electronic ground state, the lowest excited states are $|N = 1, M_N = 0, \pm 1\rangle$. The rotational transition energy $\epsilon_{eg} \sim B_e$ is on the order of 10 GHz for most polar alkali-metal dimers considered in this work. In the absence of electric fields, the first rotational excited state is triply degenerate, but a DC electric field breaks the degeneracy between the $M_N = 0$ and the $M_N = \pm 1$ sublevels (the

rotational spectrum in DC and AC electric fields is discussed in Chapter 2.4). If the polarization of the trapping lasers are collinear with the DC electric field, the rotational states of the molecule have well defined rotational angular momentum projection M_N . If the polarization of the trapping lasers have components perpendicular to the direction of the DC electric field, the axial symmetry of the system is lost and mixing of states with different projections can occur (see Section 2.7.4).

It is shown in Appendix D that in the general case of a molecule with several excited states, the exciton Hamiltonian in Eq. (5.17) can be generalized as

$$\hat{H}_e = \sum_e \hat{H}_1(e) + \sum_{e,f \neq e} \hat{H}_2(e,f), \quad (5.18)$$

where e and f denote excited states. For rotational excited states the label e represents the energy and the projection M_N . For the rotational level $N = 1$ we have $e_1 = -1$, $e_2 = 0$, and $e_3 = 1$ according to the allowed values of M_N . The Hamiltonian $\hat{H}_1(e)$ can be written in the Heitler-London approximation as

$$\hat{H}_1(e) = \sum_i (\epsilon_{eg} + D_i^e) \hat{B}_{ie}^\dagger \hat{B}_{ie} + \sum_{i,j \neq i} J_{ij}^{ee} \hat{B}_{ie}^\dagger \hat{B}_{je}, \quad (5.19)$$

and the coupling between different excited states is provided by the Hamiltonian

$$\hat{H}_2(e,f) = \frac{1}{2} \sum_{i,j \neq 1} J_{ij}^{ef} \left(\hat{B}_{ie}^\dagger \hat{B}_{jf} + \hat{B}_{ie} \hat{B}_{jf}^\dagger \right). \quad (5.20)$$

The state dependent exciton operator \hat{B}_{if}^\dagger for $f = M_N$ within the $N = 1$ rotational manifold is defined by its action on the ground state wavefunction $\hat{B}_{if}^\dagger |g_i\rangle = |f_i\rangle$, where $|g\rangle = |(0), 0\rangle$ and $|f\rangle = |(1), M_N\rangle$. The notation $|(N), M_N\rangle$ is used to indicate that in the presence of a DC electric field the rotational angular momentum N is not a good quantum number. The coupling constants appearing in Eq. (5.20) are given by ($f \neq e$)

$$J_{ij}^{ef} = \langle e_i | \langle g_j | \hat{V}_{ij} | g_i \rangle | f_j \rangle,$$

The problem of finding the lowest excited states of an ensemble of interacting molecules reduces to finding the eigenvalues and eigenvectors of the Hamiltonian in Eq. (5.18). For a molecular array with arbitrary geometry that can include vacan-

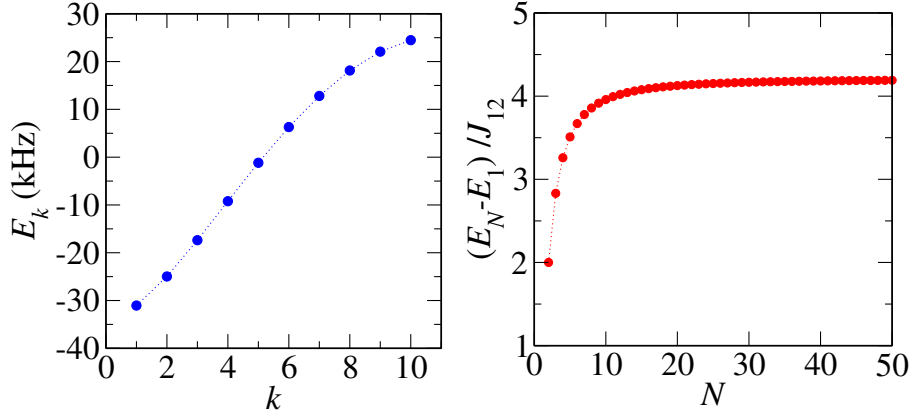


Figure 5.2: Exciton spectrum for a finite array of LiCs molecules separated by $a_L = 400$ nm. The array is in the presence of a DC electric field of 1 kV/cm oriented parallel to the array. At this electric field, the nearest-neighbour exchange constant $J_{12} = -14$ kHz. The exciton states correspond to the single-molecule transition $|(0), 0\rangle \rightarrow |(1), 0\rangle$. (a) Energies E_k centered at the single-molecule transition energy ϵ_{eg} for an array of $N = 10$ molecules. The index k labels the excitonic state. (b) Energy bandwidth $|E_N - E_1|$ as a function of the number of molecules N , in units of $|J_{12}|$.

cies, the eigenvalues and eigenvectors of the exciton Hamiltonian in Eq. (5.19) can be obtained by numerical diagonalization of the matrix $\hat{H}_1(e)$ in the basis of one-excitation states \mathcal{S}_1 . The excitonic eigenstates associated with the single-molecule excitation $|g\rangle \rightarrow |e\rangle$ can be written in the general form [99]

$$|\Psi_k^e\rangle = \sum_{i=1}^N C_{ik}^e |g_1, \dots, e_i, \dots, g_N\rangle \quad (5.21)$$

where the coefficients C_{ik}^e satisfy orthonormality conditions. Excitonic eigenstates are given by linear combinations of all the states representing the molecular ensemble having a single quantum of excitation. The square amplitudes $|C_{ik}^e|^2$ represent the probability of finding the molecule i in the excited state $|e\rangle$ if the system is in the excitonic state k . The rotational exciton state $|\Psi_k^e\rangle$ satisfies the eigenvalue equation $\hat{H}_1(e)|\Psi_k^e\rangle = E_k^e|\Psi_k^e\rangle$ and is also an eigenstate of the total projection operator $\hat{N}_Z = \sum_i \hat{N}_z$, with eigenvalue $M = \sum_i M_{N_i}$.

Figure 5.2(a) shows the excitonic energies E_k associated with the transition $|(0),0\rangle \rightarrow |(1),0\rangle$ in an 1D array of 10 LiCs molecules with lattice constant $a_L = 400$ nm. The array is in the presence of a DC electric field of 1 kV/cm oriented parallel to the array. For this field strength and orientation, $J_{12} = -14$ kHz. For an ensemble of N molecules, the dimension of the one-excitation subspace is $\mathcal{D}(\mathcal{S}_1) = N$. Therefore, there are N possible values of E_k in the spectrum. In panel (b) the width of the excitonic energy band $\Delta = |E_{k=N} - E_{k=1}|$ in units of $|J_{12}|$ is shown as a function of the number of molecules N . The bandwidth quickly converges to the asymptotic value $\Delta \approx 4$. Although the exciton bandwidth for a finite array with $N \sim 10$ molecules is similar to an infinite array, the discrete nature of the spectrum is manifest in the eigenstates. This is shown in Fig. 5.3, where the ground and the first excited excitonic states $|\Psi_{k=1}\rangle$ and $|\Psi_{k=2}\rangle$ are shown for an array of $N = 10$ molecules as in panel (a) of Fig. 5.2. The probability amplitudes C_{ik}^e for molecule i to be in the excited rotational state (see Eq. (5.21)) is plotted as a function of position. The shape of the wavefunction resembles the eigenstates of the particle in a box, in which the ground state wavefunction ($k = 1$) is peaked at the center of the interval and the first excited state ($k = 2$) is an odd function with a node at the center of the interval. In fact, the spectrum and eigenstates for a finite linear array can be obtained analytically by assuming the probability amplitudes in Eq. (5.21) to be $C_{ik} = A \sin(ik)$. The exciton wavefunction (omitting the excited state index) can be written as $|\Psi_k\rangle = \sum_i C_{ik} \hat{B}_i^\dagger |0\rangle$, where the relevant vacuum state $|0\rangle$ for this problem is the absolute ground state of the ensemble $|0\rangle \equiv |g_1, \dots, g_i, \dots, g_N\rangle$. Substituting this expansion in the Schrödinger equation $\hat{H}_1(e)|\Psi_k^e\rangle = E_k^e|\Psi_k^e\rangle$ and multiplying on the left by $\langle 0|\hat{B}_j$ we obtain the secular equation

$$(\epsilon_{eg} - E_k)C_{jk} + \sum_{j' \neq j} J_{jj'} C_{j'k} = 0. \quad (5.22)$$

We have assumed $\epsilon_{eg} \gg D_i$ and used the property $\hat{B}_n \hat{B}_{n'}^\dagger |0\rangle = \delta_{n,n'} |0\rangle$. Considering interactions between nearest-neighbours only and using $C_{ik} = A \sin(ik)$, Eq. (5.22) leads to the expression $(\epsilon_{eg} - E_k) \sin(ik) + J(2 \cos(k) \sin(ik)) = 0$, or equivalently

$$E_k = \epsilon_{eg} + 2J \cos(k). \quad (5.23)$$

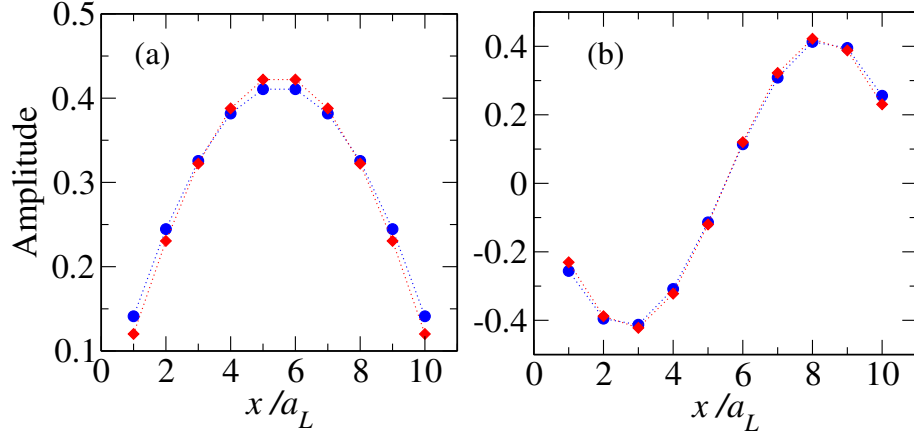


Figure 5.3: Lowest two exciton eigenstates $|\Psi_k\rangle$ for a finite array of $N = 10$ LiCs molecules with the same parameters as in panel (a) of Fig. 5.2. The ground ($k = 1$) and the first excited ($k = 2$) excitonic states of the array are shown in panels (a) and (b) respectively. The amplitude C_{ik}^e from Eq. (5.21) is plotted in the vertical axis as a function of the molecular position in units of the lattice constant a_L . The amplitudes obtained from numerical diagonalization (blue circles) and from an analytical model (red diamonds) are shown for comparison.

From the boundary condition $C_{N+1} = C_0 = 0$ for all k , the N allowed values of k are $k = n\pi/(N+1)$, with $n = 1, 2, \dots, N$. In the limit $N \rightarrow \infty$ the exciton spectrum becomes quasi-continuous. The normalized exciton wavefunction for a finite array is given by

$$|\Psi_k\rangle = \sqrt{\frac{2}{L}} \sum_i \sin\left(\frac{k\pi}{L}i\right) \hat{B}_i^\dagger |0\rangle, \quad (5.24)$$

where $L = N+1$ is the length of the quantization interval and $k = 1, \dots, N$. In Fig. 5.3 we compare the sinusoidal probability amplitudes C_{ik} with those obtained from direct numerical diagonalization including interactions beyond nearest neighbours. The difference between the results is negligible.

Exciton spectrum for homogeneous molecular arrays

For large homogeneous molecular arrays we can assume the periodic boundary conditions $C_{N+1} = C_1$ and expand the exciton operators in the site representation

as [84, 99]

$$\hat{B}_{ie} = \frac{1}{\sqrt{N}} \sum_{\mathbf{k}} \hat{B}_{\mathbf{k}e} e^{i\mathbf{k} \cdot \mathbf{R}_i}, \quad (5.25)$$

where the expansion coefficients $C_{i\mathbf{k}} = (1/\sqrt{N}) \exp(i\mathbf{k} \cdot \mathbf{R}_i)$ are eigenfunctions of the translation operator $\hat{T}_{\mathbf{R}_i}$ defined by $\hat{T}_{\mathbf{a}} \psi(\mathbf{x}) = \psi(\mathbf{x} + \mathbf{a})$. The quantum number \mathbf{k} is the wavevector defined within the first Brillouin zone. Inserting Eq. (5.25) into the one-excitation Hamiltonian $\hat{H}_1(e)$ in Eq. (5.19) gives (omitting the state index e)

$$\begin{aligned} \hat{H}_1 &= \frac{1}{N} \sum_i \sum_{\mathbf{k}, \mathbf{k}'} (\varepsilon_{eg} + D_i) e^{i(\mathbf{k}' - \mathbf{k}) \cdot \mathbf{R}_i} \hat{B}_{\mathbf{k}}^\dagger \hat{B}_{\mathbf{k}'} + \frac{1}{N} \sum_{i,j} \sum_{\mathbf{k}, \mathbf{k}'} J_{ij} e^{i\mathbf{k}' \cdot \mathbf{R}_j - i\mathbf{k} \cdot \mathbf{R}_i} \hat{B}_{\mathbf{k}}^\dagger \hat{B}_{\mathbf{k}'} \\ &= \sum_{\mathbf{k}, \mathbf{k}'} \delta_{\mathbf{k}, \mathbf{k}'} (\varepsilon_{eg} + D) \hat{B}_{\mathbf{k}}^\dagger \hat{B}_{\mathbf{k}'} + \sum_{m \neq 0} J_m e^{i\mathbf{k}' \cdot \mathbf{R}_m} \sum_{\mathbf{k}, \mathbf{k}'} \hat{B}_{\mathbf{k}}^\dagger \hat{B}_{\mathbf{k}'} \left[\frac{1}{N} \sum_i e^{i(\mathbf{k}' - \mathbf{k}) \cdot \mathbf{R}_i} \right] \\ &= \sum_{\mathbf{k}} [\varepsilon_{eg} + D + J(\mathbf{k})] \hat{B}_{\mathbf{k}}^\dagger \hat{B}_{\mathbf{k}}. \end{aligned} \quad (5.26)$$

In the second line we used the translational invariance of the system to assume $D_i = D$ and defined the distance vector $\mathbf{R}_m = \mathbf{R}_i - \mathbf{R}_j$. The diagonal form of the Hamiltonian in the third line is obtained after using the unitarity of the transformation in Eq. (5.25) $\sum_i \exp[(\mathbf{k} - \mathbf{k}') \cdot \mathbf{R}_i] = N$. The exciton spectrum for a homogeneous array with arbitrary dimensionality is thus given by

$$E_e(\mathbf{k}) = \varepsilon_{eg} + D^e + J^{ee}(\mathbf{k}), \quad (5.27)$$

where $J^{ee}(\mathbf{k}) = \sum_{m \neq 0} J_{m,0}^{ee} e^{i\mathbf{k}' \cdot \mathbf{R}_m}$ is the discrete Fourier transform of the coupling constant J_{ij} . Considering nearest-neighbour interactions only, the exciton spectrum for a 1D array is $E(k) = \varepsilon_{eg} + D + 2J \cos(ka_L)$, where a_L is the lattice constant. The bandwidth in this model is $\Delta = 4$ (see Fig. 5.2).

So far we have ignored the coupling between different exciton states induced by $\hat{H}_2(e, f)$ in Eq. (5.18). This term can be expected to be important for polar molecules where the first single-molecule excited state is triply degenerate in the absence of external fields. By using the unitary transformation in Eq. (5.25) the

exciton Hamiltonian $\hat{H}_e = \hat{H}_1 + \hat{H}_2$ can be written as

$$\hat{H}_e = \sum_{\mathbf{k}} \sum_{M,M'} [\Delta E_{eg} \delta_{M,M'} + J_{M,M'}(\mathbf{k})] \hat{B}_{\mathbf{k}M}^\dagger \hat{B}_{\mathbf{k}M'}, \quad (5.28)$$

with $J_{M,M'}(\mathbf{k}) = \sum_{m \neq 0} J_{m0}^{M,M'} e^{i\mathbf{k} \cdot \mathbf{R}_m}$. We have identified the state indices e and f with the total angular momentum projection M of the states in the one-excitation subspace $\mathcal{S}_1^e = \{|g_1, \dots, e_i, \dots, g_N\rangle : i = 1, \dots, N\}$. Because the ground state $|g\rangle = |(0), 0\rangle$ has zero projection, the value of M corresponds to the projection of the excited state e . For the first rotational level $N = 1$, we have $M = -1, 0, 1$.

The Hamiltonian in Eq. (5.28) is diagonal in the quantum number \mathbf{k} , but non-diagonal in M . The unitary transformation $\hat{B}_{\mathbf{k}M}^\dagger = \sum_{\mu} \alpha_{M,\mu} \hat{A}_{\mathbf{k}\mu}^\dagger$ to a new set of exciton operators $\hat{A}_{\mathbf{k}\mu}^\dagger$ can be used to diagonalize the Hamiltonian [99]. The coefficients $\alpha_{M,\mu}$ are the elements of the unitary matrix that diagonalizes Hamiltonian

$$\hat{H}_e(\mathbf{k}) = \begin{pmatrix} E_{-1}(\mathbf{k}) & J_{-1,0}(\mathbf{k}) & J_{-1,1}(\mathbf{k}) \\ J_{0,-1}(\mathbf{k}) & E_0(\mathbf{k}) & J_{0,1}(\mathbf{k}) \\ J_{1,-1}(\mathbf{k}) & J_{1,0}(\mathbf{k}) & E_1(\mathbf{k}) \end{pmatrix} \quad (5.29)$$

for each value of \mathbf{k} . In second-quantized notation diagonal Hamiltonian is $\hat{H} = \sum_{\mathbf{k},\mu} E_{\mu}(\mathbf{k}) \hat{A}_{\mathbf{k}\mu}^\dagger \hat{A}_{\mathbf{k}\mu}$, where the index $\mu = \alpha, \beta, \gamma$ labels the exciton eigenstates. The evaluation of the coupling functions $J_{M,M'}(\mathbf{k})$ reduces for most values of \mathbf{k} to the calculation of the dipole-dipole matrix element

$$J_{M,M'} = \langle (1)M | \langle (0)0 | V_{\text{dd}} | (0)0 \rangle | (1)M' \rangle,$$

which can be obtained using the formulas from Appendix B.

Let us consider a one-dimensional homogeneous array in the presence of a DC electric field \mathbf{E} . If the electric field is parallel to the molecular array, the axial symmetry of the Hamiltonian is preserved, and the total projection M is a good quantum number, although the projection M_N of individual molecules is not conserved. The eigenstates of exciton Hamiltonian (5.28) in this case are: $|\alpha_{\mathbf{k}}\rangle = |\Psi_{\mathbf{k},M=1}\rangle$, $|\beta_{\mathbf{k}}\rangle = |\Psi_{\mathbf{k},M=-1}\rangle$, and $|\gamma_{\mathbf{k}}\rangle = |\Psi_{\mathbf{k},M=0}\rangle$, where $|\Psi_{\mathbf{k},M}\rangle$ are eigenstates of $\hat{H}_1(e)$ in Eq. (5.19). If the electric field is perpendicular to the molec-

ular array, the axial symmetry of system is broken and the total projection M is no longer a good quantum number. In this case, off-diagonal elements of the Hamiltonian matrix (5.29) are zero only for the coupling between the exciton states with total projection $M = 0$ and $|M| = 1$. This is due to the angular dependence of the dipole-dipole matrix elements (see Appendix B). The eigenstates in this case are: $|\alpha_{\mathbf{k}}\rangle = \frac{1}{\sqrt{2}} [|\Psi_{\mathbf{k},M=1}\rangle - |\Psi_{\mathbf{k},M=-1}\rangle]$, $|\beta_{\mathbf{k}}\rangle = \frac{1}{\sqrt{2}} [|\Psi_{\mathbf{k},M=1}\rangle + |\Psi_{\mathbf{k},M=-1}\rangle]$, and $|\gamma_{\mathbf{k}}\rangle = |\Psi_{\mathbf{k},M=0}\rangle$. The dispersion curves $E_{\mu}(\mathbf{k})$ of the three exciton branches are shown in Fig. 5.4 for a 1D array of LiCs molecules ($d_0 = 5.529$ Debye, $2B_e = 11.7998$ GHz [186]) with lattice constant $a = 400$ nm in the presence of an electric field parallel and perpendicular to the array. Analogous dispersion curves can be obtained in 2D and 3D and for other directions of the electric field. The energy bands shown in Fig. 5.4 are centered at the single-molecule transitions energy. Exciton γ corresponds to the $|N=0\rangle \rightarrow |N=1, M=0\rangle$ excitation. The calculated excitonic bandwidths are of the order of 100 kHz. The broadening of the excitonic line due to the variation of the dipole-dipole interaction caused by the vibrations of the molecules about their equilibrium positions is less than 5% of its bandwidth for experimentally realizable trapping frequencies $\omega_0 \geq 100$ kHz. We will discuss more about the molecular motion in the lattice potentials in Chapter 6.

The exciton wavefunction $|\mathbf{k}, e\rangle = \hat{B}_{\mathbf{k}e}^{\dagger}|0\rangle$ describes a state with one quantum of excitation distributed equally throughout the molecules in the array, each molecule having a probability $1/N$ of being excited. This is true for idealized homogeneous arrays. A wave packet of excitons describes the state where the excitation quanta is not allowed to travel through the entire crystal. This wave packet can be written as $|\Phi_e\rangle = \sum_{\mathbf{k}} \chi_e(\mathbf{k})|\mathbf{k}, e\rangle$. This state is not associated with a definite energy. The values of the coefficients $\chi_e(\mathbf{k})$ are determined by the mechanism that localizes the exciton state. An exciton wave packet has a group velocity $\mathbf{v}_e(\mathbf{k}) = \frac{1}{\hbar} \nabla_{\mathbf{k}} E_e(\mathbf{k})$ related to the gradient of the exciton dispersion $E_e(\mathbf{k})$ along a given wavevector direction \mathbf{k} . The group velocity is independent on the specific form the wave packet, so it also describes the energy transfer velocity for one-exciton states.

The dispersion relation in Eq. (5.27) usually has an extrema for some value of the wave vector $\mathbf{k} = \mathbf{k}_0$. Around this value we can approximate the dispersion curve by a quadratic Taylor series in wave vector space $E(\mathbf{k}) = E(\mathbf{k}_0) + (\mathbf{k} - \mathbf{k}_0)^T \cdot \nabla_{\mathbf{k}} E(\mathbf{k}_0) + \frac{1}{2} (\mathbf{k} - \mathbf{k}_0)^T \cdot \nabla_{\mathbf{k}} \nabla_{\mathbf{k}} E(\mathbf{k}_0) \cdot (\mathbf{k} - \mathbf{k}_0)$, where $\nabla_{\mathbf{k}} \nabla_{\mathbf{k}} E(\mathbf{k}_0)$ is the Hessian

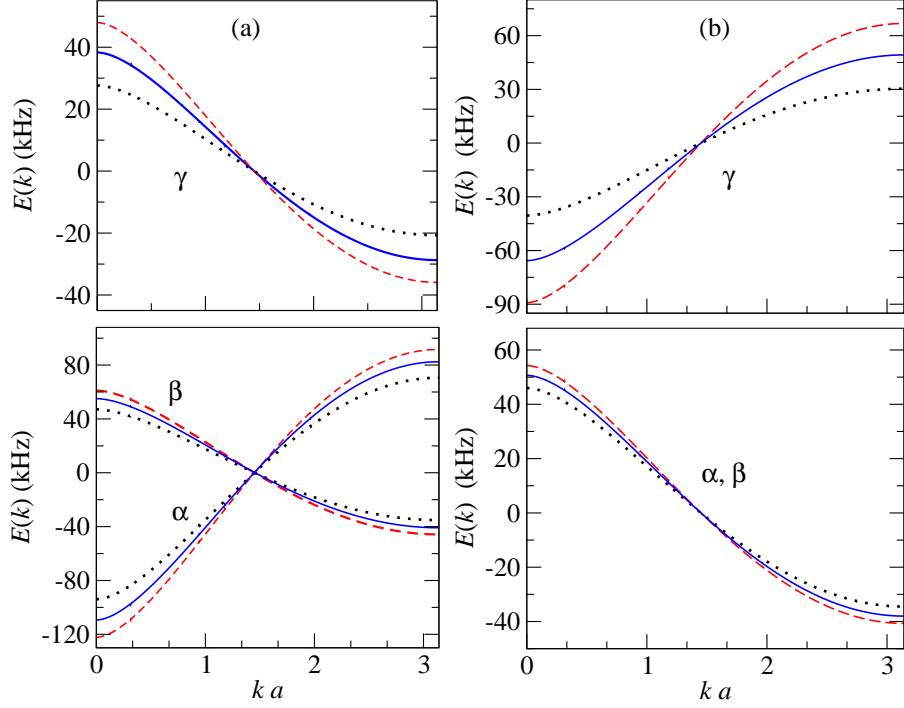


Figure 5.4: Stark effect on rotational excitons. Exciton energy $E(k)$ calculated for three lowest excitations in a 1D array of 10^5 LiCs molecules ($d_0 = 5.529$ Debye, $2B_e = 11.8$ GHz [186]) separated by 400 nm as functions of the exciton wavenumber k . Exciton states α , β and γ centered at the isolated molecule transition energies ΔE_{eg} are shown in the presence of an electric field perpendicular to the array (panel a) and parallel to the array (panel b). The electric field magnitudes are 2 kV/cm (dashed lines), 3.2 kV/cm (solid lines), 5 kV/cm (dotted lines). At these electric fields, exciton γ is separated from excitons α and β by the energy much larger than the exciton bandwidths.

matrix of second partial derivatives evaluated at \mathbf{k}_0 . If the value of $E(\mathbf{k}_0)$ is a minimum or maximum in the dispersion curve $E(\mathbf{k})$, then the directional derivative $(\mathbf{k} - \mathbf{k}_0)^T \cdot \nabla_{\mathbf{k}} E(\mathbf{k}_0)$ is zero for wave vectors close to \mathbf{k}_0 , the exciton energy is approximated by the quadratic formula $E(\mathbf{k}) \approx E(\mathbf{k}_0) + \frac{1}{2}(\mathbf{k} - \mathbf{k}_0)^T \cdot \nabla_{\mathbf{k}} \nabla_{\mathbf{k}} E(\mathbf{k}_0) \cdot (\mathbf{k} - \mathbf{k}_0)$ which for a one dimensional crystal along the x -axis with one minimum

at $k_x = 0$ reads

$$E(k) = E(k=0) + \frac{1}{2} \left. \frac{\partial^2 E(k)}{\partial k^2} \right|_{k_0} k^2 = E_0 + \frac{\hbar^2 k^2}{2m^*}, \quad (5.30)$$

where, in order to compare the exciton energy with the energy of a free particle with the same wave vector, we define the exciton effective mass

$$m^* = \hbar^2 \left(\left. \frac{\partial^2 \varepsilon(k)}{\partial k^2} \right|_{k_0} \right)^{-1}. \quad (5.31)$$

An analogous definition holds for 2D and 3D molecular arrays. When the dispersion curve is differentiable around the wave vector \mathbf{k}_0 the quadratic approximation of Eq. (5.30) can be applied. Within this approximation, quantities such as the group velocity and the effective mass of excitons are important when describing the interaction of excitons with other particles and fields.

Back to the LiCs one-dimensional array in Fig. 5.4, it is clear that when the electric field is perpendicular to the molecular array (panel (a)), excitons γ and β have negative effective mass near the origin of the Brillouin zone, i.e. their energy decreases with increasing wavevector, while the effective mass of exciton α is positive. Figure 5.4 demonstrates that the effective mass and, consequently, the group velocity of the excitons can be changed by varying the strength and the direction of the external electric field. The effective mass is an important parameter in the description of excitonic transport in impure lattices. Therefore, the possibility to manipulate the sign and magnitude of the exciton effective mass may find application in the simulation of coherent transport phenomena, as discussed later in this chapter.

In the rest of this thesis, we focus the discussion on the exciton state labelled by γ in Figure 5.4. This excitonic state has projection $M = 0$. We chose this projection because even for relatively weak electric fields $E_0 < 1$ kV/cm, the Stark shift of the rotational levels of most alkali-metal dimers is larger than the strength of the coupling between the $M = 0$ and $|M| = 1$ projections due to the dipole-dipole interaction. This is true for any orientation of the electric field. In other words, for

the states $|g\rangle = |(0), 0\rangle$ and $|e\rangle = |(1), 0\rangle$ the two-level approximation discussed in Section 5.2.2 is justified.

5.2.4 Excitons in molecules with hyperfine structure

Recent experiments have demonstrated the spectroscopic manipulation of the hyperfine state population of cold polar molecules [157]. It is possible to prepare a polar molecule in a single hyperfine state of the ground rotational level or in an arbitrary coherent superposition of hyperfine states. This motivates us to analyze the effect of the hyperfine structure on the emergence of collective excitations in an array of cold polar molecules.

In order for the two-level approximation to the exciton Hamiltonian in Eq. (5.10) to be valid, two conditions must be satisfied: (a) the transition $|g\rangle \rightarrow |e\rangle$ must be allowed; (b) the excited state $|e\rangle$ must be separated from other excited states $|e'\rangle$ by an energy larger than the dipole-dipole interaction energy U_{dd} . The additional condition $\epsilon_{eg} \gg J_{12}^{ee}$ is required for the Heitler-London approximation in Eq. (5.17) to hold.

Low magnetic fields

In the absence of magnetic fields and ignoring the effect of the trapping light, the fully coupled basis $|(NI)FM_F\rangle$ best describes the state of the molecule. In the ground rotational manifold $N = 0$, the hyperfine states are given by $|g\rangle \equiv |(0I)IM_I\rangle$. For electromagnetic fields with polarization along the Z axis, the strength of electric dipole transitions between hyperfine states is determined by the transition dipole moment $\langle e|d_Z|g\rangle \equiv \langle (NI')FM_I|\hat{d}_Z|(0I)IM_I\rangle$, which can be written as

$$\begin{aligned} \langle e|d_Z|g\rangle &= d(-1)^{F+I'+I-M_I}[(2F+1)(2I+1)(2N+1)]^{1/2} \begin{Bmatrix} 0 & I & I' \\ F & N & 1 \end{Bmatrix} \\ &\quad \times \begin{pmatrix} F & 1 & I \\ -M_I & 0 & M_I \end{pmatrix} \begin{pmatrix} N & 1 & 0 \\ 0 & 0 & 0 \end{pmatrix} \\ &= d(-1)^{N+I-M_I}(2F+1)^{1/2} \begin{pmatrix} 1 & 1 & 0 \\ 0 & 0 & 0 \end{pmatrix} \begin{pmatrix} F & 1 & I \\ -M_I & 0 & M_I \end{pmatrix}, \end{aligned} \tag{5.32}$$

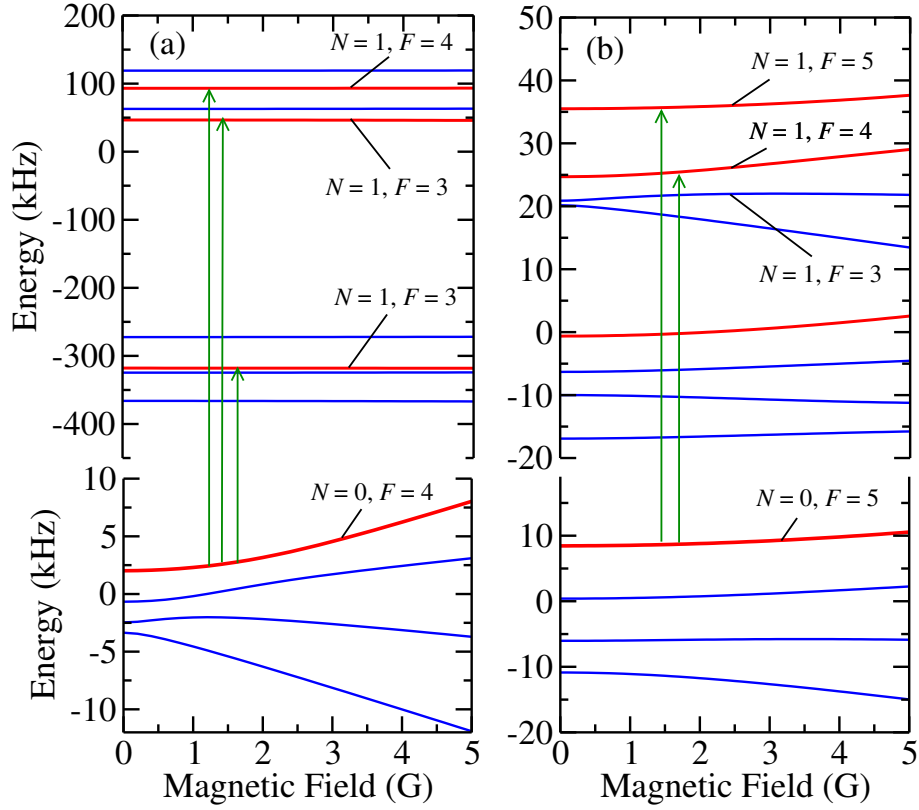


Figure 5.5: Electric dipole transitions between hyperfine states at weak magnetic fields. Panels (a) and (b) correspond to $^{41}\text{K}^{87}\text{Rb}$ and $^7\text{Li}^{133}\text{Cs}$ molecules, respectively. The Zeeman spectrum of the $N = 0$ and $N = 1$ levels are shown. Energies are given with respect to the field free rotational energies. Selected hyperfine states are labeled according to the quantum numbers N and F . States with total angular momentum projection $|M_F| \neq 0$ are omitted for clarity. Arrows indicate allowed transitions between selected states. Additional transitions are omitted.

where d is the permanent dipole moment of the molecule. The second equality in Eq. (5.32) follows from the conditions $N = 1$ and $I = I'$. As for pure rotational transitions, dipole transitions are allowed from the ground rotational level $N = 0$ to the first excited level $N = 1$. The total angular momentum of the excited state can take the values $F = I + 1, I, I - 1$, and its total spin projection M_F is equal to the nuclear spin projection in the ground level M_I . For concreteness, let us

consider $^{41}\text{K}^{87}\text{Rb}$ and $^7\text{Li}^{133}\text{Cs}$ molecules. The ground rotational manifold $N = 0$ has four hyperfine levels associated with the total angular momentum $F = I$ at zero magnetic field for both molecules. Each level is $(2F + 1)$ -fold degenerate. The hyperfine splittings are completely determined by the scalar spin-spin interaction. The associated molecular constant c_4 is approximately 0.9 kHz for KRb and 1.6 kHz for LiCs (see Table 2.1). The first rotational excited manifold $N = 1$ has 10 hyperfine levels for KRb and 12 for LiCs, with their corresponding magnetic sublevels. Figure 5.5 shows possible choices of ground and excited states $|g\rangle$ and $|e\rangle$ for KRb and LiCs molecules, at weak magnetic fields on the order of 1 Gauss.

The separation between allowed transitions should be larger than the associated exciton bandwidth $\Delta \sim 100$ kHz at optical lattice distances. Panel (a) in Fig. 5.5 shows that for KRb molecules it should be possible to choose an allowed dipole transition $|g\rangle \rightarrow |e\rangle$ that is separated from other lines by more than 200 kHz. This is the case for the transition $|(N = 0)F = 4, M_F = 0\rangle \rightarrow |(N = 1)F = 3, M_F = 0\rangle$. The nuclear spin angular momentum I is not well defined due to the anisotropy of the hyperfine Hamiltonian. For magnetic fields below 2 Gauss, the field-induced coupling between states with the same total angular momentum F is weak. At a magnetic field of 2 Gauss, for example, the ground state $|g\rangle$ in Fig. 5.5(a) has approximately 80% of $F = 5$ character. As the field increases, the F quantum number loses its relevance to describe the state. The hyperfine states in the excited rotational manifold $N = 1$ are well described using the fully coupled basis at these magnetic fields. This basis loses its meaning at larger magnetic fields than the rotational ground levels because the hyperfine splittings in the excited state are significantly larger.

Panel (b) in Fig. 5.5 suggests that for LiCs it may not be possible to isolate a dipole allowed transition at weak magnetic fields. The hyperfine splitting between excited states in the $N = 1$ rotational manifold is on the order of tens of kHz. In Chapter 2 it was shown that the dipole-dipole interaction energy between closed-shell molecules with hyperfine structure is only a fraction of the dipole-dipole energy without including hyperfine structure. For LiCs molecules separated by 400 nm this energy is about 80 kHz ignoring hyperfine structure. Therefore, a many-level exciton model as in Eq. (5.18) would be required to describe hyperfine collective excitations, since dipole-dipole interaction energy would be comparable

with the hyperfine splittings in the $N = 1$ manifold. Different exciton bands would be coupled by the dipole exchange interaction as it was shown for the rotational excitons α and β in Fig. 5.4.

So far we have ignored the effect of the trapping light on the hyperfine states of the molecule. A deep optical lattice potential can have a depth of up to tens of MHz [79]. Such deep lattices are necessary in applications where decoherence due to the motion of the molecule in the trapping potential needs to be suppressed. Optical trapping of molecules is achieved using off-resonant optical fields. The intensity of the trapping lasers is on the order of mW/cm^2 , which is not high enough to induce Raman couplings between different rotational states. The trapping laser interacts directly with the rotational angular momentum of the molecule. The off-resonant field can also interact indirectly with the nuclear spin angular momentum when this is strongly coupled to the rotational motion by the hyperfine interactions. Raman coupling between states with different rotational angular momentum N is suppressed in the presence of weak trapping lasers, but the off-resonant trapping fields may induce couplings between hyperfine states within a given rotational level at weak magnetic fields, where the fully coupled scheme $\mathbf{F} = \mathbf{N} + \mathbf{I}$ is appropriate to describe the state of the molecule.

Let us consider a one-dimensional optical lattice potential created by a standing wave with linear polarization along the Z axis (see Chapter 2)

$$\hat{H}_{\text{AC}} = -|E(\mathbf{r})|^2 \left\{ \frac{1}{3}(\alpha_{\parallel} + 2\alpha_{\perp}) + \frac{2}{3}(\alpha_{\parallel} - \alpha_{\perp})\hat{C}_{2,0}(\theta) \right\}, \quad (5.33)$$

where $E(\mathbf{r})$ is the electric field amplitude and $C_{k,q}(\theta, \phi)$ is a modified spherical harmonic. Using the methods in Appendix C, the matrix elements of the tensor operator $C_{k,q}$ in the fully coupled basis $|(NI)FM_F\rangle$ can be written as

$$\begin{aligned} & \langle (NI)FM_F | \hat{C}_{k,q} | (N'I')F'M'_F \rangle \\ &= \delta_{I,I'} (-1)^{F+F'+k+I-M_F} [(2F+1)(2F'+1)(2N+1)(2N'+1)]^{1/2} \\ & \times \begin{pmatrix} N & k & N' \\ 0 & 0 & 0 \end{pmatrix} \begin{Bmatrix} N' & F' & I \\ F & N & k \end{Bmatrix} \begin{pmatrix} F & k & F' \\ -M_F & q & M'_F \end{pmatrix}. \end{aligned} \quad (5.34)$$

Since the intensity of the trapping laser is weak, the coupling between different

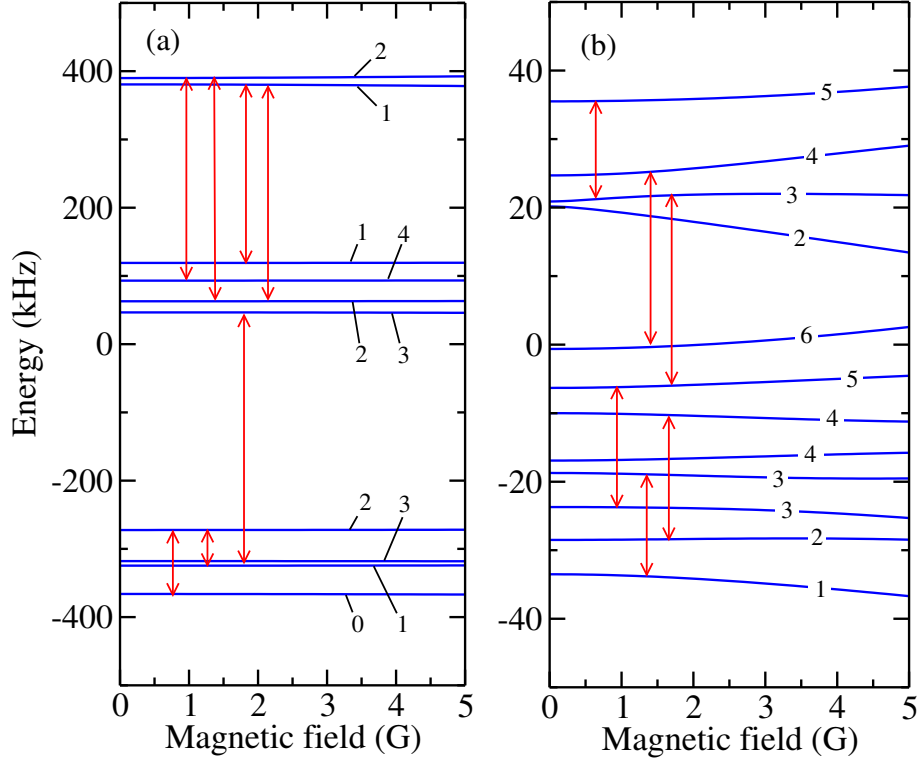


Figure 5.6: Hyperfine Raman couplings induced by an off-resonant trapping laser at weak magnetic fields. Panels (a) and (b) correspond to $^{41}\text{K}^{87}\text{Rb}$ and $^7\text{Li}^{133}\text{Cs}$ molecules, respectively. The Zeeman spectrum of the $N = 1$ levels is shown. Energies are given with respect to the field free rotational energies. The hyperfine states are labeled according to the quantum number F . States with total angular momentum projection $|M_F| \neq 0$ are omitted for clarity. Arrows indicate allowed Raman couplings induced by the field of a linearly polarized off-resonant field. Some allowed couplings are omitted.

rotational levels N and N' can be ignored. Equation (5.34) shows that the tensor light-shift operator $C_{2,0}$ in Eq. (5.33) vanishes for $N = 0$, i.e., there is no light-induced couplings between hyperfine states in the ground rotational level at weak magnetic fields. For the rotational excited state $N = 1$, the matrix element of $C_{2,0}$

gives

$$\langle FM_F|\hat{C}_{2,0}|F'M'_F\rangle = (-1)^{F+F'+I-M_F} \frac{3\sqrt{2}}{\sqrt{15}} \begin{Bmatrix} 1 & F' & I \\ F & 1 & 2 \end{Bmatrix} \begin{pmatrix} F & 2 & F' \\ -M_F & 0 & M'_F \end{pmatrix}. \quad (5.35)$$

The optical lattice light can therefore couple hyperfine states in the $N = 1$ manifold. The selection rules for the hyperfine Raman coupling are $\Delta F = 0, \pm 1, \pm 2$. The linear polarization of the field imposes the condition $\Delta M_F = 0$. When $M_F = M'_F = 0$, the selection rules $\Delta F = 0, \pm 2$ are valid. In Fig. 5.6 the hyperfine Raman couplings are shown for $^{41}\text{K}^{87}\text{Rb}$ and $^7\text{Li}^{133}\text{Cs}$ in a 1D optical lattice potential given by Eq. (5.33). This figure shows that for an optical lattice depth of a few hundred kHz, the hyperfine states of the excited rotational levels are strongly mixed in the presence of weak magnetic field collinear with the polarization of the trapping laser.

In summary, a weak off-resonant trapping laser would create hyperfine wavepackets in homonuclear and heteronuclear molecules in the presence of weak magnetic fields. This is due to the coupling between the nuclear spin of the molecule and the rotational angular momentum in rotationally excited levels $N \geq 1$. The light-matter interaction can be taken into account in the definition of the states $|g\rangle$ and $|e\rangle$ that give rise to rotational excitons in a molecular ensemble. However, the associated exchange coupling constant J_{12} would depend on the intensity fluctuations of the weak trapping laser. In addition, in the presence of combined electric, magnetic and optical fields, a field configuration that is not perfectly collinear would introduce additional couplings between states with different total angular momentum projections M_F , as it was discussed for rotational states in Section 2.7. This introduces unnecessary complications to the rotational exciton picture described in previous sections.

High magnetic fields

At high magnetic fields the leading term in the molecular Hamiltonian is the nuclear Zeeman interaction. In this regime the nuclear spin is decoupled from the rotational angular momentum. The molecular states can be described in the spin coupled basis $|NM_N\rangle|IM_I\rangle$. As shown in Appendix C, the rotational angular momentum N and the total angular momentum projection $M_N + M_I$ are good quantum

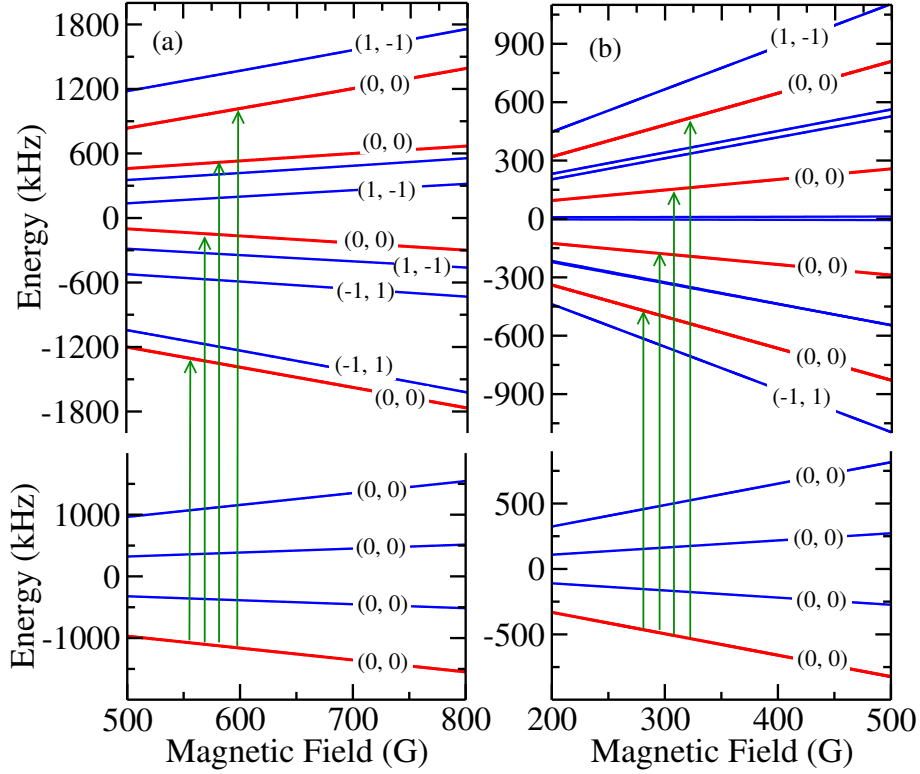


Figure 5.7: Electric dipole transitions between hyperfine states at high magnetic fields. Panels (a) and (b) correspond to $^{41}\text{K}^{87}\text{Rb}$ and $^7\text{Li}^{133}\text{Cs}$ molecules, respectively. The Zeeman spectrum of the $N = 0$ and $N = 1$ levels are shown. Energies are given with respect to the field free rotational energies. Selected hyperfine states are labeled according to their values of the rotational and nuclear spin projections (M_N, M_I). States with total angular momentum projection $|M_N + M_I| \neq 0$ are omitted for clarity. Arrows indicate allowed transitions between selected states.

numbers when Zeeman shifts are comparable with the zero field hyperfine splittings. At stronger magnetic fields, the individual projections M_N and M_I become good quantum numbers. The molecular eigenstates in this regime can be written in the spin coupled basis as $|NM_N\rangle|\phi_{M_I}\rangle$, where $|\phi_{M_I}\rangle = \sum_I a_I |I, M_I\rangle$. In the ground rotational manifold $N = 0$, the hyperfine states can be written as $|g\rangle = |N = 0, M_N = 0\rangle|\phi_{M_I}\rangle$, and in the first excited level $N = 1$ they are given by $|e\rangle = |N = 1, M_N\rangle|\psi_{M_I}\rangle$. For electromagnetic fields with polarization along the Z axis,

the strength of electric dipole allowed transitions between these hyperfine states is determined by the transition matrix element

$$\begin{aligned}\langle e|\hat{d}_Z|g\rangle &= \langle N=1, M_N=0|\hat{d}_0|N'=0, M'_N=0\rangle\langle\psi_{M_I}|\phi_{M'_I}\rangle \\ &= \delta_{M_I, M'_I}\sqrt{3}\begin{pmatrix} 1 & 1 & 0 \\ 0 & 0 & 0 \end{pmatrix}^2\langle\psi_{M_I}|\phi_{M_I}\rangle.\end{aligned}\quad (5.36)$$

Linearly polarized transitions therefore preserve the projections M_N and M_I of the hyperfine state in the ground manifold, and their intensity differs from a pure rotational transition by the nuclear overlap factor $\langle\psi_{M_I}|\phi_{M_I}\rangle$. In Figure 5.7 allowed transitions between selected hyperfine states for $^{41}\text{K}^{87}\text{Rb}$ and $^7\text{Li}^{133}\text{Cs}$ are shown at moderately high magnetic fields.

The hyperfine interactions in KRb molecules are considerably larger than in LiCs molecules. Consequently, the magnetic field strength needed to accurately describe the molecular eigenstates as the separable product $|NM_N\rangle|\phi_{M_I}\rangle$ is also larger. In panel (a) of Fig. 5.7 the Zeeman spectrum of the $N=0$ and $N=1$ levels of KRb are shown for magnetic fields larger than 500 Gauss. Below these field strength the separability of the angular momentum projections M_N and M_I in the $N=1$ level is only accurate to less than 90% of the norm of the true eigenstate. The figure shows all the allowed transitions from the $N=0$ ground rotational states with $M_N=0$ and $M_I=0$ to the hyperfine states in the first rotational level $N=1$. The intensity of these transitions is determined by the square of the transition dipole moment in Eq. (5.36). The frequencies of these transitions are separated by several hundreds of kHz, which is several times larger than the dipole-dipole interaction energy between molecules in an optical lattice. Therefore, it should be possible to define two-level exciton models as in Eq. 5.10 in optical lattices by choosing any one of these hyperfine transitions in high magnetic fields.

Panel (b) of Fig. 5.7 shows the Zeeman structure and the allowed transitions between $N=0$ and $N=1$ hyperfine states for LiCs molecules at magnetic fields above 200 Gauss. At this field strengths, the separability of the rotational and spin projections is over 99% accurate for both rotational levels. This is due to the small zero-field hyperfine splitting in the excited level. As for KRb molecules, the figure shows that it is possible to find allowed transitions separated from adjacent

lines by a few hundred kHz, which is an energy larger than the interaction energy between molecules in an optical lattice. The two-level approximation for collective excitations is thus accurate for LiCs molecules at magnetic fields of a few hundred Gauss.

At small magnetic fields we discussed how the optical trapping light induces Raman couplings between hyperfine states, and how this complicates the nature of collective excitations in molecular ensembles. Let us consider the one-dimensional optical lattice potential in Eq. (5.33). For hyperfine states described by products of the form $|NM_N\rangle|\phi_{M_I}\rangle$, the matrix elements of the tensor light shift operator $\hat{C}_{k,q}$ are given by

$$\langle\psi_{M_I}|\langle N, M_N|\hat{C}_{k,q}|N', M'_N\rangle\phi_{M'_I}\rangle = \delta_{M_I, M'_I}\langle N, M_N|\hat{C}_{k,q}|N', M'_N\rangle\langle\psi_{M_I}|\phi_{M_I}\rangle. \quad (5.37)$$

Within the same rotational level $N = N'$, the trapping potential only induces rotational Raman transitions according to the selection rules $\Delta M_N = \pm q$ (see Section 2.7). The strength of the coupling is modulated by the nuclear spin overlap factor $\langle\psi_{M_I}|\phi_{M_I}\rangle$. Contrary to the case of weak magnetic fields, different hyperfine states within a given rotational level are not mixed as a result of the interaction of the molecule with the trapping fields.

The simplification of the rotational spectrum at high magnetic fields allow us to use the simple picture of pure rotational excitons described in previous sections throughout this thesis. A common scenario in this work consists in placing the molecular ensemble in a DC electric field. The hyperfine structure of the molecule can be ignored as long as a moderately strong magnetic field parallel to the electric field is also assumed to be present. The numerical value of the dipole-dipole interaction matrix elements between hyperfine states depends on the chosen value of the magnetic field strength. The error involved in neglecting the hyperfine structure when evaluating dipole-dipole interaction energies can be made arbitrarily small by increasing the magnetic field strength to the point where the spin overlap factors become Kronecker deltas, i.e., $\langle\psi_{M_I}|\phi_{M_I}\rangle \rightarrow \delta_{\psi, \phi}$.

5.3 Controlling exciton transport with external fields

Excitons determine the optical properties of materials, energy transfer in semiconductors and mesoscopic systems [99, 108], and the reaction mechanisms in complex biological systems [187]. In molecular crystals with low excitation density, the transport properties of excitons are determined by their interaction with impurities and phonons [99], and resemble those of electrons in solids [188], or atoms in optical lattices [189]. Although the effects of phonons can be suppressed by lowering the temperature of crystals, the presence of impurities is almost unavoidable in semiconductors and organic molecular solids. Exciton - impurity interactions lead to the formation of localized exciton states [190], modifying energy transfer in crystalline materials. Therefore, it would be desirable to develop an experimentally realizable system that could be used to study exciton dynamics as a function of exciton - impurity interaction strength. In this Section it is shown that a suitably chosen two-species mixture of ultracold polar molecules loaded on an optical lattice can form a crystal where the exciton-impurity interaction can be controlled by applying an DC electric field. This can be used for the controlled creation of many-body entangled states of ultracold molecules and the time-domain quantum simulation of disorder-induced localization and delocalization of quantum particles.

As noted earlier, it has become technologically possible to create ordered ensembles of ultracold polar molecules in the ro-vibrational ground state trapped by an optical lattice with a lattice separation of about 400 nm [20]. Moreover, methods are being developed to evaporate atoms or molecules in specific lattice sites [191]. Superimposing optical lattices of different frequencies, containing two different molecular species would allow the preparation of a mixture of molecules arranged in an arbitrary array with any spatial dimensionality. For concreteness, we consider a mixture of alkali metal dimers LiCs and LiRb loaded on an optical lattice such that the array has cubic symmetry with a lattice constant $a = 400$ nm. We note, however, that the proposed mechanism of tuning exciton - impurity interactions can, in principle, be realized with any mixture of molecules A and B in a Σ electronic state, provided the rotational constant of molecule A is greater and the dipole moment of molecule A is smaller. The effects discussed in this work should

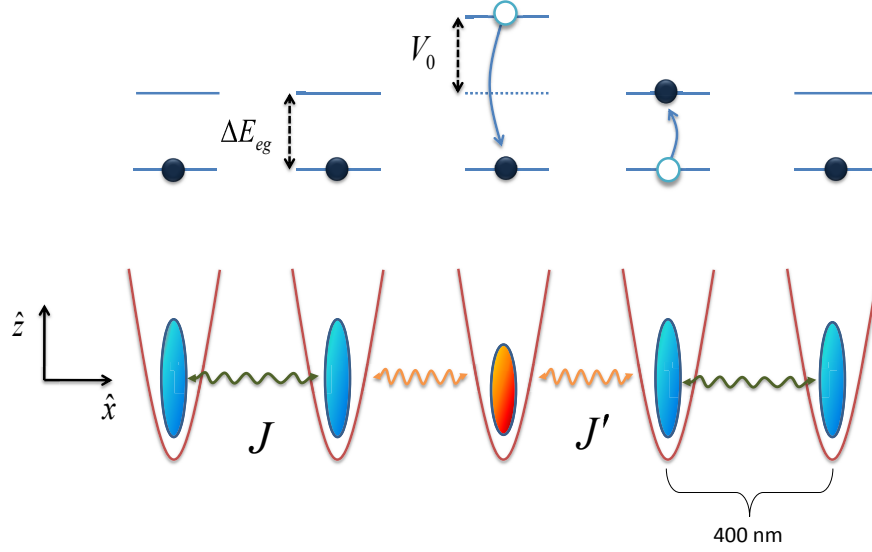


Figure 5.8: Schematic illustration of a crystal with tunable impurities. Molecules are confined by the periodic potential and are coupled by the dipole-dipole interaction, which allows the exchange of a rotational excitation between molecules in different sites. An impurity is a molecule with a different dipole moment and different rotational energy splitting, parametrized by the energy defect V_0 .

occur at smaller electric fields, if the rotational constants of molecules A and B are closer in magnitude.

5.3.1 Electric field control of exciton-impurity scattering

If a small number of LiCs molecules are replaced with molecules of a different kind, such as LiRb ($d_0 = 4.165$ Debye, $2B_e = 13.2$ GHz [186]), the translational symmetry of the lattice is disturbed, as in a solid crystal with impurities (see Fig. 5.8). Let us denote the excitation energy between the ground rotational state and a rotational excited state in the host molecules by ΔE_{eg} , and the energy of the transition between the same states in the impurity molecules by $\Delta E_{eg} + V_0$. Since

different polar molecules have different dipole moments, we denote the difference between the resonant exchange coupling constants for the impurity-host and host-host couplings by $\Delta J_{n,m}$, for molecules at sites n and m . As a starting point, we can consider a lattice with a single impurity molecule at the origin site $n = 0$. This model disordered lattice is described by the Hamiltonian [192]

$$\hat{H} = \hat{H}_0 + V_0 \hat{B}_0^\dagger \hat{B}_0 + \sum_{n \neq 0} \Delta J_{n,0} \left(\hat{B}_n^\dagger \hat{B}_0 + \hat{B}_n \hat{B}_0^\dagger \right), \quad (5.38)$$

where \hat{H}_0 is the Hamiltonian describing a single exciton

$$\hat{H}_0 = \Delta E_{eg} \sum_n \hat{B}_n^\dagger \hat{B}_n + \sum_{n,m} J_{n,m} \hat{B}_n^\dagger \hat{B}_m = \sum_{\mathbf{k}} E(\mathbf{k}) \hat{B}_{\mathbf{k}}^\dagger \hat{B}_{\mathbf{k}}. \quad (5.39)$$

The exciton-impurity interaction can thus be described as the sum of a delta-like potential with strength V_0 and a long-range perturbation due to the difference in the dipole moments of host and impurity molecules. It is well-known that the exciton-impurity interaction leads to the appearance of bound exciton states [192, 193], which are localized in real space.

Coherent exciton waves $|\Psi_e(\mathbf{k})\rangle = \hat{B}_{\mathbf{k}}^\dagger |0\rangle$, are eigenstates of the impurity-free crystal Hamiltonian characterized by a propagation direction \mathbf{k} , a wavelength $\lambda_e = 2\pi/|\mathbf{k}|$, quasimomentum $p_k = \hbar|\mathbf{k}|$, and energy $E(\mathbf{k})$. Our motivation is to find conditions under which a coherent exciton wave does not interact strongly with an impurity in an imperfect crystal, as if the impurity were transparent to exciton propagation. In order to achieve this goal, we propose to use a DC electric field to shift the rotational levels of host and impurity molecules simultaneously, which modifies the value of the exciton-impurity interaction potential V_0 . It is in general possible to find an appropriate electric at which the rotational excitation energies of two different molecules are the equal. However, depending on the choice of the molecules, the electric field required for this degeneracy may be too large to be of practical use. Fortunately, if the rotational constants of the two molecules do not differ significantly, and the permanent dipole moments are not very similar, these “matching” electric field can be easily generated in a laboratory. In Figure 5.9(a) we show the excitation energies E_{eg} for the rotational transition corresponding to $N = 0 \rightarrow N = 1$ in a field-free space, for CsF, LiCs and LiRb molecules as func-

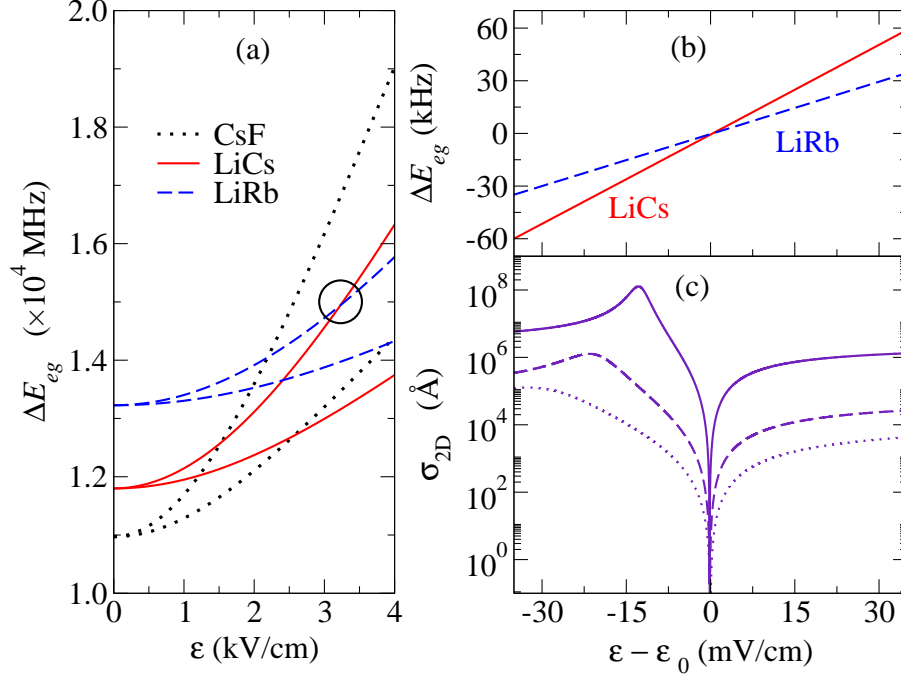


Figure 5.9: Excitation energies of non-interacting molecules in a DC electric field. Panel (a) shows the excitation energies E_{eg} for transitions $|N = 0, M_N = 0\rangle \rightarrow |N = 1, M_N\rangle$ with $M_N = 0$ (upper curve) and $M_N = \pm 1$ (lower curve) vs electric field for three polar molecules. Panel (b) shows an expanded view of the encircled area in panel (a). Panel (c) shows the exciton-impurity 2D scattering cross sections for the exciton $|\Psi_{\mathbf{k}, M_N=0}\rangle$ with $|\mathbf{k}|a = 4 \times 10^{-5}$ (solid line), $|\mathbf{k}|a = 4 \times 10^{-3}$ (dashed line), and $|\mathbf{k}|a = 4 \times 10^{-2}$ (dotted line). The calculations are for an array of LiCs molecules with one LiRb impurity. The lattice constant is $a = 400$ nm and $\mathcal{E}_0 = 3228.663$ V/cm.

tions of the strength of a DC electric field, and demonstrates that the excitation energies for these combinations of molecules become equal at certain values of the field strength. The results of Figure 5.9(a) are obtained using the spectroscopically determined values of the rotational constants and the permanent dipole moments of the molecules borrowed from the literature [186]. We select the transition corresponding to $|N = 0\rangle \rightarrow |N = 1, M_N = 0\rangle$, because the associated exciton state $|\Psi_{\mathbf{k}, M_N=0}\rangle$ is well separated from other exciton bands, so that the two-level free-

exciton Hamiltonian in Eq. (5.39) is accurate. Figure 5.9(b) is an expanded view of the energy crossing between the selected states for LiCs and LiRb molecules. The degeneracy of the transition energies shown in panel (b) should occur for any combination of molecules A and B, providing the rotational constant of molecule A is greater and the dipole moment of molecule A is smaller. Molecules with a larger difference of the dipole moments and a smaller difference of the rotational constants must exhibit the crossing of the energy differences at smaller electric fields.

The interaction of polar molecules with the electric field allows for the possibility to explore the dependence of the exciton-impurity scattering cross section not only on the exciton wavevector k , but also on the scattering strength V_0 , which is not possible to do in conventional solids. Since the potential V_0 is the difference between the rotational transition energies of the impurity and host molecules, this potential, and therefore the scattering cross section, can be tuned using a DC electric field as explained above. The cross sections for exciton - impurity scattering in 2D and 3D crystals as functions of V_0 can be obtained by solving the Lipmann-Schwinger equation as in Ref.[194]. In the effective mass approximation for excitons with $|\mathbf{k}|a \ll 1$, the cross sections in 2D and 3D crystals can be written as [194, 195]

$$\sigma_{3D}(k, V_0) = \frac{2\pi\hbar^2/|m_*|}{T_k + E_b^{(3D)}}, \quad (5.40a)$$

and

$$\sigma_{2D}(k, V_0) = \frac{4\pi^2/k}{\pi^2 + \ln^2 \left[\frac{E_b^{(2D)}(\Delta - T_k)}{T_k(\Delta - E_b^{(2D)})} \right]}, \quad (5.40b)$$

where $T_k = \hbar^2|\mathbf{k}|^2/2|m_*|$ is the kinetic energy of the exciton with effective mass m_* , and E_b is the energy of a bound state produced by scattering potential V_0 . The energy of this bound state is given by

$$E_b^{(3D)} = (2/\pi - V_0/\Delta)^2\Delta \quad \text{and} \quad E_b^{(2D)} = \Delta / [\exp(4\Delta/\pi V_0) - 1],$$

where Δ denotes the free-exciton bandwidth. Equations (5.40) show that the exciton-impurity scattering cross sections can be tuned by varying the electric field. As

shown in Figure 5.9(c), resonant enhancement of the scattering cross section occurs for $V_0 > 0$. These resonances are analogous to Feshbach resonances in atomic collisions, commonly used to tune the scattering properties of ultracold atoms [57]. In 1D, shallow bound states appear only for vanishingly small V_0 and resonances may not be observable. For an electric field perpendicular to the molecular array, the energy band for the exciton $|\Psi_{\mathbf{k},0}\rangle$ is inverted with respect to that of electrons in a solid, for example. As a consequence, the effective mass of the exciton is negative near the origin of the Brillouin zone. Due to the negative effective mass of the exciton, the bound state that leads to resonance is produced by a repulsive potential with $V_0 > 0$, as can be seen from panels (b) and (c) in Fig. 5.9. Equations (5.40) are derived in the approximation $\Delta J_{n,0} = 0$. Including $\Delta J_{n,0}$ in the calculation leads to a shift of the positions of the resonance [192] and the resonant enhancement of the scattering cross section occurs at a slightly different value of V_0 .

Figure 5.9 also suggests that the elastic mean free path of excitons $l \sim 1/\sigma n$ (n is the concentration of the impurities) can be dynamically tuned by several orders of magnitude by varying the applied electric field. According to the Ioffe-Regel criterion [196], this should allow the possibility to transfer the system dynamically from the regime of weak localization ($l \gg \lambda$) to the regime of strong localization ($l \sim \lambda$) of excitons with wavelength $\lambda = 2\pi/k$.

5.3.2 Field-induced delocalization of excitons in a disordered array

Molecular array with multiple substitutional impurities

Let us now consider a lattice with multiple impurities. It is well known that quantum particles in the presence of a random distribution of scattering centers undergo coherent localization [190]. In the system we consider in this section, we show that the localization of excitons can be tuned by an electric field. As an example, we consider localization of excitons in a 1D array of LiCs separated by 400 nm, with a random homogeneous distribution of LiRb impurities. The Hamiltonian describing an exciton in the presence of N_i substitutional impurities at positions \vec{r}_n can be

written in the site representation as

$$\begin{aligned}\hat{H} = & \Delta E_{eg} \sum_{n \neq i_n} \hat{B}_n^\dagger \hat{B}_n + \sum_{n \neq i_n} \sum_{m \neq n} J_{nm} \hat{B}_n^\dagger \hat{B}_m \\ & + \Delta E'_{eg} \sum_{i_n} \hat{B}_{i_n}^\dagger \hat{B}_{i_n} + \sum_{i_n} \sum_{n \neq i_n} J'_{n,i_n} (\hat{B}_n^\dagger \hat{B}_{i_n} + \hat{B}_n \hat{B}_{i_n}^\dagger),\end{aligned}\quad (5.41)$$

where $\Delta E'_{eg} \equiv \Delta E_{eg} + V_0$ and J'_{n,i_n} are the impurity excitation energy and the impurity-host interaction energy, respectively. We assume the concentration of impurities is low, so we can neglect impurity-impurity interactions. As it was implicitly done in Eq. 5.38, we conveniently add and subtract terms necessary to write the Hamiltonian as a sum of a zeroth-order Hamiltonian describing free excitons and a perturbation due to the presence of impurities, i.e.,

$$\begin{aligned}\hat{H} = & \Delta E_{eg} \sum_{n \neq 1}^N \hat{B}_n^\dagger \hat{B}_n + \sum_{n \neq 1}^N \sum_{m \neq n}^N J_{nm} \hat{B}_n^\dagger \hat{B}_m \\ & + V_0 \sum_{i_n}^{N_i} \hat{B}_{i_n}^\dagger \hat{B}_{i_n} + \sum_{i_n}^{N_i} \sum_{n \neq i_n}^{N_i} (J'_{n,i_n} - J_{n,i_n}) (\hat{B}_n^\dagger \hat{B}_{i_n} + \hat{B}_n \hat{B}_{i_n}^\dagger).\end{aligned}\quad (5.42)$$

We then transform the exciton operators to the wavevector representation $\hat{B}_n = (1/\sqrt{N}) \sum_{\mathbf{k}} \hat{B}_{\mathbf{k}} e^{i\mathbf{k} \cdot \mathbf{R}_n}$ to obtain

$$\begin{aligned}\hat{H} = & \sum_{\mathbf{k}} E(\mathbf{k}) \hat{B}_{\mathbf{k}}^\dagger \hat{B}_{\mathbf{k}} + \frac{V_0}{N} \sum_{\mathbf{k}} \sum_{\mathbf{q}} \hat{B}_{\mathbf{q}}^\dagger \hat{B}_{\mathbf{k}} \sum_{i_n} e^{i(\mathbf{k}-\mathbf{q}) \cdot \mathbf{i}_n} \\ & + \frac{1}{N} \sum_{i_n} \sum_{n \neq i_n} (J'_{n,i_n} - J_{n,i_n}) \left[\hat{B}_{\mathbf{q}}^\dagger \hat{B}_{\mathbf{k}} e^{i\mathbf{k} \cdot \mathbf{i}_n - i\mathbf{q} \cdot \mathbf{R}_n} + \text{h.c.} \right],\end{aligned}\quad (5.43)$$

where h.c. denotes Hermitian conjugate. In order to evaluate the summations over the impurity sites in the third term, we assume only nearest-neighbour interactions between host and impurity molecules, although there will be corrections to this approximation due to the long-range character of the dipole-dipole interaction. We then define the coupling constants $J'(a) = J'_{i_n+1,i_n}$ and $J(a) = J_{i_n+1,i_n}$ and write the third term as

$$\hat{W} = \frac{2\Delta J(a)}{N} \sum_{\mathbf{k}} \sum_{\mathbf{q}} \cos(|\mathbf{q}|a) \left[\hat{B}_{\mathbf{q}}^\dagger \hat{B}_{\mathbf{k}} \sum_{i_n} e^{i(\mathbf{k}-\mathbf{q}) \cdot \mathbf{i}_n} + \text{h.c.} \right]. \quad (5.44)$$

We have written Eq. 5.43 as the sum of three terms $\hat{H} = \hat{H}_0 + \hat{W} + \hat{V}$. The first term is the free-exciton Hamiltonian \hat{H}_0 . The second term is the exciton-impurity interaction due to the difference in transition energies, termed as diagonal disorder \hat{V} . The last term is the interaction due to the difference in interaction energies, termed as off-diagonal disorder \hat{W} . The potentials \hat{V} and \hat{W} are composed of terms that are diagonal in exciton wavevector $\mathbf{q} = \mathbf{k}$, which are responsible for an overall energy shift of the exciton band $\varepsilon(\mathbf{k})$ by the amount $(V_0 + 2\Delta J(a))(N_i/N)$, where N_i/N is the concentration of impurities. In most situations of interest for us we have $V_0 > \Delta J(a)$. If we apply an electric field such that $V_0 \rightarrow 0$, the off-diagonal disorder is the only contribution to the perturbation of free-exciton states. The terms that couple different exciton states $\mathbf{k} \neq \mathbf{q}$ are responsible for the generation of an exciton wavepacket in wavevector space, which by the uncertainty principle corresponds to a localization of the exciton wavefunction in real space. If we consider a large array of molecules with arbitrary dimensionality, we can impose periodic boundary conditions on the exciton wavefunctions and construct the Hamiltonian matrix $\hat{H} = \hat{H}_0 + \hat{W} + \hat{V}$ in the basis of free-exciton states $|\Psi_{\mathbf{k}}\rangle = \hat{B}_{\mathbf{k}}^\dagger|0\rangle$ using the following matrix elements

$$\langle\Psi_{\mathbf{k}}|\hat{H}_0|\Psi_{\mathbf{k}}\rangle = E(\mathbf{k}), \quad (5.45a)$$

$$\langle\Psi_{\mathbf{q}}|\hat{W}|\Psi_{\mathbf{k}}\rangle = \frac{2\Delta J(a)}{N} (\cos(|\mathbf{q}|a) + \cos(|\mathbf{k}|a)) \sum_{\vec{i}_n=1}^{N_i} e^{i(\mathbf{q}-\mathbf{k})\cdot\vec{i}_n}, \quad (5.45b)$$

$$\langle\Psi_{\mathbf{q}}|\hat{V}|\Psi_{\mathbf{k}}\rangle = \frac{V_0}{N} \sum_{\vec{i}_n=1}^{N_i} e^{i(\mathbf{q}-\mathbf{k})\cdot\vec{i}_n}, \quad (5.45c)$$

where $E(\mathbf{k})$ is the energy of the free-exciton (neglecting an overall energy shift). In Fig. 5.10(a) we show the energy spectrum for a one-dimensional array of $N = 100$ molecules, with 4% of homogeneously distributed LiRb impurities. An electric field perpendicular to the array is applied so that $V_0 = 80$ kHz. Panels (b) and (c) show exciton eigenstates of the impure lattice, chosen from the middle and the top of the energy spectrum, respectively. The eigenvalue problem is solved numerically by diagonalizing the complex matrix defined by Eq. (5.45).

The most noticeable feature of the spectrum in Fig. 5.10(a) is the appearance of energy levels separated from the renormalized band of exciton states. Since

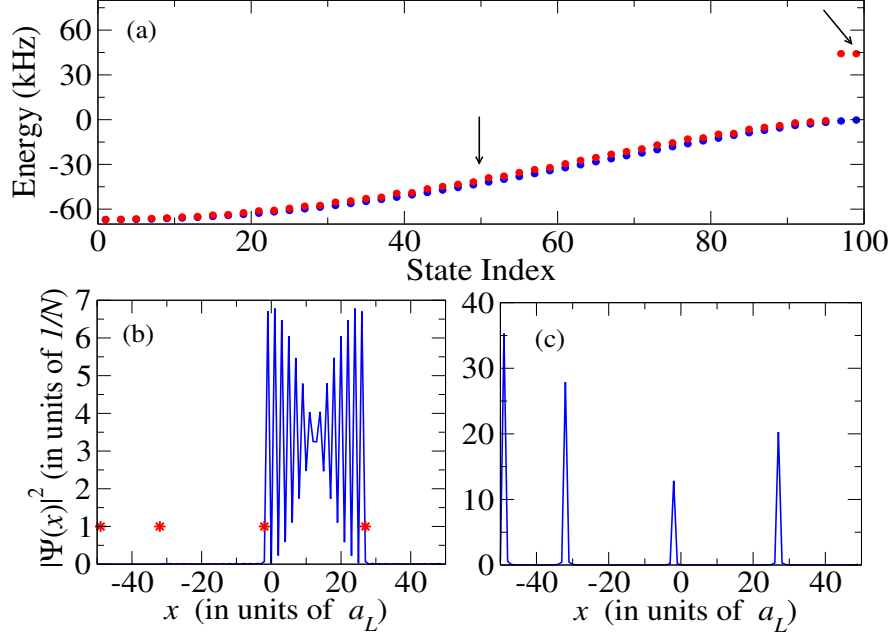


Figure 5.10: Spectrum and eigenstates of a 1D exciton in a disordered lattice of $N = 100$ LiCs molecule with 4% of LiRb molecules. A DC electric field is present such that $V_0 = 80$ kHz. Panel (a) shows the exciton spectra for the impure (red) lattice. The free-exciton band (blue) is shown for comparison. Arrows indicate the location of two chosen eigenstates: panel (b) shows a large group velocity state from the middle of the band, and panel (c) a zero group velocity state corresponding to a local level. The location of the impurities is indicated by stars in panel (b). The lattice constant is $a_L = 400$ nm.

$V_0 > 0$, these local levels have higher energy than the rest of the band. As shown in panel (c) this levels correspond to highly localized eigenstates in real space at the impurity sites. They can be considered as bound states of the exciton-impurity scattering potential. In general, states near the edges of the spectrum are highly localized, because the corresponding free-exciton states have vanishingly small group velocity. In panel (b), we show an eigenstate from the middle of the energy spectrum, which have a larger contribution from $|\mathbf{k}|a = \pi/2$ free-exciton states. These free-exciton states from the middle of the Brillouin zone have the largest

group velocity. The degree of localization of the corresponding eigenstates for the impure crystal is thus smaller.

Due to the negative effective mass of the free-excitons we consider as our basis set, the wavepackets near the top of the energy band have a large contribution of long-wavelength excitons $\mathbf{k} \approx 0$, which are accessible using microwave fields. In a disordered array, momentum is not conserved in the process of photon absorption, so in principle any exciton state is accessible using the appropriate photon energy, but those with long-wavelength character will have a larger transition dipole moment.

Field-induced disorder correlations and exciton delocalization

Let us consider a disordered array in the presence of a DC electric field such that $V_0 = 0$, i.e., the energy transition frequencies between the ground rotational state and a chosen excited state in two host and impurity molecules are the same. Because the induced dipole moments of the different molecules are not necessarily the same at this particular electric field, exciton-impurity scattering can still occur due to the terms proportional to ΔJ in Eq. (5.44), i.e., due to off-diagonal disorder. Figure 5.11 shows the probability density of a particular eigenstate of Hamiltonian (5.45) near the top of the energy spectrum, for different values of V_0 . Due to the negative effective mass of free-exciton states associated with the rotational transition $|J = 0, M_J = 0\rangle \rightarrow |J = 1, M_J = 0\rangle$, high energy eigenstates are dominated by free-exciton states with $\mathbf{k} \approx 0$. These eigenstates are localized as shown in panel (a). We note from the expression for the perturbations \hat{V} and \hat{W} , in wavevector space that two free-exciton states $|\Psi_{\mathbf{k}}\rangle$ and $|\Psi_{\mathbf{q}}\rangle$ would be decoupled to first order if the matrix element $\langle\Psi_{\mathbf{q}}|\hat{V} + \hat{W}|\Psi_{\mathbf{k}}\rangle$ vanishes. In panel (b) we show that the localized state from panel (a) corresponds adiabatically with a delocalized eigenstate obtained by applying a DC electric field at which $V_0 \approx -4\Delta J(a)$. At this field, as can be seen from Eqs. (5.45), for a given \mathbf{k} the matrix elements $\langle\hat{V}\rangle_{\mathbf{q},\mathbf{k}}$ and $\langle\hat{W}\rangle_{\mathbf{q},\mathbf{k}}$ cancel for $\mathbf{q} \approx \mathbf{k}$, which suppresses the coupling between the corresponding free-exciton states. In panel (c) we show that the eigenstates that correspond adiabatically to the localized state in panel (a), become localized for values of the electric field that do not balance the effects of V_0 and $\Delta J(a)$. We find that for local-

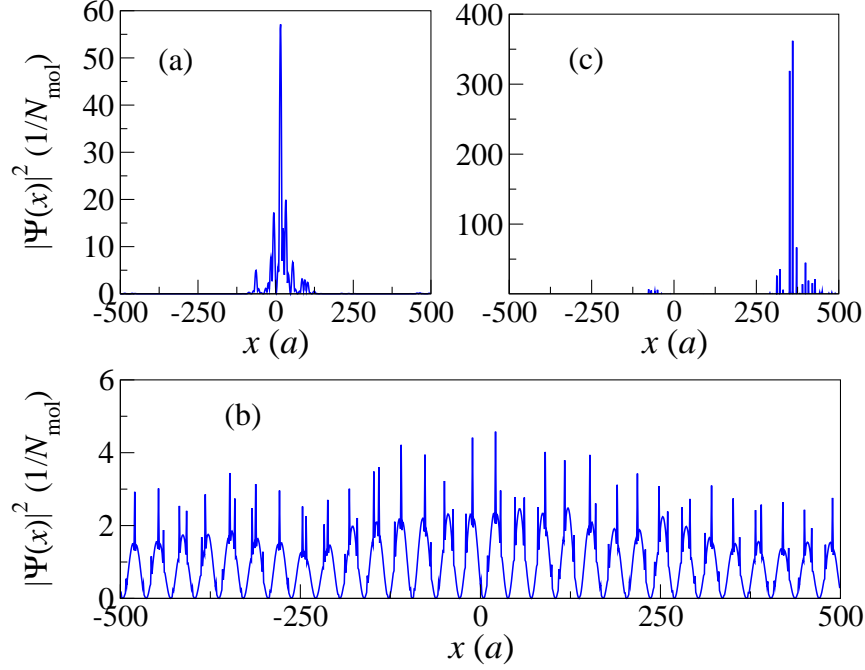


Figure 5.11: Probability density $|\Psi(x)|^2$ describing an exciton near the top of the energy spectrum for a 1D array of 1000 LiCs molecules with 10% of homogeneously and randomly distributed LiRb impurities. Panels correspond to different values of V_0 : (a) $V_0 = 0$, (b) $V_0/h = 22$ kHz, and (c) $V_0/h = 100$ kHz. The difference of the dipole moments of LiCs and LiRb molecules leads to the value $\Delta J = -6.89$ kHz.

ized eigenstates arbitrarily chosen within the energy band, we can choose a value of the electric field so that the state corresponds adiabatically to a delocalized state at some value of the electric field.

The eigenstates of quantum particles in a 1D disordered potential must be exponentially localized [190]. However, in the presence of specific correlations in the disordered potential, some localized states may undergo delocalization. For example, it follows from the results of Ref. [197] that the correlation between diagonal and off-diagonal disorder corresponding to substitutional disorder with one kind of impurities in a 1D molecular lattice with nearest neighbor interactions leads to delocalization of one eigenstate. Figure (5.11) illustrates the delocalization of

excitons in a 1D disordered system caused by this type of correlations between diagonal and off-diagonal disorder. Unlike in solids with fixed disorder, where disorder correlations lead to delocalization of one (or small number) of states, tunable disorder can be used to induce delocalization of any state in the exciton energy spectrum, as long as V_0 can be tuned to the value balancing the wavevector dependent off-diagonal disorder contribution.

5.4 Suggested applications

The system proposed here offers three unique features: (i) long-lived excitons that are stable against spontaneous decay and whose effective mass can be controlled by an external electric field; (ii) dynamically tunable impurities; (iii) possibility to arrange impurities and host molecules in various configurations and dimensions. This opens up new possibilities for quantum simulation of fundamental physical phenomena. For example, it is known that exciton - impurity scattering leads to localization of excitons in crystalline solids [190]. In particular, large cross sections for exciton - impurity scattering lead to Anderson localization. The exciton - impurity interactions in an ensemble of polar molecules with rotational excitons can be tuned from resonantly enhanced to entirely suppressed scattering, which can be used to study the dynamics of exciton localization, including the timescales for the formation of localized and delocalized states and their dependence on exciton bandwidth and exciton - impurity interaction strength. In addition, the system proposed here is ideally suited for the study of the effects of correlations in the disordered potentials. The presence of short- and long-range correlations in the disordered potentials may result in the appearance of a discrete [198, 199] or even continuous [200, 201] set of delocalized states in low-dimensional crystals. Measurements of exciton localization in a crystal with tunable impurities can be used for time-dependent quantum simulation of disorder-induced localization and delocalization of quantum particles.

Controlled spatial distributions of impurities and molecular crystals with specific arrangements of crystal particles in one, two or three dimensions may be used to study the effects of dimensionality and finite size on energy transfer in mesoscopic materials [108]. The localized states displayed in Figure 4 are many-body

entangled states of the molecules in an optical lattice. The possibility to tune exciton - impurity interactions can thus be exploited for the controlled creation of many-body entangled states of ultracold molecules, necessary for the experimental realization of quantum computation with molecular ensembles [126].

Finally, a mixture of ultracold molecules with impurities forming a sublattice may be used to study the formation of wavevector space crystals of excitons. The eigenstates of such a two-species lattice correspond to a discrete distribution in \mathbf{k} -space. Tuning the impurities by a sinusoidally varying electric field could then be used to induce resonant transitions between different k -states. In particular, it could be interesting to couple reversibly the low- k optically active, but slow (small group velocity) states with optically inactive, but fast (larger group velocity) states from the middle of the Brillouin zone. This would lead to the creation of excitonic wave packets, which can be slowed down or accelerated by an external electric field.

Chapter 6

Tunable polaron phenomena with polar molecules

6.1 Chapter overview

The description of phonons in an optical lattice of interacting molecules is presented in Sec. 6.3. In Section 6.3.3 it is shown that the phonon spectrum can be manipulated by tuning the DC electric field and the intensity of the trapping laser. Realistic estimates of the system parameters for alkali-metal dimers are also given. In Section 6.4 it is shown that the system can be described by the Holstein and the Su-Schrieffer-Heeger (SSH) polaron models in the limit of strong and weak electric field strengths, respectively.

6.2 Polaron models in condensed matter

The polaron problem falls under the general category of a particle interacting with its environment. In particular, the properties of a quantum particle depend on the strength of the interaction with a macroscopic gas of bosons. In solids and molecular aggregates the bosonic environment correspond to lattice phonons and the particle can be either a charge carrier such as an electron or hole, or an elementary excitation such as an exciton, magnon or polariton. The polaron problem in condensed matter theory is important because it is relevant to describe a wide range of physical systems of technological interest. Polaron effects are also important from a fundamental point of view, since in many solids collective quantum effects such as superconductivity arise due to the coupling of individual particles to the phonon environment [84].

Polarons are not restricted to crystalline solids. The transport properties of many organic molecular aggregates [98] and biological systems [116, 202] are determined by polaron effects. Consider the energy transfer processes between complex molecules in mesoscopic aggregates [108, 203]. The energy captured at one unit of the aggregate can be transferred incoherently to other sites via direct two-molecule interactions or through the formation of excitons [99]. Since these processes occur at room temperature, the role of quantum entanglement and coherence in excitation energy transfer in biological systems is a very interesting open question [116, 204]. In molecular systems with multiple degrees of freedom, coherence of excitons is quickly destroyed due to interactions with the environment, usually a large polymeric matrix with multiple vibrational modes. These vibrational modes constitute phonons that are coupled to the excitonic degrees of freedom which are responsible for the coherent energy transfer.

In this section three of the most commonly studied single-polaron models in condensed matter are briefly reviewed. These are the Fröhlich or large-polaron model, the Holstein or small-polaron model and the Su-Schrieffer-Heeger (SSH) model. Single-particle properties are considered using a perturbative analysis to provide a qualitative comparison between these models. A more quantitative account can be found in Ref. [205].

The polaron Hamiltonian can be written as

$$\hat{H} = \hat{H}_p + \hat{H}_{ph} + \hat{H}_{int} \quad (6.1)$$

where \hat{H}_p is the Hamiltonian describing the free particle or quasi-particle, \hat{H}_{ph} is the phonon Hamiltonian and \hat{H}_{int} describes the exciton-phonon interaction. Different polaron models assume different forms for the interaction Hamiltonian \hat{H}_{int} .

6.2.1 Fröhlich model

The Fröhlich polaron model describes the interaction between a single electron and optical phonons in a polar solid in three dimensions. Let the energy of the free electron with mass m be isotropic of the form $E(\mathbf{p}) = \mathbf{p}^2/2m$, where \mathbf{p} is momentum. Longitudinal optical phonons are represented by an Einstein model in which the phonon modes are degenerate: $\omega(\mathbf{q}) = \omega_0$, where ω is the phonon frequency and \mathbf{q} the phonon wavevector. The Fröhlich Hamiltonian [84] is given by Eq. (6.1) with

$$\hat{H}_p = \sum_{\mathbf{p}} E(\mathbf{p}) \hat{c}_{\mathbf{p}}^\dagger \hat{c}_{\mathbf{p}} \quad \hat{H}_{ph} = \hbar \omega_0 \sum_{\mathbf{q}} \hat{a}_{\mathbf{q}}^\dagger \hat{a}_{\mathbf{q}} \quad (6.2)$$

$$\hat{H}_{int} = \sum_{\mathbf{q}, \mathbf{p}} \frac{M_0}{V^{1/2}} \frac{1}{|\mathbf{q}|} \hat{c}_{\mathbf{p}+\mathbf{q}}^\dagger \hat{c}_{\mathbf{p}} \left(\hat{a}_{\mathbf{q}} + \hat{a}_{-\mathbf{q}}^\dagger \right) \quad (6.3)$$

where the operator $\hat{c}_{\mathbf{p}}^\dagger$ creates an electron with momentum \mathbf{p} , $\hat{a}_{\mathbf{q}}^\dagger$ creates a phonon with momentum \mathbf{q} , and V is the volume of the crystal. The electron-phonon coupling constant M_0 is given by

$$M_0 = -i(4\pi\alpha)^{1/2} \hbar \omega_0 \left(\frac{\hbar}{2m\omega_0} \right)^{1/4} \quad \alpha = \frac{e^2}{\hbar} \left(\frac{m}{2\hbar\omega_0} \right)^{1/2} \left(\frac{1}{\epsilon_\infty} - \frac{1}{\epsilon_0} \right). \quad (6.4)$$

The particle-phonon interaction energy depends on the phonon frequency as $\omega_0^{1/2}$ and on the phonon wavevector as $1/|\mathbf{q}|$.

Weak coupling regime

The change in the energy of the electron due to the interaction with lattice phonons can be evaluated using Rayleigh-Schrödinger (RS) perturbation theory by assuming the dimensionless coupling α to be smaller than unity. In Appendix E it is shown that to second order in M_0 the energy of the dressed electron (polaron) in atomic units ($\hbar = 1$) is

$$E_{\mathbf{p}} = E(\mathbf{p}) - \frac{\alpha \omega_0^{3/2}}{E(\mathbf{p})^{1/2}} \sin^{-1} \left(\frac{E(\mathbf{p})^{1/2}}{\omega_0^{1/2}} \right), \quad (6.5)$$

where $E(\mathbf{p}) = \mathbf{p}^2/2m$. This solution holds for $E(\mathbf{p}) < \hbar\omega_0$, otherwise energy-conserving phonon emission and absorption processes are possible and RS stationary perturbation theory is no longer applicable. This condition corresponds to the non-adiabatic limit in which the motion of the particle is faster than lattice oscillations. In the limit of a slow-moving polaron $\mathbf{p} \rightarrow 0$ the energy becomes

$$E_{p \rightarrow 0} = \frac{p^2}{2m^*} - \alpha\omega_0, \quad (6.6)$$

where the effective mass of the polaron is

$$m^* = \frac{m}{1 - \alpha/6} \approx m \left(1 + \frac{\alpha}{6} \right). \quad (6.7)$$

The ground state energy of the Fröhlich polaron $E_g = E_{\mathbf{p}=0}$ in the weak coupling regime therefore decreases linearly with ω_0 with a slope given by α . The polaron mass is larger than the bare electron mass due to the interaction between the electron and the lattice oscillators. For small α , the effective polaron mass increases linearly with the coupling strength.

The weak coupling RS perturbative results for the ground state energy and effective mass are known to be accurate up to $\alpha \sim 5$ [84]. Beyond this coupling strength the particle becomes localized in space by the strong interaction with the lattice. Equation 6.7 confirms this expectation since the effective mass m^* diverges when $\alpha = 6$.

Strong coupling regime

Following the assumption of particle localization, the strong coupling regime of the Fröhlich model was originally developed as a variational calculation for the ground state energy with a Gaussian trial wavefunction [206]. The minimum polaron energy was found to be $E_g = -\alpha^2 \omega_0 / 3\pi$. Using a path-integral formulation, the Fröhlich Hamiltonian was solved accurately for arbitrary values of α [206–209]. In the weak coupling limit $\alpha < 5$ the path-integral results are in reasonable agreement with fourth-order RS perturbation theory results that include two-phonon states [84]. In the strong coupling regime the polaron ground state energy E_0 and the effective mass m^* can be expanded as

$$E_g = -\omega_0 [0.106\alpha^2 + 2.836 + O(1/\alpha^2)], \quad (6.8)$$

and

$$\frac{m^*}{m} \approx 0.0202\alpha^4. \quad (6.9)$$

The point to remember is that in the strong coupling regime of the Fröhlich model the effective mass of the particle increases algebraically with the coupling strength. It is difficult to obtain momentum-dependent properties analytically for arbitrary values of α . Over the decades several numerical approaches have been used to address this issue [210–213]. An analysis of these numerical methods is outside the scope of this chapter.

6.2.2 Holstein model

The size of the polaron wavefunction becomes comparable to the lattice spacing in the strong coupling limit of the particle-phonon interaction. We refer to this situation as a “small” polaron problem [84, 214]. In the small polaron limit the phonon-dressed particle hops from site to site in a tight binding model. The phonons are coupled to the particle at the site where it resides. In a tight binding approach the bare energy dispersion of the particle $E(\mathbf{k})$ is not necessarily quadratic in the wavevector \mathbf{k} . In the Holstein model the discreteness of the lattice is explicitly

taken into account. The Hamiltonian in this model is given by Eq. (6.1) with

$$\hat{H}_p = \sum_{\mathbf{k}} E(\mathbf{k}) \hat{c}_{\mathbf{k}}^\dagger \hat{c}_{\mathbf{k}} \quad \hat{H}_{ph} = \sum_{\mathbf{q}} \omega_{\mathbf{q}} \hat{a}_{\mathbf{q}}^\dagger \hat{a}_{\mathbf{q}} \quad (6.10)$$

$$\hat{H}_{int} = \sum_{\mathbf{q}, \mathbf{k}} M_{\mathbf{q}} \hat{c}_{\mathbf{k}+\mathbf{q}}^\dagger \hat{c}_{\mathbf{k}} \left[\hat{a}_{\mathbf{q}} + \hat{a}_{-\mathbf{q}}^\dagger \right]. \quad (6.11)$$

In its simplest form, the Holstein model assumes Einstein phonons $\omega_{\mathbf{q}} = \omega_0$ and wavevector independent particle-phonon coupling $M_{\mathbf{q}} = g/\sqrt{N}$ [205, 214, 215].

Let us focus on a one-dimensional lattice. If the particle hopping occurs only between nearest neighbours, the dispersion relation is given by $E(k) = -2t \cos(k)$, where $t > 0$ is the hopping amplitude. Length is measured in units of the lattice constant a . Two dimensionless parameters are commonly used to describe the Holstein polaron regimes. One is the adiabaticity ratio

$$A = \frac{\hbar \omega_0}{t}, \quad (6.12)$$

and the other is the dimensionless particle-phonon coupling

$$\alpha = \frac{g^2}{2t\hbar\omega_0}. \quad (6.13)$$

For a given value of t and g , the particle-phonon coupling is weaker as the phonon frequency increases. This is in agreement with the Fröhlich model in the weak coupling regime. Large values of A correspond to the non-adiabatic limit of the system dynamics. For low phonon frequencies such that $A \ll 1$, the polaron effects become stronger.

Weak coupling regime

The weak coupling regime of the Holstein model can be treated in the same way as above for the Fröhlich polaron. The particle-phonon interaction energy g is the smallest energy scale of the problem and can be considered as a perturbation. The zero-th order state of the particle have a well defined wavevector \mathbf{k} . For a one-dimensional lattice with nearest-neighbour interactions, the energy of the polaron

up to second order in RS perturbation theory is given by

$$E_{\mathbf{k}} = -2t \cos(k) - \alpha \omega_0 \int_{-\pi}^{\pi} \frac{dq}{(2\pi)} \frac{1}{A/2 + \cos(k) - \cos(k-q)} \quad (6.14)$$

The integral can be evaluated numerically for a given value of the adiabaticity ratio $A > 4$. The integral can diverge for smaller values of A , as energy-conserving phonon emission and absorption processes become allowed and stationary perturbation theory is no longer applicable. The ground state energy depends linearly on the coupling constant α as in the Fröhlich model.

Strong coupling regime

In the strong coupling limit $\alpha \gg 1$, the energy of the particle $E(\mathbf{k})$ is the smallest energy scale of the problem. The Hamiltonian in this regime is best solved using the site representation for the particle operators, and can be partitioned as $\hat{H} = \hat{H}_0 + \hat{V}$, where

$$\hat{H}_0 = \varepsilon \hat{c}_i^\dagger \hat{c}_i + \sum_{\mathbf{q}} \omega_{\mathbf{q}} \hat{a}_{\mathbf{q}}^\dagger \hat{a}_{\mathbf{q}} + \frac{g}{\sqrt{N}} \sum_{i\mathbf{q}} \hat{c}_i^\dagger \hat{c}_i e^{i\mathbf{q} \cdot \mathbf{R}_i} (\hat{a}_{\mathbf{q}} + \hat{a}_{-\mathbf{q}}^\dagger) \quad (6.15)$$

$$\hat{V} = -t \sum_{i,j} \hat{c}_i^\dagger \hat{c}_j. \quad (6.16)$$

The partition has been chosen such that \hat{H}_0 corresponds to an independent boson model, which can be solved exactly [84]. The eigenstates of \hat{H}_0 serve as the zeroth order states in the perturbative analysis of the full Hamiltonian [215]. In Appendix E it is shown that using the canonical transformation

$$U = \exp \left[\sum_{j\mathbf{q}} \hat{c}_j^\dagger \hat{c}_j e^{i\mathbf{q} \cdot \mathbf{R}_j} \frac{M_{\mathbf{q}}}{\omega_{\mathbf{q}}} (\hat{a}_{-\mathbf{q}}^\dagger - \hat{a}_{\mathbf{q}}) \right],$$

the transformed Hamiltonian \bar{H}_0 can be written in the diagonal form

$$\bar{H}_0 \equiv \hat{U} \hat{H}_0 \hat{U}^\dagger = \hat{c}_i^\dagger \hat{c}_i (\varepsilon - \Delta E_g) + \sum_{\mathbf{q}} \omega_{\mathbf{q}} \hat{a}_{\mathbf{q}}^\dagger \hat{a}_{\mathbf{q}}, \quad (6.17)$$

where $\Delta E_g = N^{-1} \sum_{\mathbf{q}} g^2 / \omega_{\mathbf{q}}$ is the polaron shift from the single particle energy ε . The polaron shift depends on the square of the coupling energy g and is enhanced at low phonon frequencies.

The hopping of the particle between sites is determined by the operator $\hat{V} = -t \sum_{i,j} \hat{c}_i^\dagger \hat{c}_j$, where $t > 0$ is the hopping amplitude. In Appendix E it is shown that the transformed hopping operator can be written as $\bar{V} = -t \sum_{i,j} \hat{c}_i^\dagger \hat{c}_j \hat{X}_i^\dagger \hat{X}_j$, where

$$\hat{X}_i^\dagger \hat{X}_j = \exp \left[N^{-1/2} \sum_{\mathbf{q}} e^{i\mathbf{q} \cdot \mathbf{R}_j} \frac{g}{\omega_{\mathbf{q}}} \left(\hat{a}_{\mathbf{q}} - \hat{a}_{-\mathbf{q}}^\dagger \right) \right]. \quad (6.18)$$

The particle hopping is thus modulated by phonons, which are usually considered to be in a thermal equilibrium state. By taking the expectation value of the operator \bar{V} over the phonon states the hopping of the particle can be described by $\bar{V} = -\bar{t} \hat{c}_i^\dagger \hat{c}_j$, which is of the same form as the bare hopping operator \hat{V} in Eq. (6.16) but with an exponentially suppressed amplitude

$$\bar{t} = t e^{-S_T}, \quad (6.19)$$

where $e^{-S_T} = \langle i | \hat{X}_i^\dagger \hat{X}_j | i \rangle$ is the expectation value over the thermal phonon state. At low temperatures the phonon-dressed particle (polaron) can hop coherently between sites without emitting or absorbing phonons. The polaron spectrum forms a band with an exponentially suppressed bandwidth and exponentially increased effective mass near at the origin of the Brillouin zone. Incoherent hopping between sites involve the phonon absorption and emission processes. This is the dominant hopping mechanism at higher temperatures. A more comprehensive description of the small polaron problem can be found in Ref. [84].

6.2.3 Su-Schrieffer-Heeger model

The Su-Schrieffer-Heeger (SSH) model was originally introduced to describe a one-dimensional trans-polyacetylene polymer chain, which is an example of systems with phonon-modulated particle hopping [216, 217]. In the Holstein model the particle interacts with phonons locally at each lattice site. This is represented in the interaction Hamiltonian \hat{H}_{int} by its dependence on the interaction energy $M_{\mathbf{q}}$

on the phonon wavevector only. The particle hopping is due to the overlap of the particle's wavefunction in different sites and does not depend on the lattice motion. In a realistic lattice, the site position changes dynamically. The hopping amplitude t depends on the distance between lattice sites. If this distance changes as a consequence of the lattice motion, then t also varies. Since the lattice motion is quantized, the variation of t involves the creation or annihilation of phonons. The phonon-modulated hopping is represented in the interaction Hamiltonian \hat{H}_{int} by a dependence of the interaction energy on the wavevector of the particle, i.e.,

$$\hat{H}_{\text{int}} = \sum_{\mathbf{q}, \mathbf{k}} M_{\mathbf{k}, \mathbf{q}} \hat{c}_{\mathbf{k}+\mathbf{q}}^\dagger \hat{c}_{\mathbf{k}} \left[\hat{a}_{\mathbf{q}} + \hat{a}_{-\mathbf{q}}^\dagger \right]. \quad (6.20)$$

For a one-dimensional lattice with nearest-neighbour hopping we can write [218]

$$M_{k,q} = \frac{1}{\sqrt{N}} 2i\alpha_q [\sin(k+q) - \sin(k)], \quad (6.21)$$

where

$$\alpha_q = \frac{\tilde{\alpha}t}{\sqrt{2m\omega(q)}}. \quad (6.22)$$

For length measured in units of the lattice constant ($a = 1$), the parameter $\tilde{\alpha}$ is a dimensionless number, and m is the mass of the lattice oscillators.

Sharp transition in the strong coupling regime

For the Holstein and related models without phonon-mediated hopping the polaron band has a minimum at the origin of the Brillouin zone $k = 0$ for all values of the particle-phonon coupling strength. The polaron band shape changes dramatically as a function of the coupling strength, which results in the increase of the effective mass in the limit of strong coupling. The SSH and other models with phonon-modulated hopping behave differently in the limit of strong particle-phonon coupling. In this regime, the minimum energy of the polaron band occurs at a finite wavevector $k_g \neq 0$ and the bandwidth remains finite. In the weak coupling limit, the SSH model behaves analogously to the Holstein and related models. The transition from weak to strong coupling in the SSH model is sharp. Discontinuities in the polaron properties have been shown to exist for this model [205, 218]. This is con-

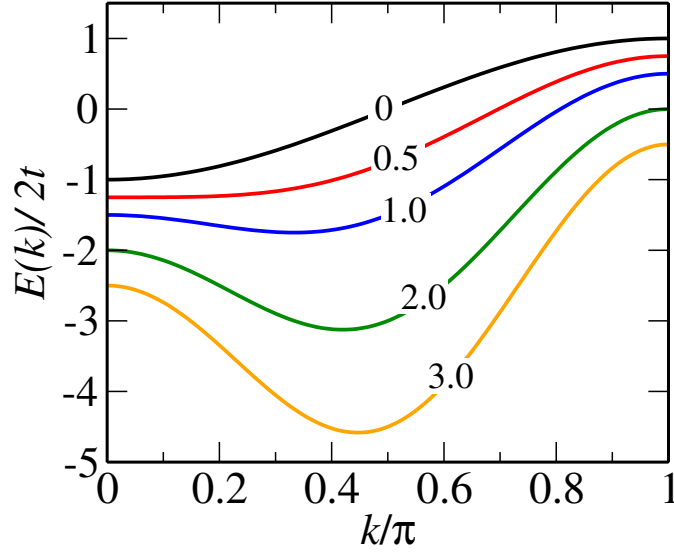


Figure 6.1: Polaron dispersion $E(k)$ (in units of $2t$) for a one-dimensional SSH model in the non-adiabatic regime $\omega_0/t \gg 1$. The curves are labeled by the value of the particle-phonon coupling constant $\lambda = 2\alpha^2/t\omega_0$. t is the particle hopping amplitude and ω_0 is the phonon frequency. The particle-phonon interaction energy is proportional to α . Energy is obtained from second-order Rayleigh-Schrödinger perturbation theory with Einstein phonons.

trary to the Holstein model for which it is known that the self-trapping crossover is continuous as the coupling strength is increased [215].

Let us consider a one-dimensional lattice in the non-adiabatic limit $\omega_0/t \gg 1$. In this limit we can use RS perturbation theory with the free particle and phonon as the zeroth order states. In Appendix E it is shown that polaron dispersion to second order in the interaction energy for optical phonons in the limit $\omega_0 \rightarrow \infty$ is given by

$$E(k) = -2t \cos(k) - t\lambda [2 - \cos(2k)] \quad (6.23)$$

where the dimensionless coupling λ is defined as

$$\lambda = \frac{2\alpha^2}{t\omega_0}. \quad (6.24)$$

The polaron dispersion in the non-adiabatic limit is shown in Fig. 6.1 for several values of λ . At the critical particle-phonon coupling $\lambda_c = 1/2$, the wavevector of the polaron ground state shifts from $k_{\text{gs}} = 0$ to a finite value. This is contrary to the behaviour of the Fröhlich or Holstein polaron models in the non-adiabatic limit where the ground state is at the origin of the Brillouin zone for all coupling strengths. The shift of the ground state to finite wavevectors is a consequence of phonon-mediated hopping. For example, a particle can hop to the neighbouring site by creating a phonon at the destination site and then hop one site further by annihilating this phonon. In Appendix E it is shown that this second order hopping has an amplitude $t_2 = -\alpha^2/\omega_0$ and leads to the term $-2t_2 \cos(2k)$ in the dispersion, which favours a minimum at $\pi/2$.

6.3 Polarons with cold molecules in optical lattices

There is currently growing interest in using ultracold atoms trapped on an optical lattice for quantum simulation of condensed matter phenomena [79, 83]. Ultracold atoms offer the possibility of designing quantum systems that are well described by models such as the Bose-Hubbard Hamiltonian [82]. However, it is difficult to design a quantum system with significant exciton - phonon couplings using ultracold atoms, primarily because the interactions between atoms trapped on an optical lattice are very weak and the external motion of the atoms is entirely determined by the trapping lattice potential. It was recently shown that polar molecules trapped on an optical lattice provide new possibilities for quantum simulation due to the presence of long-range dipole-dipole interactions [87, 195]. In this chapter, we consider the possibility that rotational excitons in an ensemble of polar molecules on an optical lattice interact with the translational motion of the molecules in the lattice potential. It is shown that under weak trapping conditions the dipole-dipole interaction between molecules can significantly couple the dynamics of rotational excitons with the lattice vibrations, and that this coupling can be tuned with an external DC electric field.

The main features of the exciton - phonon interaction in molecular aggregates can be described by a simple Holstein model [84, 214], that accounts for the deformation of the lattice potential when molecules are internally excited. The Holstein

and related models describe the coupling strength to excitons by phenomenological constants, because the complexity of the interactions with the environment make it difficult to calculate the coupling constants using ab-initio methods. Normally, information about the coupling strengths is obtained approximately from spectroscopic data [115, 116]. Therefore, it would be desirable to design an experimentally accessible many-body quantum system that would be described exactly by the Holstein Hamiltonian, with the advantage that the exciton-phonon coupling constants can be determined from first principles. Such a system could be used for quantum simulation of excitonic energy transfer in complex molecular aggregates, for example.

6.3.1 Molecular Lattice Hamiltonian

Let us consider an array of molecules trapped in a 3D optical lattice with one molecule per lattice site, without tunneling of molecules between sites [82, 83]. This has been achieved for Cs₂, Rb₂ and KRb molecules [20, 21, 137, 219]. For the ground and a few excited Bloch bands of the periodic lattice potential, molecules can be considered to vibrate harmonically around the site positions \mathbf{R}_i , with angular frequency ω_0 [79, 82]. For a given lattice direction, the equilibrium distance between different sites is given by half the wavelength of the corresponding trapping laser, i.e., $\mathbf{R}_i - \mathbf{R}_{i+1} = \lambda/2$. Under these conditions, the ensemble is described by the Hamiltonian

$$\hat{H} = \sum_i \frac{\mathbf{p}_i^2}{2m} + \frac{1}{2} m \omega_0^2 (\mathbf{r}_i - \mathbf{R}_i)^2 + B_e \mathbf{N}_i^2 - \mathbf{d}_i \cdot \mathbf{E} + \frac{1}{2} \sum_i \sum_{j \neq i} V(\mathbf{r}_i - \mathbf{r}_j), \quad (6.25)$$

where \mathbf{r}_i and \mathbf{p}_i are the position and momentum, \mathbf{N}_i is the rotational angular momentum, \mathbf{d}_i is the electric dipole, B_e is the rotational constant and m is the mass of the molecule in site i , \mathbf{E} is the DC electric field and \hat{V} is the intermolecular interaction potential. The frequency ω_0 scales as $\sqrt{I_L}$, where I_L is the intensity of the trapping laser [79]. For experimentally realizable lattice site separations $a \sim 200 - 500$ nm, V is determined by the electric dipole-dipole interaction, with a characteristic

energy $V_{dd} = d_0^2/a^3$ (in atomic units), where d_0 is the molecular permanent dipole moment. For molecules with $d_0 \sim 1 - 8$ Debye, we have $V_{dd}/h \sim 1 - 10^3$ kHz.

In Chapter 5 it was shown that the intermolecular interaction in second-quantized form contains a term that depends on the interaction between ground state molecules plus additional terms that describe the collective excitations in the lattice. Up to now we have neglected the contribution of this ground state interaction, because we were interested in the excited state properties of the ensemble. More explicitly, the quantization of the intermolecular interaction can be written as

$$\begin{aligned} \frac{1}{2} \sum_{i,j} V(\mathbf{r}_i - \mathbf{r}_j) &= \frac{1}{2} \sum_i \sum_{j \neq i} \langle g_i | \langle g_j | V_{\text{int}} | g_i \rangle | g_j \rangle + \sum_i \sum_{j \neq i} D_{ij} \hat{B}_i^\dagger \hat{B}_i + \sum_{i,j \neq i} J_{i,j} \hat{B}_i^\dagger \hat{B}_j \\ &= \frac{1}{2} \sum_i \sum_{j \neq i} \frac{U_g}{|\mathbf{r}_i - \mathbf{r}_j|^3} + \sum_i \sum_{j \neq i} D_{ij} \hat{B}_i^\dagger \hat{B}_i + \sum_{i,j \neq i} J_{i,j} \hat{B}_i^\dagger \hat{B}_j, \end{aligned} \quad (6.26)$$

where $U_g = \langle g_i | \langle g_j | V_{\text{int}} | g_i \rangle | g_j \rangle$ only depends on the internal degrees of freedom of the molecules. This separation of coordinates was demonstrated in Chapter 2, using the spherical tensor representation of the dipole-dipole interaction. The first term in the above equation can be included in the classical potential energy for the molecular motion in the lattice. We can consider the total lattice potential experienced by a molecule to be

$$U(\mathbf{r}_i) = \frac{1}{2} m \omega_0^2 (\mathbf{r}_i - \mathbf{R}_i)^2 + \frac{1}{2} \sum_{j \neq i} \frac{U_g}{|\mathbf{r}_i - \mathbf{r}_j|^3}. \quad (6.27)$$

In the limit $m \omega_0^2 \gg U_g$, the first term dominates over the second term, and the lattice dynamics is given entirely by the laser trap. In this case, interactions between molecules are responsible for the internal state dynamics only. In the opposite limit, the molecular interactions can be strong enough to displace the molecules from the site positions $\mathbf{R}_i = (X_i, Y_i, Z_i)$ to new equilibrium positions $\mathbf{R}_i^0 = (X_i^0, Y_i^0, Z_i^0)$.

The lattice Hamiltonian in Eq. 6.25 can be written in a more general way, accounting for the total potential energy of the molecular motion, as

$$\hat{H} = \sum_i \frac{\mathbf{p}_i^2}{2m} + \sum_i U(\mathbf{r}_i) + B_e \mathbf{N}_i^2 - \mathbf{d}_i \cdot \mathbf{E} + \frac{1}{2} \sum_i \sum_{j \neq i} V_{\text{ex}}(\mathbf{r}_i - \mathbf{r}_j), \quad (6.28)$$

where $U(\mathbf{r}_i)$ is given by Eq. (6.27), and V_{ex} includes only contributions of the dipole-dipole interaction that determine the collective rotational excited states of the molecular array (excitons), as well as non-linear exciton-exciton interactions.

6.3.2 Lattice Dynamics

We have seen that in general the dipole-dipole interaction will couple the translational motion of the molecules in different lattice sites. It is standard practice in condensed matter theory to analyze this motion in terms of classical normal modes, and then quantize the normal modes in the harmonic approximation for the intermolecular potential [84]. The energy spectrum of the vibrational modes is obtained by solving the equation of motion for the harmonic displacements around the equilibrium positions of the potential $U(\mathbf{r}_1, \dots, \mathbf{r}_N)$. This potential can be expanded in Taylor series in powers of small displacements defined by $\mathbf{r}_i = \mathbf{R}_i^0 + \mathbf{x}_i$. Ignoring cubic terms in \mathbf{x}_i , the potential is given by

$$U(\mathbf{x}_1, \dots, \mathbf{x}_N) = U_0 + \sum_i \left(\vec{\nabla}_{\mathbf{r}_i} U \right)_0 \cdot \mathbf{x}_i + \frac{1}{2} \sum_i \sum_j \mathbf{x}_i \cdot \left(\vec{\nabla}_{\mathbf{r}_i} \vec{\nabla}_{\mathbf{r}_j} U \right)_0 \cdot \mathbf{x}_j, \quad (6.29)$$

where the notation $()_0$ means that the derivatives are evaluated at the equilibrium positions. The first term U_0 is a constant potential energy of the equilibrium configuration, and we neglect it in the following discussion. The equilibrium positions are solutions of the equations $\vec{\nabla}_{\mathbf{r}_i} U = 0$, therefore the second term vanishes. The potential energy of the molecular motion is then given in the harmonic approximation by

$$U(\mathbf{x}_1, \dots, \mathbf{x}_N) = \frac{1}{2} \sum_{i,j} \sum_{\mu,\nu} D_{\mu i, \nu j} x_{\mu i} x_{\nu j}, \quad (6.30)$$

where the symmetric dynamical matrix elements

$$D_{\mu i, \nu j} = \frac{\partial^2 U}{\partial r_{i\mu} \partial r_{j\nu}}$$

are defined as the second derivatives of the given pair potential

$$U(\mathbf{r}_i, \mathbf{r}_j) = \frac{1}{2} m \omega_0^2 [(\mathbf{r}_i - \mathbf{R}_i)^2 + (\mathbf{r}_j - \mathbf{R}_j)^2] + \frac{1}{2} \sum_{j \neq i} \frac{U_g}{|\mathbf{r}_i - \mathbf{r}_j|^3},$$

evaluated at the equilibrium positions, i.e.,

$$D_{\mu i, \mu i} = m \omega_0^2 - \frac{3}{2} U_g \sum_{j \neq i} \left(\frac{1}{|\mathbf{R}_i^0 - \mathbf{R}_j^0|^5} - 5 \frac{(x_{\mu i}^0 - x_{\mu j}^0)^2}{|\mathbf{R}_i^0 - \mathbf{R}_j^0|^7} \right), \quad (6.31a)$$

$$D_{\mu i, \nu i} = \frac{15}{2} U_g \sum_{j \neq i} \frac{(x_{\mu i}^0 - x_{\mu j}^0)(x_{\nu i}^0 - x_{\nu j}^0)}{|\mathbf{R}_i^0 - \mathbf{R}_j^0|^7}, \quad (6.31b)$$

$$D_{\mu i, \mu j} = \frac{3}{2} U_g \left(\frac{1}{|\mathbf{R}_i^0 - \mathbf{R}_j^0|^5} - 5 \frac{(x_{\mu i}^0 - x_{\mu j}^0)^2}{|\mathbf{R}_i^0 - \mathbf{R}_j^0|^7} \right), \quad (6.31c)$$

and

$$D_{\mu i, \nu j} = -\frac{15}{2} U_g \frac{(x_{\mu i}^0 - x_{\mu j}^0)(x_{\nu i}^0 - x_{\nu j}^0)}{|\mathbf{R}_i^0 - \mathbf{R}_j^0|^7}. \quad (6.31d)$$

These expressions together with the symmetries $D_{\mu i, \mu j} = D_{\mu j, \mu i}$, $D_{\mu i, \nu j} = D_{\mu j, \nu i}$, and $D_{\mu i, \nu j} = D_{\nu j, \mu i}$, that must be satisfied for the quadratic form in Eq. (6.30), completely define all the (3×3) dynamical matrices D_{ij} , associated with the molecular displacements \mathbf{x}_i and \mathbf{x}_j . For the potential energy in Eq. (6.30), the classical equation of motion for the component $x_{\mu, i}$ of the displacement at site i is then given by

the equation [84]

$$\begin{aligned}
m \frac{d^2 x_{\mu i}(t)}{dt^2} &= - \frac{\partial U}{\partial x_{\mu i}} \\
&= - \frac{\partial}{\partial x_{\mu i}} \left\{ \frac{1}{2} D_{\mu i, \mu i} x_{\mu i}^2 + \frac{1}{2} \sum_{j \neq i} D_{\mu i, v j} x_{\mu i} x_{v j} + D_{v j, \mu i} x_{v j} x_{\mu i} \right\} \\
&= - D_{\mu i, \mu i} x_{\mu i} - \sum_{j \neq i} \sum_{v \neq \mu} D_{\mu i, v j} x_{v j}
\end{aligned} \tag{6.32}$$

where in the second line we only keep the terms that contribute to the equation of motion, and in the third line we used the symmetry of the dynamical matrix.

We look for harmonic solutions to Eq. (6.32) of the form $x_{\mu, i}(t) = \varepsilon_{\mu} e^{i(\mathbf{q} \cdot \mathbf{R}_i^0 - \omega t)}$, where ε_{μ} is a complex amplitude. Replacing this ansatz in the equation of motion, we have

$$\begin{aligned}
- m \omega^2 e^{i\mathbf{q} \cdot \mathbf{R}_i^0} e^{-i\omega t} \varepsilon_{\mu} &= - \sum_v \sum_j D_{\mu i, v j} e^{i\mathbf{q} \cdot \mathbf{R}_j^0} e^{-i\omega t} \varepsilon_v \\
m \omega^2 \varepsilon_{\mu} &= \sum_v D_{\mu, v}(\mathbf{q}) \varepsilon_v
\end{aligned} \tag{6.33}$$

which is an eigenvalue equation, for the dynamical matrix in Fourier space given by ($i = j$ terms are included)

$$D_{\mu, v}(\mathbf{q}) = \sum_j D_{\mu i, v j} e^{i\mathbf{q} \cdot (\mathbf{R}_j^0 - \mathbf{R}_i^0)}. \tag{6.34}$$

Assuming periodic boundary conditions, we can solve this eigenvalue problem for the polarization vectors $\vec{\varepsilon}$, for each allowed value of the wavevector \mathbf{q} . The eigenvalues $\lambda_{\varepsilon}(\mathbf{q}) = m \omega_{\varepsilon}^2(\mathbf{q})$ give the energy associated with the Fourier mode \mathbf{q} , of the motion along the polarization direction $\vec{\varepsilon}$. The most general solution of the equation of motion for the displacement $\mathbf{x}_i(t)$ is the linear combination of the form

$$\mathbf{x}_i = \sqrt{\frac{1}{Nm}} \sum_{\mathbf{q}} \sum_s \hat{\varepsilon}_s(\mathbf{q}) \Phi_s(\mathbf{q}) e^{i(\mathbf{q} \cdot \mathbf{R}_i^0 - \omega_s(\mathbf{q})t)}, \tag{6.35}$$

where the eigenvectors $\vec{\varepsilon}_s(\mathbf{q}) = \sqrt{m} \hat{\varepsilon}_s(\mathbf{q}) \Phi_s(\mathbf{q})$ are normalized by the mass of the molecules. The index s labels the three allowed eigenvectors of Eq. 6.33. Starting

with the Hamiltonian for the vibrational motion of the molecules in the form

$$H_{\text{vib}} = \sum_i \frac{1}{2} m \dot{\mathbf{x}}_i^2 + \frac{1}{2} \sum_{i,j \neq i} \sum_{\mu,\nu} D_{\mu,\nu} (\mathbf{R}_i^0 - \mathbf{R}_j^0) x_{\mu i} x_{\nu j}, \quad (6.36)$$

and inserting the expression for the displacements in terms of normal modes, Eq. 6.35, one can rewrite the vibrational Hamiltonian in terms of the normal coordinates $\Phi_s(\mathbf{q})$ as [84]

$$H_{\text{vib}} = \frac{1}{2} \sum_{\mathbf{q}} \sum_s [\dot{\Phi}_s(\mathbf{q}) \dot{\Phi}_s(-\mathbf{q}) + \omega_s^2(\mathbf{q}) \Phi_s(\mathbf{q}) \Phi_s(-\mathbf{q})]. \quad (6.37)$$

The mode amplitudes $\Phi_s(\mathbf{q})$ satisfy the relations $\Phi_s(\mathbf{q}) = \Phi_s^*(-\mathbf{q})$, which then allows us to use the standard method of canonical quantization of promoting the field variable $\Phi_s(\mathbf{q})$ to an operator using the well-known relations

$$\Phi_s(\mathbf{q}) = \sqrt{\frac{\hbar}{2\omega_s(\mathbf{q})}} (\hat{a}_{\mathbf{q},s} + \hat{a}_{\mathbf{q},s}^\dagger) ; \dot{\Phi}_s(\mathbf{q}) = -i\sqrt{\frac{\hbar\omega_s(\mathbf{q})}{2}} (\hat{a}_{\mathbf{q},s}^\dagger - \hat{a}_{-\mathbf{q},s}), \quad (6.38)$$

which preserve the canonical commutation relations $[x_{\mu i}, \dot{x}_{\nu j}] = i\hbar\delta_{\mu,\nu}\delta_{i,j}$. In terms of the new operators, the molecular displacements can be written as

$$\mathbf{x}_i = \sum_{\mathbf{q},s} \sqrt{\frac{\hbar}{2mN\omega_s(\mathbf{q})}} \hat{\epsilon}_s(\mathbf{q}) (\hat{a}_{\mathbf{q},s} + \hat{a}_{-\mathbf{q},s}^\dagger) e^{i\mathbf{q} \cdot \mathbf{R}_i^0}, \quad (6.39)$$

and the vibrational Hamiltonian assumes the diagonal form

$$\hat{H}_{\text{vib}} = \sum_{\mathbf{q}} \sum_s \hbar\omega_s(\mathbf{q}) \left[\hat{a}_{\mathbf{q},s}^\dagger \hat{a}_{\mathbf{q},s} + \frac{1}{2} \right]. \quad (6.40)$$

The operator $\hat{a}_{\mathbf{q},s}^\dagger$ creates a phonon with wavevector \mathbf{q} and polarization s , from the vacuum state with no vibrational excitations in the corresponding Fourier mode. The phonon energy dispersion $\hbar\omega_s(\mathbf{q})$ is obtained by solving the eigenvalue problem in Eq. (6.33).

6.3.3 External field control of phonon dynamics

The previous sections describe the standard formalism to analyze the lattice dynamics of an array of interacting molecules in an optical lattice trap. Similar ideas are also used to describe an array of atomic ions trapped individually in microtraps [220]. In analogy with ion arrays, in arrays of polar molecules it is the competition between the external trapping forces and the intermolecular forces what determines the phonon dynamics. In contrast with ion arrays, the ratio between the competing forces can be manipulated by tuning a DC electric field or by changing the intensity of the trapping laser. In this section we analyze the external field dependence of the phonon spectrum for infinite and finite molecular arrays. We restrict the discussion to one spatial dimension for simplicity, but extensions to higher dimensionality are straightforward.

Finite one-dimensional array with repulsive interactions

When the displacement of the molecules from their equilibrium positions is small, the potential energy of the molecular array can be defined as $U(\mathbf{r}_1, \dots, \mathbf{r}_N) = \sum_1^N U(\mathbf{r}_i)$, where $U(\mathbf{r}_i)$ is given by Eq. (6.27). The molecular coordinates can be rewritten as $\mathbf{r}_i = \mathbf{R}_i + \mathbf{x}_i$, and express the potential in terms of the relative displacements \mathbf{x}_i from the optical lattice trap minima \mathbf{R}_i , i.e.,

$$U = \sum_i \frac{1}{2} m \omega_0^2 \mathbf{x}_i^2 + \frac{1}{2} \sum_i \sum_{j \neq i} \frac{U_g}{|\mathbf{x}_i - \mathbf{x}_j + \mathbf{R}_i - \mathbf{R}_j|^3}. \quad (6.41)$$

For a cubic optical lattice symmetry with lattice minima separated by $a_L = \lambda_L/2$, where λ_L is the wavelength of the trapping laser, we can express the coordinates in units of a_L , and the potential energy in units of $m \omega_0^2 a_L^2$. The resulting generic potential energy for a one-dimensional array is

$$F(v_1, \dots, v_N) = \frac{U}{m \omega_0^2 a^2} = \sum_i \frac{v_i^2}{2} + \frac{1}{2} \sum_i \sum_{j \neq i} \frac{\kappa}{|v_i - v_j + i - j|^3}, \quad (6.42)$$

where $v_i = (x_i - R_i)/a_L$ and

$$\kappa = \frac{(U_g/a_L^5)}{m\omega_0^2} \quad (6.43)$$

is a force constant ratio that parametrizes the relative strength of the dipole-dipole and laser trapping forces. The potential $F(v_1, \dots, v_N)$ is generic for an arbitrary polar molecule.

Alternatively, we can consider the periodicity of the optical lattice potential explicitly. We can always choose a laser configuration for which the optical trapping potential is separable in three orthogonal directions, as can be obtained with three retro-reflecting beams with polarizations orthogonal to each other [36]. In this case, we can consider a one dimensional array given by a standing wave laser with polarization along the \hat{z} axis, propagating along the x direction. If the dipole-dipole interaction is negligible along the yz -plane, the total lattice potential along the x axis is

$$U = \sum_i V_0 \cos^2(k_L x_i) + \frac{1}{2} \sum_i \sum_{j \neq i} \frac{U_g}{|x_i - x_j|^3}. \quad (6.44)$$

The first terms describes the optical lattice potential with finite depth $V_0 = |E_0|^2 \alpha_{\text{eff}}$, generated by the standing wave laser with intensity $I_L = c\epsilon_0 |E_0|^2/2$ and wavevector $k_L = 2\pi/\lambda_L = \pi/a_L$. α_{eff} is the effective dynamic polarizability of the molecular state being trapped at the frequency of the trapping laser (see Chapter 2). Since in the Mott-insulator phase the molecules are localized near the minima of the potential [79], we can rewrite the coordinates in terms of the displacements $v_i = x_i - X_i$. We can rescale the coordinates in units of a_L and the energies in units of the lattice depth V_0 , which results in the generic potential energy

$$G(v_1, \dots, v_N) = \frac{U}{V_0} = \sum_i \cos^2(\pi(v_i + i)) + \frac{1}{2} \sum_i \sum_{j \neq i} \frac{\rho}{|v_i - v_j + i - j|^3}, \quad (6.45)$$

where

$$\rho = \frac{V_g}{V_0} \quad (6.46)$$

is the ratio between the ground state dipole-dipole interaction energy $V_g = U_g/a_L^3$ and the optical lattice depth V_0 . For small displacements $x_i \ll 1/k_L$, the expansion of $\cos^2(k_L x_i)$ in Eq. (6.44) up to quadratic terms in x_i leads to the relation $m\omega_0^2 =$

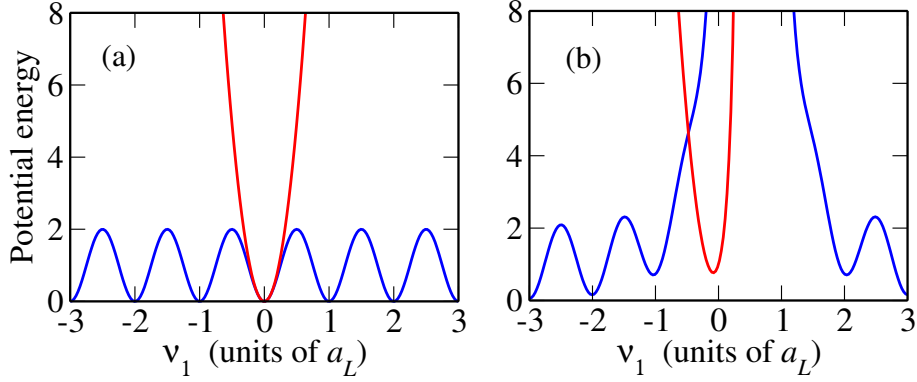


Figure 6.2: Dimensionless sinusoidal $G(v_1, v_2)$ (blue) and scaled-quadratic $(2\pi^2) \times F(v_1, v_2)$ (red) potentials, evaluated along the path $v_1 = -v_2$, for two interacting molecules: (a) The minimum of both potentials coincide at $v_1 = 0 = v_2$ when $U_g = 0$, meaning that the molecules are separated by one lattice constant a_L ; (b) For strong repulsive dipole-dipole interaction ($V_g/V_0 = 2\pi^2$), the potential G does not have a minimum at $v_1 \approx 0$, but F still predicts a stable minimum at near zero displacement. $V_g = U_g/a_L^3$ is the dipole-dipole energy and V_0 is the optical lattice trap depth.

$2V_0k_L^2$. Using this expression, we can relate κ and ρ as

$$\kappa = \frac{\rho}{2\pi^2}. \quad (6.47)$$

Therefore, the functions $F(v_1, \dots, v_N)$ in Eq. (6.42) and $G(v_1, \dots, v_N)$ in Eq. (6.45) have their minima at the same positions for two values of κ and ρ related by Eq. (6.47). This equivalence is only valid for values of $\kappa \ll 1$, since otherwise the finite depth of the optical lattice potential in G is important. As an illustration of this point, we show in Fig. 6.2 the difference between the equilibrium positions predicted by $F(v_1, v_2)$ and $G(v_1, v_2)$ when the repulsive dipole-dipole interaction is much larger than the lattice trap depth V_0 . We therefore restrict our discussion to moderate interaction strengths, i.e., $V_g \sim V_0$, because we are interested in the limit where the lattice has an important effect on the phonon dynamics.

In order to find the equilibrium geometry associated with the potential G in Eq. (6.45), we use the commercial software *Mathematica* to find the global minimum of the potential, using three different direct search algorithms that do not

ρ	0.1	1
v_1	-0.0008156 (-0.0153162)	-0.0079563 (-0.117283)
v_2	-0.0000503 (-0.0016473)	-0.0006791 (-0.0324155)
v_3	0.0000000 (0.0000000)	0.0000000 (0.0000000)
v_4	0.0000503 (0.0016473)	0.0006791 (0.0324155)
v_5	0.0008156 (0.0153162)	0.0079563 (0.117283)

Table 6.1: Displacements $v_i = x_i - X_i$ from the position of the optical lattice minima X_i , in units of $a_L = \lambda_L/2$, for a 1D array of five polar molecules. The interaction strength is parametrized by the ration $\rho = (U_g/a_L^3)/V_0$. Dipole-dipole interactions only up to the next-nearest neighbour are taken into account. λ_L is the wavelength of the trapping laser, and V_0 is the optical lattice depth. The values in parenthesis correspond to a quadratic approximation for the lattice site potentials.

evaluate the derivatives of G . We shift the value of the lattice potential as $\cos^2 \alpha = 1 - \sin^2 \alpha$, so there is a minimum at $\alpha = 0$, when there are no interactions. The results are shown in Tables 6.1 for $N = 5$. For $N = 10$ the solutions are of the same order of magnitude as for $N = 5$. Since the potential is periodic, we restrict ourselves to the solutions with $|v_i| < 1$, because we assume there is no tunneling of molecules between different lattices. Although the repulsive interactions are comparable to the lattice depth ($\rho \sim 1$), the equilibrium positions for an array of interacting molecules \mathbf{R}_i^0 are not significantly perturbed with respect to a non-interacting array, i.e., $\mathbf{R}_i^0 \approx \mathbf{R}_i$, where \mathbf{R}_i is the position of the optical lattice minima.

Finite one-dimensional arrays with attractive interactions

For a infinite homogeneous array, the phonon frequencies may not be well defined for $\kappa < 0$, which is an indication of instabilities in the lattice potential energy. We want to analyze in more detail the stability of a finite one-dimensional molecu-

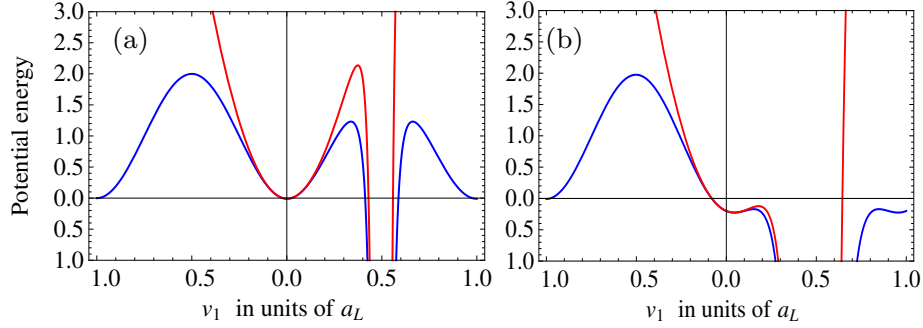


Figure 6.3: Dimensionless sinusoidal $G(v_1, v_2)$ (blue) and scaled quadratic $(2\pi^2) \times F(v_1, v_2)$ (red) potentials, evaluated along the path $v_1 = -v_2$, for two interacting molecules: (a) A relatively weak attractive dipole-dipole interaction ($\rho = 0.01$) creates a local minimum at $v_1 \approx 0$, which keeps the molecules separated by one lattice constant a_L ; (b) For a stronger attractive interaction ($\rho \sim 0.1$), the potentials G and F do not have stable minimum at $v_1 \approx 0$. ρ is the ratio between the dipole-dipole energy and the optical lattice trap depth.

lar array with attractive interactions. Understanding the conditions under which the lattice potential is not strong enough to counteract the attractive dipole-dipole interaction between molecules is important if one considers a two- or three-dimensional optical lattice of molecules where an exciton can propagate in orthogonal directions. In the lattice direction parallel to an applied electric field (attractive interaction), excitons have a positive effective mass, and a negative effective mass in the directions perpendicular to the field (repulsive interaction). This anisotropy can in principle be exploited in experiments that probe the linear and non-linear response of the molecular ensemble to microwave fields.

Let us again consider two interacting molecules in an optical lattice with lattice constant a_L . Figure 6.3 shows the potential $G(v_1, v_2)$ along the path $v_1 = -v_2$ in coordinate space. Although the strength of the potential is smaller than the lattice depth, i.e., $\rho < 1$, the local minimum at $v_1 = v_2 \approx 0$ becomes vanishingly shallow for a ratio $\rho \sim 0.2$, which would result in the approach of the molecules, leading to a collisional loss. Therefore, the laser trapping forces would not be strong enough to support a Mott-insulator phase for relatively small dipole-dipole interaction strengths. For values of ρ that support relatively deep local minima

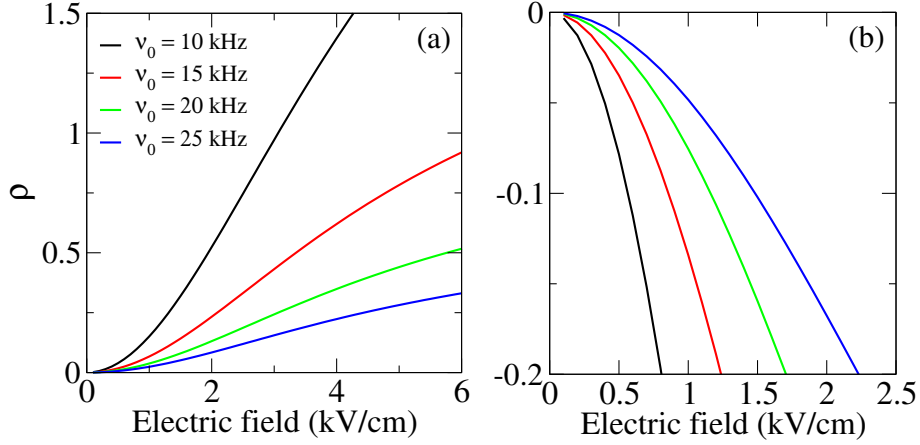


Figure 6.4: Ratio $\rho = (U_g/a_L^3)/V_0$ between the dipole-dipole energy and the optical lattice depth, for a one-dimensional array of LiCs molecules separated by $a = 400$ nm as a function of the electric field and trapping frequency $\nu_0 = \omega_0/2\pi$: (a) Field perpendicular to the array; (b) Field parallel to the array.

away from the instability in the potential ($\rho \sim 0.01$), the displacement of the equilibrium position from the optical lattice minima are $v_i \ll 10^{-5}$ (in units of a_L) for an array of five molecules. The same holds holds for an array with an arbitrary number of molecules. Figure 6.3 also shows that an attractive dipole-dipole interaction arising from the permanent dipole moments of the molecules in their rotational ground state can lower the effective trap depth of the optical lattice, which might be relevant for studies of dipolar quantum phases [64, 85, 86].

6.3.4 Typical parameters for alkali dimers in optical lattices

In order to illustrate the distinct physical regimes for the lattice dynamics, let us consider LiCs molecules as an example of an alkali-metal dimer with relatively large dipole moment. Since the phonon spectrum is characterized by the parameter $\rho = (U_g/a_L^3)/V_0$, or equivalently $\kappa = \rho/2\pi^2$, in principle we have complete control over the phonon dynamics because the lattice depth ω_0 scales linearly with with the trapping laser intensity I_L , and U_g can be manipulated by changing the strength an external DC electric field, as well as its orientation with respect to the

array axis. In Figure 6.4 we show typical values of ρ for different trapping frequencies $\nu_0 = \omega_0/2\pi$ and electric field strengths parallel and perpendicular to the array. For arrays of LiCs molecules that are perpendicular to an applied electric field, the condition $\rho \sim 1$ we imposed previously implies that for relatively small trapping frequencies ν_0 from 10 to 15 kHz, DC electric fields of up to 10 kV/cm can be applied to the array without disturbing the geometrical arrangement of the molecules in the optical lattice. Electric fields larger than (approx.) 3 kV/cm are perturbative for LiCs molecules, so that the mixing of the rotational ground state $N = 0$ with rotational excited states higher than $N = 1$ cannot be neglected.

For attractive interactions, Fig. 6.4 shows that an array of LiCs molecules is stable for DC electric fields larger than 2 kV/cm only for trapping frequencies ν_0 much larger than 20 kHz, according to the criteria $\rho \leq 0.2$ we identified above. Trapping frequencies on the order of 100 kHz can be easily achieved experimentally by increasing the intensity of the trapping laser. We will see later in this chapter, however, that for trapping frequencies larger than 30 - 50 kHz, the phonon dynamics is only weakly coupled to the collective rotational degrees of freedom (excitons), regardless of the strength and orientation of the electric field. For lower trapping frequencies on the order of 10 kHz, an array of LiCs molecules with attractive interactions is stable for parallel electric fields of strength smaller than 0.5 kV/cm. In this trapping frequency regime the exciton-phonon coupling is strong, and is mainly characterized by non-local spatial correlations and phonon-modulated hopping that are believed to be absent in natural systems such as molecular crystals and photosynthetic complexes [116].

6.3.5 Frequency of lattice vibrations in a finite array

In the limit of non-interacting molecules, the vibrational frequency of the molecules in the optical lattice potential is ω_0 for the lowest Bloch band. In the harmonic approximation, higher bands have energy $n\hbar\omega_0$, with n an integer. For small enough ratio between the lattice depth and the dipole-dipole interaction between molecules in their rotational ground state, the vibrations of the molecules become correlated, and the collective vibrational motion of the molecular array can be described in

terms of normal modes. For a large number of molecules, these normal modes can be described more conveniently in terms of phonons.

In general, the vibrational analysis of the normal modes of a finite lattice can be performed by solving the equations of motion numerically, given the form of the dynamical matrix in Eq. (6.31). For instance, let us consider an one-dimensional array of N molecules that in equilibrium are separated by a distance a_L , given by the optical lattice potential. We saw in the previous section that even in the presence of dipole-dipole interactions, the equilibrium positions of the molecules \mathbf{R}_i^0 are given by the trapping potential. We define the mass-weighted molecular displacements \mathbf{q}_i as

$$\mathbf{q}_i = \sqrt{m}\mathbf{x}_i = \sqrt{m}(\mathbf{r}_i - \mathbf{R}_i^0), \quad (6.48)$$

and divide the kinetic and potential energy of the array by ω_0^2 to rewrite the Hamiltonian in Eq. 6.36 as

$$H' \equiv \frac{H}{\omega_0^2} = \frac{1}{2} \sum_{i,\mu} q_{\mu,i}^2 + \frac{1}{2} \sum_{i,j} \sum_{\mu,\nu} K_{\mu i, \nu j} q_{\mu,i} q_{\nu,j} \quad (6.49)$$

where $K_{\mu i, \nu j} = D_{\mu i, \nu j} / m\omega_0^2$ is a dimensionless dynamical matrix, $D_{\mu i, \nu j}$ given by Eqs. (6.31). Associated with the Hamiltonian in Eq. (6.49) are the equations of motion for the $3N$ variables $q_{\mu,i}$ ($i = 1, \dots, N$ and $\mu = x, y, z$)

$$\frac{1}{\omega_0^2} \frac{d^2 q_{\mu i}}{dt^2} = -K_{\mu i, \mu i} q_{\mu i} - \sum_{j \neq i} \sum_{\nu \neq \mu} K_{\mu i, \nu j} q_{\nu j}. \quad (6.50)$$

We look for real harmonic solutions of the form $q_{\mu i} = A_{\mu i} \cos(\omega t + \delta)$, and obtain the secular equation

$$\sum_j \sum_\nu (K_{\mu i, \nu j} - \delta_{\mu i, \nu j} \lambda) A_{\nu j} = 0, \quad (6.51)$$

where $\lambda = \omega^2 / \omega_0^2$. Equation (6.51) is an eigenvalue equation for the matrix \mathcal{K} , with matrix elements $K_{\mu i, \nu j}$. The eigenvector Φ_k of the matrix \mathcal{K} , associated with the eigenvalue λ_k , are the normal modes of vibration of the array. The mass-weighted oscillation amplitudes at site i of the array are given by the coefficients $A_{\mu i}$ of the eigenvector Φ_k . For the k -th normal mode, all molecules oscillate with the same frequency given by $\omega_k / \omega_0 = \sqrt{\lambda_k}$. As we did for an array with periodic

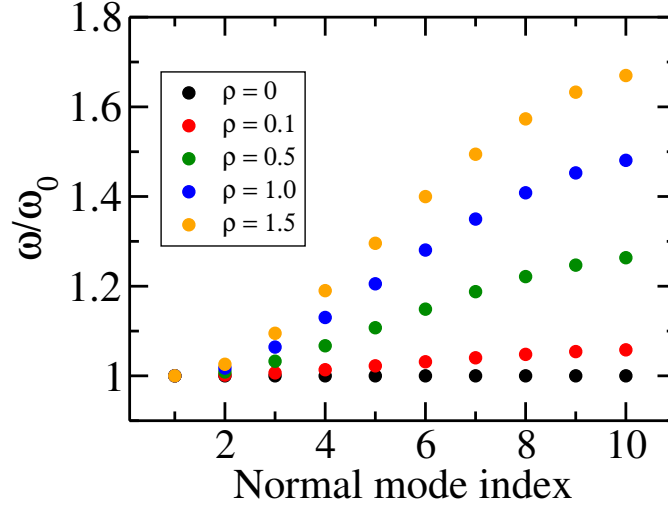


Figure 6.5: Normal mode frequencies for a one-dimensional array of 10 polar molecules as a function of the ratio $\rho = (U_g/a_L^3)/V_0$. V_0 is the depth of the optical lattice potential, with trapping frequency ω_0 . U_g/a_L^3 is the dipole-dipole energy between molecules separated by a distance a_L , where a_L is half the wavelength of the trapping laser.

boundary conditions in Section 6.3.2, by introducing the normal coordinates Q_k , Eq. (6.49) can be written in the diagonal form

$$H' = \frac{1}{2} \sum_k \{ \dot{Q}_k^2 + \lambda_k Q_k^2 \}, \quad (6.52)$$

with $\lambda = \sqrt{\omega_k/\omega_0}$, which can be quantized using the canonical formalism, as in Section 6.3.2. We then identify the normal coordinate Q_k with the amplitude of the motion in the normal mode Φ_k , whose frequency ω_k we find by solving Eq. (6.51).

As an example, let us consider a one-dimensional array of $N = 10$ molecules. In this case the matrix \mathcal{K} has elements

$$K_{i,i} = 1 + 6\kappa \sum_{j \neq i} \frac{1}{|i-j|^5}; \quad K_{i,j} = -6\kappa \frac{1}{|i-j|^5}, \quad (6.53)$$

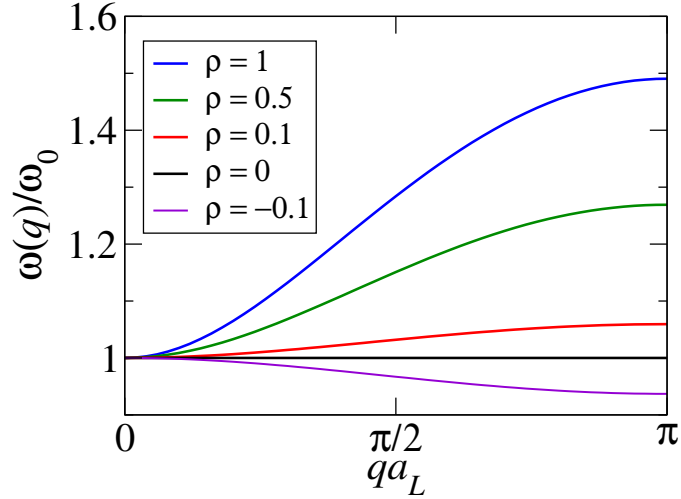


Figure 6.6: Phonon spectrum $\omega(\mathbf{q})/\omega_0$ for an infinite one-dimensional array of polar molecules in an optical lattice with trapping frequency ω_0 , for different values of the parameter $\rho = (U_g/a_L^3)/V_0$.

where $\kappa = (1/2\pi^2)\rho$, with ρ the ratio between the dipole-dipole interaction energy U_g/a_L^3 and the lattice depth V_0 . Figure 6.5 shows the normal mode frequencies ω_k , in units of ω_0 , for an array of 10 polar molecules with repulsive dipole-dipole interactions, for different values of ρ . We denote by Δ the energy difference between the highest and lowest frequency modes, i.e., the width of the spectrum. Figure 6.5 shows that Δ increases with ρ . For $\rho \sim 1$, we find $\Delta \approx \hbar\omega_0/2$. For an array of 10 molecules with attractive interactions, we restrict ourselves to values of $\rho \leq -0.2$, in order to ensure stability of the array. In this case we find that $\Delta \leq 0.13 \hbar\omega_0$.

6.3.6 Phonon spectrum of an infinite array

In section 6.3.2 we looked for solutions of the equations of motion of the form $x_{\mu,i}(t) = \varepsilon_{\mu} e^{i(\mathbf{q} \cdot \mathbf{R}_i^0 - \omega t)}$, where ε_{μ} is a complex amplitude. This is convenient for very large arrays for which periodic boundary conditions are accurate. Let us consider an infinite array of molecules directed along the z axis. In this case, Eq. (6.33) becomes an algebraic equation for the frequency $\omega(\mathbf{q})$, with the dynamical matrix

D_z is given by

$$\begin{aligned} D_z(\mathbf{q}) &= D_{zi,zi} + \sum_{j \neq i} D_{zi,zj} e^{i\mathbf{q} \cdot (\mathbf{R}_j^0 - \mathbf{R}_i^0)} \\ &= m\omega_0^2 + \frac{12U_g}{a^5} \sum_{l>0} \frac{1 - \cos(l\mathbf{q}a_L)}{l^5}, \end{aligned} \quad (6.54)$$

where Eq. (6.31) was used. The phonon dispersion for the linear chain is obtained as the positive root $\omega(\mathbf{q})/\omega_0 = \sqrt{D_z(\mathbf{q})/m\omega_0^2} \equiv \sqrt{\mathcal{K}_z(\mathbf{q})}$, given by

$$\omega(\mathbf{q}) = \omega_0 \sqrt{1 + 12\kappa\gamma(\mathbf{q})}, \quad (6.55)$$

where $\kappa = U_g/a_L^5/m\omega_0^2 \equiv \rho/2\pi^2$, and $\gamma(\mathbf{q}) = \sum_{m>0} (1 - \cos(m\mathbf{q}a_L))/m^5$. Figure 6.6 shows the phonon frequencies $\omega(\mathbf{q})$, in units of ω_0 , for different values of the parameter ρ . For a given value of $\rho > 0$ the phonon bandwidth in the homogeneous case approximately equal to the bandwidth obtained for a finite array in Fig. 6.5. For repulsive molecular interactions in the ground state $\rho > 0$, the phonon dispersion has a minimum at the origin of the Brillouin zone, but the sound velocity $v_s = d\omega(q)/dq$ vanishes at the minimum. It takes an energy larger than the gap ω_0 for a sound wave to propagate in the array. In the limit where the lattice potential is negligibly small compared to the dipolar interaction $\rho \rightarrow \infty$, the phonon frequency in Eq. 6.55 becomes $\omega(q) \approx \eta \sin(2qa_L)$ in the nearest neighbour approximation, where $\eta = \sqrt{12U_g/ma_L^5}$. Phonon are acoustic in this regime and the sound velocity is $v_s = 2\eta a_L$ at $q = 0$. This case has been considered in detail in Ref. [103].

6.3.7 Exciton-phonon interaction

In mesoscopic systems such as a photosynthetic complex consisting of a few number of interacting monomers ($N \sim 10$), coupled to a finite number of environmental modes, the non-Markovian limit of exciton-phonon coupling is believed to be important in preserving the quantum coherence between monomers at room temperature [115, 116]. Non-Markovian behaviour is generally characterized by the inability of the environment to dissipate the energy transferred from the system of interest, so that energy can be transferred back to the system [221].

The ability to generate arrays of polar molecules in optical lattices with arbitrary dimensionality and size would allow for studies of mesoscopic open quantum dynamics, in the limit of markovian and non-markovian system-bath coupling. The system would consist of rotational states of the molecules, coherently coupled by the dipole-dipole interaction, and the bath would correspond to the motional degrees of freedom of the molecules in the lattice potential. An interesting possibility would be the creation of small arrays of polar molecules ($N \sim 10$), that is decoupled from the rest of the molecular ensemble. Starting from a Mott-insulator phase with unit filling with a large number of molecules $N \sim 10^3 - 10^5$, it should be possible to generate smaller molecular arrays by evaporating molecules at specific sites, either by collisions with an electron beam or by selective molecular ionization. It is therefore important to understand the coupling of rotational excitons with lattice vibrations, in the limit of small number of molecules.

The excitonic part of the dipole-dipole operator, V_{ex} , depends on the instantaneous position of the molecules. This naturally couples the internal states with the relative motion of the molecules. We can separate V_{ex} in a component of that depends on the ro-vibrational coordinates of the molecules only, and a components that mix the internal and translational coordinates by defining a Taylor expansion of the pair potential $V_{\text{ex}}(\mathbf{r}_i - \mathbf{r}_j)$ around the equilibrium distance $\mathbf{R}_{ij}^0 = \mathbf{R}_i^0 - \mathbf{R}_j^0$, in powers of the small displacement \mathbf{x}_i from the equilibrium positions, i.e., $\mathbf{r}_i = \mathbf{R}_i^0 + \mathbf{x}_i$. Keeping only the first order term in the expansion, the potential can be written as

$$V_{\text{ex}}(\mathbf{r}_{ij}) \approx V_{\text{ex}}(\mathbf{R}_{ij}^0) + (\hat{\mathbf{x}}_i - \hat{\mathbf{x}}_j) \cdot \vec{\nabla}_{\mathbf{r}_{ij}} V_{\text{ex}}(\mathbf{r}_{ij}) \Big|_{\mathbf{r}_{ij}=\mathbf{R}_{ij}^0} \quad (6.56)$$

where $\mathbf{r}_{ij} = \mathbf{r}_i - \mathbf{r}_j$, and the derivatives of the potential are evaluated at the equilibrium positions. As a result of these separation internal and external motion, the total Hamiltonian in Eq. (6.28) can be written as the sum: $\hat{H} = \hat{H}_{\text{ex}} + \hat{H}_{\text{vib}} + \hat{H}_{\text{int}}$, where

$$\hat{H}_{\text{ex}} = \sum_i B_e \mathbf{N}_i^2 - \mathbf{d}_i \cdot \mathbf{E} + \frac{1}{2} \sum_i \sum_{j \neq i} V_{\text{ex}}(\mathbf{R}_i^0 - \mathbf{R}_j^0), \quad (6.57)$$

and

$$\hat{H}_{\text{int}} = \frac{1}{2} \sum_{i,j \neq i} (\mathbf{x}_i - \mathbf{x}_j) \cdot \vec{\nabla} V(\mathbf{r}_{ij}) \Big|_{\mathbf{r}_{ij}=\mathbf{R}_{ij}^0}. \quad (6.58)$$

\hat{H}_{vib} is the Hamiltonian describing the vibrational modes of the array (phonons). At this point we quantize the rotational motion of a polar molecule in the presence of the DC electric field, as well as the dipole-dipole interaction between molecules at fixed distance \mathbf{R}_{ij}^0 . The procedure was explained in detail in Chapter 5. In a similar way, we can quantize the internal degrees of freedom in gradient operator $\vec{\nabla}V(\mathbf{r}_{ij})$ evaluated at fixed positions. Therefore, by using first and second quantization, the internal state dynamics can be described by the sum of the exciton Hamiltonian and the exciton-phonon interaction as

$$\begin{aligned}\hat{H}_{\text{ex}} + \hat{H}_{\text{int}} = & \sum_i (\epsilon_{eg} + \sum_{j \neq i} D_{ij}) \hat{B}_i^\dagger \hat{B}_i + \sum_{i,j \neq i} J_{i,j} \hat{B}_i^\dagger \hat{B}_j \\ & + \sum_i \left(\sum_{j \neq i} (\mathbf{x}_i - \mathbf{x}_j) \cdot \vec{\nabla}_{\mathbf{r}_{ij}} D(\mathbf{R}_{ij}) \right) \hat{B}_i^\dagger \hat{B}_i \\ & + \sum_{i,j \neq i} (\mathbf{x}_i - \mathbf{x}_j) \cdot \vec{\nabla}_{\mathbf{r}_{ij}} J(\mathbf{R}_{ij}) \hat{B}_i^\dagger \hat{B}_j. \quad (6.59)\end{aligned}$$

In Section 6.3.2 we analyzed the vibrational normal modes of an infinite molecular array in Fourier space assuming periodic boundary conditions. The molecular displacements \mathbf{x}_i appearing in the linear exciton-vibration coupling term in Eq. (6.59) can then be expressed as a Fourier expansion using Eq. (6.39). In Appendix E it is shown that the linear exciton-phonon coupling \hat{H}_{int} in Eq. (6.59) can be written as

$$\hat{H}_{\text{int}} = \frac{1}{\sqrt{N}} \sum_{\mathbf{q}\lambda} \sum_{\mathbf{k}} M_\lambda(\mathbf{k}, \mathbf{q}) \hat{B}_{\mathbf{k}+\mathbf{q}}^\dagger \hat{B}_{\mathbf{k}} \left(\hat{a}_{\mathbf{q},\lambda} + \hat{a}_{-\mathbf{q},\lambda}^\dagger \right), \quad (6.60)$$

where the coupling constant satisfies $M^*(\mathbf{k}, \mathbf{q}) = M(\mathbf{k} + \mathbf{q}, -\mathbf{q})$ in order to ensure hermiticity of the Hamiltonian. The strength of the coupling of an exciton state \mathbf{k} is not the same for all phonon modes (\mathbf{q}, λ) .

Let us consider a finite molecular array. It is advantageous to describe the vibrational motion of the molecules in terms of normal coordinates \mathbf{Q}_i , with $i = 1, \dots, N$. These are related to the mass-weighted cartesian displacements $\mathbf{q}_i \equiv \sqrt{m}\mathbf{x}_i$ by a unitary transformation U , constructed from the normalized eigenvectors of the dynamical matrix \mathcal{K} , defined in Eq. (6.49). In matrix notation, we can thus

express the cartesian displacements \mathbf{x}_i in terms of normal coordinates as

$$x = \frac{1}{\sqrt{m}} U Q \quad (6.61)$$

where $x^T = (x_{11}, \dots, x_{1i}, x_{2i}, x_{3i}, \dots, x_{3N})$, with $x_{\mu i}$ denoting the μ -th component of the displacement of the i -th molecule in the array.

The normal coordinates \mathbf{Q}_k can be separated into three orthogonal directions, for example the cartesian axes. Each direction ν of the normal mode k can be quantized canonically as

$$\hat{Q}_{\nu k} = \sqrt{\frac{\hbar}{2\omega_{k\nu}}} (\hat{a}_{\nu k}^\dagger + \hat{a}_{\nu k}), \quad (6.62)$$

where $\hat{a}_{\nu k}^\dagger$ creates a phonon in mode k along the ν -direction. In the harmonic approximation, the phonon Hamiltonian in Eq. 6.52, which is valid for an array of arbitrary size and geometry, can then be written as

$$\hat{H}_{\text{ph}} = \sum_k \sum_\nu \hbar \omega_{k\nu} \left(\hat{a}_{\nu k}^\dagger \hat{a}_{\nu k} + \frac{1}{2} \right). \quad (6.63)$$

Using the expansion of the cartesian displacements $x_{\mu i}$ in terms of normal coordinates $Q_{\nu k}$, we can write the components of the relative displacement $\mathbf{x}_i - \mathbf{x}_j$ as

$$x_{\mu i} - x_{\mu j} = \frac{1}{\sqrt{m}} \sum_k \left(u_{\mu i}^{\mu k} - u_{\mu j}^{\mu k} \right) Q_{\nu k}, \quad (6.64)$$

where $u_{\mu i}^{\mu k}$ is the element of the U matrix in the (μi) row and (μk) column. The exciton-phonon Hamiltonian in Eq. 6.59 can then be written as

$$\begin{aligned} \hat{H}_{\text{int}} = & \sum_{k,\mu} \sqrt{\frac{\hbar}{2m\omega_{k\mu}}} \sum_i \left[\sum_{j \neq i} \left(u_{\mu i}^{\mu k} - u_{\mu j}^{\mu k} \right) \partial_\mu D(\mathbf{R}_{ij}) \right] \left(\hat{a}_{\mu k}^\dagger + \hat{a}_{\mu k} \right) \hat{B}_i^\dagger \hat{B}_i \\ & + \sum_{k,\mu} \sqrt{\frac{\hbar}{2m\omega_{k\mu}}} \sum_{i,j \neq i} \left(u_{\mu i}^{\mu k} - u_{\mu j}^{\mu k} \right) \partial_\mu J(\mathbf{R}_{ij}) \left(\hat{a}_{\mu k}^\dagger + \hat{a}_{\mu k} \right) \hat{B}_i^\dagger \hat{B}_j, \end{aligned} \quad (6.65)$$

which is separable in the orthogonal directions μ . We can write the interaction Hamiltonian along the μ -direction as

$$\hat{H}_{\text{int}}^{\mu} = \sum_i \sum_k g_{D_i}^{\mu k} \left(\hat{a}_{\mu k}^{\dagger} + \hat{a}_{\mu k} \right) \hat{B}_i^{\dagger} \hat{B}_i + \sum_{i,j \neq i} \sum_k g_{J_{ij}}^{\mu k} \left(\hat{a}_{\mu k}^{\dagger} + \hat{a}_{\mu k} \right) \hat{B}_i^{\dagger} \hat{B}_j, \quad (6.66)$$

where $g_{D_i}^{\mu k}$ is the coupling constant for the term that is diagonal in exciton degrees of freedom. It corresponds to the variation of the rotational energy shift $D_i = \sum_{j \neq i} D_{i,j}$ due to the vibrational motion of the molecules in the lattice potential. This term has been extensively studied in the literature [84, 205, 215, 222]. The magnitudes of the constants $g_{D_i}^{\mu k}$ for solids and chromophoric aggregates are normally deduced from spectroscopic measurements. In our case, it is given by the expression

$$g_{D_i}^{\mu k} = \sqrt{\frac{\hbar}{2m\omega_{k\mu}}} \sum_{j \neq i} \left(u_{\mu i}^{\mu k} - u_{\mu j}^{\mu k} \right) \partial_{\mu} D(\mathbf{r}_{ij}^0), \quad (6.67)$$

where $\partial_{\mu} D(\mathbf{r}_{ij})$ is the μ -th component of the gradient of $D(\mathbf{r}_{ij})$ with respect to the variable \mathbf{r}_{ij} , evaluated at the equilibrium distance \mathbf{r}_{ij}^0 .

The coupling constant $g_{J_{ij}}^{\mu k}$ is given by

$$g_{J_{ij}}^{\mu k} = \sqrt{\frac{\hbar}{2m\omega_{k\mu}}} \left(u_{\mu i}^{\mu k} - u_{\mu j}^{\mu k} \right) \partial_{\mu} J(\mathbf{r}_{ij}^0), \quad (6.68)$$

and parametrizes the off-diagonal exciton-phonon coupling. It has received much less attention in the literature than the diagonal term, partly because it is believed to be smaller for most molecular solids and aggregates [116, 223], but also because when including this term in the Hamiltonian, analytic approaches fail in the strong coupling regime [84]. In the system proposed here this term cannot be neglected because the magnitude of D_{12} in comparison with J_{12} can be at most a factor of 10 larger in the limit of large electric fields.

For an optical lattice of polar molecules, the above equations are accurate provided there is no tunneling of molecules between lattice sites, i.e., the ensemble is in the Mott-insulator phase. The coupling between rotational and translational degrees of freedom occurs due to the long-range character of the dipole-dipole inter-

action, and not due to the particular form of the trapping potential. For instance, if we consider anharmonic corrections to the optical lattice potential, we would only need to include additional terms in Eq. (6.66), which can affect the exciton-phonon interaction dynamics [224]. The simplified form of the excitonic Hamiltonian \hat{H}_{ex} in Eq. (6.59) is accurate when the excited state $|e\rangle$ is well separated from other rotational states, which can always be achieved by applying a DC electric field of moderate strength [195, 225]. Since we are neglecting exciton-exciton interactions, this model is valid in the limit of low excitation density.

The exciton-phonon interaction operator in Eq. (6.66) corresponds to a generalized polaron model that has been used to study energy transfer and polaron effects in molecular crystals and photosynthetic complexes [84, 214, 223]. The main advantages of the realization of a generalized polaron model using polar molecules in optical lattices can be summarized as follow:

- From the knowledge of the trapping potential and the fact that the dipole-dipole interactions is the leading contribution to the intermolecular interaction, Eqs. (6.67) and (6.68) provide an accurate estimate of the strength of the exciton-phonon coupling. Deriving an expression for the coupling constants from first principles for a real solid or molecular aggregate is not practical due to the complexity of the system.
- The potential use of the generalized polaron Hamiltonian for finite arrays of polar molecules with arbitrary geometry, in which concepts such as momentum conserving exciton-phonon scattering are irrelevant, can lead to interesting studies of quantum dynamics of excitonic degrees of freedom in a mesoscopic phonon bath, which is believed to be highly non-Markovian [114–116].

6.4 Polaron regimes in static electric fields

We have developed a microscopic model to describe the coupling of rotational excitons to the lattice vibrations that can in principle be solved numerically for a molecular array with arbitrary geometry and trapping frequency, in the presence of a DC electric field. For simplicity, here we focus on a finite one-dimensional array

of $^1\Sigma$ polar molecules. Quasi-1D arrays within a 3D optical lattice can be obtained when the coupling J_{ij} is significant along one direction of the lattice only. Control of the coupling of rotational excitons to the lattice phonons is thus possible due to the indirect dependence of the coupling constants $g_{D_i}^k$ and $g_{J_{ij}}^k$ on two experimental parameters: the optical lattice laser intensity and the DC electric field. For instance the phonon-modulated hopping term is proportional to $g_{J_{ij}}^k \propto \sqrt{(1/m\omega_0)}(J_{12}/a)$, where ω_0 scales with the intensity as $\sqrt{I_L}$ and J_{12} depends on the strength and orientation of the electric field with respect to the array.

The Hamiltonian that describes a one-dimensional array of N polar molecules is given by

$$\begin{aligned} \hat{H} = & \sum_i (\epsilon_{eg} + \sum_{j \neq i} D_{ij}) \hat{B}_i^\dagger \hat{B}_i + \sum_{i,j \neq i} J_{ij} \hat{B}_i^\dagger \hat{B}_j + \sum_k \hbar \omega_k \left(\hat{a}_k^\dagger \hat{a}_k + \frac{1}{2} \right) \\ & + \sum_i \sum_k g_{D_i}^k \left(\hat{a}_k^\dagger + \hat{a}_k \right) \hat{B}_i^\dagger \hat{B}_i + \sum_{i,j \neq i} \sum_k g_{J_{ij}}^k \left(\hat{a}_k^\dagger + \hat{a}_k \right) \hat{B}_i^\dagger \hat{B}_j, \quad (6.69) \end{aligned}$$

where the coupling constants $g_{D_i}^k$ and $g_{J_{ij}}^k$ are given by Eqs. (6.67) and (6.68) in terms of the vibrational normal modes and frequencies of the array, and the spatial derivatives of the dipole-dipole constants D_{ij} and J_{ij} . This Hamiltonian is sometimes referred to as a Holstein-Peierls model [226, 227].

In order to quantify the strength of this coupling for realistic trapping conditions, we analyze the eigenvalues of the polaron Hamiltonian in Eq. (6.69) for a given molecular species in a finite 1D array. We can diagonalize the total Hamiltonian $\hat{\mathcal{H}}$ numerically for an array of σ molecules in the site basis

$$|g_1, \dots, e_i, \dots, g_\sigma\rangle |v_1, v_2, \dots, v_\sigma\rangle,$$

where v_k is the occupation number of the phonon mode k . The phonon basis is truncated by including states with up to a given phonon occupation v_{\max} . The value of v_{\max} is increased iteratively until the calculated observable is converged. The Hamiltonian is partitioned as $\hat{\mathcal{H}} = \hat{H}_0 + \hat{H}_{\text{int}}$, where $\hat{H}_0 = \hat{H}_{\text{ex}} + \hat{H}_{\text{ph}}$. The ground state energy E_g of the non-interacting Hamiltonian \hat{H}_0 is chosen as a reference. Any interaction between rotational excitons and the lattice vibrations of the molecules shifts the ground state E_g towards lower energies. The polaron shift of the ground

state ΔE_g can be used as a measure of the exciton-phonon coupling strength [84, 205]. The stronger the coupling to phonons, the larger the polaron shift.

As an illustrative example, we use a finite array of LiCs molecules ($d = 5.5$ Debye [15]) separated by $a_L = 400$ nm. The polaron shift ΔE_g is evaluated as a function of the optical lattice trap frequency ω_0 for strong and weak DC electric fields.

6.4.1 Strong fields: Holstein regime

In Appendix E it is shown that the exciton-phonon coupling constant for a homogeneous one-dimensional array with Einstein phonons can be written as

$$M(k, q) = 2i\alpha_D g(q) + 2i\alpha_J [g(k+q) - g(k)], \quad (6.70)$$

where $g(k) = \sum_{m>0} \sin(mka_L)/m^4$ is a mode-coupling function. The Holstein-type interaction energy α_D is defined as

$$\alpha_D = \frac{\tilde{\alpha} D_{12}}{\sqrt{2m\omega_E}} \left[\frac{\hbar}{a_L^2} \right]^{1/2}, \quad (6.71)$$

where ω_E is the Einstein phonon frequency and $\tilde{\alpha} = -3$. The SSH-type interaction energy is

$$\alpha_J = \frac{\tilde{\alpha} J_{12}}{\sqrt{2m\omega_E}} \left[\frac{\hbar}{a_L^2} \right]^{1/2}. \quad (6.72)$$

For the Holstein model discussed in Section 6.2, the exciton-phonon interaction Hamiltonian is given by $M(k, q) = ig$. This simplified form of the coupling corresponds to the first term in Eq. (6.70) with $g \equiv 2\alpha_D$, when the mode-coupling function $g(q)$ is set to unity. Holstein-type exciton-phonon interaction dominates over SSH interactions when $D_{12} \gg J_{12}$. For closed-shell polar alkali-metal dimers, this condition can be achieved to some extent at large DC electric field strengths for any orientation of the field with respect to the molecular array (see Chapter 3). In Fig. 6.7 the magnitude of the ratio $\alpha_D/\alpha_J = D_{12}/J_{12}$ is plotted as a function of the dimensionless field strength dE/B_e . For LiCs molecules $dE/B_e = 1$ corresponds to $E \approx 2$ kV/cm. The value of the ratio D_{12}/J_{12} is independent of the orientation of the field with respect to the array axis. Figure 6.7 shows that for alkali-metal

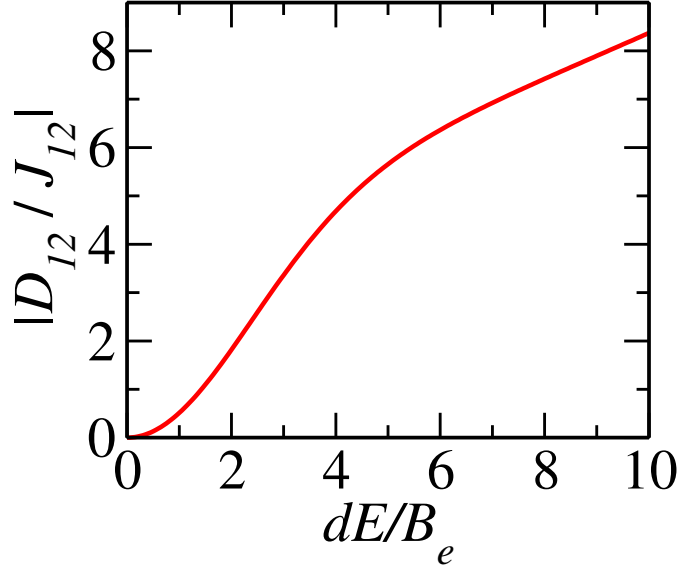


Figure 6.7: Diagonal (Holstein) to off-diagonal (SSH) exciton-phonon coupling ratio $|\alpha_D/\alpha_J| = |D_{12}/J_{12}|$ as a function of the dimensionless DC electric field strength dE/B_e .

dimers the effect of phonon-modulated hopping cannot be neglected even in strong electric fields $dE/B_e \sim 10$. In Section 6.3.2 we discussed the lattice stability in the presence of large electric fields. In order for strong Holstein-type exciton-phonon coupling to be achieved, the value of α_D can be increased by decreasing the trapping frequency ω_0 , increasing the electric field strength, or both simultaneously. However, the ratio $\rho = V_g/V_0$ between the ground state dipole-dipole interaction energy V_g and the trap depth V_0 needs to be less than unity in order for the displacement of the molecules from their equilibrium positions in the lattice potential to be small. This restriction imposes a limit on the achievable values of the coupling energies α_D and α_J . In panel (a) of Figure 6.8 the polaron ground state shift ΔE_g for a one-dimensional array of 10 LiCs molecules is plotted as a function of the trapping frequency $\omega_0/2\pi$. The electric field is 9.0 kV/cm and is oriented perpendicular to the molecular array. At this field strength the diagonal-to-nondiagonal exciton-phonon coupling ratio is $|D_{12}/J_{12}| \approx 5$ and the stability ratio $V_g/V_0 < 1$ for $\omega_0/2\pi \geq 15$ kHz. The Holstein coupling strength can be parametrized by the

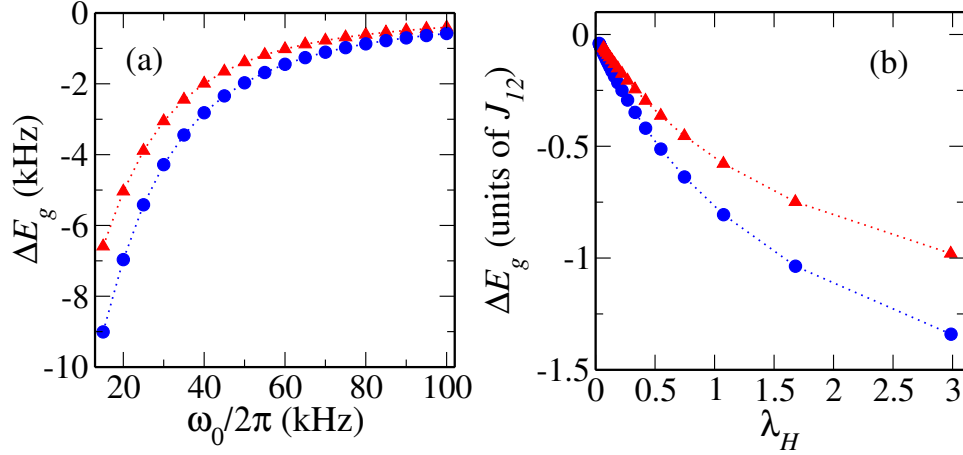


Figure 6.8: Shift of the polaron ground state energy ΔE_g from its value for non-interacting excitons and phonons for 10 LiCs molecules separated by 400 nm, as a function of the exciton-phonon coupling strength. (a) ΔE_g in kHz versus trapping frequency ω_0 for $|D_{12}|/|J_{12}| \approx 5$ in a DC electric field of 9 kV/cm perpendicular to the array. (b) $\Delta E_g/J_{12}$ versus the dimensionless Holstein coupling strength $\lambda_H = 2\alpha_D^2/J_{12}\hbar\omega_0$. α_D is proportional to D_{12} . Circles correspond to the polaron Hamiltonian including diagonal (Holstein) and off-diagonal (SSH) exciton-phonon interactions. Triangles correspond to Holstein coupling only.

dimensionless quantity [215, 218]

$$\lambda_H = \frac{2\alpha_D^2}{J_{12}\hbar\omega_0}. \quad (6.73)$$

In panel (b) the same polaron shift ΔE_g as in panel (a) is shown in units of the exciton hopping amplitude J_{12} as a function of $\lambda_H \propto 1/\omega_0^2$. The data presented this way allows for better comparison with the literature [205] and is independent of the molecular species. The energies shown in Fig. 6.8 are obtained using an iterative process. The polaron shifts ΔE_g are converged to within 0.5% of their values. For the smallest frequencies $\omega_0/2\pi < 20$ kHz, the energy converges when including up to four phonons in the array, arranged in a combinatorial way throughout the 10 lattice sites. For the largest frequencies $\omega_0/2\pi > 50$ kHz the energy converges when including up to two phonons in the array. The numerical procedure takes

into account the phonon dispersion $\omega(k)$ and the discrete mode-coupling functions $g(k)$ defined in Eqs. 6.67 and 6.68. Therefore, the results do not directly relate to the standard Holstein model described in Section 6.2, for which all phonons modes are degenerate and couple equally to excitons.

In Fig. 6.8 the polaron shift is also evaluated only for diagonal exciton-phonon coupling. In order to eliminate the effect of phonon-modulated hopping, the energy α_J is set to zero while the other parameters in the Hamiltonian are kept constant. The polaron shift ΔE_g in this case is 27% to 30% smaller than the value including both diagonal and off-diagonal coupling in the range of frequencies considered. This relative difference between the curves at a given frequency is comparable with the value of the ratio $\alpha_J/\alpha_D \approx 0.2$ at the electric field used.

Polaron effects are dominant in the strong coupling regime of the exciton-phonon interaction. The ground state energy shift from its value in the absence of exciton-phonon interaction is an indicator of the strength of the coupling. In the strong coupling regime, the polaron shift ΔE_g is larger than the hopping amplitude of the particle J_{12} [84, 205, 215, 222]. Panel (b) of Fig. 6.8 shows evidence that an array of molecules in an optical lattice can be prepared in the strong exciton-phonon coupling regime. Even at large electric fields, where Holstein-type couplings dominate, the contribution of phonon-modulated hopping processes to the properties of rotational polarons can be significant.

The one-dimensional polaron spectrum has been calculated by direct diagonalization of the Hamiltonian in Eq. (6.69) in real space for a finite array. It is important to understand the size dependence of the results obtained as the conclusions regarding the strength of the exciton-phonon coupling may vary with the number of molecules in the array. Let us consider a one-dimensional array in the weak exciton-phonon coupling regime. This can be achieved at large trapping frequencies ω_0 for any electric field strength. For larger frequencies, convergence of the polaron ground state energy is achieved after including a maximum of two phonons in the array. The phonon basis is thus small enough so that the size of the array can be increased to $N > 10$. For an homogeneous lattice in the limit $N \rightarrow \infty$, Rayleigh-Schrödinger (RS) perturbation theory gives an accurate estimate of the polaron ground state energy in the regime $\hbar\omega_0/J_{12} \gg 1$. Figure 6.9 shows the polaron shift ΔE_g for a one-dimensional molecular array as a function of the number

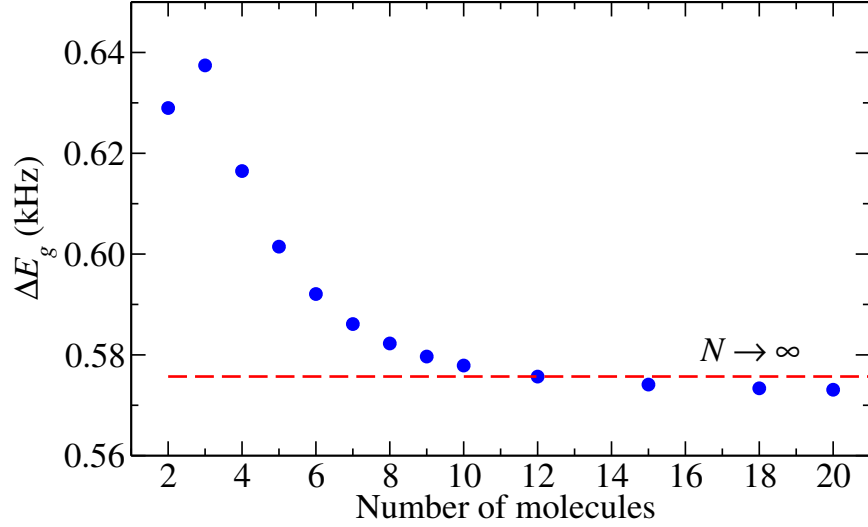


Figure 6.9: Polaron shift ΔE_g for a one-dimensional array of LiCs molecules separated by $a_L = 400$ nm, as a function of the number of molecules. The lattice parameters are: $\omega_0/2\pi = 100$ kHz, $J_{12} = 6.66$ kHz, and $D_{12} = -33.32$ kHz (perpendicular DC electric field). The dashed horizontal line corresponds to the shift for an infinite homogeneous array, calculated using weak-coupling perturbation theory.

of molecules N . The polaron shift ΔE_g has its maximum value for $N = 3$, for all the trapping frequencies considered here ($\nu_0 = 10 - 100$ kHz). For $N > 3$, the polaron shift decreases monotonically towards an asymptotic value. This asymptotic value has been estimated using second-order RS perturbation theory as in Appendix E, where only one-phonon states are included. The coupling constant $M(k, q)$ for a homogeneous array is given in Eq. (6.70). The wavevector integrals have been evaluated numerically neglecting the phonon dispersion. By replacing the dipole-dipole energies used in Fig. 6.9, we obtain the perturbative result $\Delta E_g^{RS} = 575.6979$ Hz, which corresponds to the $N \rightarrow \infty$ asymptote in the figure. For comparison, the shift for a finite array of 20 molecules is $\Delta E_g = 573.0533$ Hz. Figure 6.9 shows that at least in the weak coupling regime, the polaron spectrum for lattice sizes $N \geq 10$ agrees reasonably well with the results for a infinite homogeneous lattice. It is difficult to consider arrays with $N > 10$ for stronger exciton-phonon couplings

because the dimension of the Hilbert space is prohibitively large ($\mathcal{D} \gg 10^4$), as more phonons are required to converge the energies.

6.4.2 Weak fields: SSH regime

The ratio between Holstein-type diagonal coupling to phonons and off-diagonal coupling increases rapidly with the magnitude of the electric field (see Fig. 6.7). For weak electric fields such that $dE/B_e < 1$, the ratio $\alpha_D/\alpha_J = D_{12}/J_{12}$ is small and the dominant contribution to polaron behavior in the molecular array is given by phonon-modulated exciton hopping as described in the SSH model (Section 6.2). The phonon dispersion for a homogeneous array depends on the ratio V_g/V_0 , where V_0 is the optical lattice depth and $V_g = \langle g_1 g_2 | \hat{V}_{dd} | g_1 g_2 \rangle$ is the ground state dipole-dipole interaction. In the weak field regime, the phonon dispersion can safely be ignored because V_g is suppressed by parity selection rules.

The particle-phonon coupling strength in the SSH model can be parametrized in analogy with the Holstein model by

$$\lambda_{\text{SSH}} \equiv \frac{2\alpha_J^2}{J_{12}\hbar\omega_0} = \frac{\tilde{\alpha}^2 J_{12}}{m\omega_0^2 a_L^2} = \frac{18}{\pi^2} \left(\frac{E_R}{J_{12}} \right) \frac{1}{A^2}. \quad (6.74)$$

where in the second equality we have used $\tilde{\alpha} = -3$ and $E_R = \hbar\pi^2/2ma_L^2$. As in the Holstein model, the adiabaticity ratio $A = \hbar\omega_0/J_{12}$ is used to characterize the polaron behaviour. Equation 6.74 states that for a given value of A , the dimensionless coupling strength λ_{SSH} increases with the ratio E_R/J_{12} which depends linearly on the lattice constant a_L . In other words, for fixed ω_0 and J_{12} , the coupling is stronger for lighter molecules and longer lattices. For a given lattice constant a_L and molecular mass m , the exciton-phonon coupling is stronger for molecules with larger dipole moments, as the first equality in Eq. (6.74) shows.

In Section 6.2 a sharp polaron transition in the SSH model was described in the non-adiabatic limit $A \gg 1$ using perturbation theory. Using diagrammatic techniques, it has been shown that this single-polaron transition also occurs in the adiabatic limit $A < 1$ [218]. This transition has yet to be observed experimentally. The tunability of the dipole-dipole interaction and the phonon frequency in arrays of cold molecules in optical lattices opens the possibility of observing this sharp

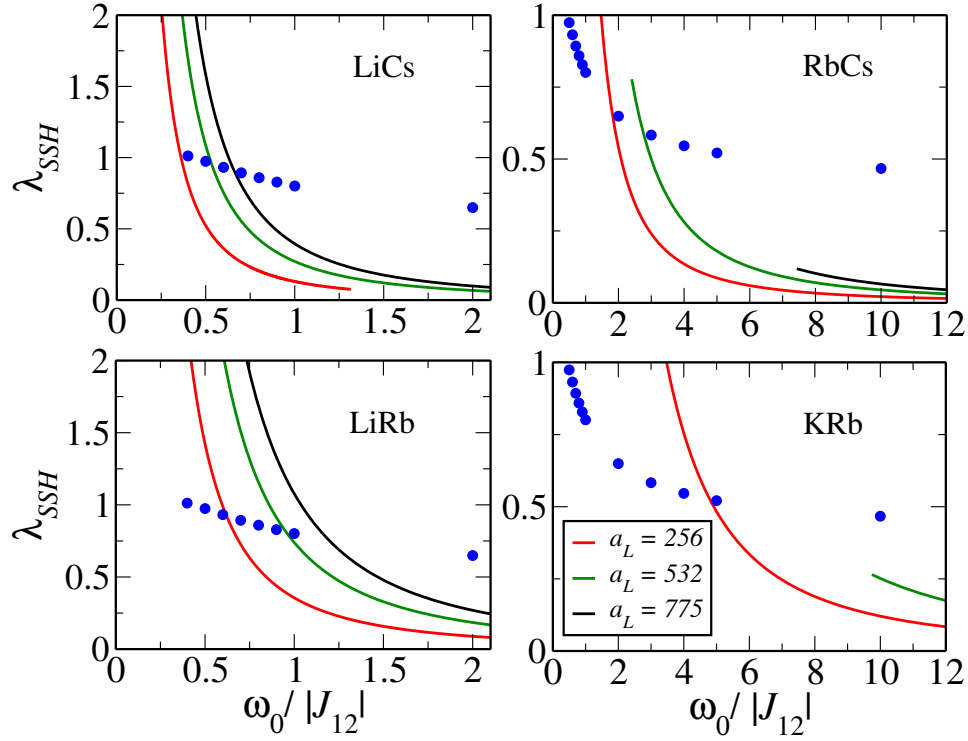


Figure 6.10: Polaron phase diagram in the SSH model for selected alkali dimers. The phase boundary between the weak and strong coupling regimes is shown in circles. Lines corresponds to the set of parameters that can be achieved with a given molecular species. These lines correspond to the experimentally relevant lattice constants $a_L = 256$ nm, $a_L = 532$ nm and $a_L = 775$ nm (from left to right). For each line, the frequency varies in the range $\omega_0/2\pi = 1 - 100$ kHz. A weak DC electric field E is present with strength $dE/B_e = 1$. The ratio between diagonal and off-diagonal exciton-phonon coupling is $\alpha_D/\alpha_J = -0.5$. The phase boundary data were obtained by M. Berciu using the method in Ref. [218].

transition using current technology. In Figure 6.10 the calculated polaron phase diagram is shown for a one-dimensional array. The data was obtained by M. Berciu using the Momentum Average (MA) approximation, a recently-developed semi-analytical technique to evaluate the polaron Green's function [213, 218, 228, 229].

Above the transition line, the SSH polaron is in the strong coupling regime where the minimum of the dispersion is displaced from the origin of the Brillouin zone ($k_0 \neq 0$). Below the line, the polaron behaviour is similar to the Holstein model, with band narrowing and energy minimum at $k_0 = 0$. The phase diagram is universal and includes a small but finite contribution from diagonal exciton-phonon coupling. The phonon spectrum is gapped (optical) and dispersionless. Figure 6.10 also shows a region of parameters that can be achieved with cold molecules in optical lattices. Several alkali-metal dimers are considered. The trapping frequency $\omega_0/2\pi$ varies in the range 1 kHz to 100 kHz. The molecular ensemble is assumed to be in the Mott insulator phase for at least the three lowest Bloch bands, so that tunneling of molecules between sites is suppressed. For each molecular species, the lattice constants $a_L = 256$ nm, $a_L = 532$ nm and $a_L = 775$ nm are used to evaluate λ_{SSH} . These correspond to experimentally relevant trapping wavelengths $\lambda_L = 2a_L$. Each curve is obtained for an electric field perpendicular to the array with strength $dE_Z/B_e = 1$. At this field strength, the ratio α_D/α_J is approximately 0.5 and the phonon dispersion is negligible. In Table 6.2 the electric field strength corresponding to $dE_Z/B_e = 1$ is presented for the molecular species used in Fig. 6.10.

The molecular parameters of LiRb and LiCs molecules are favorable for the observation of the sharp single-polaron transition induced by phonon-modulated hopping in the presence of weak DC electric fields. Figure 6.10 shows that transition from weak to strong coupling occurs within the frequency interval $\omega_0/2\pi = 4 - 5$ kHz for LiCs and LiRb molecules for an array with lattice constant $a_L = 532$ nm, which is most common in experiments [219]. For an array with a larger lattice constant $a_L = 775$ nm, the transition occurs at frequencies $\omega_0/2\pi < 2$ kHz. For the shortest lattice spacing considered here $a_L = 256$ nm, the transition occurs at $\omega_0/2\pi \approx 26$ kHz for both LiCs and LiRb molecules. These frequency estimates assume that the lattice potential is harmonic, which is valid only for the lowest vibrational levels of the potential. For very shallow lattices with only a few bound states, the anharmonic nature of the lattice potential needs to be taken into account.

For molecules with small dipole moments $d < 1$ Debye, it is difficult to observe the transition to the strong coupling regime. Figure 6.10 shows that for an array of KRb molecules the polaron transition is predicted to be observable only at the

	RbCs	LiRb	LiCs	KRb
E (kV/cm)	0.78	1.39	2.12	3.69

Table 6.2: Electric field at which $dE/B_e = 1$ selected closed-shell polar molecules. d is the permanent dipole moment and B_e is the rotational constant. Molecular parameters are taken from Ref. [230].

shortest lattice constant $a_L = 256$ nm, in the range of trapping frequencies considered. However, it is possible to enhance the effect of phonon-modulating hopping by increasing the value of J_{12} while keeping the rest of the parameters constant. By increasing the transition dipole moment d_{eg} , the magnitude of $J_{12} \propto d_{eg}^2$ increases. We have seen in Chapter 3 that a DC electric field decreases the magnitude of J_{12} (see Fig. 3.1). It was shown in Section 3.3 that this is caused by the mixing of rotational states of opposite parity. On the contrary, in Section 3.5 it was shown that J_{12} increases in the presence of an off-resonant optical field, which induces Raman couplings between rotational states of the same parity. However, the intensities necessary to modify J_{12} significantly are greater than 10^8 W/cm² for the molecules considered here. At such intensities, only pulsed fields much shorter than a microsecond can be easily produced in the laboratory [149, 231]. However, one can use continuous-wave (CW) infrared lasers to induce Raman couplings between rotational states of the same parity such that the hopping amplitude J_{12} is increased with respect to its field-free value.

Let us consider creating superpositions of rotational states that preserve the parity of the states $|g\rangle$ and $|e\rangle$ via the Raman couplings illustrated in Fig. 6.11. The intermediate states denoted $|E_{\text{even}}\rangle$ and $|E_{\text{odd}}\rangle$ may correspond to rotational states of the first vibrational excited state. Each three-level scheme in Fig. 6.11 corresponds to a lambda-configuration as used in stimulated Raman adiabatic passage techniques (STIRAP) [232]. The laser fields create coherences between the rotational states of the same parity. Let us consider the field-dressed ground and excited states be given by

$$|g\rangle = a_0|N=0\rangle + a_2|N=2\rangle \equiv a_0|0\rangle + a_2|2\rangle, \quad (6.75)$$

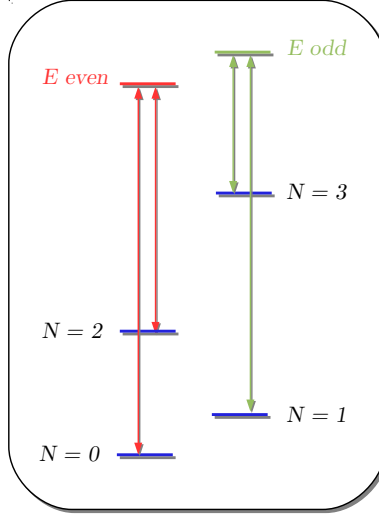


Figure 6.11: Energy level scheme for parity-preserving Raman couplings via the intermediate rovibrational states $|E_{\text{even}}\rangle$ and $|E_{\text{odd}}\rangle$. The rovibrational states in the even and odd manifolds are not coupled by external fields. The angular momentum projection of the rotational states involved is $M_N = 0$.

and

$$|e\rangle = a_1|1\rangle + a_3|3\rangle. \quad (6.76)$$

We have assumed $M_N = 0$ for the rotational states involved and ignored contributions from the intermediate states $|E_{\text{even}}\rangle$ and $|E_{\text{odd}}\rangle$ in the eigenstates. The one-excitation two-particle state is

$$|e\rangle|g\rangle = a_1a_0|1\rangle|0\rangle + a_1a_2|1\rangle|2\rangle + a_3a_0|3\rangle|0\rangle + a_3a_2|3\rangle|2\rangle. \quad (6.77)$$

Using this expression and its hermitian conjugate, the hopping amplitude $J = \langle g|\langle e|V_{dd}|e\rangle|g\rangle$ can be written as

$$\begin{aligned} J = & |a_0a_1|^2\langle 0|\langle 1|\hat{V}_{dd}|1\rangle|0\rangle + |a_1a_2|^2\langle 2|\langle 1|\hat{V}_{dd}|1\rangle|2\rangle + |a_2a_3|^2\langle 2|\langle 3|V_{dd}|3\rangle|2\rangle \\ & + 2|a_1|^2\text{Re}(a_0a_2^*)\langle 0|\langle 1|\hat{V}_{dd}|1\rangle|2\rangle + 2|a_2|^2\text{Re}(a_1a_3^*)\langle 2|\langle 1|\hat{V}_{dd}|3\rangle|2\rangle \\ & + 2\text{Re}(a_0a_3a_1^*a_2^*)\langle 2|\langle 1|\hat{V}_{dd}|3\rangle|0\rangle, \end{aligned} \quad (6.78)$$

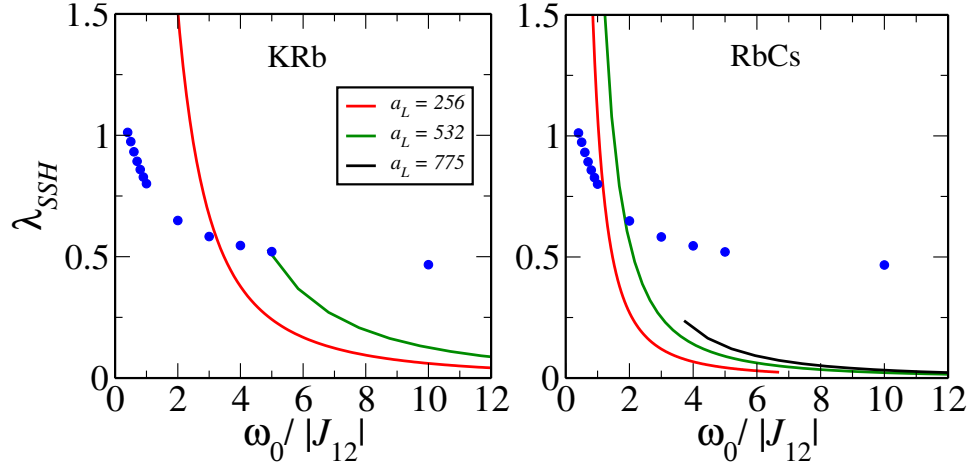


Figure 6.12: Polaron phase diagram for KRb and RbCs molecules in the presence of near resonant laser fields. The labeling of the curves is identical to Fig. 6.10, but the exciton hopping amplitude J_{12} is enhanced by a factor of two due to Raman couplings between rovibrational states of the same parity.

where $\text{Re}(z)$ denotes the real part of z .

Using the methods in Appendix B, the dipole-dipole interaction matrix elements above can be evaluated. The six matrix elements in Eq. (6.78) are $\langle 0|\langle 1|\hat{V}_{dd}|1\rangle|0\rangle = 1/3$, $\langle 2|\langle 1|\hat{V}_{dd}|1\rangle|2\rangle = 4/15$, $\langle 2|\langle 3|\hat{V}_{dd}|3\rangle|2\rangle = 9/35$, $\langle 0|\langle 1|\hat{V}_{dd}|1\rangle|2\rangle = 2\sqrt{5}/15$, $\langle 2|\langle 1|\hat{V}_{dd}|3\rangle|2\rangle = 2\sqrt{21}/35$ and $\langle 2|\langle 1|\hat{V}_{dd}|3\rangle|0\rangle = \sqrt{105}/35$. The energies are given in units of $U_{dd}(1 - 3\cos^2\theta)$, where $U_{dd} = d^2/a_L^3$ and θ is the angle between the molecular array and the quantization axis. Inserting this values in Eq. (6.78) gives

$$\begin{aligned}
 J = & \frac{1}{3}|a_0a_1|^2 + \frac{4}{15}|a_1a_2|^2 + \frac{9}{35}|a_2a_3|^2 + \frac{4\sqrt{5}}{15}|a_1|^2\text{Re}(a_0a_2^*) \\
 & + \frac{4\sqrt{21}}{35}|a_2|^2\text{Re}(a_1a_3^*) + \frac{4\sqrt{105}}{35}\text{Re}(a_0a_3a_1^*a_2^*).
 \end{aligned}
 \tag{6.79}$$

In the absence of external fields, the nearest neighbour hopping amplitude is thus $J_{12} = 1/3$, since $a_0 = a_1 = 1$ and $a_2 = a_3 = 0$. By tuning the intensity and

relative phase of the lasers used to prepare the even and odd rotational superpositions in Eqs. (6.75) and (6.76), the value of J_{12} can be modified. For example, for the real and positive values $a_0 = a_1 = a_2 = a_3 = 1/\sqrt{2}$ we obtain the field-dressed hopping amplitude $J_{12} \approx 0.787$. This value is approximately 2.4 times larger than the field-free hopping. Figure 6.12 shows the range of parameters in the polaron phase diagram that can be achieved with KRb and RbCs molecules when the hopping amplitude is enhanced by a factor of two ($J_{12} \rightarrow 2J_{12}$) using the Raman coupling scheme depicted in Fig. 6.11. The curves corresponding to different lattice constants a_L are significantly shifted towards the strong coupling region of the phase diagram when the Raman coupling scheme is considered (compare with Fig. 6.10). However, the curve corresponding to $a_L = 532$ nm does not cross the phase boundary in the frequency range considered $\omega_0/2\pi = 1 - 50$ kHz for KRb molecules. Shorter lattice separations would facilitate the observation of the transition. For RbCs molecules, increasing the hopping amplitude J_{12} by a factor of two also shifts the lines in the phase diagram towards the strong coupling phase. The transition frequency for $a_L = 532$ nm, however, is in the same range of values $\omega_0/2\pi = 1 - 2$ kHz as in Fig. 6.10, although the value of λ_{SSH} at $\omega_0/2\pi = 1$ kHz is larger.

In summary, by trapping molecules with large dipole moments such as LiCs and LiRb in optical lattices with site separation of up to several hundred nanometers, it should be possible to observe a recently predicted single-polaron sharp transition due to phonon-modulated hopping. For molecules with smaller dipole moments such as KRb, the transition should be observable only for small site separations $a_L < 500$ nm. It is possible to enhance the effect of phonon-modulated hopping by using near resonant laser fields to induce Raman couplings between rotational states of the same parity. This enhancement, however, does not have a dramatic effect on the range of available parameters in the polaron phase diagram.

Chapter 7

Entanglement of cold molecules using off-resonant light

7.1 Chapter overview

This chapter presents a method to generate long-range entanglement of molecular pairs using strong off-resonant pulses, in the absence of static fields. In Section 7.2 the basic notions of molecular alignment with strong pulses are reviewed. The dipole-dipole interaction between molecules in the presence of strong off-resonant fields is revisited in Sec. 7.3. The proposed scheme to generate long-distance entanglement between polar molecules is explained in Secs. 7.4 and 7.5. The chapter ends in with an analysis of specific entanglement measures that are relevant for current experiments in Sec. 7.6. Here the possibility is also discussed to use cold molecules in optical lattices to test Bell's inequalities and to create many-particle entanglement.

7.2 Molecular alignment with adiabatic pulses

7.2.1 Single molecule alignment

In Chapter 2 it was shown that a far-detuned optical field polarizes a molecule in the electronic ground state and interacts with the instantaneously induced dipole moment resulting in an energy shift represented by the Hamiltonian

$$\hat{H}_{AC} = - \sum_p \sum_{p'} E_p(\mathbf{r}) \hat{\alpha}_{p,p'} E_{p'}^*(\mathbf{r}), \quad (7.1)$$

where $\hat{\alpha}_{p,p'}$ is a component of the polarizability tensor in the laboratory frame. For non-rotating molecules, Eq. (7.1) corresponds to a constant energy shift of a given vibronic state. For freely rotating molecules, the Hamiltonian \hat{H}_{AC} couples the rotational states of the molecule. For a laser field with linear polarization along the Z axis, it was shown in Sec. 2.5 that Eq. (7.1) can be written as

$$\hat{H}_{AC} = \hat{N}^2 - \frac{2}{3} \Omega_I \mathcal{D}_{0,0}^{(2)}(\theta), \quad (7.2)$$

where $\mathcal{D}_{0,0}^{(2)} = (3 \cos^2 \theta - 1)/2$ and $\Omega_I = \varepsilon^2(\alpha_{\parallel} - \alpha_{\perp})/4B_e$ is proportional to the intensity of the laser field. The eigenvalues and eigenstates of this Hamiltonian were analyzed in some detail in Secs. 2.5 and 3.5 for weak fields ($\Omega_I \ll 1$) and strong fields ($\Omega_I \gg 1$), respectively.

From a classical point of view, the electric field of a strong off-resonant optical pulse exerts a torque on the rotating axis of a diatomic molecule. This torque induces alignment of the molecular axis along the polarization axis of the pulse. Since the electric field of the pulse oscillates rapidly at optical frequencies, the direction of the instantaneous dipole moment of the molecule oscillates at the same frequency as the field. Therefore, there is no net orientation of the molecule in space on timescales longer than an optical cycle. As a result of the molecule-field interaction, the molecules are aligned in space without a well-defined orientation. The degree of alignment for diatomic molecules is commonly expressed by the expectation value $\mathcal{A} = \langle \cos^2 \theta \rangle$, which is an observable quantity [149, 231]. This quantity can be directly related to the angular distribution of the molecule in the

laboratory frame:

$$\langle \cos^2 \theta \rangle = \begin{cases} 1 & \Rightarrow \text{alignment parallel to reference axis} \\ 0 & \Rightarrow \text{alignment perpendicular to reference axis} \end{cases} \quad (7.3)$$

where θ is the angle between the molecular axis and the field polarization axis (reference axis). The alignment factor $\mathcal{A} = \langle \cos^2 \theta \rangle$ for a molecule in the rotational eigenstate $|N, M_N\rangle$ can be easily evaluated using $\cos^2 \theta = (1/3)(1 + 2C_{2,0})$, where $C_{2,0}$ is a modified spherical harmonic,

$$\mathcal{A}_{N,M_N} = \langle NM_N | \cos^2 \theta | NM_N \rangle = \frac{1}{3} + \frac{2}{3} \left[\frac{N(N+1) - 3M_N^2}{(2N-1)(2N+3)} \right]. \quad (7.4)$$

This expectation value is state-dependent. For the ground state $|N=0, M_N=0\rangle$ the alignment factor is $\mathcal{A}_{0,0} = 1/3 \approx 0.3$ and for the excited state $|N=1, M_N=0\rangle$ we have $\mathcal{A}_{1,0} = 0.6$.

7.2.2 Adiabatic vs non-adiabatic alignment

In the presence of a strong linearly polarized off-resonant pulse ($\Omega_I \gg 1$ in Eq. (7.2)), the rotational wavefunction is given by the superposition

$$|\Psi(t)\rangle = \sum_N C_N(t) |N, M_N\rangle. \quad (7.5)$$

This state can be viewed as a rotational wavepacket in angular momentum space \mathbf{N} . A broad wavepacket in angular momentum space corresponds to a narrow angular distribution of the molecule due to the uncertainty principle¹. The degree of alignment of a rotational wavepacket is therefore larger than the alignment of rotational eigenstates. The alignment of a rotational wavepacket given by Eq. (7.5) evolves in time according to the evolution of the wavepacket under the influence of the laser pulse, i.e.,

$$\langle \Psi(t) | \cos^2 \theta | \Psi(t) \rangle = \sum_N \sum_{N'} C_N(t) C_{N'}^*(t) \langle N' M_N | \cos^2 \theta | NM_N \rangle. \quad (7.6)$$

¹The variables (θ, \mathbf{N}) form a canonical conjugate pair in classical mechanics.

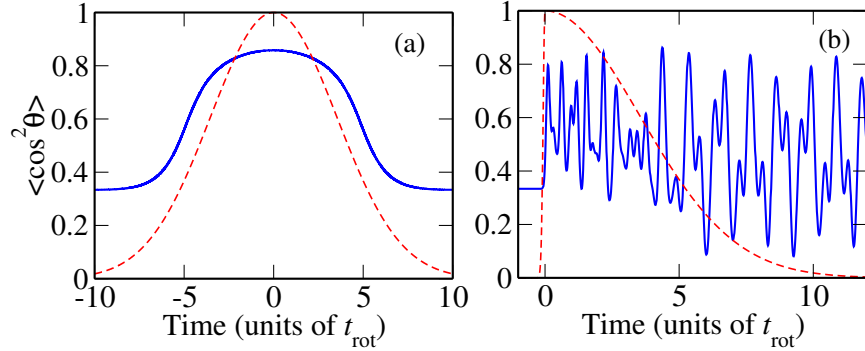


Figure 7.1: Single molecule alignment for adiabatic and non-adiabatic Gaussian pulses. (a) *adiabatic* pulse with $t_{\text{on}} = t_{\text{off}} = 5 t_{\text{rot}}$. (b) *non-adiabatic* pulse with $t_{\text{on}} = 0.1 t_{\text{rot}}$ and $t_{\text{off}} = 5 t_{\text{rot}}$. In both panels the peak intensity is if $\Omega_0 = 50$. The red-dotted line shows the pulse envelope normalized to unity. Time is in units of $t_{\text{rot}} = \hbar/B_e$.

The temporal evolution of a rotational wavepacket under the influence of a strong optical pulse can be divided into two broad categories: adiabatic and non-adiabatic dynamics. These terms refer to the comparison between the pulse duration and the timescale for the rotational motion of the molecules $t_{\text{rot}} = \hbar/B_e$. Let us consider a molecule in the rotational eigenstate $|\Psi(0)\rangle = |NM_N\rangle$ long before the laser pulse is applied. If the pulse is several times longer than t_{rot} the evolution is adiabatic and the rotational wavefunction $|\Psi(t)\rangle$ returns to the initial state $|N, M_N\rangle$ after the pulse is over [231]. When the pulse duration is comparable or shorter than t_{rot} the wavefunction $|\Psi(t)\rangle$ after the pulse is over is given by the rotational wavepacket in Eq. (7.5) with time-dependent amplitudes $C_N(t) = C_N \exp(-iE_N t/\hbar)$. After the pulse is gone, each component of the wavepacket evolves according to its stationary phase $iE_N t/\hbar$. Due to the discrete nature of the rotational spectrum, the evolution of the wavefunction density $|\Psi(t)|^2$ is periodic [149]: $|\Psi(t)\rangle = \pm |\Psi(t + nT_R)\rangle$, where $T_R = \pi\hbar/B_e$ is the rotational period and n is an integer.

In Figure 7.1 molecular alignment under adiabatic and non-adiabatic evolution is shown. The molecule is initially in the rovibrational ground state $|\Psi(0)\rangle = |0, 0\rangle$. A strong off-resonant optical pulse is applied along the Z axis. The intensity parameter is given by $\Omega_I = f(t)^2 \Omega_0$. The electric field envelope of the pulse is

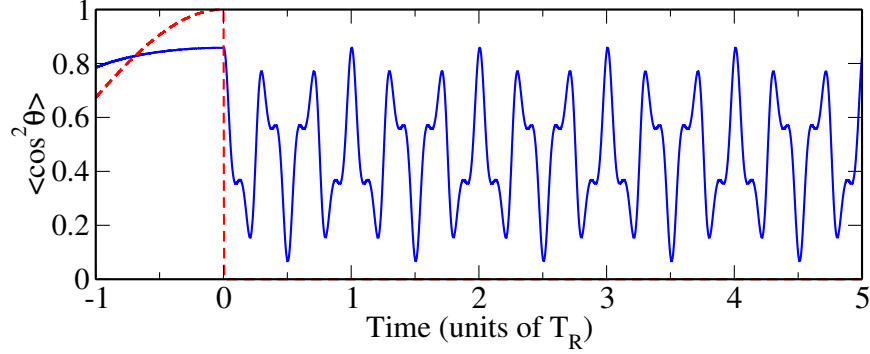


Figure 7.2: Rotational wavepacket revival structure for a non-adiabatic pulse with peak intensity $\Omega_0 = 50$, $t_{\text{on}} = 5 t_{\text{rot}}$ and $t_{\text{off}} = 0.01 t_{\text{rot}}$. The degree of alignment right after the pulse is over revives at integer multiples of the rotational period $T_R = \pi\hbar/B_e \equiv \pi t_{\text{rot}}$. The pulse profile is shown in dotted line.

chosen to be a Gaussian defined by

$$f(t) = \begin{cases} e^{-(t/t_{\text{on}})^2} & t \leq 0 \\ e^{-(t/t_{\text{off}})^2} & t \geq 0 \end{cases}, \quad (7.7)$$

where t_{on} and t_{off} are time constants that determine the shape of the pulse. For a symmetric pulse ($t_{\text{on}} = t_{\text{off}} = t_0$) the pulse duration τ_p is characterized by the full width at half maximum (FWHM), i.e., $\tau_p = 2\sqrt{\ln 2}t_0$. The results in Fig. (7.1) are obtained for a symmetric Gaussian with peak intensity $\Omega_0 = 50$ with varying turn-on and turn-off time constants. The revival structure of a non-adiabatic pulse with a fast turn-off time is shown in Fig. 7.2. The degree of alignment immediately after the pulse is off revives at later times that are integer multiples of the rotational period $T_R = \pi t_{\text{rot}}$.

7.3 Dipolar interactions in strong off-resonant fields

Let us consider the dipole-dipole interaction between molecules in the presence of a strong off-resonant optical field with linear polarization. The Hamiltonian

describing a single molecule \hat{H}_{AC} is given in Eq. (7.2) and its lowest eigenvalues are plotted in Fig. 3.6. We limit the discussion to the opposite parity states g and e from the lowest tunneling doublet. These states form a two-level system since they are not mixed with other rotational states due to intermolecular interactions.

An approximate form of the interaction Hamiltonian matrix $\mathcal{H} = \hat{H}_1 + \hat{H}_2 + \hat{V}_{12}$ was presented in Chapter 3 (see Eq. (3.12), for the case where the transition energy $\varepsilon_e - \varepsilon_g$ is larger than the magnitude of the exchange coupling matrix element J_{12} . This condition is satisfied for closed-shell molecules in static electric fields (Section 3.3) and open-shell molecules in combined electric and magnetic fields (Section 3.4). The lowest two rotational states $|g\rangle$ and $|e\rangle$ in the presence of a strong off-resonant field become very closely spaced as the field intensity increases (see Fig. 3.6). For high laser intensities the energy splitting $\varepsilon_e - \varepsilon_g$ for two interacting polar molecules is comparable to or smaller than the energy of their mutual interaction. In this intensity regime, the interaction-induced transition $|g_1 g_2\rangle \rightarrow |e_1 e_2\rangle$ is energetically allowed if the molecules are initially in the ground state. By setting the energy reference $\varepsilon_g = 0$, the Hamiltonian matrix \mathcal{H} in the subspace $\mathcal{V}_2 = \{|g_1 g_2\rangle, |e_1, e_2\rangle, |g_1, e_2\rangle, |e_1 g_2\rangle\}$ can be written in block-diagonal form

$$\mathcal{H} = \left(\begin{array}{cc|cc} 0 & J_{12} & 0 & 0 \\ J_{12} & 2\varepsilon_e & 0 & 0 \\ \hline 0 & 0 & \varepsilon_e & J_{12} \\ 0 & 0 & J_{12} & \varepsilon_e \end{array} \right). \quad (7.8)$$

The eigenstates of the upper block can be written as

$$|\Phi_1\rangle = a|g_1 g_2\rangle + b|e_1 e_2\rangle \quad \text{and} \quad |\Phi_2\rangle = b|g_1 g_2\rangle - a|e_1 e_2\rangle, \quad (7.9)$$

with eigenvalues $E_1 = \varepsilon_e - K$ and $E_2 = \varepsilon_e + K$, where $K = \sqrt{\varepsilon_e^2 + J_{12}^2}$. The states $|\Phi_1\rangle$ and $|\Phi_2\rangle$ are entangled composite states due to the non-separability of its single-particle components. The eigenstates of the lower block are the symmetric and antisymmetric entangled states

$$|\Psi_+\rangle = \frac{1}{\sqrt{2}} \{|g_1 e_2\rangle + |e_1 g_2\rangle\} \quad \text{and} \quad |\Psi_-\rangle = \frac{1}{\sqrt{2}} \{|g_1 e_2\rangle - |e_1 g_2\rangle\}, \quad (7.10)$$

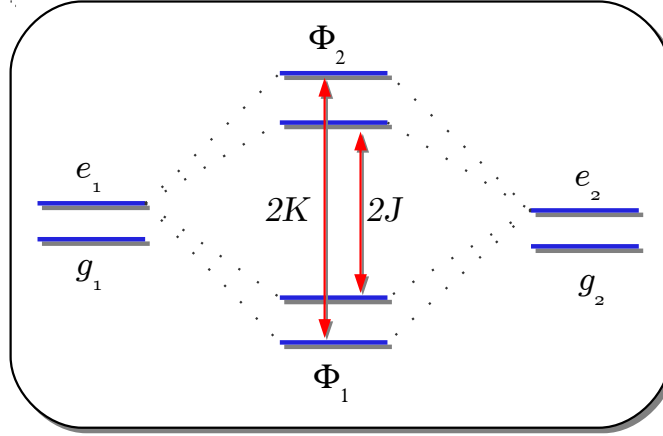


Figure 7.3: Two-molecule level scheme for interaction J_{12} greater than the transition energy ϵ_e . The ground and highest excited state $|\Phi_1\rangle = a|g_1g_2\rangle + b|e_1e_2\rangle$ and $|\Phi_2\rangle = b|g_1g_2\rangle - a|e_1e_2\rangle$ are separated in energy by $2K$, where $K = \sqrt{\epsilon_e^2 + J^2}$. J is the exchange coupling constant.

already discussed in Section 3.4.3. Their corresponding eigenvalues are $E_- = \epsilon_e - J_{12}$ and $E_+ = \epsilon_e + J_{12}$. The two-molecule energy level scheme when $|J_{12}| > \epsilon_e$ is illustrated in Fig. 7.3. This situation should be compared with the regime considered in Sections 3.3 and 3.4, where only the subradiant and superradiant states $|\Psi_-\rangle$ and $|\Psi_+\rangle$ are entangled.

7.4 Entanglement of polar molecules in the absence of DC fields

7.4.1 Time-evolution of two-molecule states

The results of this Section suggest an interesting possibility for generating molecular entanglement using strong off-resonant pulses in the limit of cold and ultracold temperatures. Polar molecules can be initially prepared in the rovibrational ground state $|g\rangle$ in the absence of DC electric fields. The molecules can be confined in optical traps created by weak off-resonant fields (see Section 2.7). The initial wavefunction for a pair of interacting molecules is the stationary state $|\Psi(0)\rangle = |g_1g_2\rangle$.

A strong linearly polarized off-resonant field can then be used to bring the energy of the excited state $|e\rangle$ close to degeneracy with the ground state. In this regime the dipole exchange interaction between two molecules leads to an arbitrary superposition of the form

$$|\Psi(t)\rangle = a(t)|g_1g_2\rangle + b(t)|e_1e_2\rangle e^{-i2\varepsilon_e t/\hbar} \quad (7.11)$$

with no contribution from the one-excitation subspace $\{|g_1e_2\rangle, |e_1g_2\rangle\}$ because the Hamiltonian in Eq. (7.8) is block-diagonal. Let us rewrite the sub-block involving the states $|g_1g_2\rangle$ and $|e_1e_2\rangle$ as

$$\mathcal{H} = \begin{pmatrix} -\varepsilon_e & J_{12} \\ J_{12} & \varepsilon_e \end{pmatrix}, \quad (7.12)$$

where the zero of energy is defined to be half the excitation energy $\hbar\omega_e = 2\varepsilon_e$. Inserting the wavefunction in Eq. (7.11) into the time-dependent Schrödinger equation $i\hbar\partial_t|\Psi(t)\rangle = \mathcal{H}|\Psi(t)\rangle$ with \mathcal{H} given by Eq. (7.12) results in the system of equations

$$\begin{aligned} i\hbar \frac{d}{d\tau} a(t) &= b(t) J_{12} e^{-2i\varepsilon_e t/\hbar} \\ i\hbar \frac{d}{d\tau} b(t) &= a(t) J_{12} e^{2i\varepsilon_e t/\hbar}. \end{aligned} \quad (7.13)$$

In the case where the energy splitting ε_e is instantaneously made of the same order as J_{12} and both energy parameters are kept for a very long time, the probability amplitude of the doubly excited state $P_b(t) = |b(t)|^2$ oscillates in time as

$$P_b(t) = \frac{J_{12}^2}{\hbar K} \sin^2(Kt), \quad (7.14)$$

where $\hbar K = \sqrt{\varepsilon_e^2 + J_{12}^2}$. We have assumed the initial condition $a(0) = 1$ and $b(0) = 0$. The probability amplitude $P_a(t)$ is obtained from Eq (7.14) and the normalization condition. Two molecules initially in the ground state therefore undergo periodic exchange processes between the states $|g_1g_2\rangle$ and $|e_1e_2\rangle$ with Rabi frequency K for

$J_{12}/K \sim 1$. In the limit $J_{12}/\varepsilon_e \rightarrow 0$, the oscillation period $1/K$ tends to infinity, and the amplitude of the oscillation tends to zero.

In order to study the more general case where both the dipolar coupling $J_{12}(t)$ and the excited energy $\varepsilon_e(t)$ are time-dependent, the two-molecule wavefunction can be expanded as

$$|\Psi(t)\rangle = a(t)|g_1g_2\rangle + b(t)|e_1e_2\rangle. \quad (7.15)$$

Inserting this expression in the Schrödinger equation, expressing energy in units of the rotational constant B_e and time in units of $t_{\text{rot}} = \hbar/B_e$ gives the following system of differential equations

$$\begin{aligned} i \frac{d}{d\tau} a(\tau) &= J(\tau)b(\tau) \\ i \frac{d}{d\tau} b(\tau) &= J(\tau)a(\tau) + 2E(\tau)b(\tau), \end{aligned} \quad (7.16)$$

where $J = J_{12}/B_e$, $E = \varepsilon_e/B_e$, and $\tau = t/t_{\text{rot}}$. The timescale t_{rot} corresponds roughly to the rotational period of a molecule [149, 150], which is on the order of picoseconds for most diatomic molecules. The dipole-dipole energy scale $U_{dd} = d^2/R^3$ defines the interaction timescale $t_{dd} = \hbar/U_{dd}$, which depends on the relative distance between molecules. The ratio between the rotational and interaction timescales t_{dd}/t_{rot} is larger than unity for distances larger than the characteristic length²

$$R_0 = (d^2/B_e)^{1/3}. \quad (7.17)$$

If the pulse is adiabatic with respect to the rotational timescales ($\tau_p \gg t_{\text{rot}}$), the state of a single molecule is given by an eigenstate of the Hamiltonian in Eq. (7.2) at all times. In this case, Eq. 7.16 can be solved numerically using the intensity parameter $\Omega_I(t) = f^2(t)\Omega_0$ to evaluate the time-dependent Hamiltonian parameters $J(t)$ and $E(t)$ from the curves in Figs. 3.6 and 3.9 for $\lambda = 0$. The strength of the pulse $\Omega_0 = \varepsilon^2 \Delta\alpha / 4B_e$ is determined by the peak electric field amplitude.

²This equation in S.I. units reads $R_0 = (d^2/4\pi\varepsilon_0 B_e)^{1/3}$, where $\varepsilon_0 \approx 8.854 \times 10^{-12} \text{ CV}^{-1}\text{m}^{-1}$ is the electric constant. In atomic units $4\pi\varepsilon_0 = 1$.

7.4.2 Molecular parameters for alkali-metal dimers

For polar alkali-dimers, the magnitude of the dipole moment d is a few Debye and the rotational constant are in the range $10^2 - 10^3$ GHz. The characteristic length $R_0 = (d^2/B_e)^{1/3}$ is therefore a few nanometers. The strength of the light-matter interaction is parametrized by $\Omega_I = |\epsilon|^2(\alpha_{\parallel} - \alpha_{\perp})/4B_e$. The S.I. units of the polarizability anisotropy $\Delta\alpha = \alpha_{\parallel} - \alpha_{\perp}$ are $[\text{CV}^{-1}\text{m}^2]$, but is commonly presented in units of volume $[\text{cm}^3]$. These two choices of units are related by $\alpha[\text{C V}^{-1}\text{m}^2] = 4\pi\epsilon_0 10^{-6} \alpha_V[\text{cm}^3]$, where ϵ_0 is the electric constant. The square electric field amplitude $|\epsilon|^2$ of the traveling wave is related to its intensity by $I = c\epsilon_0 n |\epsilon|^2/2$, where $n \approx 1$ is the refractive index of the medium and c is the speed of light. The intensity parameter Ω_I can thus be written as

$$\Omega_I = \left(\frac{1}{c\epsilon_0} \right) \frac{I\Delta\alpha}{2B_e} = \left(\frac{4\pi}{c} \right) \frac{I\Delta\alpha_V}{2B_e} \quad (7.18)$$

In Table 7.1 the laser intensity I_0 corresponding to a light-matter interaction parameter $\Omega_I = 1$ is presented for selected polar alkali-metal dimers. Predicted values for the polarizability anisotropy $\Delta\alpha_V$ and rotational constants for the rovibrational ground state $B_{v=0} \approx B_e$ are taken from Ref. [230]. For alkali-dimers I_0 is on the order of $10^7 - 10^8$ W/cm². Continuous laser beams with frequencies in the mid-infrared region ($\lambda = 1064$ nm) can have intensities on the order of 10^8 W/cm² when focused to micrometer size regions [233, 234]. Intensities higher than 10^{10} W/cm² can be achieved with laser pulses. Strong laser pulses are routinely used in molecular alignment experiments, with pulse durations varying from less than a femtosecond to hundreds of nanoseconds [149].

7.4.3 Entanglement length scale

In the presence of an off-resonant field, the excitation energy ϵ_e between the field-dressed states $|g\rangle$ and $|e\rangle$ is equal to the dipole-dipole interaction energy for molecules whose separation is on the order of the *entanglement length*

$$R_e = (d^2/\epsilon_e)^{1/3}. \quad (7.19)$$

	d (D)	$\Delta\alpha_V$ (a_0^3)	B_e (cm^{-1})	I_0 (10^8 Wcm^{-2})	R_0 (nm)	t_{rot} (ps)
RbCs	1.238	441	0.0290	0.4	6.4	1.15
KRb	0.615	360	0.0386	0.7	3.7	0.86
LiCs	5.529	327	0.1940	3.8	9.3	0.17
LiRb	4.168	280	0.2220	5.0	7.3	0.15

Table 7.1: Molecular parameters for selected polar alkali-metal dimers: I_0 is the laser intensity corresponding to $\Omega_I = (4\pi/c)I_0\Delta\alpha_V/2B_e = 1$, $R_0 = (d^2/B_e)^{1/3}$ is the characteristic length of the dipole-dipole interaction and $t_{\text{rot}} = \hbar/B_e$ is the timescale of the rotational motion. Values of the polarizability anisotropy $\Delta\alpha_V$, dipole moment d and rotational constant B_e are taken from Ref. [230].

For two molecules separated within this length, mixing of the composite states $|g_1g_2\rangle$ and $|e_1e_2\rangle$ is energetically allowed. The entanglement length R_e increases exponentially with the intensity parameter Ω_I . This is shown in Fig. 7.4, where the distance is expressed in units of R_0 .

7.4.4 Dynamical entanglement generation

The dynamical generation of entanglement between a molecular pair can be studied by solving the time-dependent Schrödinger equation (7.16). The doubly excited state probability $P_b(t)$ is the figure of merit for the non-separability of the composite wavefunction $|\Psi\rangle = a|g_1g_2\rangle + b|e_1e_2\rangle$ at any given time. When $P_b \equiv |b|^2 = 0$, the two-particle state is separable.

Let us consider a pair of polar molecules separated by a distance $R > R_0$, where both molecules are initially in their rotational ground states, i.e., $|\Psi(0)\rangle = |g_1g_2\rangle$. The intermolecular distance R is a free parameter that determines the interaction timescale t_{dd} . The ratio $t_{\text{dd}}/t_{\text{rot}} = (R/R_0)^3$ can thus be used to parametrize the intermolecular distance. As an illustration of the results, in Fig. 7.5 the evolution of the doubly excited state probability $P_b(t)$ is shown for pulse of moderate peak intensity $\Omega_0 = 40$ and $t_{\text{on}} = t_{\text{off}} = 200 t_{\text{rot}}$. Curves are shown for intermolecular distances $R = 5 R_0$ and $R = 10 R_0$. Figure 7.5 shows that for molecules separated by a distance larger than the entanglement length R_e , the laser pulse does not populate the

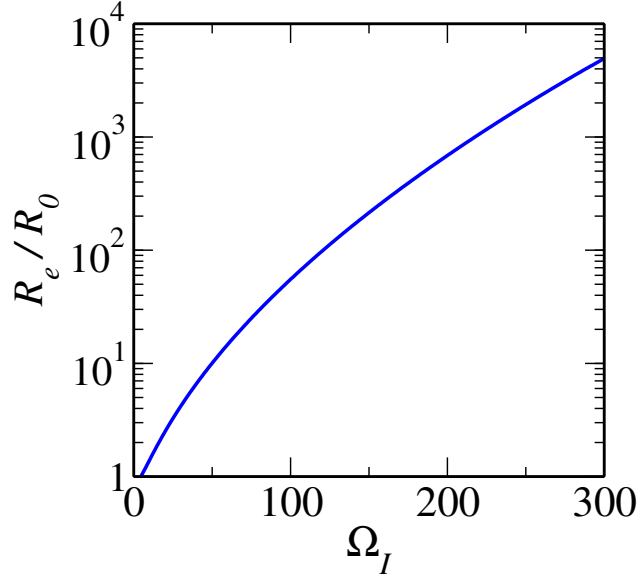


Figure 7.4: Entanglement length R_e in units of $R_0 = (d^2/B_e)^{1/3}$, as a function of the laser intensity parameter Ω_I . The vertical axis is in logarithmic scale.

doubly excited state significantly. For distances smaller than R_e , the two-molecule state can have a significant contribution from the state $|e_1 e_2\rangle$, even after the pulse is over. For $\Omega_0 = 40$, the entanglement length is $R_e = 6.7 R_0$. For concreteness, the example in Fig. (7.5) for KRb molecules would correspond to a pulse with peak intensity $I = 28 \times 10^8 \text{ W/cm}^2$ and $t_{\text{on}} = t_{\text{off}} = 0.17 \text{ ns}$. These parameters can be easily achieved in experiments [149, 231]. The associated entanglement length is $R_e = 24.7 \text{ nm}$.

7.4.5 Pulse shape effects

The entanglement length increases exponentially with the laser intensity (see Fig. 7.4). Therefore, high intensity pulses are needed to couple weakly interacting molecules separated by distances several orders of magnitude larger than R_0 . The dipole-dipole interaction time t_{dd} increases with the intermolecular distance as R^3 . Pulse durations on the order of the interaction time are needed in order to cou-

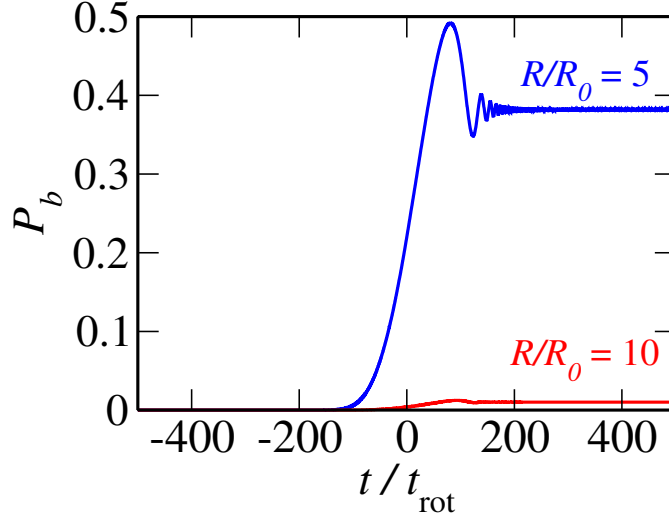


Figure 7.5: Dynamical entanglement generation with a moderately strong pulse. The probability amplitude $P_b(t)$ of the doubly excited state $|e_1 e_2\rangle$ is shown for the peak intensity parameter $\Omega_0 = 40$. The entanglement length is $R_e = 6.7 R_0$. Two intermolecular distances $R > R_0$ are plotted. The pulse has a symmetric Gaussian profile centered at $t = 0$ with $t_{\text{on}} = t_{\text{off}} = 200 t_{\text{rot}}$. Length is in units of $R_0 = (d^2/B_e)^{1/3}$.

ple the states $|g_1 g_2\rangle$ and $|e_1 e_2\rangle$ significantly. For distances a few times R_0 , the interaction time is on the order of $100 t_{\text{rot}}$ (see Fig. 7.5). Increasing the entanglement length by one order of magnitude would require increasing the pulse duration 1000 times longer. As an illustration, let us consider a pulse with peak intensity $\Omega_0 = 150$. The associated entanglement length is $R_e = 214 R_0$. The evolution of doubly excited state $P_b(t)$ is shown in Fig. (7.6) for the intermolecular distances $R = 30 R_0$, $R = 50 R_0$ and $R = 100 R_0$. The corresponding interaction times are $t_{\text{dd}} = 0.27 \times 10^5 t_{\text{rot}}$, $t_{\text{dd}} = 1.25 \times 10^5 t_{\text{rot}}$ and $t_{\text{dd}} = 10 \times 10^5 t_{\text{rot}}$ respectively. For LiRb molecules, these intermolecular distances correspond to a few hundred nanometers and the longer interaction time is 150 nanoseconds. The peak intensity for $\Omega_0 = 150$ is $I = 1.5 \times 10^{10} \text{ W/cm}^2$.

Figure 7.6 shows that the evolution $P_b(t)$ is strongly dependent on the distance between molecules. The figure also shows that for a pulse longer than the interac-

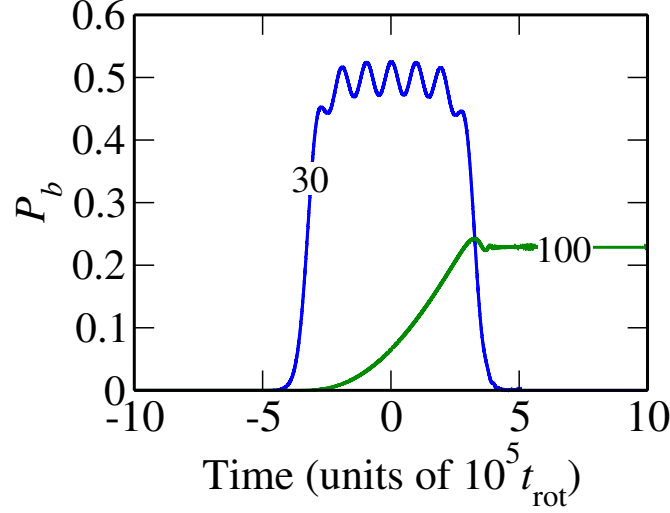


Figure 7.6: Entanglement generation with strong pulses of different duration. Plotted is the probability amplitude $P_b(t)$ of the doubly excited state $|e_1 e_2\rangle$ for $\Omega_0 = 150$. The entanglement length is $R_e = 214 R_0$. The curves are labeled by the intermolecular distance: $R = 30R_0$ ($t_{dd} = 0.27 \times 10^5 t_{rot}$) and $R = 100R_0$ ($t_{dd} = 10 \times 10^5 t_{rot}$). The pulse is a symmetric Gaussian centered at $t = 0$ with $t_{on} = t_{off} = 6.25 \times 10^5 t_{rot}$ (FWHM = $10.4 \times 10^5 t_{rot}$).

tion time at a certain distance ($R = 30R_0$ and $R = 50R_0$), the wavefunction returns adiabatically into initial state $|\Psi\rangle = |g_1 g_2\rangle$ after the pulse is over, and the two-particle entanglement is lost. For intermolecular separations such that the interaction time t_{dd} is longer than the pulse turn-on and turn-off times ($R = 100 R_0$ in Fig. (7.6), a strong laser pulse creates the superposition

$$|\Psi\rangle = a|g_1 g_2\rangle + b|e_1 e_2\rangle e^{-i2\omega_{01}t}, \quad (7.20)$$

after the pulse is over. The relative phase between the superposition states rotates with frequency $2\omega_{01}$, where $\omega_{01} = 2B_e/\hbar$ is the transition frequency between the states $|g\rangle = |N = 0, M_N = 0\rangle$ and $|e\rangle = |N = 1, M_N = 0\rangle$. The magnitude of the coefficient b depends on the duration and intensity of the applied pulse.

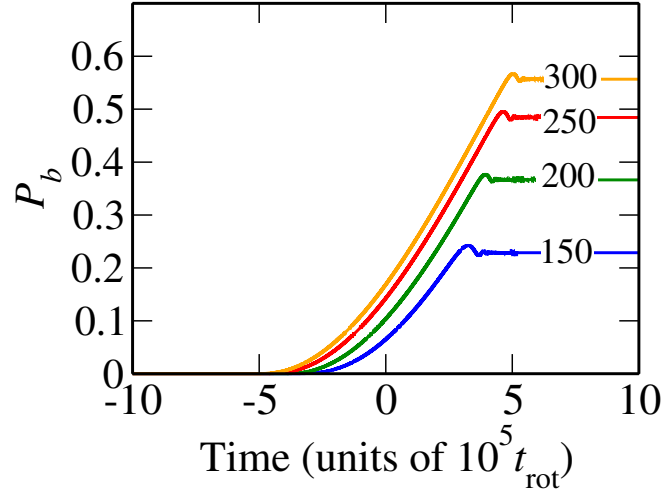


Figure 7.7: Entanglement generation with strong pulses of different peak intensity. Probability amplitude $P_b(t)$ of the doubly excited state $|e_1 e_2\rangle$ for $\Omega_0 = 150$, $\Omega_0 = 200$, $\Omega_0 = 250$ and $\Omega_0 = 300$. The curves are labeled by the value of Ω_0 . The intermolecular distance is $R = 100R_0$ for all curves and the interaction time is $t_{\text{dd}} = 10 \times 10^5 t_{\text{rot}}$. The laser pulse has Gaussian profile centered at $t = 0$ with $t_{\text{on}} = t_{\text{off}} = 6.25 \times 10^5 t_{\text{rot}}$.

For a given intermolecular distance R , the peak intensity of the laser Ω_0 can be increased in order to enhance the doubly excited state amplitude b in Eq. (7.20). This is the case for non-adiabatic pulses with respect to the dipole-dipole interaction time t_{dd} . In Figure 7.7 this is shown for two molecules separated by $R = 100 R_0$ (730 nm for LiRb molecules). The laser pulse turn-on and off times are $t_{\text{on}} = t_{\text{off}} = 6.25 \times 10^5 t_{\text{rot}}$ (93.8 ns for LiRb molecules), which gives a pulse width comparable with the interaction time $t_{\text{dd}} = 10 \times 10^5 t_{\text{rot}}$. As the peak intensity parameter Ω_0 is increased from 150 to 300, the value of the probability amplitude after the pulse is over $P_b(t \rightarrow \infty)$ increases significantly. For LiRb molecules the peak intensities used in Fig. 7.7 are on the order of 10^{11} W/cm², but for KRb molecules the required intensities are an order of magnitude smaller due to its larger polarizability and smaller rotational constant.

7.4.6 Field-free entanglement in optical lattices

Let us now consider the interaction of polar molecules with a strong off-resonant pulse when molecules are trapped in individual sites of an optical lattice. The smallest lattice site separations that can be achieved in experiments are $a_L = 400 - 600$ nm [20, 79]. For most alkali-dimers in Table 7.1, these distances correspond roughly to $R = 100 R_0$. In Figure 7.7 it was shown that for such distances it is possible to achieve field-free two-molecule entanglement using pulses that are adiabatic with respect to the rotational time t_{rot} , but non-adiabatic with respect to the dipole-dipole interaction time t_{dd} . In adiabatic alignment experiments, optical pulses with peak intensities $I \sim 10^{12}$ W/cm² and FWHM $\sim 10 - 100$ ns can be easily produced [149, 231]. The doubly excited state population P_b is shown in Fig. 7.8 for several pulse widths. The peak intensity parameter is $\Omega_0 = 200$ for all curves. When the FWHM is smaller than the interaction time t_{dd} , the achieved value of P_b is significantly smaller than for a pulse width on the order of t_{dd} . The magnitude of P_b after the pulse is over can be increased by increasing the width of the pulse. However, for a pulse width much larger than t_{dd} the two-molecule evolution is adiabatic (see Fig. 7.6) and P_b vanishes after the pulse is over. For concreteness, the dipole-dipole interaction time t_{dd} for the optical lattice distance $R = 500$ nm is 26.4 ns for LiCs, 48.2 ns for LiRb, 548 ns for RbCs and 2.83 μ s for KRb molecules. Molecules with larger dipole moments such as LiCs and LiRb have interaction times of a few tens of nanoseconds, whereas t_{dd} for weakly polar molecules such as KRb is on the order of microseconds for optical lattice distances. It should therefore be possible to generate field-free entanglement of highly polar molecules (see Eq. (7.20)) using strong off-resonant pulses with pulse durations $\tau_p \sim 10$ ns (FWHM) and peak intensities $I \sim 10^9 - 10^{11}$ W/cm². Laser pulses with these requirements are routinely used in studies of adiabatic molecular alignment of molecules [231]. For weakly polar molecules, the necessary pulses to generate field-free entanglement are much longer, which limits the achievable peak intensities significantly.

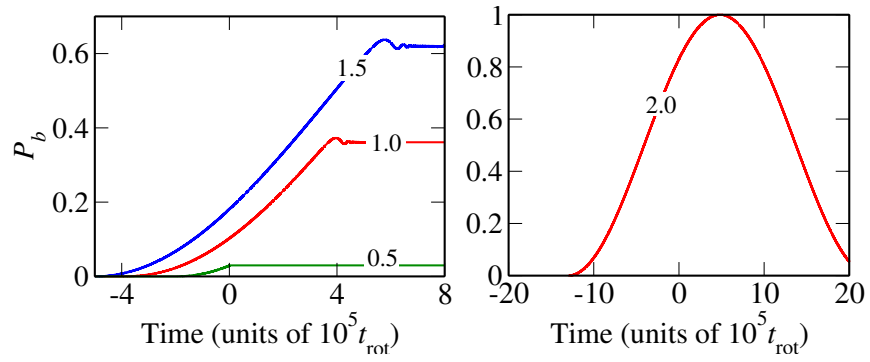


Figure 7.8: Entanglement generation for polar molecules in optical lattices. Probability amplitude $P_b(t)$ of the doubly excited state $|e_1 e_2\rangle$ for $\Omega_0 = 200$ as a function of the pulse width τ_p (Gaussian FWHM). Each curve is labeled by the value of the ratio τ_p/t_{dd} , for $t_{\text{dd}} = 10^6 t_{\text{rot}}$. This corresponds to the optical lattice intermolecular distance $R = 100 R_0$.

7.5 Entanglement in combined DC fields and optical pulses

7.5.1 Novel couplings induced by the DC electric field

The discussion in the preceding section is no longer valid when molecules are in the presence of an additional DC electric field. As shown in Fig. (3.9), in the presence of collinear static and off-resonant fields the exchange coupling J_{12} becomes negligibly small for large intensity parameters, even for very weak dc electric fields. This is the case for the states $|g\rangle$ and $|e\rangle$ from the lowest tunneling doublet in Fig. (3.6). Conversely, the dipole-dipole matrix elements that are diagonal in the molecular states such as $V_{12}^{gg} = \langle g_1 g_2 | \hat{V}_{12} | g_1 g_2 \rangle$ and $V_{12}^{ee} = \langle e_1 g_2 | \hat{V}_{12} | e_1 g_2 \rangle$ increase with the laser intensity, as shown in Fig. (3.10). In the limit where the excitation energy ϵ_e is comparable with the dipole-dipole energy scale U_{dd} , the matrix elements

$$A_{12} = \langle e_1 g_2 | \hat{V}_{12} | g_1 g_2 \rangle \quad \text{and} \quad B_{12} = \langle e_1 g_2 | \hat{V}_{12} | e_1 e_2 \rangle \quad (7.21)$$

also contribute to the dynamics of two-molecule states. These matrix elements vanish in the absence of static electric fields. In a weak DC electric field with $\lambda \ll 1$ and a weak AC field with $\Omega_I \ll 1$, the matrix element A_{12} for the rotational ground and excited states $|g\rangle = a|N=0, M_N=0\rangle + b|N=1, M_N=0\rangle$ and $|e\rangle = -b|N=0, M_N=0\rangle + a|N=1, M_N=0\rangle$, with $a \gg b > 0$, can be written as

$$A_{12} = 2J_{12}^{(0,0)} ab(a^2 - b^2) \quad (7.22)$$

where $J_{12}^{(0,0)} = \langle 1, 0 | \langle 0, 0 | \hat{V}_{12} | 0, 0 \rangle | 1, 0 \rangle = \langle 1, 0 | \langle 1, 0 | \hat{V}_{12} | 0, 0 \rangle | 0, 0 \rangle$ is the field-free exchange constant. The matrix element A_{12} thus has the same sign as J_{12} for weak DC and AC electric fields. The same holds for the matrix element B_{12} . For larger fields, the value of the matrix elements A_{12} and B_{12} are obtained by constructing two-molecule states from the eigenstates of the single-molecule Hamiltonian $\hat{H} = \hat{H}_R + \hat{H}_{DC} + \hat{H}_{AC}$ in Eq. (3.17), for a collinear configuration. It is important to control the overall phase of the two-particle states constructed in this procedure. For example, if the state $|e_1 g_2\rangle$ is multiplied by an overall π -phase, i.e., $|e_1 g_2\rangle \rightarrow -|e_1 g_2\rangle$, the matrix element in Eq. (7.22) changes sign, which

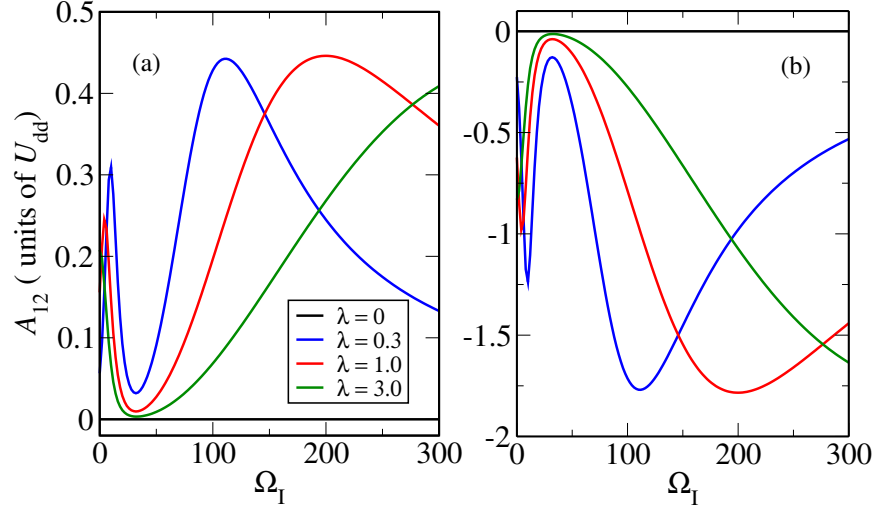


Figure 7.9: Interaction energy $A_{12} = \langle e_1 g_2 | \hat{V}_{12} | g_1 g_2 \rangle$ for two molecules in their ground $|g\rangle$ and first excited $|e\rangle$ rotational states, in the presence of collinear DC electric with strength λB_e and CW far-detuned optical fields with strength $\Omega_I B_e$, where B_e is the rotational constant. Panels (a) and (b) correspond to a perpendicular and parallel orientation, respectively, of the intermolecular axis with respect to the field axis. The dipole-dipole energy is in units of $U_{dd} = d^2/R_{12}^3$.

is an unphysical result. This is not an issue in the evaluation of the matrix elements $J_{12} = \langle e_1 g_2 | \hat{V}_{12} | g_1 e_2 \rangle$ and $V_{12}^{eg} = \langle e_1 g_2 | \hat{V}_{12} | e_1 g_2 \rangle$ because the overall phase of the states in the degenerate subspace can be chosen such that the sign of the dipole-dipole matrix elements depend on the orientation of an external field as $(1 - 3\cos^2\theta)$, where θ is the angle between the intermolecular axis and the external field along the Z-axis. As Eq. (7.22) suggests, the sign of the matrix elements A_{12} is equal to the sign of the field-free exchange constant $J^{(0,0)}$ and the field-dress exchange constant J_{12} (see Eq. (3.5)).

The matrix element $B_{12} = \langle e_1 g_2 | \hat{V}_{12} | e_1 e_2 \rangle$ can be written assuming weak DC and AC electric fields as

$$B_{12} \approx 2J^{(0,0)}ab(b^2 - a^2) = -A_{12}. \quad (7.23)$$

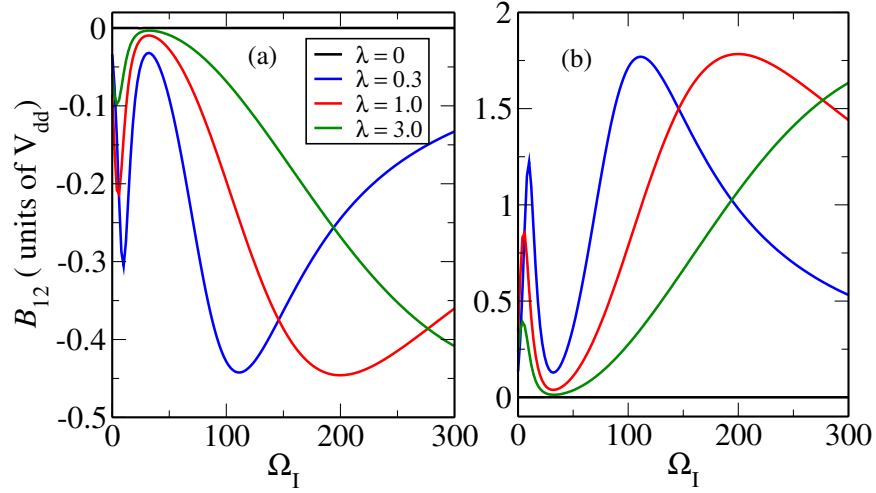


Figure 7.10: Interaction energy $B_{12} = \langle e_{1g} | \hat{V}_{12} | e_1 e_2 \rangle$ for two molecules in their ground $|g\rangle$ and first excited $|e\rangle$ rotational states, in the presence of collinear DC electric with strength λB_e and CW far-detuned optical fields with strength $\Omega_I B_e$, where B_e is the rotational constant. Panels (a) and (b) correspond to a perpendicular and parallel orientation, respectively, of the intermolecular axis with respect to the field axis. The dipole-dipole energy is in units of $U_{dd} = d^2/R_{12}^3$.

This relation between A_{12} and B_{12} holds for small DC electric field parameter $\lambda < 1$ and for arbitrary AC field strengths. Figures 7.9 and 7.10 show the dependence of these dipole-dipole energies on the intensity parameter Ω_I for weak and intermediate DC electric field strengths. The dependence of A_{12} and B_{12} on the DC field strength, for different AC field parameters, is shown in Figure 7.11. It is shown that the relation $B_{12} \approx -A_{12}$ only holds for weak electric fields since B_{12} changes sign at some large value of the DC field strength ($\lambda > 1$) which depends on the strength of an applied AC field. The magnitude of the couplings A_{12} and B_{12} is zero in the absence of a DC electric field and has a maximum in the region of weak DC fields. The position of the weak field maximum is shifted towards $\lambda = 0$ as the strength of the AC field increases.

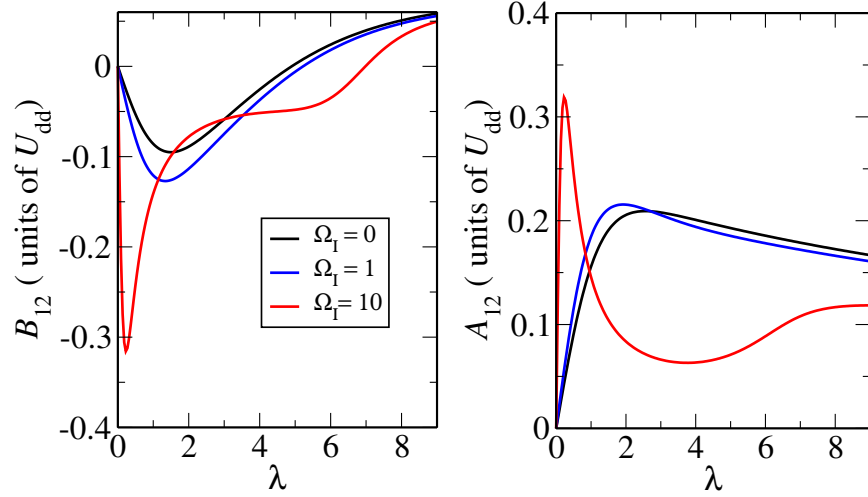


Figure 7.11: Dipole-dipole couplings A_{12} and B_{12} as a function of the DC electric field strength λ in the presence of a far-detuned optical field with strength Ω_I . The intermolecular axis is perpendicular to the field axis. The dipole-dipole energy is in units of $U_{dd} = d^2/R_{12}^3$.

In the presence of collinear static and strong off-resonant fields, the two-molecule Hamiltonian matrix in Eq. (7.8) can be rewritten in the basis $\mathcal{V}_2 = \{|g_1g_2\rangle, |e_1, e_2\rangle, |g_1, e_2\rangle, |e_1g_2\rangle\}$ as

$$\mathcal{H} = \left(\begin{array}{cc|cc} -\epsilon_e & J_{12} & A_{12} & A_{12} \\ J_{12} & \epsilon_e + V_{12}^{ee} - V_{12}^{gg} & B_{12} & B_{12} \\ \hline A_{12} & B_{12} & V_{12}^{eg} - V_{12}^{gg} & J_{12} \\ A_{12} & B_{12} & J_{12} & V_{12}^{eg} - V_{12}^{gg} \end{array} \right). \quad (7.24)$$

In this expression, the energy reference is chosen as $V_{12}^{gg} + \epsilon_e$. The matrix element A_{12} couple the state with no excitations $|g_1g_2\rangle$ with the degenerate states in the one-excitation subspace $|e_1g_2\rangle$ and $|g_1e_2\rangle$. This type of coupling is typically achieved by one-photon absorption of electromagnetic radiation near resonance with the transition $|g\rangle \rightarrow |e\rangle$. In this case, the dipole-dipole interaction between

molecules induces such transitions. Analogously, the matrix element B_{12} couples the one-excitation subspace with the doubly-excited state $|e_1 e_2\rangle$.

The eigenstates of the Hamiltonian in Eq. (7.24) can be written as

$$|\Phi\rangle = a|g_1 g_2\rangle + b|e_1 g_2\rangle + c|g_1 e_2\rangle + d|e_1 e_2\rangle, \quad (7.25)$$

where the coefficients depend on intensity of the off-resonant field and the strength of the DC electric field.

7.5.2 Spatial bounds for entanglement generation

Let us consider a pair of molecules in the presence of a static electric field. A strong laser pulse is applied whose polarization is collinear with the direction of the DC field. The direction of the intermolecular axis is perpendicular to the direction of the fields. The static electric field couples states of opposite parity and in particular the states of the lowest tunneling doublet $|g\rangle$ and $|e\rangle$. The static electric field breaks the degeneracy between the tunneling doublet states. The single excitation energy ε_e increases linearly with the DC field strength for $\lambda \ll 1$ (see Fig. 3.8). As the excitation energy increases due to the linear Stark shift, the entanglement length $R_e \equiv (B_e/\varepsilon_e)^{1/3} R_0$ for a given intensity of the applied laser pulse is smaller than in the absence of DC electric fields. While R_e increases exponentially with the intensity parameter Ω_I in the absence of static fields, it reaches an asymptotic limit when a DC field is present. Figure 7.12 shows that this limit decreases rapidly to $R_e \sim R_0$ even for weak DC electric fields.

When a static field is present, the wavefunction for a pair polar molecules due to the action of a strong optical pulse can be written as

$$|\Psi(t)\rangle = a(t)|g_1 g_2\rangle + b(t)|e_1, e_2\rangle e^{-i\varepsilon_2 t/\hbar} + c(t)|e_1 g_2\rangle e^{-i\varepsilon_1 t/\hbar} + d(t)|g_1, e_2\rangle e^{-i\varepsilon_1 t/\hbar} \quad (7.26)$$

where $\varepsilon_2 = 2\varepsilon_e + V_{12}^{ee} - V_{12}^{gg}$ and $\varepsilon_1 = \varepsilon_e + V_{12}^{eg} - V_{12}^{gg}$. The time-dependent Schrödinger equation for the wavefunction $|\Psi(t)\rangle$ reduces to the dimensionless system of equa-

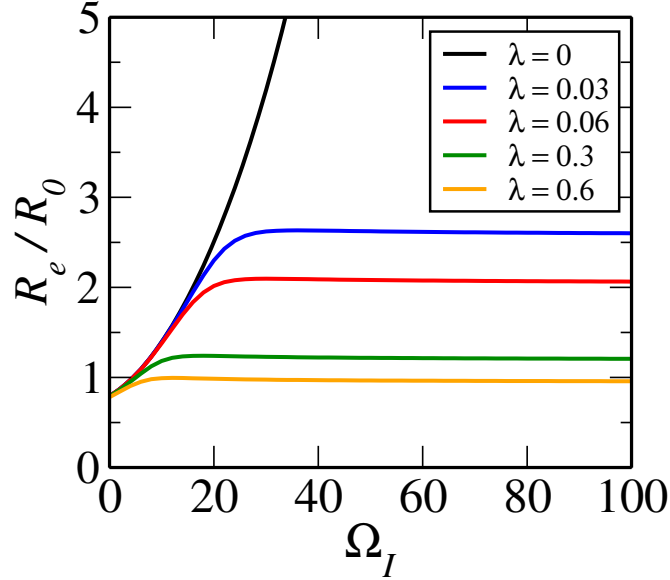


Figure 7.12: Entanglement length R_e in units of $R_0 = (d^2/B_e)^{1/3}$, as a function of the laser intensity parameter Ω_I for several values of the DC field strength parameter λ . R_e increases exponentially when $\lambda = 0$ and reaches an asymptotic limit for $\lambda \neq 0$.

tions

$$\begin{aligned}
 i \frac{d}{d\tau} a(\tau) &= b(\tau) J(\tau) e^{-i\omega_2(\tau)\tau} + c(\tau) A(\tau) e^{-i\omega_1(\tau)\tau} + d(\tau) A(\tau) e^{-i\omega_1(\tau)\tau} \\
 i \frac{d}{d\tau} b(\tau) &= b(\tau) J(\tau) e^{i\omega_2(\tau)\tau} + c(\tau) B(\tau) e^{i[\omega_2(\tau) - \omega_1(\tau)]\tau} + d(\tau) A(\tau) e^{i[\omega_2(\tau) - \omega_1(\tau)]\tau} \\
 i \frac{d}{d\tau} c(\tau) &= a(\tau) A(\tau) e^{i\omega_1(\tau)\tau} + b(\tau) B(\tau) e^{-i[\omega_2(\tau) - \omega_1(\tau)]\tau} + d(\tau) J(\tau) \\
 i \frac{d}{d\tau} d(\tau) &= a(\tau) A(\tau) e^{i\omega_1(\tau)\tau} + b(\tau) B(\tau) e^{-i[\omega_2(\tau) - \omega_1(\tau)]\tau} + d(\tau) J(\tau),
 \end{aligned} \tag{7.27}$$

where $J = J_{12}/B_e$, $A = A_{12}/B_e$, $B = B_{12}/B_e$, $E_1 = \varepsilon_1/B_e$, $E_2 = \varepsilon_2/B_e$ and $\tau = B_e t/\hbar$. The two-level system in Eq. (7.16) is obtained from the first two equations by setting $A_{12} = B_{12} = V_{12}^{ee} = V_{12}^{gg} = 0$.

Let us consider a molecular pair in the presence of a weak DC electric field of strength $\lambda \ll 1$. For such values of λ , the entanglement length R_e has an upper bound as the intensity of an applied off-resonant field increase. We assume that the polarization of the laser pulse is collinear with the static field and the intermolecular axis is perpendicular to the direction of the fields. In Fig. 7.5 it was shown that in the absence of DC fields, a pulse of moderate intensity generates an entangled two-particle state when the molecules are initially in the ground rotational state. If a very weak DC electric field is present, the magnitude of the coupling constants A_{12} and B_{12} are smaller than the energy splitting ϵ_e for any peak intensity Ω_0 (see Fig. 7.11). Consequently, the populations $P_c(t) = |c(t)|^2$ and $P_d(t) = |d(t)|^2$ of the singly excited states $|e_1g_2\rangle$ and $|g_1e_2\rangle$ are negligible after the pulse is over and the evolution of the doubly excited state $P_b(t)$ resembles the result obtained in the absence of static fields. As shown in Fig. 7.12, the entanglement length decreases rapidly with the field strength to a few times the characteristic length R_0 . The couplings A_{12} and B_{12} however increase with the strength of the static field. Significant population of the singly excited state $|e_1g_2\rangle$ and $|g_1e_2\rangle$ can only be achieved for molecules separated by distances on the order R_0 , by using pulses with duration $\tau_p \sim t_{dd} \approx 1 - 10 t_{\text{rot}}$. For intermolecular separations larger than the entanglement length, a laser pulse only weakly perturbs the initial wavefunction $|\Psi(0)\rangle = |g_1g_2\rangle$. The results in Figs. 7.13 and 7.14 illustrate these conclusions.

In Fig. 7.13 a very weak static field with $\lambda = 0.001$ is considered. The upper bound of the entanglement length is $R_e \approx 8 R_0$. The evolution of the two-particle wavefunction $|\Psi(t)\rangle$ is obtained by solving Eq. (7.27) numerically. Panel (a) corresponds to the distance $R = 5 R_0$ for which the interaction time is $t_{dd} = 125 t_{\text{rot}}$. An off-resonant Gaussian pulse with duration $\tau_p = 333 t_{\text{rot}}$ (FWHM) and peak intensity $\Omega_0 = 40$ is applied to the system. After the pulse is over, the doubly excited population P_b resembles the result obtained in the absence of DC fields from Fig. 7.5. For this very weak static field, the occupation of the singly excited states is negligibly small (inset). Panel (b) shows a similar result for a smaller intermolecular distance $R = 2 R_0$ and shorter pulse $\tau_p = 21.3 t_{\text{rot}}$. The ratio between the pulse width τ_p and the interaction time t_{dd} as well as the peak intensity is the same in both cases.

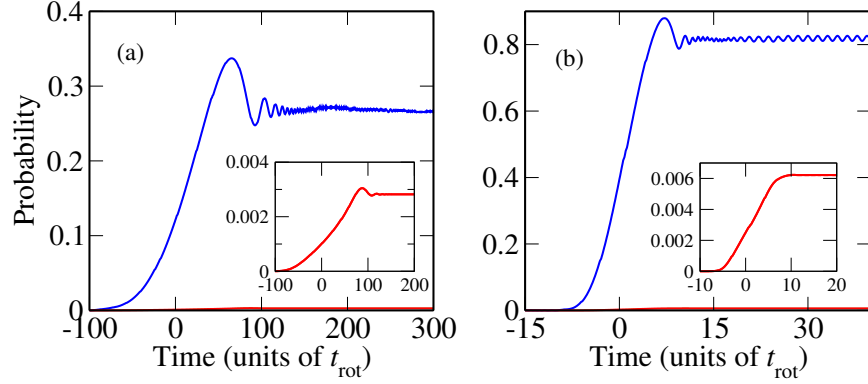


Figure 7.13: Entanglement generation in combined AC and weak DC electric fields. The static field strength parameter is $\lambda = 0.001$. (a) Probability amplitudes for the doubly excited state $|e_1e_2\rangle$ (blue line) and for the singly excited states $|e_1g_2\rangle$ and $|g_1e_2\rangle$ (red line). The pulse width is $\tau_p = 333t_{\text{rot}}$ and the intermolecular distance is $R = 5R_0$. (b) The same as panel (a) for $R = 2R_0$ and $\tau_p = 21.3t_{\text{rot}}$. The pulse has a symmetric Gaussian profile centered at $t = 0$. The peak intensity parameter is $\Omega_0 = 40$ in both panels. The inset shows an expanded view of the singly excited probability.

A relatively stronger DC electric field with $\lambda = 0.1$ is considered in Fig. 7.14. Panel (a) corresponds to the intermolecular distance $R = 1.5 R_0$ and a Gaussian pulse with duration $\tau_p = 9 t_{\text{rot}}$ (FWHM) is applied. The molecules are initially in their ground states. After the pulse is over the population of the singly excited states P_c and P_d are significantly larger than the doubly excited population P_b . This is because the peak intensity $\Omega_0 = 80$ is chosen so that the value of A_{12} and B_{12} are larger than J_{12} during the interaction with the pulse. Panel (b) shows a similar result for $R = 2 R_0$, $\tau = 21.3 t_{\text{rot}}$ and the same peak intensity as in panel (a). The entanglement length in both panels is bounded by $R_e \approx 1.7 R_0$.

Although the results in Figs. 7.5 ($\lambda = 0$) and 7.13 ($\lambda = 0.001$) are similar, there is a fundamental difference regarding the intermolecular distances for which significant entanglement can be achieved. Let us consider alkali-metal dimers for which $R_0 \sim 1 - 10$ nm. In the absence of static fields, the entanglement length R_e can reach hundreds of nanometers using laser pulses with peak intensities $I \sim 10^{10}$

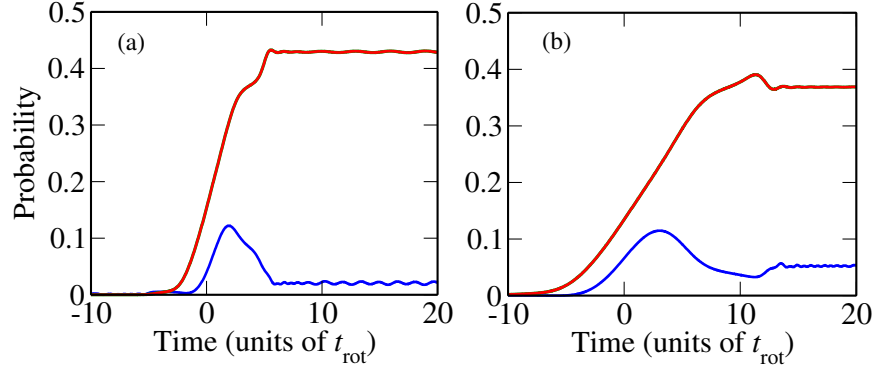


Figure 7.14: Entanglement generation in combined AC and moderate DC electric fields. The static field strength parameter is $\lambda = 0.1$. (a) Probability amplitudes for the doubly excited state $|e_1 e_2\rangle$ (blue line) and for the singly excited states $|e_1 g_2\rangle$ and $|g_1 e_2\rangle$ (red line). The pulse width is $\tau_p = 9t_{\text{rot}}$ and the intermolecular distance is $R = 1.5R_0$. (b) The same as panel (a) for $R = 2R_0$ and $\tau_p = 21.3t_{\text{rot}}$. The pulse has a symmetric Gaussian profile centered at $t = 0$. The peak intensity parameter is $\Omega_0 = 80$ in both panels.

W/cm^2 . In the presence of even a small electric field with $\lambda = 0.001$ ($E_{\text{DC}} \sim 1 \text{ V}/\text{cm}$ for LiCs) the entanglement length cannot be increased beyond a few tens of nanometers by increasing the laser intensity (see Fig. 7.12). This restricts the applicability of the entanglement generation scheme to highly dense molecular samples, for which collisional decoherence can be expected to be much stronger than in dilute samples such as optical lattices.

7.6 Quantification of entanglement using cold molecules

7.6.1 Orientation correlation for entangled molecules

The degree of orientation of a single molecule can be measured by the expectation value $\langle \cos \theta \rangle$. The operator $\hat{O} = \hat{C}_{1,0} = \cos \theta$ couples rotational states of different parity (see Sec. 2.4 for the matrix element). Therefore for a molecule in free space or in the presence of an off-resonant field, the orientation factor $\langle \cos \theta \rangle = 0$. The orientation correlation between two molecules can be defined as

the expectation value $E(t_a, t_b) = \langle \hat{\mathcal{O}}_a(t_a) \otimes \hat{\mathcal{O}}_b(t_b) \rangle$ [139, 140, 155], where $\hat{\mathcal{O}}_i(t_i) = \hat{U}_i^\dagger(t_i) \hat{\mathcal{O}}(0) \hat{U}_i(t_i)$. The free evolution operator $\hat{U}_i(t_i) = \exp[-i\hat{H}_i t_i/\hbar]$ is determined by the rotational Hamiltonian $\hat{H}_i = B_e \mathbf{N}_i^2$.

Let us consider two molecules described by the state

$$|\Psi\rangle = a|g_1 g_2\rangle + b|e_1 e_2\rangle \equiv a|00\rangle + b|11\rangle, \quad (7.28)$$

where we use $|g\rangle \equiv |N=0\rangle$ and $|e\rangle \equiv |N=1\rangle$ (omitting the label $M_N=0$). The density matrix $\rho = |\Psi\rangle\langle\Psi|$ describes the combined state of two qubits. The concurrence $C(\rho)$ of the bipartite state quantifies the degree of entanglement of the combined system [169]. The quantity $C(\rho)$ varies between zero and unity, where these extrema correspond to separable (non-entangled) and maximally-entangled states, respectively. The pairwise concurrence for qubits is defined as $C(\rho) = \max\{0, \sqrt{\lambda_1} - \sqrt{\lambda_2} - \sqrt{\lambda_3} - \sqrt{\lambda_4}\}$, where $(\lambda_1, \lambda_2, \lambda_3, \lambda_4)$ are the eigenvalues (in order of decreasing energy) of the non-hermitian matrix $\rho\tilde{\rho}$, where $\tilde{\rho} = (\hat{\sigma}_y \otimes \hat{\sigma}_y)\rho^*(\hat{\sigma}_y \otimes \hat{\sigma}_y)$. For the pure state $\rho = |\Psi\rangle\langle\Psi|$ given by Eq.(7.28), the concurrence is given by

$$C(\rho) = 2|ab|. \quad (7.29)$$

It should be clear from the results of Section 7.4 (see Fig. 7.7) that by choosing the appropriate laser intensity and pulse duration, it is possible to prepare a molecular pair separated by hundreds of nanometers in a state ρ with an arbitrary value of $0 \leq C(\rho) \leq 1$ using off-resonant optical fields.

Using the state in Eq. (7.28), the two-time orientation correlation function $E(t_a, t_b)$ can be written as

$$E(t_a, t_b) = \frac{1}{3} (2|ab|) \cos(\omega_{10}t_a + \omega_{10}t_b + \theta_{ba}) \quad (7.30)$$

where we have defined $a^*b = |ab|e^{i\theta_{ba}}$ and $\omega_{10} = 2B_e/\hbar$. The correlation function is invariant under particle exchange. If the concurrence of the state $\rho = |\Psi\rangle\langle\Psi|$ vanishes, the orientation correlation function vanishes for all times. The maximum value of the correlator $|E(t_a, t_b)| = \lambda_{\max}^2$ is achieved for maximally-entangled states with $|a| = |b| = 1/\sqrt{2}$. In Eq. (7.30), $\lambda_{\max} = 1/\sqrt{3}$ is the maximum eigen-

value of the single-molecule orientation operator $\hat{O} = \cos \theta$ in the subspace $\mathcal{S} = \{|N=0, M_N=0\rangle, |N=1, M_N=0\rangle\}$.

The correlation function not only depends on the magnitude of the concurrence $C(\rho)$ but on the relative phase θ_{ba} between the basis states $|00\rangle$ and $|11\rangle$. For $\theta_{ba} = 0$ and $\theta_{ba} = \pi$ the maximally-entangled states correspond to the symmetric and antisymmetric Bell states $\frac{1}{\sqrt{2}}(|00\rangle + |11\rangle)$ and $\frac{1}{\sqrt{2}}(|00\rangle - |11\rangle)$ respectively. The associated correlation functions are $E_+(t_a, t_b) = (1/3) \cos(\omega_{10}t_a + \omega_{10}t_b)$ and $E_-(t_a, t_b) = -(1/3) \cos(\omega_{10}t_a + \omega_{10}t_b)$.

7.6.2 Violation of Bell's inequalities in optical lattices

The objection to the completeness of quantum mechanics as a theory of Nature made by Eistein, Podolsky and Rosen (EPR) derives from preconceived notions about locality and reality. The EPR theorem can be stated as follows: *If the predictions of quantum mechanics are correct and if physical reality can be described in a local way, then quantum mechanics is necessarily incomplete, as some “elements of reality” exist in Nature that are ignored by this theory* [235, 236]. In fact, quantum mechanics predicts that when two spins are prepared in an entangled state with space-like separation, and the spin projections are measured independently for each spin, there are correlations between the measurements performed on each particle that are beyond the predictions of classical probability. A complete analysis of this and related topics can be found in Ref. [236]. For illustrative purposes, let us summarize the EPR scheme and its consequences: Two spin-1/2 particles are prepared in the triplet Bell state

$$|\Phi^+\rangle_{AB} = \frac{1}{\sqrt{2}}(|0\rangle_A|0\rangle_B + |1\rangle_A|1\rangle_B).$$

The two particles are separated by a distance large enough so there can be no communication between them. The spin projection $\hat{\sigma}_z$ is measured on particle A by Alice³. If the result of the measurement is +1, then the state of particle B in a distant lab by Bob can be found to be $|0\rangle_B$ when the measurement of $\hat{\sigma}_z$ is performed. If the result of Alice's measurement is -1, this immediately establishes the state

³Alice and Bob are conventional labels for two different observers.

of Bob's particle to be $|1\rangle_B$. This apparent influence between two measurements performed at remote locations challenges the classical notions of locality. These non-local correlations are preserved if Alice chooses to measure $\hat{\sigma}_x$ instead. If the result of her measurement of the x -projection is $+1$, then the state of Bob's particle is found to be $\frac{1}{\sqrt{2}}(|0\rangle_B - |1\rangle_B)$ when the measurement of $\hat{\sigma}_x$ is performed. Alice can therefore establish either of two incompatible properties of Bob's qubit. Since there is no quantum state with well defined values of both $\hat{\sigma}_z$ and $\hat{\sigma}_x$ observables (the operators do not commute), these properties of Bob's qubit could not both have been established at the source in some remote past. This contradicts the notions of reality which state that a system has preexisting properties if they can be predicted with certainty prior to their measurement. The combination of realism and locality is called local realism [169, 236].

Bell's inequality has nothing to do with quantum mechanics, but it is the result of analyzing the measurement correlations in the EPR experiment assuming the conditions of local realism. The derivation of Bell's inequality is presented in Appendix F. The result of a measurement Alice might perform is denoted by A . This result depends on her choice of measuring direction \vec{a} for the spin projection, and also on the statistical and unknown variables λ (hidden-variables) that determine the state of the particle when they are produced at the source. This dependence on λ is imposed by the assumptions of realism. Locality is imposed by writing $A = A(\vec{a}, \lambda)$, i.e., Alice's result A does not depend on Bob's choice of the measurement direction \vec{b} . If Alice and Bob measure their spins along the \vec{a} and \vec{b} directions, the correlation between the results according to classical probability theory can be written as

$$E(\vec{a}, \vec{b}) = \int d\lambda \rho(\lambda) A(\vec{a}, \lambda) B(\vec{b}, \lambda).$$

Bell's theorem states that products of classical correlations between measurements involving two different measurement directions for each particle satisfy the following inequality

$$|E(\vec{a}, \vec{b}) + E(\vec{a}, \vec{b}') + E(\vec{a}', \vec{b}) - E(\vec{a}', \vec{b}')| \leq 2\lambda_{\max}^2. \quad (7.31)$$

This is a general result satisfied under the assumptions of local realism. λ_{\max} is the maximum eigenvalue of the observable being measured in the qubit basis.

We have assumed that each qubit space has the same dimensionality. For spin-1/2 particles the maximum eigenvalue of the spin projection operator $\vec{a} \cdot \vec{\sigma}$ is unity, where the components of $\vec{\sigma}$ are the Pauli matrices. Experimental violations of the Bell's inequality have been established using a pair of entangled photons over distances of several kilometers and also with massive elementary particles created in high-energy collisions [237–242]. Bell's inequality is satisfied by all separable states. Not all entangled bipartite states violate this inequality.

Let us consider two polar molecules prepared in an entangled state $\rho = |\Psi\rangle\langle\Psi|$ given by Eq. (7.28). In Appendix F it is shown that there is an equivalence between the orientations of the measurement apparatuses \vec{a} and \vec{b} in the EPR scheme and the times t_a and t_b corresponding to the free rotational evolution of each molecule. The orientation correlation function $E(t_a, t_b)$ for the state ρ is given in Eq. (7.30). Following the equivalence between spin and rotational states, the magnitude of the quantity

$$S = E(t_a, t_b) + E(t_a, t'_b) + E(t'_a, t_b) - E(t'_a, t'_b). \quad (7.32)$$

can be used to test violations of local realism. In order to establish violations of the Bell's inequality it is sufficient to set $t_a = t_b = 0$ and $t'_a = t'_b = t$ in Eq. (7.32) and evaluate the expectation value of

$$S_1(t) = E(0, 0) + E(0, t) + E(t, 0) - E(t, t). \quad (7.33)$$

using the expression in Eq. (7.30) for $E(t_a, t_b)$. In Fig. 7.15 the magnitude of expectation value $\langle S_1(t) \rangle$ is plotted as a function of time for several parent states ρ with different concurrences $C(\rho)$ and relative phase θ_{ba} . Time is shown in units of the rotational period $T_R = \pi\hbar/B_e$. Each panel in Fig. 7.15 corresponds to an entangled state $|\Psi\rangle = |a||00\rangle + |b|e^{i\theta_{ba}}|11\rangle$ with a given relative phase θ_{ba} . The upper bound imposed by local realism over the magnitude of quantity of $\langle S_1(t) \rangle$ is $2\lambda_{\max}^2 = 2/3$. For the states shown in Fig. 7.15, this limit is violated over a wide range of times within a rotational period. The figure also shows that the amount by which the local realism threshold is violated depends on the value of the concurrence $C(\rho)$ of the entangled state. Panel (a) shows, for example, that only states whose concurrence is larger than 0.8 can be used to measure violations of Bell's inequality. Maximally-entangled states with $C(\rho) = 1$ exceed the local

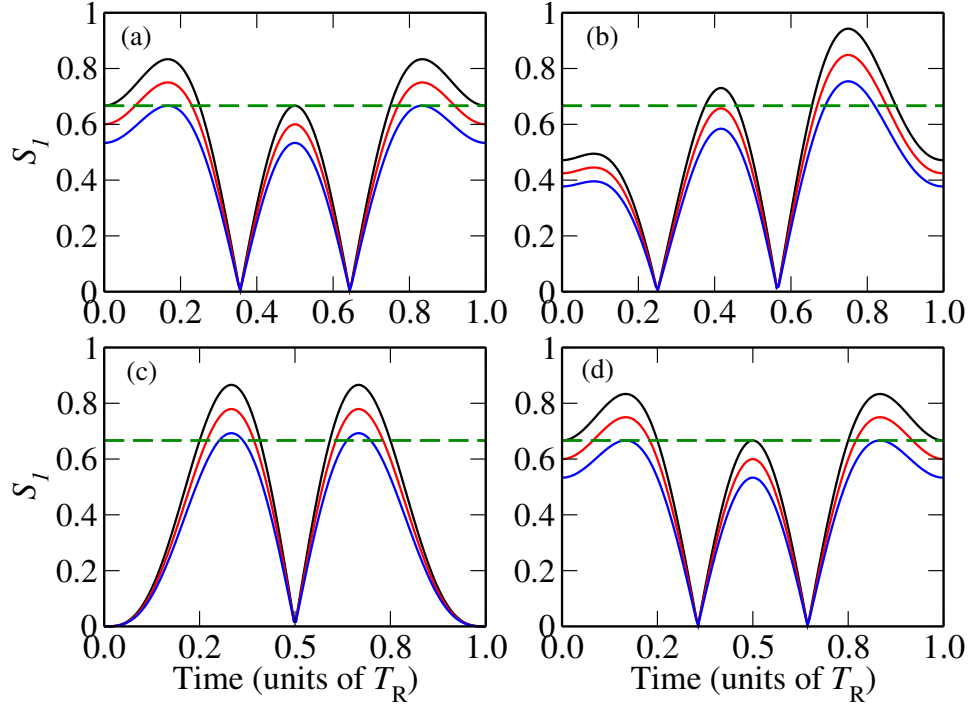


Figure 7.15: Violation of Bell's inequality for molecular orientation correlations. The absolute value of $S_I(t) = E(0,0) + E(0,t) + E(t,0) - E(t,t)$ is plotted as a function of time for several bipartite states $|\Psi\rangle = |a\rangle|00\rangle + |b|e^{i\theta_{ba}}|11\rangle$. Each panel shows $|S_I|$ for three values of the concurrence: $C = 1.0$ (black line), $C = 0.9$ (red line), and $C = 0.8$ (blue line). Different panels correspond to a different value of the relative phase θ_{ba} : (a) $\theta_{ba} = 0$; (b) $\theta_{ba} = \pi/4$; (c) $\theta_{ba} = \pi/2$; (d) $\theta_{ba} = \pi$. $E(t,t')$ is the two-time orientation correlation. Time in is units of the rotational period $T_R = \pi\hbar/B_e$.

realism bound by the largest amount. In panel (b) the state with relative phase $\theta_{ba} = \pi/4$ exceeds the local realism threshold by approximately 41% at $t = (3/4)T_R$. This is the maximum violation achievable in a bipartite state of two-dimensional qubits, and is known as the Cirel'son bound [243]

The results in Fig. 7.15 show that it is possible to use polar molecules in optical traps to test theories of quantum mechanics that include local realism as a requirement. It is beyond the scope of this chapter to analyze in detail the exper-

imental requirements necessary to perform Bell-type tests with trapped molecules that are free of so-called logical “loopholes” [236]. Nevertheless, one can comment on the most evident advantages between an experimental setup that uses trapped molecules and other schemes that use photons or elementary particles.

Entangled photon pairs have the advantage of being easy to produce using non-linear crystals and propagate over long distances, but single photons are difficult to detect [236]. Kaons are massive mesons produced in particle accelerators. Pairs of entangled Kaons can be detected indirectly by measuring their decay products. Although Kaons are easier to detect than photons, they undergo an intrinsic decay process that limits their detection efficiency [241]. Molecules in optical traps can be detected with high efficiency using spectroscopic methods or by photo-ionization. The orientation of molecules can be detected with near unit efficiency using ultrashort laser pulses that dissociate the molecule [149]. In summary, entangled molecular pairs can therefore be easily detected using standard techniques, the decay of rotational states is negligible, and the dephasing of the entangled state in the optical traps can be minimized.

In order to test the non-locality of quantum mechanics, it is necessary that the entangled particles are space-like separated, so that no communication can occur between them. Otherwise the experiments cannot rule out theories in which the information about the experimental setting chosen (possibly at random) by Alice is transmitted to the other particle’s location, affecting the outcome of Bob’s measurement. This is known as the “communication loophole”. Experiments with entangled photons have demonstrated non-locality over distances of several kilometers [239]. For Bell-type test with polar molecules in optical traps, measurement of the orientation using ultrashort pulses can be performed in a timescale of hundreds of femtoseconds [231], which is shorter than the rotational period $T_R \sim 1$ ps of most diatomic molecules. In the scheme described in this section, measurement of the orientation of two distant molecules is performed at different times. The Bell inequality in Eq. (7.33) involves the two-time correlation function $E(t, 0) = E(0, t)$. The time origin can be set by the measurement of the orientation of one molecule, while the measurement of the orientation of the other molecule is delayed by a time t . In order to rule out possible communication between the molecules prior to the second measurement, the separation R between the entangled molecules should be

larger than $cT_R \approx 300 \mu\text{m}$, where c is the speed of light. Such distances are possible to achieve using optical lattices, or by trapping individual molecules in two separated dipole traps. Even in experiments where the intermolecular distance R is only a few hundred nanometers, the violation of Bell's inequality can be used to demonstrate entanglement between molecules and also, as Fig. 7.15 shows, to measure the concurrence $C(\rho)$ of the bipartite state created by off-resonant pulses.

7.6.3 Tripartite and many-particle entanglement

The method described in this chapter to create bipartite entanglement can be naturally extended to systems with a larger number of molecules. Let us consider a system of three polar molecules fixed in space by an optical trap. For illustrative purposes we assume the geometry of the arrangement to be either linear or triangular. The Hamiltonian for a tripartite system of molecules can be written as

$$\hat{H} = \hat{H}_1 + \hat{H}_2 + \hat{H}_3 + \hat{V}_{12} + \hat{V}_{13} + \hat{V}_{23}, \quad (7.34)$$

where $\hat{H}_i = \hat{H}_R + \hat{H}_{AC}$ is the sum of the rotational Hamiltonian and the light-matter interaction operator. \hat{V}_{ij} is the dipole-dipole interaction operator. It was shown in Section 7.4 that for molecules initially in the rotational ground state the combined effect of a strong off-resonant optical field and the dipole-dipole interaction does not lead to transitions outside the rotational manifold $\mathcal{S} = \{|g\rangle, |e\rangle\}$, where $|g\rangle$ and $|e\rangle$ correspond to opposite parity states of the lowest field-dressed tunneling doublet and to the bare rotational states $|N=0, M_N=0\rangle$ and $|N=1, M_N=1\rangle$ in the absence of fields. The eight-dimensional tripartite basis set contains the ground state subspace $\mathcal{S}_0 = \{|ggg\rangle\}$, a singly-excited subspace $\mathcal{S}_1 = \{|gge\rangle, |geg\rangle, |egg\rangle\}$, a doubly-excited subspace $\mathcal{S}_2 = \{|gee\rangle, |ege\rangle, |eeg\rangle\}$, and the triply-excited subspace $\mathcal{S}_3 = \{|eee\rangle\}$. In the absence of DC electric fields or near resonant mi-

crowave fields, the Hamiltonian in Eq. (7.34) can be written in matrix form as

$$\hat{H} = \left(\begin{array}{cccc|cccc} 0 & J_{12} & J_{13} & J_{23} & 0 & 0 & 0 & 0 \\ J_{12} & 2\varepsilon_e & 0 & 0 & 0 & 0 & 0 & 0 \\ J_{13} & 0 & 2\varepsilon_e & 0 & 0 & 0 & 0 & 0 \\ J_{23} & 0 & 0 & 2\varepsilon_e & 0 & 0 & 0 & 0 \\ \hline 0 & 0 & 0 & 0 & \varepsilon_e & 0 & 0 & J_{12} \\ 0 & 0 & 0 & 0 & 0 & \varepsilon_e & 0 & J_{13} \\ 0 & 0 & 0 & 0 & 0 & 0 & \varepsilon_e & J_{23} \\ 0 & 0 & 0 & 0 & J_{12} & J_{13} & J_{23} & 3\varepsilon_e \end{array} \right), \quad (7.35)$$

where the upper block involves the subspaces \mathcal{S}_0 and \mathcal{S}_2 , and the lower block involves \mathcal{S}_1 and \mathcal{S}_3 . The two sub-blocks are uncoupled in the absence of parity breaking interactions. If the molecules are initially in their rotational ground state, i.e., $|\Psi(0)\rangle = |ggg\rangle$, then using the method described in this chapter, it is possible to create an entangled tripartite state of the form

$$|\Psi(t)\rangle = a(t)|ggg\rangle + b(t)|eeg\rangle + c(t)|ege\rangle + d(t)|gee\rangle, \quad (7.36)$$

after exposing the molecules to a single off-resonant optical pulse. The magnitudes and phases of the superposition coefficients in Eq. (7.36) can be manipulated by tuning the peak intensity and duration of the pulse.

The degree of tripartite entanglement not only depends on the details of the laser pulse but also on the geometry of the molecular arrangement. In Section 7.4 it was shown that the pulse duration can be chosen such that only pairs of molecules separated by a given distance can be entangled (see Figs. 7.6 and 7.8). Molecular pairs whose distance is smaller or larger than the target separation would not be affected by the pulse and remain in their initial state. For example, Fig. 7.8 shows the effect of varying the pulse width τ_p in the amount of entanglement ($|b|^2$ maps the bipartite concurrence $C(\rho) = 2|ab|$ for two molecules separated by a distance $R = 100 R_0$, where R_0 is the characteristic length defined in Eq. (7.17). The figure shows that the molecules remain in their ground states for a pulse duration either half or twice the dipole-dipole interaction time t_{dd} at the distance $R = 100 R_0$. These

correspond to relative distance variations $\Delta R/R \approx 20\%$ and $\Delta R \approx 25\%$ from below and above the target distance, respectively.

Instead of considering a triangular geometry where each molecular pair has the same separation distance, as it is implied in Eq. (7.34), one can consider a linear array of molecules with the equal nearest-neighbour separation $R_{12} = R_{23}$. If the duration of the laser pulse is chosen to match the interaction time at the distance R_{12} then qubits 1 and 3 are not entangled with each other, even when the coupling V_{13} is not zero. In this case, the tripartite state after the pulse is over is given by Eq. (7.36) with $c(t) = 0$.

Additional possibilities can be explored by coupling the sub-spaces $\mathcal{S}_0 \oplus \mathcal{S}_2$ and $\mathcal{S}_1 \oplus \mathcal{S}_3$. This coupling can be achieved by applying a DC electric field, which breaks the parity of the rotational states. However, as discussed in Section 7.5 the entanglement length R_e (see Eq. (7.19)) is severely reduced due to the linear Stark shift of the states $|g\rangle$ and $|e\rangle$. Even for molecules whose separation distance R is on the order of the characteristic length R_0 , the couplings between states in different sub-blocks are not selective. This is shown for the bipartite case in Eq. (7.24). It would be desirable for applications to prepare tripartite entangled states given by arbitrary superpositions of the complete basis spanning the tripartite Hilbert space. This could be achieved with polar molecules using combined off-resonant laser pulses and near resonant microwave pulses. For example, let us consider a two-step scheme to prepare a tripartite system in a Werner state [169]

$$|W\rangle = \alpha|gge\rangle + \beta|geg\rangle + \gamma|egg\rangle. \quad (7.37)$$

The system consists of three polar molecules in a triangular arrangement. Each molecule is initially in the ground rovibrational state, i.e., $|\Psi(0)\rangle = |ggg\rangle$. Assuming the molecules can be addressed individually, a near resonant microwave π -pulse is applied to each molecule to completely transfer the population to the triply excited state $|eee\rangle$. A single off-resonant laser pulse can then be applied to create the desired Werner state by coupling the \mathcal{S}_3 and \mathcal{S}_1 subspaces via the dipole-dipole interaction. The intensity and duration of the pulse can be chosen such that the remaining population in the triply-excited state is negligibly small.

Single molecule resolution can be implemented in practice using gradients of external fields to shift the rotational levels differently at different positions.

The idea of using combined microwave and laser pulses to prepare an arbitrary entangled state is not limited by the geometry and size of the molecular arrangement. The schemes for generation of tripartite and many-particle entanglement described in this section should find direct application in optical lattices of polar molecules, which can be useful in the development of quantum computation with cold molecules.

Chapter 8

Conclusion

8.1 Overall conclusions of the dissertation

The field of trapped cold molecules has advanced significantly in the last years after the preparation of dense ensembles of ultracold molecules in the rovibrational ground state by several groups [15–21]. Current experimental effort in the field aims toward the observation of novel quantum phenomena that would be difficult to achieve using ultracold atoms. The internal structure of simple diatomic molecules is more complex than the structure of atoms. The consequences of this are twofold. On one hand, direct laser cooling of a molecular sample is prohibitively difficult because a molecule in an electronic excited state can decay radiatively to several rovibrational states in the ground electronic level, which makes laser cooling inefficient. On the other hand, the rich internal structure of molecules allows for stronger interactions with static and dynamic electric and magnetic fields. This provides the basic mechanism for external field control of molecular processes. The additional controllability that cold molecules offer is the driving force of many research efforts in this field, including this dissertation.

The research presented in this thesis offers new possibilities for studying binary and many-particle quantum phenomena with a high degree of controllability. The results obtained are timely as they integrate with current experimental research in the field, in particular with recent advances such as the preparation of an insulator phase of cold polar molecules in optical lattices [219]. Some of the proposed sys-

tems in this thesis rely on the ability to trap individual molecules in optical microtraps. The recent experimental success in this direction significantly enhances the relevance of the theoretical proposals in this thesis. The quantum control schemes proposed here are simple enough to be relevant for experimental work, but the underlying physics is rich enough to also promote further theoretical exploration. The scientific questions that can be addressed using the results in this dissertation are important in the field of cold molecules, and also in other areas of modern science.

8.2 Contributions of the dissertation

In Chapter 1 the specific goals of this dissertation were categorized under three general topics: cold collisions and controlled chemistry, quantum entanglement and quantum information, and tunable condensed-matter phenomena. The scientific goals pursued in each of these directions are ambitious since their achievement would constitute an important advancement not only in the field of cold molecules, but would also stimulate progress in other areas of physical chemistry and physics.

8.2.1 Cold collisions and controlled chemistry

In Chapter 4 a general scheme is proposed to achieve coherent control of collisions between non-identical particles at ultracold temperatures. Coherent control of molecular dynamics has been successfully demonstrated for a number of unimolecular processes, but schemes for coherent control of bimolecular processes has proven difficult to achieve. The method proposed here uses a static field to induce quantum interference between two collision channels, so that the outcome of a single collision event can be controlled by tuning the interference pattern with laser fields. The scheme was successfully illustrated numerically for non-reactive atomic scattering at ultracold temperatures. The branching ratio between elastic and inelastic scattering of alkali-metal atoms can be increased by tuning the control parameters. Although the degree of controllability of the elastic-to-inelastic ratio does not exceed that achievable with other methods, the results obtained here constitute an important first step towards the demonstration of coherent control of molecular reactive scattering in ultracold gases. This contribution has been recently discussed in Ref. [244] and may stimulate further research efforts towards

understanding the role of quantum coherence in chemical reactivity, which is an important open question in physical chemistry.

The main strength of the coherent control scheme proposed in this thesis is its generality. The same mechanism can be used to control atomic and molecular scattering, reactive and non-reactive. However, control is demonstrated here for a single collision process. Subsequent collisions in an ensemble of particles may quickly destroy the interference between collisions channels upon which the control scenario is based. On the other hand, if the collisional noise is small enough it may be used to relax the narrow energy degeneracy conditions necessary to achieve interference of scattering states, thus assisting coherent control. The results presented in this dissertation are still applicable in situations where the effects of subsequent collisions can be ignored, such as the scattering of atoms and molecules in supersonic beams. However, general conclusions about possible applications of the control scheme proposed here cannot be made until the effects of collisional decoherence in ultracold gases are taken into account.

8.2.2 Tunable condensed-matter phenomena

In Chapters 5 and 6 it is demonstrated that an ensemble of polar molecules trapped in an optical lattice can be used to study excitonic and polaronic phenomena with a high degree of controllability. For an array of interacting molecules in the electronic and rovibrational ground state, the lowest energy excited state corresponds to a single rotational exciton. Excitons are collective states that determine the response of the system to electromagnetic fields and the energy transport processes in the array. Exciton-related phenomena are ubiquitous in semiconductors, insulators, and biological systems at room temperature. In many cases it is possible to design the excitonic properties of a material using microfabrication techniques, but there are intrinsic phenomena such as the energy transport efficiency that are difficult to control microscopically. The intrinsic decay of electronic excitons is an additional obstacle to the microscopic control of exciton dynamics. The interaction of excitons with ever-present impurities and phonons determine the energy transport properties of the system and also the linear and nonlinear interactions with light.

Chapter 5 shows that excitonic phenomena in an array of interacting ultracold molecules can be tuned using static electric and magnetic fields. Control is possible due to the electric field dependence of the dipole-dipole interaction between molecules (see Chapter 3). Using current technology it is possible to engineer not only the geometry and chemical composition of the array, but also the properties of individual molecules. This offers a degree of controllability that is not possible in condensed-matter systems. The exciton-impurity interaction in a two-species optical lattice can be tuned using a static electric field. It is well-known that the multiple scattering of particles or quasi-particles by impurities leads to localization in one dimension. Here it is shown that an initially localized state in a one-dimensional array can be delocalized by choosing the electric field strength such that the effects of diagonal and non-diagonal disorder compensate each other. Moreover, the method works for any local state in the exciton spectrum. The possibility of tuning the exciton-impurity and exciton-exciton interaction dynamically may offer insight into the nature of Anderson localization that would be difficult to obtain with other systems.

Chapter 6 demonstrates that an optical lattice with polar molecules supports phonons that interact with rotational excitons in a controlled way. The exciton-phonon interaction is a prototype example of a particle interacting with a bosonic environment. This type of interaction is of fundamental importance in the description of condensed matter and open quantum systems in general. Therefore, providing insight into the nature of phonons in molecular optical lattices is a significant contribution to the understanding of ultracold molecular arrays. In classical terms, optical lattice phonons correspond to small displacement of the molecules from their equilibrium positions under the combined effect of the optical trapping forces and the dipole-dipole interaction between molecules. The phonon spectrum is gapped and its bandwidth depends on the strength of an applied electric field. The molecular array is stable for a wide range of electric fields and trapping frequencies. It is shown that lattice instabilities can occur when the dipole-dipole interaction energy is comparable with the optical trap depth, either for repulsive or attractive interactions. The interaction of rotational excitons with lattice phonons can be tuned independently by changing the trapping laser intensity and the static electric field. A large molecular array can be described by a generalized polaron

Hamiltonian with tunable parameters. Smaller arrays or individual molecules can be described by a spin-boson model. In the limit of large electric fields, the dominant effect of phonons is the fluctuation of the molecular site energies. In this limit the array can be described by a Holstein polaron model, widely used in condensed matter theory to describe electron and energy transport in solids, molecular aggregates and biological complexes. In the limit of weak electric fields, the system can be described by the Su-Schrieffer-Heeger (SSH) polaron model, which is used to describe particle and energy transport in polymers with phonon-modulated hopping. In most materials the effect of phonon-modulated hopping is assumed to be smaller than the diagonal particle-phonon interaction at each site, and is usually neglected. It has been recently shown however, that polaron properties are dramatically different in the strong coupling regime of the SSH model. In Holstein-type polaron models, particle and energy transport is exponentially suppressed in the strong coupling regime. On the contrary, phonon-modulated hopping facilitates transport even in the strong coupling regime of the SSH model. This behaviour has yet to be observed experimentally. Arrays of cold polar molecules in optical lattices may therefore provide a unique playground to study a wide range of polaron phenomena with a high degree of tunability.

The work on rotational exciton and polaron phenomena presented in this thesis is applicable to a wide range of problem involving cold molecular arrays. Exciton and polaron effects described here can be easily observed in current experiments with polar molecules in optical lattices. Two-species optical lattices may be produced in the near future. The system studied here contains many of the basic ingredients necessary for important processes in condensed-matter to occur such as exciton-polariton condensation and size-enhanced nonlinear response to the electromagnetic field for technological applications. Moreover, since rotational excitons can be mapped into spin-waves, an ensemble of excitons in a molecular array can be used to simulate quantum magnetism. The multiplicity of possible applications of this contribution and the general importance of these is one of the main strengths of this work.

8.2.3 Quantum entanglement and quantum information

Chapter 7 describes a method to generate entanglement between polar molecules using a single off-resonant optical pulse. The molecules are initially in their rovibrational ground state and entanglement arises from a dipole exchange process while the pulse is present. The exchange process occurs in the absence of static electric fields and the molecules remain entangled long after the pulse is over. The intermolecular distance at which molecules become entangled and the amount of entanglement created (as measured by pairwise concurrence) is determined by the pulse duration and intensity. Intermolecular distances of up to several hundred nanometers are considered, that are relevant for molecules trapped in optical lattices. The method presented here can be used to produce maximally entangled bipartite and many-particle states in a deterministic way. Quantum entanglement is an important resource in quantum computation and quantum communication protocols. The research in this dissertation therefore provides the physical basis for novel implementations of quantum information processing with cold molecules.

The entanglement generation scheme presented in this dissertation imposes very few conditions for an experimental realization. This is one of the main strengths of this contribution. Intense nanosecond mid-infrared pulses are routinely used in molecular alignment experiments and individual molecules have been successfully trapped in optical lattices. Unlike other proposals to generate entanglement in molecular arrays, the scheme proposed here can thus be easily realized with current technology. However, the effects of decoherence need to be taken into account for better comparison with experimental conditions. Although the coherence time in optical lattices exceeds seconds and it is limited by radiative processes, the effect of the tensor light-shift and the motion of the molecule in the trapping potential might lead to dephasing of the prepared entangled state on microsecond timescales. These effects are not considered here and are subject of future work.

8.3 Future research directions

8.3.1 Nonlinear quantum optics in the microwave domain

Designing novel materials with large nonlinear susceptibilities to electromagnetic fields is an important technological challenge. Materials with fast nonlinear response to off-resonant optical fields are used in optical communication and computing [245, 246]. Crystalline solids, polymers and molecular aggregates are widely used nonlinear materials in the optical domain [245]. The molecular properties of these materials can be engineered to enhance their second-order and third-order susceptibilities. Materials with giant susceptibilities are needed in order to study nonlinear optics in the quantum regime for applications in quantum computation and communication [247].

Progress in laser cooling and trapping of atoms has stimulated the study of photon-photon interactions at the single-photon level [94, 248], using atomic ensembles as a medium with enhanced nonlinearities in the optical domain [249–251]. Recent breakthroughs in circuit quantum electrodynamics using superconducting qubits [252, 253] have made possible the study of nonlinear quantum optics in the microwave domain [254, 255]. Ultracold atomic ensembles and superconducting qubits can have large third-order susceptibilities $\chi^{(3)}$, but second-order nonlinear processes are suppressed due to the centrosymmetric nature of these systems. Nonlinear materials with finite $\chi^{(2)}$ optical susceptibility are commonly used for technological applications [245–247], but materials with large second-order nonlinearities in the microwave domain are less common [256]. It is then desirable to design a tunable system with a large $\chi^{(2)}$ microwave susceptibility. This system could be used to produce and manipulate the quantum states of microwave fields. In particular, a tunable second-order nonlinear material could be used to generate entangled pairs of microwave photons on demand via parametric down-conversion processes [247].

Arrays of cold polar molecules in the presence of a DC electric field can be used as a nonlinear medium for microwave fields. Polar molecules trapped on optical lattices are described in Chapters 5 and 6. Dipolar molecular crystals in static electric fields are non-centrosymmetric and highly anisotropic due to the long-range

dipole-dipole interaction between the molecular units. The second-order nonlinearity of the proposed system can be exploited to study nonlinear quantum optical processes in the microwave domain that are not allowed by symmetry in systems such as superconducting qubits in stripline cavity resonators [254] or semiconductor quantum dots [256]. Applications of this system range from precision measurements to quantum teleportation and quantum communication protocols.

8.3.2 Quantum computation with cold homonuclear molecules

An ensemble of polar molecules in an optical lattice has become an attractive candidate for the implementation of scalable quantum computation [117]. Polar molecules have a number of properties that are advantageous in comparison with other implementations based on trapped particles. Long-lived rotational qubit states and long-range dipole-dipole logic gates are the main features that distinguish molecular arrays from neutral atoms and ions [120–124]. Proposed schemes for quantum computation with trapped molecules exploit the dipole moment induced by a static electric field in analogy with the magnetic dipole moment in NMR quantum computing [126, 131–133]. These theoretical proposals offer significant advantages over more established architectures such as trapped-ion quantum computing, but they also suffer from limitations that make their experimental realization difficult. In particular, single-qubit addressability is achieved by introducing electric field gradients on top of the polarizing static fields, due to the sub-micrometer distances considered between molecules. At larger distances the dipolar interactions between molecules are too weak to be of practical use. Quantum entanglement is an important resource in quantum information processing. For current proposals using arrays of polar molecules it has been shown that the degree of bipartite entanglement is small [141]. It is desirable to design an array of molecular qubits in an optical lattice where an arbitrary amount of entanglement between molecular pairs can be created, with molecules separated by tens of micrometers to allow spectroscopic resolution of single qubits, in the absence of DC electric fields. This system could be used as a scalable and robust quantum computer architecture.

An ensemble of homonuclear molecules trapped on an optical lattice can be used for quantum information processing. Entanglement between molecules can

be induced by strong off-resonant laser pulses. The mechanism of dynamical entanglement generation with long optical pulses is described in Chapter 7 for polar molecules. The dipole-dipole interaction between molecules is responsible for the entanglement of molecules while the pulse is on. For homonuclear molecules, there is no direct dipole-dipole interaction. However, a polarizable molecule acquires a dipole moment in the presence of a strong off-resonant field. Homonuclear molecules can interact via their induced dipoles while the field is present. These induced interactions can lead to entanglement in the rotational degrees of freedom due to laser-assisted resonance energy transfer (LARET) [257]. This process is well-known for electronic degrees of freedom in atoms and molecules, but has not been exploited for rotational degrees of freedom of molecules in their ground electronic state. Moreover, preliminary results show that for molecules separated by tens of micrometers, entanglement can be built in a step-wise manner by applying a sequence of long off-resonant optical pulses. The mechanism for this is analogous to piece-wise adiabatic passage [258, 259]. Large intermolecular separation facilitates single-qubit manipulations. In summary, extending the ideas presented in this thesis to arrays of nonpolar diatomic and polyatomic molecules may lead to novel quantum computing architectures that are competitive with established implementations such as trapped ions or NMR-based systems.

8.3.3 Coherent control of ultracold molecular reactions

Control of molecular reactivity using laser fields is a long sought after goal in physical chemistry [171, 260]. In a simplified form, the effect of the laser consists in activating a certain reactive channel by preparing at least one of the reactants in a particularly reactive quantum state. The desired outcome of a reaction can thus be controlled by choosing the laser fields appropriately. In thermal samples, the coherence created by lasers can be quickly destroyed by internal energy conversion processes or collisions. Proposed schemes for coherent control of collisions rely on the preparation of fragile superposition states in which the internal and external degrees of freedom are correlated [244]. The preparation of such superpositions leads to quantum interference between reaction channels, that may be difficult to achieve in thermal gases. At ultracold temperatures, the randomizing effect of col-

lisions can be minimized. Therefore, in this temperature regime where the wave nature of molecular motion is predominant, coherent control schemes based on path-interference may provide an interesting tool to control chemical reactivity. Ultracold molecular gases in specific internal states can be easily produced using current technology. It is therefore desirable to have a scheme to control ultracold molecular reactions using pathway interference induced by electromagnetic pulsed. This may provide insight into the role of internal state coherence in chemical reactivity.

Recent experimental results show that quantum effects, such as nuclear spin symmetry, can be used to dramatically alter collision cross sections in ultracold reactions, such as $K_2 + Rb_2 \rightarrow 2KRb$, as well as $KRb + K \rightarrow K_2 + Rb$ and $KRb + Rb \rightarrow K + Rb_2$ [43, 158]. These experimental studies have generated important theoretical questions regarding quantum effects in such reactions and the ability of quantum control techniques to eliminate unwanted events. In particular, the coherent control scheme developed in this dissertation may provide an easily realizable method to control the chemical reactivity in ultracold gases. Modifications to kinetic theory necessary to relate the dynamical scattering calculations with experimental observables may be needed to account for the field-induced scattering interferences.

Bibliography

- [1] Weinstein Jonathan D., deCarvalho Robert, Guillet Thierry, Friedrich Bretislav, and Doyle John M. Magnetic trapping of calcium monohydride molecules at millikelvin temperatures. *Nature*, 395(6698):148–150, Sep 1998. 10.1038/25949.
- [2] Bethlem Hendrick L., Berden Giel, and Meijer Gerard. Decelerating neutral dipolar molecules. *Phys. Rev. Lett.*, 83(8):1558–1561, Aug 1999.
- [3] Bethlem Hendrick L., Berden Giel, Crompvoets Floris M. H., Jongma Rienk T., van Roij Andre J. A., and Meijer Gerard. Electrostatic trapping of ammonia molecules. *Nature*, 406(6795):491–494, Aug 2000. 10.1038/35020030.
- [4] Crompvoets Floris M.H., Bethlem Hendrick L., Jongma Rienk T., and Meijer Gerard. A prototype storage ring for neutral molecules. *Nature*, 411(6834):174–176, May 2001. 10.1038/35075537.
- [5] Bochinski J. R., Hudson Eric R., Lewandowski H. J., Meijer Gerard, and Ye Jun. Phase space manipulation of cold free radical oh molecules. *Phys. Rev. Lett.*, 91(24):243001, Dec 2003.
- [6] Junglen T., Rieger T., Rangwala S. A., Pinkse P. W. H., and Rempe G. Two-dimensional trapping of dipolar molecules in time-varying electric fields. *Phys. Rev. Lett.*, 92(22):223001, Jun 2004.
- [7] Wang D., Qi J., Stone M. F., Nikolayeva O., Wang H., Hattaway B., Gensemer S. D., Gould P. L., Eyler E. E., and Stwalley W. C. Photoassociative production and trapping of ultracold krb molecules. *Phys. Rev. Lett.*, 93(24):243005, Dec 2004.
- [8] Hudson Eric R., Bochinski J. R., Lewandowski H. J., Sawyer Brian C., and Ye Jun. Efficient stark deceleration of cold polar molecules. *The European*

Physical Journal D - Atomic, Molecular, Optical and Plasma Physics,
31(2):351–358.

- [9] Rieger T., Junglen T., Rangwala S. A., Pinkse P. W. H., and Rempe G. Continuous loading of an electrostatic trap for polar molecules. *Phys. Rev. Lett.*, 95(17):173002, Oct 2005.
- [10] S D Kraft and P Staunum and J Lange and L Vogel and R Wester and M Weidemüller. Formation of ultracold lics molecules. *Journal of Physics B: Atomic, Molecular and Optical Physics*, 39(19):S993, 2006.
- [11] van de Meerakker Sebastiaan Y. T., Bethlem Hendrick L., and Meijer Gerard. Taming molecular beams. *Nat Phys*, 4(8):595–602, Aug 2008. 10.1038/nphys1031.
- [12] Regal Cindy A., Ticknor Christopher, Bohn John L., and Jin Deborah S. Creation of ultracold molecules from a fermi gas of atoms. *Nature*, 424(6944):47–50, Jul 2003. 10.1038/nature01738.
- [13] Sage Jeremy M., Sainis Sunil, Bergeman Thomas, and DeMille David. Optical production of ultracold polar molecules. *Phys. Rev. Lett.*, 94(20):203001, May 2005.
- [14] Volz T., Syassen N., Bauer D. M., Hansis E., Durr S., and Rempe G. Preparation of a quantum state with one molecule at each site of an optical lattice. *Nat Phys*, 2(10):692–695, Oct 2006. 10.1038/nphys415.
- [15] J. Deiglmayr, A. Grochola, M. Repp, K. Mortlbauer, C. Gluck, J. Lange, O. Dulieu, R. Wester, and M. Weidemuller. Formation of ultracold polar molecules in the rovibrational ground state. *Phys. Rev. Lett.*, 101(13):133004–4, 09 2008.
- [16] Knoop S., Mark M., Ferlaine F., Danzl J. G., Kraemer T., Nägerl H.-C., and Grimm R. Metastable feshbach molecules in high rotational states. *Phys. Rev. Lett.*, 100(8):083002, Feb 2008.
- [17] Nemitz N., Baumer F., Münchow F., Tassy S., and Görlitz A. Production of heteronuclear molecules in an electronically excited state by photoassociation in a mixture of ultracold yb and rb. *Phys. Rev. A*, 79(6):061403, Jun 2009.
- [18] K. K. Ni, S. Ospelkaus, M. H. G. de Miranda, A. Pe’er, B. Neyenhuis, J. J. Zirbel, S. Kotochigova, P. S. Julienne, D. S. Jin, and J. Ye. A high

phase-space-density gas of polar molecules. *Science*, 322(5899):231–235, 10 2008.

- [19] Danzl Johann G., Haller Elmar, Gustavsson Mattias, Mark Manfred J., Hart Russell, Bouloufa Nadia, Dulieu Olivier, Ritsch Helmut, and Nägerl Hanns-Christoph. Quantum gas of deeply bound ground state molecules. *Science*, 321(5892):1062–1066, Aug 2008. 10.1126/science.1159909.
- [20] Johann G. Danzl *et al.* Deeply bound ultracold molecules in an optical lattice. *New J. Phys.*, 11(5):055036, 2009.
- [21] F. Lang *et al.* Ultracold triplet molecules in the rovibrational ground state. *Phys. Rev. Lett.*, 101(13):133005, 09 2008.
- [22] J. Doyle, B. Friedrich, R. V. Krems, and F. Masnou-Seeuws. Quo vadis, cold molecules? *Eur. Phys. J. D*, 32:149, 2004.
- [23] R. V. Krems. Molecules near absolute zero and external field control of atomic and molecular dynamics. *Int. Rev. Phys. Chem.*, 24:99, 2005.
- [24] Roman V. Krems. Cold controlled chemistry. *Phys. Chem. Chem. Phys.*, 10:4079, 2008.
- [25] Lincoln D. Carr, David DeMille, Roman V. Krems, and Jun Ye. Cold and ultracold molecules: science, technology and applications. *New J. Phys.*, 11(5):055049, 2009.
- [26] Ticknor Christopher. Energy dependence of scattering ground-state polar molecules. *Phys. Rev. A*, 76(5):052703, Nov 2007.
- [27] Ticknor Christopher. Collisional control of ground state polar molecules and universal dipolar scattering. *Phys. Rev. Lett.*, 100(13):133202, Apr 2008.
- [28] J L Bohn and M Cavagnero and C Ticknor. Quasi-universal dipolar scattering in cold and ultracold gases. *New Journal of Physics*, 11(5):055039, 2009.
- [29] Michael Cavagnero and Catherine Newell. Inelastic semiclassical collisions in cold dipolar gases. *New Journal of Physics*, 11(5):055040, 2009.
- [30] Volpi Alessandro and Bohn John L. Magnetic-field effects in ultracold molecular collisions. *Phys. Rev. A*, 65(5):052712, May 2002.

- [31] R. V. Krems and A. Dalgarno. Quantum-mechanical theory of atom-molecule and molecular collisions in a magnetic field: Spin depolarization. *The Journal of Chemical Physics*, 120(5):2296–2307, 2004.
- [32] Tscherbul T. V. and Krems R. V. Controlling electronic spin relaxation of cold molecules with electric fields. *Phys. Rev. Lett.*, 97(8):083201, Aug 2006.
- [33] T. V. Tscherbul and R. V. Krems. Quantum theory of chemical reactions in the presence of electromagnetic fields. *The Journal of Chemical Physics*, 129(3):034112, 2008.
- [34] Wallis Alisdair O. G. and Hutson Jeremy M. Production of ultracold nh molecules by sympathetic cooling with mg. *Phys. Rev. Lett.*, 103(18):183201, Oct 2009.
- [35] R. Grimm, M. Weidemüller, and Y.B. Ovchinnikov. Optical dipole traps for neutral atoms. *Advances in atomic, molecular, and optical physics*, 42:95–170, 2000.
- [36] P. S. Jessen, I. H. Deutsch, Benjamin Bederson, and Herbert Walther. *Optical Lattices*, volume Volume 37, pages 95–138. Academic Press, 1996.
- [37] D. S. Petrov and G. V. Shlyapnikov. Interatomic collisions in a tightly confined bose gas. *Phys. Rev. A*, 64(1):012706, Jun 2001.
- [38] Li Z., Alyabyshev S. V., and Krems R. V. Ultracold inelastic collisions in two dimensions. *Phys. Rev. Lett.*, 100(7):073202, Feb 2008.
- [39] Z. Li and R. V. Krems. Inelastic collisions in an ultracold quasi-two-dimensional gas. *Phys. Rev. A*, 79(5):050701, May 2009.
- [40] H R Sadeghpour and J L Bohn and M J Cavagnero and B D Esry and I I Fabrikant and J H Macek and A R P Rau. Collisions near threshold in atomic and molecular physics. *Journal of Physics B: Atomic, Molecular and Optical Physics*, 33(5):R93, 2000.
- [41] Micheli A., Pupillo G., Büchler H. P., and Zoller P. Cold polar molecules in two-dimensional traps: Tailoring interactions with external fields for novel quantum phases. *Phys. Rev. A*, 76(4):043604, Oct 2007.
- [42] Micheli Andrea, Idziaszek Zbigniew, Pupillo Guido, Baranov Mikhail A., Zoller Peter, and Julienne Paul S. Universal rates for reactive ultracold polar molecules in reduced dimensions. *Phys. Rev. Lett.*, 105(7):073202, Aug 2010.

- [43] de Miranda M. H. G., Chotia A., Neyenhuis B., Wang D., Quemener G., Ospelkaus S., Bohn J. L., Ye J., and Jin D. S. Controlling the quantum stereodynamics of ultracold bimolecular reactions. *Nat Phys*, 7(6):502–507, Jun 2011. 10.1038/nphys1939.
- [44] Moshe Shapiro and Paul Brumer. Coherent control of molecular dynamics. *Rep. Prog. Phys.*, 66:859–942, 2003.
- [45] Moshe Shapiro and Paul Brumer. *Principles of the Quantum Control of Molecular Processes*. Wiley, Hoboken, New Jersey, 2003.
- [46] Southwell Karen. Ultracold matter. *Nature*, 416(6877):205–205, Mar 2002. 10.1038/416205a.
- [47] Wolfgang Ketterle. Nobel lecture: When atoms behave as waves: Bose-einstein condensation and the atom laser. *Rev. Mod. Phys.*, 74(4):1131–1151, Nov 2002.
- [48] J. R. Anglin and W. Ketterle. Bose-einstein condensation of atomic gases. *Nature*, 416:211, 2002.
- [49] Pitaevskii Lev and Stringari Sandro. The quest for superfluidity in fermi gases. *Science*, 298(5601):2144–2146, Dec 2002. 10.1126/science.1080087.
- [50] Giorgini Stefano, Pitaevskii Lev P., and Stringari Sandro. Theory of ultracold atomic fermi gases. *Rev. Mod. Phys.*, 80(4):1215–1274, Oct 2008.
- [51] Chu Steven. Nobel lecture: The manipulation of neutral particles. *Rev. Mod. Phys.*, 70(3):685–706, Jul 1998.
- [52] Phillips William D. Nobel lecture: Laser cooling and trapping of neutral atoms. *Rev. Mod. Phys.*, 70(3):721–741, Jul 1998.
- [53] Claude Cohen-Tannoudji. Manipulating atoms with photons. *Physica Scripta*, 1998(T76):33, 1998.
- [54] John Weiner. *Cold and ultracold collision in quantum microscopic and mesoscopic systems*. Cambridge University Press, UK, 2003.
- [55] Burnett Keith, Julienne Paul S., Lett Paul D., Tiesinga Eite, and Williams Carl J. Quantum encounters of the cold kind. *Nature*, 416(6877):225–232, Mar 2002. 10.1038/416225a.

- [56] V I Balykin and V G Minogin and V S Letokhov. Electromagnetic trapping of cold atoms. *Reports on Progress in Physics*, 63(9):1429, 2000.
- [57] Cheng Chin, Rudolf Grimm, Paul Julienne, and Eite Tiesinga. Feshbach resonances in ultracold gases. *Reviews of Modern Physics*, 82(2):1225, 2010.
- [58] Morsch Oliver and Oberthaler Markus. Dynamics of bose-einstein condensates in optical lattices. *Rev. Mod. Phys.*, 78(1):179–215, Feb 2006.
- [59] Santos L., Shlyapnikov G. V., Zoller P., and Lewenstein M. Bose-einstein condensation in trapped dipolar gases. *Phys. Rev. Lett.*, 85(9):1791–1794, Aug 2000.
- [60] Yi S. and You L. Trapped atomic condensates with anisotropic interactions. *Phys. Rev. A*, 61(4):041604, Mar 2000.
- [61] Lushnikov Pavel M. Collapse of bose-einstein condensates with dipole-dipole interactions. *Phys. Rev. A*, 66(5):051601, Nov 2002.
- [62] Ronen Shai, Bortolotti Daniele C. E., and Bohn John L. Radial and angular rotons in trapped dipolar gases. *Phys. Rev. Lett.*, 98(3):030406, Jan 2007.
- [63] Dutta O. and Meystre P. Ground-state structure and stability of dipolar condensates in anisotropic traps. *Phys. Rev. A*, 75(5):053604, May 2007.
- [64] T Lahaye and C Menotti and L Santos and M Lewenstein and T Pfau. The physics of dipolar bosonic quantum gases. *Reports on Progress in Physics*, 72(12):126401, 2009.
- [65] Griesmaier Axel, Werner Jörg, Hensler Sven, Stuhler Jürgen, and Pfau Tilman. Bose-einstein condensation of chromium. *Phys. Rev. Lett.*, 94(16):160401, Apr 2005.
- [66] Lahaye T., Metz J., Fröhlich B., Koch T., Meister M., Griesmaier A., Pfau T., Saito H., Kawaguchi Y., and Ueda M. d-wave collapse and explosion of a dipolar bose-einstein condensate. *Phys. Rev. Lett.*, 101(8):080401, Aug 2008.
- [67] P. G Kevrekidis, D. J. Frantzeskakis, and R. Carretero-González, editors. *Emergent Nonlinear Phenomena in Bose-Einstein Condensates*. Springer, 2008.
- [68] Pedri P. and Santos L. Two-dimensional bright solitons in dipolar bose-einstein condensates. *Phys. Rev. Lett.*, 95(20):200404, Nov 2005.

- [69] Nath R., Pedri P., and Santos L. Stability of dark solitons in three dimensional dipolar bose-einstein condensates. *Phys. Rev. Lett.*, 101(21):210402, Nov 2008.
- [70] Cooper N. R., Rezayi E. H., and Simon S. H. Vortex lattices in rotating atomic bose gases with dipolar interactions. *Phys. Rev. Lett.*, 95(20):200402, Nov 2005.
- [71] Yi S. and Pu H. Vortex structures in dipolar condensates. *Phys. Rev. A*, 73(6):061602, Jun 2006.
- [72] Baranov M. A., Mar'enko M. S., Rychkov Val. S., and Shlyapnikov G. V. Superfluid pairing in a polarized dipolar fermi gas. *Phys. Rev. A*, 66(1):013606, Jul 2002.
- [73] M A Baranov and Ł Dobrek and M Lewenstein. Bcs pairing in a trapped dipolar fermi gas. *New Journal of Physics*, 6(1):198, 2004.
- [74] Köhl Michael, Moritz Henning, Stöferle Thilo, Günter Kenneth, and Esslinger Tilman. Fermionic atoms in a three dimensional optical lattice: Observing fermi surfaces, dynamics, and interactions. *Phys. Rev. Lett.*, 94(8):080403, Mar 2005.
- [75] Iskin M. and Sá de Melo C. A. R. Ultracold heteronuclear molecules and ferroelectric superfluids. *Phys. Rev. Lett.*, 99(11):110402, Sep 2007.
- [76] Miyakawa Takahiko, Sogo Takaaki, and Pu Han. Phase-space deformation of a trapped dipolar fermi gas. *Phys. Rev. A*, 77(6):061603, Jun 2008.
- [77] Hemmerich A. and Hänsch T. W. Two-dimesional atomic crystal bound by light. *Phys. Rev. Lett.*, 70(4):410–413, Jan 1993.
- [78] Grynberg G., Lounis B., Verkerk P., Courtois J.-Y., and Salomon C. Quantized motion of cold cesium atoms in two- and three-dimensional optical potentials. *Phys. Rev. Lett.*, 70(15):2249–2252, Apr 1993.
- [79] Immanuel Bloch. Ultracold quantum gases in optical lattices. *Nat. Phys.*, 1(1):23–30, 10 2005.
- [80] D. Jaksch, C. Bruder, J. I. Cirac, C. W. Gardiner, and P. Zoller. Cold bosonic atoms in optical lattices. *Phys. Rev. Lett.*, 81(15):3108–3111, Oct 1998.

- [81] Greiner Markus, Mandel Olaf, Esslinger Tilman, Hansch Theodor W., and Bloch Immanuel. Quantum phase transition from a superfluid to a mott insulator in a gas of ultracold atoms. *Nature*, 415(6867):39–44, Jan 2002. 10.1038/415039a.
- [82] Maciej Lewenstein, Anna Sanpera, Veronica Ahufinger, Bogdan Damski, Aditi Sen, and Ujjwal Sen. Ultracold atomic gases in optical lattices: mimicking condensed matter physics and beyond. *Adv. Phys.*, 56(2):243–379, 2007.
- [83] Immanuel Bloch, Jean Dalibard, and Wilhelm Zwerger. Many-body physics with ultracold gases. *Rev. Mod. Phys.*, 80(3):885, 07 2008.
- [84] Gerald D. Mahan. *Many-particle physics*. Plenum Publishers, New York, 3rd edition, 2000.
- [85] Góral K., Santos L., and Lewenstein M. Quantum phases of dipolar bosons in optical lattices. *Phys. Rev. Lett.*, 88(17):170406, Apr 2002.
- [86] C Trefzger and C Menotti and B Capogrosso-Sansone and M Lewenstein. Ultracold dipolar gases in optical lattices. *Journal of Physics B: Atomic, Molecular and Optical Physics*, 44(19):193001, 2011.
- [87] A. Micheli, G. K. Brennen, and P. Zoller. A toolbox for lattice-spin models with polar molecules. *Nat. Phys.*, 2:341, 2006.
- [88] Osterloh Klaus, Barberán Nuria, and Lewenstein Maciej. Strongly correlated states of ultracold rotating dipolar fermi gases. *Phys. Rev. Lett.*, 99(16):160403, Oct 2007.
- [89] Menotti C., Trefzger C., and Lewenstein M. Metastable states of a gas of dipolar bosons in a 2d optical lattice. *Phys. Rev. Lett.*, 98(23):235301, Jun 2007.
- [90] H. P. Buchler, E. Demler, M. Lukin, A. Micheli, N. Prokof’ev, G. Pupillo, and P. Zoller. Strongly correlated 2d quantum phases with cold polar molecules: Controlling the shape of the interaction potential. *Physical Review Letters*, 98(6):060404, 2007.
- [91] Capogrosso-Sansone B., Trefzger C., Lewenstein M., Zoller P., and Pupillo G. Quantum phases of cold polar molecules in 2d optical lattices. *Phys. Rev. Lett.*, 104(12):125301, Mar 2010.

- [92] Pollet L., Picon J. D., Büchler H. P., and Troyer M. Supersolid phase with cold polar molecules on a triangular lattice. *Phys. Rev. Lett.*, 104(12):125302, Mar 2010.
- [93] He Liang and Hofstetter Walter. Supersolid phase of cold fermionic polar molecules in two-dimensional optical lattices. *Phys. Rev. A*, 83(5):053629, May 2011.
- [94] Gorshkov Alexey V., Manmana Salvatore R., Chen Gang, Demler Eugene, Lukin Mikhail D., and Rey Ana Maria. Quantum magnetism with polar alkali-metal dimers. *Phys. Rev. A*, 84(3):033619, Sep 2011.
- [95] Gorshkov Alexey V., Manmana Salvatore R., Chen Gang, Ye Jun, Demler Eugene, Lukin Mikhail D., and Rey Ana Maria. Tunable superfluidity and quantum magnetism with ultracold polar molecules. *Phys. Rev. Lett.*, 107(11):115301, Sep 2011.
- [96] Guido Pupillo, Andrea Micheli, Hans-Peter Büchler, and Peter Zoller. Condensed matter physics with cold polar molecules. In Roman V. Krems, William C. Stwalley, and Bretislav Friedrich, editors, *Cold molecules: Theory, experiment and applications*, chapter 12. CRC Press, Boca Raton, 2009.
- [97] J. Frenkel. On the transformation of light into heat in solids. ii. *Phys. Rev.*, 37(17):1276–1294, 1931.
- [98] T. Kobayashi. *J-Aggregates*. World Scientific Publishing, 1996.
- [99] Vladimir Agranovich. *Excitations in Organic Solids*. Oxford University Press, Oxford, DDDD 2008.
- [100] Frank C. Spano. The spectral signatures of frenkel polarons in h- and j-aggregates. *Acc. Chem. Res.*, 43(3):429–439, 12 2009.
- [101] Marco Koschorreck, Daniel Pertot, Enrico Vogt, Bernd Frohlich, Michael Feld, and Michael Kohl. Attractive and repulsive fermi polarons in two dimensions. *Nature*, advance online publication, 2012. 10.1038/nature11151.
- [102] Rabl P., DeMille D., Doyle J. M., Lukin M. D., Schoelkopf R. J., and Zoller P. Hybrid quantum processors: Molecular ensembles as quantum memory for solid state circuits. *Phys. Rev. Lett.*, 97(3):033003, Jul 2006.

- [103] P. Rabl and P. Zoller. Molecular dipolar crystals as high-fidelity quantum memory for hybrid quantum computing. *Phys. Rev. A*, 76(4):042308, 10 2007.
- [104] Andre A., DeMille D., Doyle J. M., Lukin M. D., Maxwell S. E., Rabl P., Schoelkopf R. J., and Zoller P. A coherent all-electrical interface between polar molecules and mesoscopic superconducting resonators. *Nat Phys*, 2(9):636–642, Sep 2006. 10.1038/nphys386.
- [105] Savvidis P. G., Baumberg J. J., Stevenson R. M., Skolnick M. S., Whittaker D. M., and Roberts J. S. Angle-resonant stimulated polariton amplifier. *Phys. Rev. Lett.*, 84(7):1547–1550, Feb 2000.
- [106] Amo A., Liew T. C. H., Adrados C., Houdre R., Giacobino E., Kavokin A. V., and Bramati A. Exciton-polariton spin switches. *Nat Photon*, 4(6):361–366, Jun 2010. 10.1038/nphoton.2010.79.
- [107] Das Ayan, Heo Junseok, Jankowski Marc, Guo Wei, Zhang Lei, Deng Hui, and Bhattacharya Pallab. Room temperature ultralow threshold gan nanowire polariton laser. *Phys. Rev. Lett.*, 107(6):066405, Aug 2011.
- [108] G.D. Scholes and G. Rumbles. Excitons in nanoscale systems. *Nat. Mat.*, 5:683–696, 2006.
- [109] F. Tassone and Y. Yamamoto. Exciton-exciton scattering dynamics in a semiconductor microcavity and stimulated scattering into polaritons. *Physical Review B*, 59(16), 04 1999.
- [110] J. Kasprzak, M. Richard, S. Kundermann, A. Baas, P. Jeambrun, J. M. J. Keeling, F. M. Marchetti, M. H. Szymanska, R. Andre, J. L. Staehli, V. Savona, P. B. Littlewood, B. Deveaud, and Le Si Dang. Bose-einstein condensation of exciton polaritons. *Nature*, 443(7110):409–414, 09 2006.
- [111] Deng Hui, Haug Hartmut, and Yamamoto Yoshihisa. Exciton-polariton bose-einstein condensation. *Rev. Mod. Phys.*, 82(2):1489–1537, May 2010.
- [112] Hohjai Lee, Yuan-Chung Cheng, and Graham R. Fleming. Coherence Dynamics in Photosynthesis: Protein Protection of Excitonic Coherence. *Science*, 316(5830):1462–1465, 2007.
- [113] Yuan-Chung Cheng and Graham R. Fleming. Dynamics of light harvesting in photosynthesis. *Annu. Rev. Phys. Chem.*, 60(1):241–262, 2009.

- [114] Patrick Rebentrost *et al.* Environment-assisted quantum transport. *New J. Phys.*, 11(3):033003, 2009.
- [115] M. B. Plenio and S. F. Huelga. Dephasing-assisted transport: quantum networks and biomolecules. *New J. Phys.*, 10(11):113019, 2008.
- [116] Mohan Sarovar *et al.* Quantum entanglement in photosynthetic light-harvesting complexes. *Nat. Phys.*, 6(6):462–467, 06 2010.
- [117] S. F. Yelin, D. DeMille, and R. Côté. Quantum information processing with ultracold polar molecules. In R. V. Krems, W. C. Stwalley, and B. Friedrich, editors, *Cold molecules: Theory, Experiment and Applications*. Taylor & Francis, Boca Raton, 2009.
- [118] Mayle Michael, González-Férez Rosario, and Schmelcher Peter. Controlling molecular orientation through radiative rotational transitions in strong static electric fields. *Phys. Rev. A*, 75(1):013421, Jan 2007.
- [119] Deiglmayr J., Repp M., Dulieu O., Wester R., and Weidemüller M. Population redistribution in optically trapped polar molecules. *The European Physical Journal D - Atomic, Molecular, Optical and Plasma Physics*, 65(1):99–104.
- [120] I. H. Deutsch, G. K. Brennen, and P. S. Jessen. Quantum computing with neutral atoms in an optical lattice. In S. L. Braustein, H.-K. Lo, and P. Kok, editors, *Scalable Quantum Computers: Paving the Way to Realization*. Wiley-VCH Verlag GmbH & Co., 2005.
- [121] Jaksch D., Briegel H.-J., Cirac J. I., Gardiner C. W., and Zoller P. Entanglement of atoms via cold controlled collisions. *Phys. Rev. Lett.*, 82(9):1975–1978, Mar 1999.
- [122] Cirac J. I. and Zoller P. Quantum computations with cold trapped ions. *Phys. Rev. Lett.*, 74(20):4091–4094, May 1995.
- [123] Haffner H., Hansel W., Roos C. F., Benhelm J., Chek al-kar D., Chwalla M., Korber T., Rapol U. D., Riebe M., Schmidt P. O., Becher C., Guhne O., Dur W., and Blatt R. Scalable multiparticle entanglement of trapped ions. *Nature*, 438(7068):643–646, Dec 2005. 10.1038/nature04279.
- [124] H. Häffner, C.F. Roos, and R. Blatt. Quantum computing with trapped ions.
- [125] Michael A. Nielsen and Isaac L. Chuang. *Quantum Computation and Quantum Information*. Cambridge University Press, 2000.

- [126] D. DeMille. Quantum computation with trapped polar molecules. *Physical Review Letters*, 88(6), 2002.
- [127] Kuznetsova Elena, Côté Robin, Kirby Kate, and Yelin S. F. Analysis of experimental feasibility of polar-molecule-based phase gates. *Phys. Rev. A*, 78(1):012313, Jul 2008.
- [128] Lee Chaohong and Ostrovskaya Elena A. Quantum computation with diatomic bits in optical lattices. *Phys. Rev. A*, 72(6):062321, Dec 2005.
- [129] Yelin S. F., Kirby K., and Côté Robin. Schemes for robust quantum computation with polar molecules. *Phys. Rev. A*, 74(5):050301, Nov 2006.
- [130] Charron Eric, Milman Pérola, Keller Arne, and Atabek Osman. Quantum phase gate and controlled entanglement with polar molecules. *Phys. Rev. A*, 75(3):033414, Mar 2007.
- [131] Gershenfeld Neil A. and Chuang Isaac L. Bulk spin-resonance quantum computation. *Science*, 275(5298):350–356, Jan 1997. 10.1126/science.275.5298.350.
- [132] Warren Warren S. The usefulness of nmr quantum computing. *Science*, 277(5332):1688–1690, Sep 1997. 10.1126/science.277.5332.1688.
- [133] Glaser Steffen J. Nmr quantum computing. *Angew. Chem. Int. Ed.*, 40(1):147–149, 2001.
- [134] R. Zadoyan, D. Kohen, D.A. Lidar, and V.A. Apkarian. The manipulation of massive ro-vibronic superpositions using time–frequency-resolved coherent anti-stokes raman scattering (tfrcars): from quantum control to quantum computing. *Chemical Physics*, 266(2–3):323–351, 2001.
- [135] Glenn David R., Lidar Daniel A., and Apkarian V. Ara. Quantum logic gates in iodine vapor using time–frequency resolved coherent anti-stokes raman scattering: a theoretical study. *Molecular Physics*, 104(8):1249–1266, 2006. doi: 10.1080/00268970500525713.
- [136] Pellegrini P. and Desouter-Lecomte M. Quantum gates driven by microwave pulses in hyperfine levels of ultracold heteronuclear dimers. *The European Physical Journal D - Atomic, Molecular, Optical and Plasma Physics*, 64(1):163–170, Sep 2011.
- [137] C. Ospelkaus *et al.* Ultracold heteronuclear molecules in a 3d optical lattice. *Phys. Rev. Lett.*, 97(12):120402–4, 09 2006.

- [138] Amodsen Chotia, Brian Neyenhuis, Steven A. Moses, Bo Yan, Jacob P. Covey, Michael Foss-Feig, Ana Maria Rey, Deborah S. Jin, and Jun Ye. Long-lived dipolar molecules and feshbach molecules in a 3d optical lattice. *arXiv:1110.4420v1*.
- [139] Milman P., Keller A., Charron E., and Atabek O. Bell-type inequalities for cold heteronuclear molecules. *Phys. Rev. Lett.*, 99(13):130405, Sep 2007.
- [140] Milman P., Keller A., Charron E., and Atabek O. Molecular orientation entanglement and temporal bell-type inequalities. *The European Physical Journal D - Atomic, Molecular, Optical and Plasma Physics*, 53(3):383–392, 2009.
- [141] Qi Wei, Sabre Kais, Bretislav Friedrich, and Dudley Herschbach. Entanglement of polar molecules in pendular states. *The Journal of Chemical Physics*, 134(12):124107, 2011.
- [142] John Brown and Alan Carrington. *Rotational Spectroscopy of Diatomic Molecules*. Cambridge University Press.
- [143] Richard Zare. *Angular Momentum*.
- [144] Hong Ran and J Aldegunde and Jeremy M Hutson. Hyperfine structure in the microwave spectra of ultracold polar molecules, 2010.
- [145] Aldegunde J., Rivington Ben A., uchowski Piotr S., and Hutson Jeremy M. Hyperfine energy levels of alkali-metal dimers: Ground-state polar molecules in electric and magnetic fields. *Phys. Rev. A*, 78(3):033434, Sep 2008.
- [146] Aldegunde J. and Hutson Jeremy M. Hyperfine energy levels of alkali-metal dimers: Ground-state homonuclear molecules in magnetic fields. *Phys. Rev. A*, 79(1):013401, Jan 2009.
- [147] Shuman E. S., Barry J. F., and DeMille D. Laser cooling of a diatomic molecule. *Nature*, 467(7317):820–823, Oct 2010. 10.1038/nature09443.
- [148] Derek A. Long. *The Raman Effect: a unified treatment of the theory of Raman scattering by molecules*. John Wiley & Sons, 2002.
- [149] Tamar Seideman and Edward Hamilton. Nonadiabatic alignment by intense pulses. concepts, theory, and directions. *Advances In Atomic, Molecular, and Optical Physics*, 52:289–329, 2005.

- [150] Friedrich Bretislav and Herschbach Dudley. Alignment and trapping of molecules in intense laser fields. *Phys. Rev. Lett.*, 74(23):4623–4626, Jun 1995.
- [151] Keith D. Bonin and Vitaly V. Kresin. *Electric-Dipole Polarizabilities of Atoms, Molecules, and Clusters*. World Scientific Press, 1997.
- [152] S. Kotochigova and E. Tiesinga. Controlling polar molecules in optical lattices. *Physical Review A*, 73(4):041405, 2006.
- [153] Svetlana Kotochigova and David DeMille. Electric-field-dependent dynamic polarizability and state-insensitive conditions for optical trapping of diatomic polar molecules. *Physical Review A*, 82(6):063421, 2010.
- [154] J. Deiglmayr, M. Aymar, R. Wester, M. Weidemüller, and O. Dulieu. Calculations of static dipole polarizabilities of alkali dimers: Prospects for alignment of ultracold molecules. *J. Chem. Phys.*, 129(064309), 2008.
- [155] Mikhail Lemesko. Shaping interactions between polar molecules with far-off-resonant light. *Phys. Rev. A*, 83(5):051402, May 2011.
- [156] Anthony Stone. *The Theory of Intermolecular Forces*. Oxford University Press, 2000.
- [157] Ospelkaus S., Ni K.-K., Quémener G., Neyenhuis B., Wang D., de Miranda M. H. G., Bohn J. L., Ye J., and Jin D. S. Controlling the hyperfine state of rovibronic ground-state polar molecules. *Phys. Rev. Lett.*, 104(3):030402, Jan 2010.
- [158] S. Ospelkaus, K.-K. Ni, D. Wang, M. H. G. de Miranda, B. Neyenhuis, G. Quémener, P. S. Julienne, J. L. Bohn, D. S. Jin, and J. Ye. Quantum-state controlled chemical reactions of ultracold potassium-rubidium molecules. *Science*, 327(5967):853–857, 2010. 10.1126/science.1184121.
- [159] Masao Takamoto, Feng-Lei Hong, Ryoichi Higashi, and Hidetoshi Katori. An optical lattice clock. *Nature*, 435(7040):321–324, 2005. 10.1038/nature03541.
- [160] M. Brieger. Stark effect, polarizabilities and the electric dipole moment of heteronuclear diatomic molecules in $^1\Sigma$ states. *Chemical Physics*, 89:275–295, 1984.
- [161] M L Wall and L D Carr. Emergent timescales in entangled quantum dynamics of ultracold molecules in optical lattices. *New Journal of Physics*, 11(5):055027, 2009.

- [162] Kevin M. Jones, Eite Tiesinga, Paul D. Lett, and Paul S. Julienne. Ultracold photoassociation spectroscopy: Long-range molecules and atomic scattering. *Rev. Mod. Phys.*, 78:483, 2006.
- [163] Okano M., Hara H., Muramatsu M., Doi K., Uetake S., Takasu Y., and Takahashi Y. Simultaneous magneto-optical trapping of lithium and ytterbium atoms towards production of ultracold polar molecules. *Applied Physics B: Lasers and Optics*, 98(4):691–696.
- [164] Maussang Kenneth, Egorov Dima, Helton Joel S., Nguyen Scott V., and Doyle John M. Zeeman relaxation of caF in low-temperature collisions with helium. *Phys. Rev. Lett.*, 94(12):123002, Mar 2005.
- [165] Di Rosa M. D. Laser-cooling molecules. *The European Physical Journal D - Atomic, Molecular, Optical and Plasma Physics*, 31(2):395–402.
- [166] D. M. Egorov. PhD thesis, Harvard University, 2004.
- [167] Hudson J. J., Sauer B. E., Tarbutt M. R., and Hinds E. A. Measurement of the electron electric dipole moment using ybF molecules. *Phys. Rev. Lett.*, 89(2):023003, Jun 2002.
- [168] T. V. Tscherbul and R. V. Krems. Manipulating spin-dependent interactions in rotationally excited cold molecules with electric fields. *The Journal of Chemical Physics*, 125(19):194311, 2006.
- [169] Stephen M. Barnett. *Quantum Information*. Oxford University Press, 2009.
- [170] Marvin L. Goldberger and Kenneth M. Watson. *Collision Theory*. John Wiley & Sons, 1964.
- [171] Moshe Shapiro and Paul Brumer. Coherent control of collisional events: Bimolecular reactive scattering. *Phys. Rev. Lett.*, 77(12):2574, 1996.
- [172] Alexander Abrashevich, Moshe Shapiro, and Paul Brumer. Coherent control of atom-diatom reactive scattering: isotopic variants of H+H₂ in three dimensions. *Chem. Phys.*, 267:81–92, 2001.
- [173] Carlos A. Arango, Moshe Shapiro, and Paul Brumer. Cold atomic collisions: Coherent control of penning and associative ionization. *Phys. Rev. Lett.*, 97:193202(4), 2006.
- [174] Carlos A. Arango, Moshe Shapiro, and Paul Brumer. Coherent control of collision processes: Penning versus associative ionization. *The Journal of Chemical Physics*, 125(9):094315, 2006.

- [175] Keith Burnett, Paul S. Julienne, Paul D. Lett, Eite Tiesinga, and Carl J. Williams. Quantum encounters of the cold kind. *Nature*, 416:225, March 2002.
- [176] M. J. Wright, J. A. Pechkis, J. L. Carini, S. Kallush, R. Kosloff, and P. L. Gould. Coherent control of ultracold collisions with chirped light: Direction matters. *Phys. Rev. A*, 75:51401, 2007.
- [177] Ph. Courteille, R. S. Freeland, D. J. Heinzen, F. A. van Abeelen, and B. J. Verhaar. Observation of a feshbach resonance in cold atom scattering. *Physical Review Letters*, 81(1), 1998.
- [178] Z. Li and R. V. Krems. Electric-field-induced feshbach resonances in ultracold alkali-metal mixtures. *Phys. Rev. A*, 75:032709–1(8), 2007.
- [179] Bout Marcelis, Boudewijn Verhaar, and Servaas Kokkelmans. Total control over ultracold interactions via electric and magnetic fields. *Phys. Rev Lett.*, 100:153201, 2008.
- [180] Roman V. Krems. Controlling collisions of ultracold atoms with dc electric fields. *Phys. Rev Lett.*, 96(12):123202(4), 2006.
- [181] C. J. Foot. Oxford University Press, 2005.
- [182] Marcel Mudrich, Stephan Kraft, K. Singer, R. Grimm, Allard Mosk, and Matthias Weidemüller. Sympathetic cooling with two atomic species in an optical trap. *Phys. Rev Lett.*, 88(25):253001(4), 2002.
- [183] Robert Duane Cowan. *The theory of atomic structure and spectra*. Los Alamos series in basic and applied sciences. University of California Press, 1981.
- [184] J C Camparo and R P Frueholz. A dressed atom interpretation of adiabatic rapid passage. *Journal of Physics B: Atomic and Molecular Physics*, 17(20):4169–4178, 1984.
- [185] John R. Taylor. *Scattering Theory: The quantum theory of non-relativistic collisions*. Dover, 1972.
- [186] M. Aymar and O. Dulieu. Calculation of accurate permanent dipole moments of the lowest [^{sup} 1,3] σ [^{sup} +] states of heteronuclear alkali dimers using extended basis sets. *J. Chem. Phys.*, 122(20):204302–9, 05 2005.

- [187] Chao-Ping Hsu. The electronic couplings in electron transfer and excitation energy transfer. *Acc. Chem. Res.*, 42(4):509–518, 02 2009.
- [188] A. H. Zewail, D. D. Smith, and J. Lemaistre. Dynamics of molecular excitons: disorder, coherence and dephasing. In E. I. Rashba and M. D. Sturge, editors, *Excitons*, volume 2 of *Modern Problems in Condensed Matter Sciences*, page 665. North Holland, Amsterdam, 1982.
- [189] L. Fallani, J. E. Lye, V. Guarrera, C. Fort, and M. Inguscio. Ultracold atoms in a disordered crystal of light: Towards a bose glass. *Phys. Rev. Lett.*, 98:130404, 2007.
- [190] H. Fukuyama and S. Hikami. *Anderson Localization*. Springer, Berlin, 1982.
- [191] P. Würtz, T. Langen, T. Gericke, A. Koglbauer, H. Ot, et al. Need title. *Phys. Rev. Lett.*, 103:080404, 2009.
- [192] O.A. Konobeev and Yu. V. Dubovskii. Cross section for scattering of a free exciton by impurities in a molecular crystal. *Sov. Phys -Solid State*, 6:2071, 1965.
- [193] I. Avgin and D. L. Huber. Localized states in 1d frenkel exciton systems: A comparison between infinite-range and nearest-neighbor transfer for normal and inverted bands. *The Journal of Physical Chemistry B*, 113(43):14112–14117, 2009. PMID: 19788261.
- [194] Marina Litinskaya. Exciton polariton kinematic interaction in crystalline organic microcavities. *Physical Review B (Condensed Matter and Materials Physics)*, 77(15):155325–12, 04 2008.
- [195] Felipe Herrera, Marina Litinskaya, and Roman V. Krems. Tunable disorder in a crystal of cold polar molecules. *Phys. Rev. A*, 82:033428, 2010.
- [196] A. F. Ioffe and A. R. Regel. Need title. *Prog. Semicond.*, 4:237, 1960.
- [197] L. Tessieri and F. M. Izrailev. One-dimensional tight-binding models with correlated diagonal and off-diagonal disorder. *Physica E: Low-dimensional Systems and Nanostructures*, 9(3):405–417, 2001.
- [198] David H. Dunlap, H-L. Wu, and Philip W. Phillips. Absence of localization in a random-dimer model. *Physical Review Letters*, 65(1):88, 1990.

- [199] V. Bellani, E. Diez, R. Hey, L. Toni, L. Tarricone, G. B. Parravicini, F. Domínguez-Adame, and R. Gómez-Alcalá;. Experimental evidence of delocalized states in random dimer superlattices. *Physical Review Letters*, 82(10):2159, 1999.
- [200] F. M. Izrailev and A. A. Krokhn. Localization and the mobility edge in one-dimensional potentials with correlated disorder. *Physical Review Letters*, 82(20):4062, 1999.
- [201] U. Kuhl, F. M. Izrailev, A. A. Krokhn, and H.-J. Stockmann. Experimental observation of the mobility edge in a waveguide with correlated disorder. *Applied Physics Letters*, 77(5):633–635, 2000.
- [202] Guo-Meng Zhao *et al.* Evidence for polaronic supercarriers in the copper oxide superconductors $\text{La}_{2-x}\text{Sr}_x\text{CuO}_4$. *Nature*, 385:236–239, 1997.
- [203] G. S. Engel *et al.* Evidence for wavelike energy transfer through quantum coherence in photosynthetic systems. *Nature*, 446:782–786, 2007.
- [204] Shaul Mukamel. Multidimensional femtosecond correlation spectroscopies of electronic and vibrational excitations. *Annu. Rev. Phys. Chem.*, 51(1):691–729, 2000.
- [205] Dominic Marchand. *Polaron physics beyond the Holstein model*. PhD thesis, University of British Columbia, September 2011.
- [206] J. T. Devreese. Polarons. 14:383, 1996.
- [207] Feynman R. P. Slow electrons in a polar crystal. *Phys. Rev.*, 97(3):660–665, Feb 1955.
- [208] Feynman R. P., Hellwarth R. W., Iddings C. K., and Platzman P. M. Mobility of slow electrons in a polar crystal. *Phys. Rev.*, 127(4):1004–1017, Aug 1962.
- [209] Gerlach B. and Löwen H. Analytical properties of polaron systems or: Do polaronic phase transitions exist or not? *Rev. Mod. Phys.*, 63(1):63–90, Jan 1991.
- [210] Prokof'ev Nikolai V. and Svistunov Boris V. Polaron problem by diagrammatic quantum monte carlo. *Phys. Rev. Lett.*, 81(12):2514–2517, Sep 1998.

- [211] De Filippis G., Cataudella V., Mishchenko A. S., Perroni C. A., and Nagaosa N. Optical conductivity of a doped mott insulator: The interplay between correlation and electron-phonon interaction. *Phys. Rev. B*, 80(19):195104, Nov 2009.
- [212] Hohenadler Martin, Evertz Hans Gerd, and von der Linden Wolfgang. Quantum monte carlo and variational approaches to the holstein model. *Phys. Rev. B*, 69(2):024301, Jan 2004.
- [213] Goodvin Glen L., Berciu Mona, and Sawatzky George A. Green's function of the holstein polaron. *Phys. Rev. B*, 74(24):245104, Dec 2006.
- [214] T. Holstein. Studies of polaron motion : Part i. the molecular-crystal model. *Ann. Phys.*, 8(3):325–342, 1959.
- [215] Aldo H. Romero, David W. Brown, and Katja Lindenberg. Polaron effective mass, band distortion, and self-trapping in the holstein molecular-crystal model. *Phys. Rev. B*, 59(21):13728, 1999.
- [216] Su W. P., Schrieffer J. R., and Heeger A. J. Solitons in polyacetylene. *Phys. Rev. Lett.*, 42(25):1698–1701, Jun 1979.
- [217] Heeger A. J., Kivelson S., Schrieffer J. R., and Su W. P. Solitons in conducting polymers. *Rev. Mod. Phys.*, 60(3):781–850, Jul 1988.
- [218] Marchand D. J. J., De Filippis G., Cataudella V., Berciu M., Nagaosa N., Prokof'ev N. V., Mishchenko A. S., and Stamp P. C. E. Sharp transition for single polarons in the one-dimensional su-schrieffer-heeger model. *Phys. Rev. Lett.*, 105(26):266605, Dec 2010.
- [219] Chotia Amodsen, Neyenhuis Brian, Moses Steven A., Yan Bo, Covey Jacob P., Foss-Feig Michael, Rey Ana Maria, Jin Deborah S., and Ye Jun. Long-lived dipolar molecules and feshbach molecules in a 3d optical lattice. *Phys. Rev. Lett.*, 108(8):080405, Feb 2012.
- [220] Leibfried D., Blatt R., Monroe C., and Wineland D. Quantum dynamics of single trapped ions. *Rev. Mod. Phys.*, 75(1):281–324, Mar 2003.
- [221] Günter Mahler and Volker A. Weberrub. *Quantum Networks: Dynamics of Open Nanostructures*. Springer, 1998.
- [222] Jai Singh. *Excitation Energy Transfer Processes in Condensed Matter: Theory and Applications*. Physics of Solids and Liquids. Plenum Press, 1994.

- [223] Y. Zhao V. Chernyak T. Meier and S. Mukamel. Polarons, localization, and excitonic coherence in superradiance of biological antenna complexes. *J. Chem. Phys.*, 107(10):3876, 1997.
- [224] Y. Zolotaryuk, P. L. Christiansen, and J. Juul Rasmussen. Polaron dynamics in a two-dimensional anharmonic holstein model. *Phys. Rev. B*, 58(21):14305, 12 1998.
- [225] J Pérez-Ríos, F Herrera, and R V Krems. External field control of collective spin excitations in an optical lattice of 2 molecules. *New J. Phys.*, 12(10):103007, 2010.
- [226] Hannewald K., Stojanović V. M., Schellekens J. M. T., Bobbert P. A., Kresse G., and Hafner J. Theory of polaron bandwidth narrowing in organic molecular crystals. *Phys. Rev. B*, 69(7):075211, Feb 2004.
- [227] Dongmeng Chen, Jun Ye, Haijun Zhang, and Yang Zhao. On the munnsilbey approach to polaron transport with off-diagonal coupling and temperature-dependent canonical transformations. *The Journal of Physical Chemistry B*, 115(18):5312–5321, 2011.
- [228] Berciu Mona. Green’s function of a dressed particle. *Phys. Rev. Lett.*, 97(3):036402, Jul 2006.
- [229] Goodvin Glen L. and Berciu Mona. Momentum average approximation for models with electron-phonon coupling dependent on the phonon momentum. *Phys. Rev. B*, 78(23):235120, Dec 2008.
- [230] Johannes Deiglmayr, Mireille Aymar, Roland Wester, Matthias Weidemuller, and Olivier Dulieu. Calculations of static dipole polarizabilities of alkali dimers: Prospects for alignment of ultracold molecules. *The Journal of Chemical Physics*, 129(6):064309, 2008.
- [231] Hirofumi Sakai, C. P. Safvan, Jakob Juul Larsen, Karen Marie Hilligsoe, Kasper Hald, and Henrik Stapelfeldt. Controlling the alignment of neutral molecules by a strong laser field. *J. Chem. Phys.*, 110:10235–10238, 1999.
- [232] K. Bergmann, H. Theuer, and B. W. Shore. Coherent population transfer among quantum states of atoms and molecules. *Reviews of Modern Physics*, 70(3), 1998.
- [233] Teruki Sugiyama, Takuji Adachi, and Hiroshi Masuhara. Crystallization of glycine by photon pressure of a focused cw laser beam. *Chem. Lett.*, 36(12):1480, 2007.

- [234] Rungsimanon Thitiporn, Yuyama Ken-ichi, Sugiyama Teruki, Masuhara Hiroshi, Tohnai Norimitsu, and Miyata Mikiji. Control of crystal polymorph of glycine by photon pressure of a focused continuous wave near-infrared laser beam. *The Journal of Physical Chemistry Letters*, 1(3):599–603, 2010. doi: 10.1021/jz900370x.
- [235] A. Einstein, B. Podolsky, and N. Rosen. Can quantum-mechanical description of physical reality be considered complete? *Phys. Rev.*, 47:777–780, 1935.
- [236] F. Laloe. Do we really understand quantum mechanics? strange correlations, paradoxes, and theorems. *American Journal of Physics*, 69(6):655–701, 2001.
- [237] Freedman Stuart J. and Clauser John F. Experimental test of local hidden-variable theories. *Phys. Rev. Lett.*, 28(14):938–941, Apr 1972.
- [238] Aspect Alain, Grangier Philippe, and Roger Gérard. Experimental tests of realistic local theories via bell’s theorem. *Phys. Rev. Lett.*, 47(7):460–463, Aug 1981.
- [239] Weihs Gregor, Jennewein Thomas, Simon Christoph, Weinfurter Harald, and Zeilinger Anton. Violation of bell’s inequality under strict einstein locality conditions. *Phys. Rev. Lett.*, 81(23):5039–5043, Dec 1998.
- [240] Tittel W., Brendel J., Zbinden H., and Gisin N. Violation of bell inequalities by photons more than 10 km apart. *Phys. Rev. Lett.*, 81(17):3563–3566, Oct 1998.
- [241] A Apostolakis et al. An epr experiment testing the non-separability of the ψ_{000} wave function. *Physics Letters B*, 422(1–4):339–348, 1998.
- [242] N. Gisin and A. Go. Epr test with photons and kaons: Analogies. *American Journal of Physics*, 69(3):264–270, 2001.
- [243] Cirel’son B. S. Quantum generalizations of bell’s inequality. *Letters in Mathematical Physics*, 4(2):93–100, 1980.
- [244] Moshe Shapiro and Paul Brumer. *Quantum Control of Molecular Processes*. Wiley-VCH, 2011.
- [245] R. W. Boyd. *Nonlinear Optics*. Elsevier, 3rd edition, 2008.
- [246] G. I. Papadimitriou. Optical switching: Switch fabrics, techniques, and architectures. *J. Lightw. Technol.*, 21:384, 2003.

- [247] C. C. Gerry and P. L. Knight. *Introductory Quantum Optics*. Cambridge University Press, 2005.
- [248] M. D. Lukin and A. Imamoglu. Nonlinear optics and quantum entanglement of ultraslow single photons. *Phys. Rev. Lett.*, 84:1419, 2000.
- [249] A. K. Mohapatra et al. A giant electro-optic effect using polarizable dark states. *Nat Phys*, 4:890–894, 2008.
- [250] J. D. Pritchard et al. Cooperative atom-light interaction in a blockaded rydberg ensemble. *Phys. Rev. Lett.*, 105:193603, 2010.
- [251] S. Sevincli, N. Henkel, C. Ates, and T. Pohl. Nonlocal nonlinear optics in cold rydberg gases. *Phys. Rev. Lett.*, 107:153001, 2011.
- [252] A. Blais et al. Cavity quantum electrodynamics for superconducting electrical circuits: An architecture for quantum computation. *Phys. Rev. A*, 69:062320, 2004.
- [253] A. Wallraff et al. Strong coupling of a single photon to a superconducting qubit using circuit quantum electrodynamics. *Nature*, 431:162–167, 2004.
- [254] M. A. Castellanos-Beltran et al. Amplification and squeezing of quantum noise with a tunable josephson metamaterial. *Nat Phys*, 4:929–931, 2008.
- [255] C. Lang et al. Observation of resonant photon blockade at microwave frequencies using correlation function measurements. *Phys. Rev. Lett.*, 106:243601, 2011.
- [256] C. Emary, B. Trauzettel, and C. W. J. Beenakker. Emission of polarization-entangled microwave photons from a pair of quantum dots. *Phys. Rev. Lett.*, 95:127401, 2005.
- [257] Allcock Philip, Jenkins Robert D., and Andrews David L. Laser-assisted resonance-energy transfer. *Phys. Rev. A*, 61(2):023812, Jan 2000.
- [258] Shapiro E. A., Milner V., Menzel-Jones C., and Shapiro M. Piecewise adiabatic passage with a series of femtosecond pulses. *Phys. Rev. Lett.*, 99(3):033002, Jul 2007.
- [259] Shapiro Evgeny A., Pe'er Avi, Ye Jun, and Shapiro Moshe. Piecewise adiabatic population transfer in a molecule via a wave packet. *Phys. Rev. Lett.*, 101(2):023601, Jul 2008.

- [260] Paul Brumer and Moshe Shapiro. Coherence chemistry: controlling chemical reactions [with lasers]. *Accounts of Chemical Research*, 22(12):407–413, 1989.
- [261] Clauser John F., Horne Michael A., Shimony Abner, and Holt Richard A. Proposed experiment to test local hidden-variable theories. *Phys. Rev. Lett.*, 23(15):880–884, Oct 1969.

Appendix A

Effective Hamiltonian for a molecule in a far-off resonant field

In this Appendix a detailed derivation of the light-shift operator \hat{H}_{AC} in Eq. (2.32) is provided. The starting point of the derivation is the time-dependent Schrödinger equation for the state vector

$$i\hbar \frac{d}{dt} |\Psi(t)\rangle = \hat{\mathcal{H}} |\Psi(t)\rangle, \quad (\text{A.1})$$

where $\hat{\mathcal{H}} = \hat{H}_{\text{mol}} + \hat{V}(t)$. The eigenstates of the molecular Hamiltonian \hat{H}_{mol} are denoted as $|evr\rangle$ and describe the electronic (e), vibrational (v) and rotational (r) degrees of freedom. The light-matter interaction Hamiltonian $\hat{V}(t)$ can be written as

$$\hat{V}(t) = -\mathbf{d} \cdot \mathbf{E}(\mathbf{r}, t) = -\mathbf{d} \cdot \left[\mathbf{E}^{(+)}(\mathbf{r}, t) e^{-i\omega t} + \mathbf{E}^{(-)}(\mathbf{r}, t) e^{i\omega t} \right], \quad (\text{A.2})$$

where the periodic time-dependence of the electric field has been separated into its usual positive and negative frequency components. The complex amplitudes satisfy $\mathbf{E}^{(-)} = [\mathbf{E}^{(+)}]^*$. The remaining time-dependence of the field amplitudes is

kept to account for pulsed interactions. The state vector $|\Psi(t)\rangle$ can be written as

$$|\Psi(t)\rangle = \sum_r C_{e_i v_i r}(t) |e_i v_i r\rangle e^{-iE_{e_i v_i r} t / \hbar} + \sum_{e_j, v_j, r} C_{e_j v_j r}(t) |e_j v_j r\rangle e^{-iE_{e_j v_j r} t / \hbar}, \quad (\text{A.3})$$

where the contribution of the initial state has been singled out ($i \neq j$). Inserting this expression in Eq. (A.1) and multiplying the resulting expression by $\langle e_i v_i n' | \exp(\frac{i}{\hbar} E_{e_i v_i r'} t)$ gives the set of coupled first-order differential equations for the coefficients of the initial vibronic state (for notational convenience we set $|e_i v_i r\rangle \equiv |ir\rangle$)

$$\begin{aligned} i\hbar \frac{d}{dt} C_{ir'}(t) &= \sum_r C_{ir}(t) \langle ir' | \hat{V}(t) | ir \rangle e^{i(E_{ir'} - E_{ir})t / \hbar} \\ &+ \sum_r \sum_{j \neq i} C_{jr}(t) \langle ir' | \hat{V}(t) | jr \rangle e^{i(E_{ir'} - E_{jr})t / \hbar}. \end{aligned} \quad (\text{A.4})$$

The equations for the coefficients $C_{jr}(t)$ are obtained by inserting Eq. (A.3) into Eq. (A.1), and multiplying the resulting expression by $\langle e_j v_j r' | \exp(iE_{e_j v_j r'} t / \hbar)$ gives

$$\begin{aligned} i\hbar \frac{d}{dt} C_{j'r'}(t) &= \sum_r C_{ir}(t) \langle j'r' | \hat{V}(t) | ir \rangle e^{i(E_{j'r'} - E_{ir})t / \hbar} \\ &+ \sum_r \sum_{j' \neq i} C_{jr}(t) \langle j'r' | \hat{V}(t) | jr \rangle e^{i(E_{j'r'} - E_{jr})t / \hbar}. \end{aligned} \quad (\text{A.5})$$

The closed system of coupled equations (A.4) and (A.5) derive directly from the Schrödinger equation and do not involve any approximation. If the molecule is initially in a state within the vibronic state $|e_i v_i\rangle$, then when the frequency ω of the light-matter interaction operator $\hat{V}(t)$ in Eq. (A.2) is far detuned with respect to the transition frequency $E_{in} - E_{jn}$ for $i \neq j$, the population of higher vibronic states can be neglected in Eq. (A.5). The resulting equation can be integrated by assuming the electric field amplitudes $\mathbf{E}^{(\pm)}(\mathbf{r}, t)$ and the state amplitudes in the initial vibronic state $C_{ir}(t)$ vary much slowly than terms oscillating at the frequency $(E_{j'r'} - E_{ir}) / \hbar \mp \omega$. Since $C_{j'r'}(t=0) = 0$, the integrated amplitude from Eq. A.5

can be written as

$$C_{j'r'}(t) = \sum_r \left\{ \frac{\langle j'r' | \mathbf{d} \cdot \mathbf{E}^{(+)} | ir \rangle}{E_{j'r'} - E_{ir} - \hbar\omega} \left[e^{i(\omega_{j'r',ir} - \omega)t} - 1 \right] + \frac{\langle j'r' | \mathbf{d} \cdot \mathbf{E}^{(-)} | ir \rangle}{E_{j'r'} - E_{ir} + \hbar\omega} \left[e^{i(\omega_{j'r',ir} + \omega)t} - 1 \right] \right\} C_{ir}(t), \quad (\text{A.6})$$

where $\hbar\omega_{j'r',ir} = E_{j'r'} - E_{ir}$. In the far-detuned limit $\hbar\omega \ll E_{e'v'n'} - E_{eiv_in}$, both terms in the above equation contribute equally to the summation. Inserting Eq. (A.6) in the second term of Eq. (A.4), substituting Eq. (A.2) and rearranging indices we obtain the equation for the evolution of the rotational manifold in the initial vibronic state

$$\begin{aligned} i\hbar \frac{d}{dt} C_{ir'} &= \sum_{r''} C_{ir''}(t) \langle ir' | \hat{V}(t) | ir'' \rangle e^{i(E_{ir'} - E_{ir''})t/\hbar} \\ &\quad - \sum_{r''} \sum_{jr} C_{ir''}(t) \left[\langle ir' | \mathbf{d} \cdot \mathbf{E}^{(+)} | jr \rangle e^{i(\omega_{ir',jn} - \omega)t} + \langle ir' | \mathbf{d} \cdot \mathbf{E}^{(-)} | jr \rangle e^{i(\omega_{ir',jn} + \omega)t} \right] \\ &\quad \times \left[\frac{\langle jr | \mathbf{d} \cdot \mathbf{E}^{(+)} | ir'' \rangle}{E_{jr} - E_{ir''} - \hbar\omega} \left(e^{i(\omega_{jr,ir''} - \omega)t} - 1 \right) + \frac{\langle jr | \mathbf{d} \cdot \mathbf{E}^{(-)} | ir'' \rangle}{E_{jr} - E_{ir''} + \hbar\omega} \left(e^{i(\omega_{jr,ir''} + \omega)t} - 1 \right) \right] \end{aligned} \quad (\text{A.7})$$

The first term in this expression corresponds to single-photon light-matter interactions involving rotational degrees of freedom, which can be ignored if the field is far-detuned from the rotational transition frequencies. The second term contains the two-photon contributions to the state evolution. The time-dependence of the two-photon kernel can be simplified by ignoring the contributions that depend on the light frequency ω . Only two terms in the evolution kernel are time-independent, which lead to the approximate Hamiltonian evolution for rotational states

$$i\hbar \frac{d}{dt} C_{ir'}(t) = \sum_{r''} C_{ir''}(t) \langle r' | \hat{H}_{AC} | r'' \rangle e^{i(E_{ir'} - E_{ir''})t/\hbar}, \quad (\text{A.8})$$

where the effective Hamiltonian can be written as

$$\hat{H}_{AC} = - \sum_j \frac{\langle i | \mathbf{d} \cdot \mathbf{E}^{(-)} | j \rangle \langle j | \mathbf{d} \cdot \mathbf{E}^{(+)} | i \rangle}{E_j - E_i - \hbar\omega} + \frac{\langle i | \mathbf{d} \cdot \mathbf{E}^{(+)} | j \rangle \langle j | \mathbf{d} \cdot \mathbf{E}^{(-)} | i \rangle}{E_j - E_i + \hbar\omega}. \quad (\text{A.9})$$

The rotational state summation in Eq. (A.9) has been ignored because the light-frequency is far-detuned from the rotational transition frequencies.

The matrix elements of \hat{H}_{AC} in Eq. (A.8) can be written in a more convenient form by expanding the electric field amplitudes and the dipole operator in spherical basis using the definition [143]

$$\mathbf{A} = \sum_q A_q \hat{\mathbf{e}}_q^*, \quad (\text{A.10})$$

where $q = -1, 0, 1$. Equation (A.9) can be rewritten as

$$\hat{H}_{AC} = -\mathbf{E}^{(+)} \cdot \overleftrightarrow{\alpha}(\omega_-) \cdot \mathbf{E}^{(-)} - \mathbf{E}^{(-)} \cdot \overleftrightarrow{\alpha}(\omega_+) \cdot \mathbf{E}^{(+)} \quad (\text{A.11})$$

where the positive and negative frequency components of the polarizability tensor are given by

$$\overleftrightarrow{\alpha}(\omega_{\pm}) = \sum_j \frac{\langle i|\mathbf{d}|j\rangle\langle j|\mathbf{d}|i\rangle}{E_j - E_i \pm \hbar\omega}. \quad (\text{A.12})$$

Expanding the dipole operator \mathbf{d} using Eq. (A.10) we write the polarizability tensor as

$$\overleftrightarrow{\alpha}(\omega_-) = \sum_{q,q'} \left[\sum_j \frac{\langle i|d_q^\dagger|j\rangle\langle j|d_{q'}|i\rangle}{E_j - E_i - \hbar\omega} \right] \hat{\mathbf{e}}_q \otimes \hat{\mathbf{e}}_{q'}^*, \quad (\text{A.13})$$

and

$$\overleftrightarrow{\alpha}(\omega_+) = \sum_{q,q'} \left[\sum_j \frac{\langle i|d_{q'}|j\rangle\langle j|d_q^\dagger|i\rangle}{E_j - E_i + \hbar\omega} \right] \hat{\mathbf{e}}_{q'}^* \otimes \hat{\mathbf{e}}_q. \quad (\text{A.14})$$

The electric field amplitudes $\mathbf{E}^{(\pm)}$ can also be expanded in spherical basis using Eq. (A.10) and its complex conjugate. Using Eqs. (A.13) and (A.14), the effective light-matter Hamiltonian \hat{H}_{AC} is written as in Eq. (2.32)

$$\hat{H}_{AC} = - \sum_{p,p'} \alpha_{p,p'}(\omega) E_p(\mathbf{r}) E_p^*(\mathbf{r}), \quad (\text{A.15})$$

where $E_p(\mathbf{r}) \equiv E_p^{(+)}(\mathbf{r})$ and the components of the dynamical polarizability tensor in spherical basis are given by

$$\alpha_{p,p'}(\omega) = \sum_j \frac{\langle i|d_p^\dagger|j\rangle\langle j|d_{p'}|i\rangle}{E_j - E_i - \hbar\omega} + \frac{\langle i|d_{p'}|j\rangle\langle j|d_p^\dagger|i\rangle}{E_j - E_i + \hbar\omega}. \quad (\text{A.16})$$

Appendix B

Dipole-dipole interaction in spherical tensor form

In this appendix we derive Eq. (2.48) using basic angular momentum algebra, assuming that the intermolecular axis between the interacting molecules is fixed in space, but the relative distance between the molecules is arbitrary.

Let us denote the dipole moments of molecules A and B as \mathbf{d}_A and \mathbf{d}_B , dipole-dipole interaction is given by the classical expression

$$V_{dd}(\mathbf{R}) = \left(\frac{1}{|\mathbf{R}|^3} \right) \{ \mathbf{d}_A \cdot \mathbf{d}_B - 3(\mathbf{d}_A \cdot \hat{\mathbf{R}}) \cdot (\mathbf{d}_B \cdot \hat{\mathbf{R}}) \}, \quad (\text{B.1})$$

where $\hat{\mathbf{R}} = \mathbf{R}/|\mathbf{R}|$. The term $(\mathbf{d}_A \cdot \hat{\mathbf{R}}) \cdot (\mathbf{d}_B \cdot \hat{\mathbf{R}})$ has the tensorial form [143]

$$(\mathbf{d}_A \cdot \hat{\mathbf{R}}) \cdot (\mathbf{d}_B \cdot \hat{\mathbf{R}}) = \left[\left[\mathbf{d}_A^{(1)} \otimes \hat{\mathbf{R}}^{(1)} \right]^{(0)} \otimes \left[\mathbf{d}_B^{(1)} \otimes \hat{\mathbf{R}}^{(1)} \right]^{(0)} \right]^{(0)}, \quad (\text{B.2})$$

which can be recoupled in order to separate the dipole tensor from the position tensors. The recoupling of these four tensors involves the evaluation of a $9j$ symbol

with a vanishing element, giving

$$(\mathbf{d}_A \cdot \hat{\mathbf{R}}) \cdot (\mathbf{d}_B \cdot \hat{\mathbf{R}}) = \sum_k (2k+1) \begin{Bmatrix} 1 & 1 & k \\ 1 & 1 & k \\ 0 & 0 & 0 \end{Bmatrix} \left[[\mathbf{d}_A^{(1)} \otimes \mathbf{d}_B^{(1)}]^{(k)} \otimes [\hat{\mathbf{R}}^{(1)} \otimes \hat{\mathbf{R}}^{(1)}]^{(k)} \right]^{(0)}. \quad (\text{B.3})$$

The coupling to two tensors of the same rank into a zero-rank tensor is given by

$$\left[T^{(k)} \otimes U^{(k)} \right]_0^{(0)} = (2k+1)^{-1/2} \sum_q (-1)^{k-q} T(k, q) \cdot U(k, -q), \quad (\text{B.4})$$

and we have that $\vec{T} \cdot \vec{U} = -3^{1/2} [T^{(1)} \otimes U^{(1)}]^{(0)}$. $T^{(k)}$ and $U^{(k)}$ are irreducible spherical tensors of rank k , acting on different spaces. We use Eqs. (B.2) to (B.4) to rewrite Eq. (B.1) as

$$\hat{V}_{dd}(\mathbf{R}) = -\frac{3}{|\mathbf{R}|^3} \sum_q (-1)^{-q} [\mathbf{d}_A^{(1)} \otimes \mathbf{d}_B^{(1)}]_q^{(2)} [\hat{\mathbf{R}}^{(1)} \otimes \hat{\mathbf{R}}^{(1)}]_{-q}^{(2)}, \quad (\text{B.5})$$

which is a summation over the products of the components of two rank-two tensors, one depends on the orientation of the electric dipole moments of the molecules, and the other depends on the coordinates of the unit vector $\hat{\mathbf{R}}$. The contraction $T_{-q}^{(2)} = [\hat{\mathbf{R}}^{(1)} \otimes \hat{\mathbf{R}}^{(1)}]_{-q}^{(2)}$ can be written in terms of spherical harmonics as [143]

$$T_{-q}^{(2)} = \left(\frac{8\pi}{15} \right)^{1/2} Y_{2,-q}(\theta, \phi). \quad (\text{B.6})$$

Thus, by using Eq. (B.6), we rewrite Eq. (B.5) to obtain

$$\hat{V}_{dd}(\mathbf{R}) = -\sqrt{\frac{6\pi}{5}} \left(\frac{2}{R^3} \right) \sum_q (-1)^{-q} Y_{2,-q}(\theta_R, \phi_R) [\mathbf{d}_A^{(1)} \otimes \mathbf{d}_B^{(1)}]_q^{(2)}. \quad (\text{B.7})$$

We are interested in evaluating the matrix elements $\hat{V}_{dd}(\mathbf{R})$ in the uncoupled basis $\{|N_A M_{N_A}\rangle |N_B M_{N_B}\rangle\}$. The matrix element of $\hat{V}_{dd}(\mathbf{R})$ can be evaluated by specifying the orientation of the vector $\hat{\mathbf{R}}$ with respect to the space-fixed z axis.

Substitution of the expression for the spherical harmonics in Eq. (B.7) gives

$$\begin{aligned} \hat{V}_{dd}(\mathbf{R}) = & -\frac{\sqrt{3}}{R^3} \left\{ \frac{\sqrt{2}}{2} (3 \cos^2 \theta - 1) [\mathbf{d}_A^{(1)} \otimes \mathbf{d}_B^{(1)}]_0^{(2)} \right. \\ & + \sqrt{3} e^{i\phi} \cos \theta \sin \theta [\mathbf{d}_A^{(1)} \otimes \mathbf{d}_B^{(1)}]_{-1}^{(2)} - \sqrt{3} e^{-i\phi} \cos \theta \sin \theta [\mathbf{d}_A^{(1)} \otimes \mathbf{d}_B^{(1)}]_1^{(2)} \\ & \left. + \frac{\sqrt{3}}{2} e^{i2\phi_R} \sin^2 \theta [\mathbf{d}_A^{(1)} \otimes \mathbf{d}_B^{(1)}]_{-2}^{(2)} + \frac{\sqrt{3}}{2} e^{-i2\phi_R} \sin^2 \theta [\mathbf{d}_A^{(1)} \otimes \mathbf{d}_B^{(1)}]_2^{(2)} \right\}. \end{aligned} \quad (\text{B.8})$$

The operator $\hat{V}_{dd}(R, \theta_R)$ is thus a sum of terms with distinct physical meaning according to the Wigner-Eckart theorem [143]; two terms associated with transitions that change the total projection $M_{N_A} + M_{N_B}$ by two units, two that change the value by one unit, and one term that conserves the total projection. In order to evaluate the matrix elements of the operator in Eq. (B.8), using the basis $|N_A M_{N_A}\rangle |N_B M_{N_B}\rangle$, the rank-two tensors involving the dipole operators \mathbf{d}_A and \mathbf{d}_B can be decoupled to give

$$[\mathbf{d}_A^{(1)} \otimes \mathbf{d}_B^{(1)}]_q^{(2)} = (-1)^q (5)^{1/2} \sum_{q_A} \begin{pmatrix} 1 & 1 & 2 \\ q_A & q_B & q \end{pmatrix} d_{q_A}^{(1)} d_{q_B}^{(1)}, \quad (\text{B.9})$$

where $q_A + q_B + q = 0$. The problem is thus reduced to the evaluation of the single-molecule matrix element $\langle N M_N | d_q^{(1)} | N' M'_N \rangle$. The components of the dipole tensor in the space fixed coordinate systems $d_q^{(1)}$ in Eq. (B.9) are related to the permanent dipole moment of the molecule in the the body-fixed z axis by the expression

$$d_{qs}^{(1)} = \sum_{qb=-1}^1 D_{qs,qb}^*(\phi, \theta, \chi) d_{qb}^{(1)} = d_0 D_{qs,0}^*(\phi, \theta, \chi), \quad (\text{B.10})$$

where d_0 is the permanent dipole moment of the molecule, and $D_{qs,qb}^*(\phi, \theta, \chi)$ is an element the inverse rotation matrix. The elements with $q_b = 0$ correspond to the modified spherical harmonics $C_{1,qs}(\phi, \theta)$ [143]. We then use the Wigner-Eckart theorem to evaluate the matrix element of the modified spherical harmonics of rank one as

$$\langle N M_N | C_{1,q} | N' M'_N \rangle = (-1)^{N-M_N} \begin{pmatrix} N & 1 & N' \\ -M_N & q & M'_N \end{pmatrix} \langle N || C^{(1)} || N' \rangle, \quad (\text{B.11})$$

with the reduced matrix element

$$\langle N || C^{(1)} || N' \rangle = (-1)^N [(2N+1)(2N'+1)]^{1/2} \begin{pmatrix} N & 1 & N' \\ 0 & 0 & 0 \end{pmatrix}. \quad (\text{B.12})$$

We now use Eqs. (B.12), (B.11), (B.10) and (B.9), to write the the matrix element

$$\begin{aligned} \langle N_A M_{N_A} | \langle N_B M_{N_B} | \hat{V}_{dd}(R, \theta_R) | N'_A M'_{N_A} \rangle | N'_B M'_{N_B} \rangle &= - \left(\frac{d_A d_B}{R^3} \right) (-1)^{-M_{N_A} - M_{N_B}} \\ &\times [(2N_A+1)(2N'_A+1)(2N_B+1)(2N'_B+1)]^{1/2} \begin{pmatrix} N_A & 1 & N'_A \\ 0 & 0 & 0 \end{pmatrix} \begin{pmatrix} N_B & 1 & N'_B \\ 0 & 0 & 0 \end{pmatrix} \\ &\times \left\{ \frac{3\sqrt{5}}{2} e^{-i2\phi} \sin^2 \theta \times D_2 + \frac{3\sqrt{5}}{2} e^{i2\phi_R} \sin^2 \theta \times D_{-2} + \sqrt{\frac{15}{2}} (3 \cos^2 \theta - 1) \times D_0 \right. \\ &\left. - 3\sqrt{5} \sin \theta \cos \theta e^{-i\phi} \times D_1 + 3\sqrt{5} \sin \theta \cos \theta e^{i\phi} \times D_{-1} \right\}, \end{aligned} \quad (\text{B.13})$$

where d_A and d_B are the permanent electric dipole moments of the molecules. This is Eq. (2.48), where we have defined the constants D_k as the summations

$$\begin{aligned} D_{-2} &= \sum_{q_A} \begin{pmatrix} 1 & 1 & 2 \\ q_A & 2-q_A & -2 \end{pmatrix} \begin{pmatrix} N_A & 1 & N'_A \\ -M_{N_A} & q_A & M'_{N_A} \end{pmatrix} \begin{pmatrix} N_B & 1 & N'_B \\ -M_{N_B} & 2-q_A & M'_{N_B} \end{pmatrix} \\ D_2 &= \sum_{q_A} \begin{pmatrix} 1 & 1 & 2 \\ q_A & -2-q_A & 2 \end{pmatrix} \begin{pmatrix} N_A & 1 & N'_A \\ -M_{N_A} & q_A & M'_{N_A} \end{pmatrix} \begin{pmatrix} N_B & 1 & N'_B \\ -M_{N_B} & -2-q_A & M'_{N_B} \end{pmatrix} \\ D_0 &= \sum_{q_A} \begin{pmatrix} 1 & 1 & 2 \\ q_A & -q_A & 0 \end{pmatrix} \begin{pmatrix} N_A & 1 & N'_A \\ -M_{N_A} & q_A & M'_{N_A} \end{pmatrix} \begin{pmatrix} N_B & 1 & N'_B \\ -M_{N_B} & -q_A & M'_{N_B} \end{pmatrix} \\ D_{-1} &= \sum_{q_A} \begin{pmatrix} 1 & 1 & 2 \\ q_A & 1-q_A & -1 \end{pmatrix} \begin{pmatrix} N_A & 1 & N'_A \\ -M_{N_A} & q_A & M'_{N_A} \end{pmatrix} \begin{pmatrix} N_B & 1 & N'_B \\ -M_{N_B} & 1-q_A & M'_{N_B} \end{pmatrix} \\ D_1 &= \sum_{q_A} \begin{pmatrix} 1 & 1 & 2 \\ q_A & -1-q_A & 1 \end{pmatrix} \begin{pmatrix} N_A & 1 & N'_A \\ -M_{N_A} & q_A & M'_{N_A} \end{pmatrix} \begin{pmatrix} N_B & 1 & N'_B \\ -M_{N_B} & -1-q_A & M'_{N_B} \end{pmatrix}. \end{aligned}$$

These quantities are labeled according to their effect on the total projections $M_{N_A} + M_{N_B}$. In practice, once the quantum numbers in the bra and the ket are chosen, only

one of these constants will be non-zero. In fact, only a single term in the a given sum survives the selection rules imposed by the 3-j symbols.

Appendix C

Hyperfine structure of closed-shell diatomic molecules

In this Appendix we provide expressions for the matrix elements of the molecular Hamiltonian that describes the hyperfine structure of the rotational levels. The molecular Hamiltonian in the absence of external fields is defined in Eq. (2.13) and the Zeeman interaction in Eq. (2.20). Below we present the matrix elements for each Hamiltonian term in two basis states relevant for this thesis:

- (a) $|(NI)FM_F\rangle$ Fully coupled basis (weak fields),
- (b) $|NM_N\rangle|(I_1I_2)IM_I\rangle$ Spin coupled basis (intermediate fields),

The use of either basis is arbitrary since a state in a given basis can be written as a linear combination of states in another basis. However, the choice of the basis is physically motivated by the strength of an external DC electric or magnetic field, a particular choice of basis states is suitable to represent the Hamiltonian matrix in a form close to diagonal.

For each matrix element in the fully coupled basis, we outline the steps of its derivation using standard results of angular momentum algebra [142, 143]. The expressions for the matrix elements in other basis sets can be obtained using the same methods.

C.1 Fully coupled basis: $\mathbf{I} = \mathbf{I}_1 + \mathbf{I}_2$ and $\mathbf{N} + \mathbf{I} = \mathbf{F}$

Electric quadrupole interaction \hat{H}_Q

Good quantum numbers: F , and M_F .

(a) *Decouple total nuclear spin and rotational angular momenta for Atom 1*

$$\begin{aligned} \langle (NI)FM_F | \hat{H}_{Q_1} | (N'I')FM_F \rangle &= \\ &= (-1)^{N'+F+I} \begin{Bmatrix} I' & N' & F \\ N & I & 2 \end{Bmatrix} \\ &\quad \times \langle N || -e\hat{T}^{(2)}(\nabla E_1) || N' \rangle \langle (I_1 I_2)I || \hat{T}^{(2)}(Q_1) || (I_1 I_2)I' \rangle \end{aligned}$$

(b) *Decouple quadrupole reduced matrix element for atom 1*

$$\begin{aligned} \langle (I_1 I_2)I || \hat{T}^{(2)}(Q_1) || (I_1 I_2)I' \rangle &= \\ &= (-1)^{I'+I_1+I_2} [(2I+1)(2I'+1)]^{1/2} \begin{Bmatrix} I_1 & I' & I_2 \\ I & I_1 & 2 \end{Bmatrix} \langle I_1 || \hat{T}^{(2)}(Q_1) || I_1 \rangle \end{aligned}$$

(c) *Insert definitions for the reduced matrix elements*

$$\langle N || -e\hat{T}^{(2)}(\nabla E_1) || N' \rangle = (-1)^N [(2N+1)(2N'+1)]^{1/2} \begin{pmatrix} N & 2 & N' \\ 0 & 0 & 0 \end{pmatrix} \frac{eq}{2}$$

$$\langle I_1 || \hat{T}^{(2)}(Q_1) || I_1 \rangle = \frac{Q}{2} \begin{pmatrix} I_1 & 2 & I_1 \\ -I_1 & 0 & I_1 \end{pmatrix}^{-1}$$

(e) Repeat procedure for Atom 2 and collect results to obtain final expression

$$\begin{aligned}
& \langle (NI)FM_F | \hat{H}_Q | (N'I')FM_F \rangle = \\
& = (-1)^{F+N'+N+I+I_1+I_2} [(2N+1)(2N'+1)(2I+1)(2I'+1)]^{1/2} \\
& \times \begin{pmatrix} N & 2 & N' \\ 0 & 0 & 0 \end{pmatrix} \begin{Bmatrix} I' & N' & F \\ N & I & 2 \end{Bmatrix} \\
& \times \left[(-1)^{I'} \begin{pmatrix} I_1 & 2 & I_1 \\ -I_1 & 0 & I_1 \end{pmatrix}^{-1} \begin{Bmatrix} I_1 & I' & I_2 \\ I & I_1 & 2 \end{Bmatrix} \frac{(eqQ)_1}{4} \right. \\
& \left. + (-1)^I \begin{pmatrix} I_2 & 2 & I_2 \\ -I_2 & 0 & I_2 \end{pmatrix}^{-1} \begin{Bmatrix} I_2 & I' & I_1 \\ I & I_2 & 2 \end{Bmatrix} \frac{(eqQ)_2}{4} \right] \quad (C.1)
\end{aligned}$$

Note: Coupling between rotational levels can be ignored because $eqQ \ll B_e$.

Scalar spin-spin interaction \hat{H}_{SC}

Good quantum numbers: N , I , F , and M_F .

(a) Rewrite the scalar product

$$\mathbf{I}_1 \cdot \mathbf{I}_2 = \frac{1}{2} \{ \mathbf{I}^2 - \mathbf{I}_1^2 - \mathbf{I}_2^2 \}$$

(b) Decouple total spin and rotational angular momenta for \mathbf{I}^2 term

$$\begin{aligned}
& \langle (NI)FM_F | \mathbf{I}^2 | (NI)FM_F \rangle = \\
& = (-1)^{F-M_F} \begin{pmatrix} F & 0 & F \\ -M_F & 0 & M_F \end{pmatrix} \langle (NI)F || \mathbf{I}^2 || (NI)F \rangle \\
& = (-1)^{F+N+I} (2F+1)^{1/2} \begin{Bmatrix} I & F & N \\ F & I & 0 \end{Bmatrix} \langle I || \mathbf{I}^2 || I \rangle
\end{aligned}$$

(c) Decouple total spin and rotational angular momenta for \mathbf{I}_1^2 term

$$\begin{aligned}
& \langle (NI)FM_F | \mathbf{I}_1^2 | (NI)FM_F \rangle = \\
& = (-1)^{F+N+I} (2F+1)^{1/2} \begin{Bmatrix} I & F & N \\ F & I & 0 \end{Bmatrix} \langle (I_1 I_2)I || \mathbf{I}_1^2 || (I_1 I_2)I \rangle
\end{aligned}$$

(d) *Decouple the nuclear spin of individual atoms*

$$\begin{aligned} \langle (I_1 I_2) I || \mathbf{I}_1^2 || (I_1 I_2) I \rangle &= \\ &= (-1)^{I+I_1+I_2} (2I+1) \left\{ \begin{array}{ccc} I_1 & I & I_2 \\ I & I_1 & 0 \end{array} \right\} \langle I_1 || \mathbf{I}_1^2 || I_1 \rangle \end{aligned}$$

(e) *Insert expression for reduced matrix elements*

$$\langle j || \mathbf{j}^2 || j \rangle = j(j+1)(2j+1)^{1/2}$$

(e) *Repeat steps (c)-(d) for the term \mathbf{I}_2^2 and collect results to obtain final expression*

$$\langle (NI) F M_F | \hat{H}_{\text{SC}} | (NI) F M_F \rangle = \frac{c_4}{2} [I(I+1) - I_1(I_1+1) - I_2(I_2+1)] \quad (\text{C.2})$$

Nuclear spin-rotation interaction \hat{H}_{SR}

Good quantum numbers: N , F , and M_F .

(a) *Decouple total nuclear spin and rotational angular momenta for Atom 1*

$$\langle (NI) F M_F | \mathbf{N} \cdot \mathbf{I}_1 | (NI') F M_F \rangle = (-1)^{N'+F+I} \left\{ \begin{array}{ccc} I' & N & F \\ N & I & 1 \end{array} \right\} \langle N || \mathbf{N} || N \rangle \langle I || \mathbf{I}_1 || I' \rangle$$

(b) *Decouple nuclear spin reduced matrix element for Atom 1*

$$\begin{aligned} \langle (I_1 I_2) I || \mathbf{I}_1 || (I_1 I_2) I' \rangle &= [(2I+1)(2I'+1)]^{1/2} (-1)^{I'+I_1+I_2+1} \\ &\times \left\{ \begin{array}{ccc} I_1 & I' & I_2 \\ I & I_1 & 1 \end{array} \right\} \langle I_1 || \mathbf{I}_1 || I_1 \rangle \end{aligned} \quad (\text{C.3})$$

$$\langle I_1 || \mathbf{I}_1 || I_1 \rangle = [I_1(I_1+1)(2I_1+1)]^{1/2}$$

(c) Repeat procedure for Atom 2 and collect results to obtain final expression

$$\begin{aligned}
& \langle (NI)FM_F | \hat{H}_{\text{SR}} | (N'I')FM_F \rangle = \\
& = (-1)^{F+N+I+I_1+I_2+1} [N(2N+1)(N+1)(2I+1)(2I'+1)]^{1/2} \\
& \quad \times \left\{ \begin{matrix} I' & N & F \\ N & I & 1 \end{matrix} \right\} \left[(-1)^{I'} \left\{ \begin{matrix} I_1 & I' & I_2 \\ I & I_1 & 1 \end{matrix} \right\} c_1 + (-1)^I \left\{ \begin{matrix} I_2 & I' & I_1 \\ I & I_2 & 1 \end{matrix} \right\} c_2 \right]
\end{aligned} \tag{C.4}$$

Tensor spin-spin interaction \hat{H}_{T}

Good quantum numbers: F and M_F .

$$\begin{aligned}
& \langle (NI)FM_F | \hat{H}_{\text{T}} | (N'I')FM_F \rangle = \\
& = -c_3 \sqrt{30} (-1)^{N+N'+F+I} \begin{pmatrix} N & 2 & N' \\ 0 & 0 & 0 \end{pmatrix} [(2I+1)(2I'+1)]^{1/2} \\
& \quad \times [(2N+1)(2N'+1)]^{1/2} \times [I_1(I_1+1)(2I_1+1)I_2(I_2+1)(2I_2+1)]^{1/2} \\
& \quad \times \left\{ \begin{matrix} I' & N' & F \\ N & I & 2 \end{matrix} \right\} \left\{ \begin{matrix} I_1 & I_1 & 1 \\ I_2 & I_2 & 1 \\ I & I' & 2 \end{matrix} \right\}
\end{aligned} \tag{C.5}$$

Zeeman interaction \hat{H}_B

Magnetic field along Z axis. Good quantum numbers: N, M_F

$$\begin{aligned}
\langle (NI)FM_F | \hat{H}_B | (NI')F'M_F \rangle = & \\
= & -\mu_B B_Z (-1)^{N+I'+I_1+I_2-M_F} [(2F+1)(2F'+1)(2I+1)(2I'+1)]^{1/2} \\
& \times \left\{ \begin{matrix} I' & F' & N \\ F & I & 1 \end{matrix} \right\} \left(\begin{matrix} F & 1 & F' \\ -M_F & 0 & M'_F \end{matrix} \right) \\
& \times \left[g_1 (-1)^{I'} [I_1(I_1+1)(2I_1+1)]^{1/2} \left\{ \begin{matrix} I_1 & I' & I_2 \\ I & I_1 & 1 \end{matrix} \right\} \right. \\
& \left. + g_2 (-1)^I [I_2(I_2+1)(2I_2+1)]^{1/2} \left\{ \begin{matrix} I_2 & I' & I_1 \\ I & I_2 & 1 \end{matrix} \right\} \right] \quad (C.6)
\end{aligned}$$

Stark interaction \hat{H}_E

Electric field along Z axis. Good quantum numbers: I, M_F

$$\begin{aligned}
\langle (NI)FM_F | \hat{H}_E | (N'I)F'M_F \rangle = & \\
= & dE_Z (-1)^{F+F'+I-M_F} [(2F+1)(2F'+1)(2N+1)(2N'+1)]^{1/2} \\
& \times \left\{ \begin{matrix} N' & F' & I \\ F & N & 1 \end{matrix} \right\} \left(\begin{matrix} F & 1 & F' \\ -M_F & 0 & M'_F \end{matrix} \right) \left(\begin{matrix} N & 1 & N' \\ 0 & 0 & 0 \end{matrix} \right) \quad (C.7)
\end{aligned}$$

C.2 Spin coupled basis: $\mathbf{I} = \mathbf{I}_1 + \mathbf{I}_2$

Electric quadrupole interaction \hat{H}_Q

Good quantum number: N , and $M_N + M_I$. ($\Delta N = \pm 2$ coupling ignored)

$$\begin{aligned}
& \langle NM_N IM_I | \hat{H}_Q | NM'_N I' M'_I \rangle = \\
& = (-1)^{I+I_1+I_2-M_N-M_I} [(2N+1)(2N'+1)(2I+1)(2I'+1)]^{1/2} \begin{pmatrix} N & 2 & N \\ 0 & 0 & 0 \end{pmatrix} \\
& \times \left[\frac{(eqQ)_1}{4} (-1)^{I'} \begin{Bmatrix} I_1 & I' & I_2 \\ I & I_1 & 2 \end{Bmatrix} \begin{pmatrix} I_1 & 2 & I_1 \\ -I_1 & 0 & I_1 \end{pmatrix}^{-1} \right. \\
& \quad \left. + \frac{(eqQ)_2}{4} (-1)^I \begin{Bmatrix} I_2 & I' & I_1 \\ I & I_2 & 2 \end{Bmatrix} \begin{pmatrix} I_2 & 2 & I_2 \\ -I_2 & 0 & I_2 \end{pmatrix}^{-1} \right] \\
& \times \sum_{p=-2}^2 (-1)^p \begin{pmatrix} N & 2 & N \\ -M_N & p & M'_N \end{pmatrix} \begin{pmatrix} I & 2 & I' \\ M_I & -p & M'_I \end{pmatrix} \tag{C.8}
\end{aligned}$$

Nuclear spin-rotation interaction \hat{H}_{SR}

Good quantum numbers: N , M_N , M_I .

$$\begin{aligned}
& \langle NM_N IM_I | \hat{H}_{SR} | NM'_N I' M'_I \rangle = \\
& = (-1)^{N+I+I_1+I_2-M_N-M_I+1} [N(N+1)(2N+1)(2I+1)(2I'+1)]^{1/2} \\
& \times \left[c_1 (-1)^{I'} [I_1(I_1+1)(2I_1+1)]^{1/2} \begin{Bmatrix} I_1 & I' & I_2 \\ I & I_1 & 1 \end{Bmatrix} \right. \\
& \quad \left. + c_2 (-1)^I [I_2(I_2+1)(2I_2+1)]^{1/2} \begin{Bmatrix} I_2 & I' & I_1 \\ I & I_2 & 1 \end{Bmatrix} \right] \\
& \times \sum_{p=-1}^1 (-1)^p \begin{pmatrix} N & 1 & N' \\ -M_N & p & M'_N \end{pmatrix} \begin{pmatrix} I & 1 & I' \\ M_I & -p & M'_I \end{pmatrix} \tag{C.9}
\end{aligned}$$

Scalar spin-spin interaction \hat{H}_{SC}

Good quantum numbers: N, M_N, I, M_I

$$\langle NM_N IM_I | \hat{H}_{\text{SC}} | NM_N IM_I \rangle = \frac{c_4}{2} [I(I+1) - I_1(I_1+1) - I_2(I_2+1)] \quad (\text{C.10})$$

Tensor spin-spin interaction \hat{H}_{T}

Good quantum numbers: $N, M_N + M_I$. ($\Delta N = \pm 2$ coupling ignored)

$$\begin{aligned} \langle NM_N IM_I | \hat{H}_{\text{T}} | NM_N I' M_I \rangle = \\ = -c_3 \sqrt{30} (-1)^{I-M_N-M_I} (2N+1) \begin{pmatrix} N & 2 & N \\ 0 & 0 & 0 \end{pmatrix} [(2I+1)(2I'+1)]^{1/2} \\ \times [I_1(I_1+1)(2I_1+1)I_2(I_2+1)(2I_2+1)]^{1/2} \begin{Bmatrix} I_1 & I_1 & 1 \\ I_2 & I_2 & 1 \\ I & I' & 2 \end{Bmatrix} \\ \times \sum_{p=-2}^2 (-1)^p \begin{pmatrix} N & 2 & N \\ -M_N & p & M'_N \end{pmatrix} \begin{pmatrix} I & 2 & I' \\ -M_I & -p & M'_I \end{pmatrix} \end{aligned} \quad (\text{C.11})$$

Zeeman interaction \hat{H}_{B}

Magnetic field along Z axis. Good quantum numbers: N, M_N, M_I

$$\begin{aligned} \langle NM_N IM_I | \hat{H}_{\text{B}} | NM_N I' M_I \rangle = \\ = \mu_B B_Z (-1)^{I+I_1+I_2-M_I} [(2I+1)(2I'+1)]^{1/2} \begin{pmatrix} I & 1 & I' \\ -M_I & 0 & M_I \end{pmatrix} \\ \times \left[g_1 (-1)^{I'} [I_1(I_1+1)(2I_1+1)]^{1/2} \begin{Bmatrix} I_1 & I' & I_2 \\ I & I_1 & 1 \end{Bmatrix} \right. \\ \left. + g_2 (-1)^I [I_2(I_2+1)(2I_2+1)]^{1/2} \begin{Bmatrix} I_2 & I' & I_1 \\ I & I_2 & 1 \end{Bmatrix} \right] \end{aligned} \quad (\text{C.12})$$

Appendix D

Hamiltonian for an ensemble of interacting molecules

In this appendix we present the derivation of the model Hamiltonian for an ensemble of interacting many-level molecules. The derivation follows closely the treatment in Ref. [99]. In this Appendix many intermediate steps missing in the literature are provided. The starting point is the second-quantized Hamiltonian in Eq. (5.6) ¹

$$\hat{H} = \sum_{i,f} \epsilon_f \hat{b}_{if}^\dagger \hat{b}_{if} + \frac{1}{2} \sum_{i,j \neq i} \sum_{f,f'} \sum_{g,g'} \langle fg | V_{ij} | f'g' \rangle \hat{b}_{if}^\dagger \hat{b}_{jg}^\dagger \hat{b}_{if'} \hat{b}_{jg'}. \quad (\text{D.1})$$

This Hamiltonian can be simplified by restricting the number of matrix elements of the interaction operator \hat{V}_{ij} . In the following we divide the terms in Eq. (D.1) according to the states involved in the interaction. We make use of the normalization condition

$$\sum_f \hat{n}_{if} + \hat{n}_{i0} = 1, \quad (\text{D.2})$$

where $\hat{n}_{if} = \hat{b}_{if}^\dagger \hat{b}_{if}$ is a number operator.

¹The notation in this Appendix differs from the main text in that g here denotes any excited state. The ground state here is denoted by 0.

D.1 Single-particle energies

Using Eq. (D.2), the first term in Eq. (D.1) can be written as

$$\sum_i \left[\epsilon_0 \left(1 - \sum_f \hat{n}_{if} \right) + \sum_f \epsilon_f \hat{n}_{if} \right] = \sum_i \epsilon_0 + \sum_{i,f} (\epsilon_f - \epsilon_0) \hat{n}_{if} \quad (\text{D.3})$$

D.2 Two-body interaction

For simplicity, the summations over site indices $\frac{1}{2} \sum_{ij}$ are omitted in this section. The interaction operator \hat{V}_{ij} is hermitian and its matrix elements are real.

Ground-ground electrostatic interaction $\langle 00 | V_{ij} | 00 \rangle$

This matrix element represents the electrostatic interaction between two ground state molecules. By setting $f' = g' = f = g$ in Eq. (D.1), the corresponding term in Eq. (D.1) can be written as

$$\begin{aligned} \langle 00 | V_{ij} | 00 \rangle \hat{n}_{i0} \hat{n}_{j0} &= \langle 00 | V_{ij} | 00 \rangle \left(1 - \sum_f \hat{n}_{if} \right) \left(1 - \sum_g \hat{n}_{jg} \right) \\ &= \langle 00 | V_{ij} | 00 \rangle \left(1 - \sum_f \hat{n}_{if} - \sum_f \hat{n}_{jf} + \sum_{f,g} \hat{n}_{if} \hat{n}_{jg} \right), \quad (\text{D.4}) \end{aligned}$$

One term does not depend on the occupation of excited states. The remaining terms depend linearly and quadratically on the excited state occupation.

Ground state mediated excitation $\langle f0 | V_{ij} | 00 \rangle = \langle 0f | V_{ij} | 00 \rangle$

These matrix elements describe a transition to an excited state in one molecule, mediated by the presence of another molecule in its ground state. The corresponding

terms in Eq. (D.1) are

$$\begin{aligned}
& \langle f0|V_{ij}|00\rangle \left(\hat{b}_{if}^\dagger \hat{b}_{j0}^\dagger \hat{b}_{i0} \hat{b}_{j0} + \text{h.c.} \right) + \langle 0f|V_{ij}|00\rangle \left(\hat{b}_{i0}^\dagger \hat{b}_{jf}^\dagger \hat{b}_{i0} \hat{b}_{j0} + \text{h.c.} \right) \\
&= \langle f0|V_{ij}|00\rangle \left(\hat{b}_{if}^\dagger \hat{b}_{i0} + \text{h.c.} \right) \left(1 - \sum_g \hat{n}_{jg} \right) \\
&\quad + \langle 0f|V_{ij}|00\rangle \left(\hat{b}_{jf}^\dagger \hat{b}_{j0} + \text{h.c.} \right) \left(1 - \sum_g \hat{n}_{ig} \right)
\end{aligned} \tag{D.5}$$

where h.c. denotes hermitian conjugate.

Excited-ground electrostatic interaction $\langle f0|V_{ij}|g0\rangle = \langle 0f|V_{ij}|0g\rangle$

These matrix elements represent the electrostatic interaction between a molecule in an excited state and another molecule in the ground state. The corresponding terms in Eq. (D.1) are

$$\begin{aligned}
& \langle f0|V_{ij}|g0\rangle \left(\hat{b}_{if}^\dagger \hat{b}_{j0}^\dagger \hat{b}_{ig} \hat{b}_{j0} + \text{h.c.} \right) + \langle 0f|V_{ij}|0g\rangle \left(\hat{b}_{i0}^\dagger \hat{b}_{jf}^\dagger \hat{b}_{i0} \hat{b}_{jg} + \text{h.c.} \right) \\
&= \langle f0|V_{ij}|g0\rangle \left(\hat{b}_{if}^\dagger \hat{b}_{ig} + \hat{b}_{ig}^\dagger \hat{b}_{if} \right) \left(1 - \sum_{f'} \hat{n}_{jf'} \right) \\
&\quad + \langle 0f|V_{ij}|0g\rangle \left(\hat{b}_{jf}^\dagger \hat{b}_{jg} + \hat{b}_{jg}^\dagger \hat{b}_{jf} \right) \left(1 - \sum_{f'} \hat{n}_{if'} \right).
\end{aligned} \tag{D.6}$$

Single-excitation exchange interaction $\langle f0|V_{ij}|0g\rangle = \langle 0f|V_{ij}|g0\rangle$

These matrix elements describe the exchange of an excitation from one molecule to another. The corresponding terms in Eq. (D.1) are (including terms with $g = f$)

$$\langle f0|V_{ij}|0g\rangle \left(\hat{b}_{if}^\dagger \hat{b}_{j0}^\dagger \hat{b}_{i0} \hat{b}_{jg} + \text{h.c.} \right) + \langle 0f|V_{ij}|g0\rangle \left(\hat{b}_{i0}^\dagger \hat{b}_{jf}^\dagger \hat{b}_{ig} \hat{b}_{j0} + \text{h.c.} \right) \tag{D.7}$$

In the second line we used the fact that the creation and annihilation operators commute if they have different indices.

Fission and fusion of excitations $\langle fg|V_{ij}|f'0\rangle = \langle gf|V_{ij}|0f'\rangle$

These class of matrix elements couple states with a single excitation and states with two excitations. One of the allowed processes involves an excited molecule and a ground state molecule. The molecular excitation is split into two excitation residing in each molecule. This process is known as excitation fission. In the hermitian conjugate processes the excitations in two molecules are combined into a single molecule, leaving one molecule in its ground state (excitation fusion). The corresponding terms in Eq. (D.1) are

$$\langle fg|V_{ij}|f'0\rangle \left(\hat{b}_{if}^\dagger \hat{b}_{jg}^\dagger \hat{b}_{if'} \hat{b}_{j0} + \text{h.c.} \right) + \langle gf|V_{ij}|0f'\rangle \left(\hat{b}_{ig}^\dagger \hat{b}_{jf}^\dagger \hat{b}_{i0} \hat{b}_{jf'} + \text{h.c.} \right) \quad (\text{D.8})$$

In the case where at least two of the state indices are equal, the corresponding terms describe the excitation of one molecule induced by the excitation in another molecule. These terms are analogous to the ground-state induced excitations in Eq. (D.5). For $f' = f$ we have the contributions

$$\langle fg|V_{ij}|f0\rangle \left(\hat{b}_{if}^\dagger \hat{b}_{jg}^\dagger \hat{b}_{if} \hat{b}_{j0} + \text{h.c.} \right) + \langle gf|V_{ij}|0f\rangle \left(\hat{b}_{ig}^\dagger \hat{b}_{jf}^\dagger \hat{b}_{i0} \hat{b}_{jf} + \text{h.c.} \right) \quad (\text{D.9})$$

Double-excitation exchange interaction $\langle fg|V_{ij}|00\rangle = \langle gf|V_{ij}|00\rangle$

These matrix elements couple the two-molecule ground state $|00\rangle$ and doubly-excited states. In a system with at least four molecules, these couplings lead to the exchange of two excitations between pairs of molecules. The corresponding terms in Eq. (D.1) are

$$\langle fg|V_{ij}|00\rangle \left(\hat{b}_{if}^\dagger \hat{b}_{jg}^\dagger \hat{b}_{i0} \hat{b}_{j0} + \text{h.c.} \right) + \langle gf|V_{ij}|00\rangle \left(\hat{b}_{ig}^\dagger \hat{b}_{jf}^\dagger \hat{b}_{i0} \hat{b}_{j0} + \text{h.c.} \right) \quad (\text{D.10})$$

Excited-excited interaction $\langle fg|V_{ij}|f'g'\rangle = \langle gf|V_{ij}|g'f'\rangle$

These matrix elements represent interactions between two molecules in excited states. There are many possible terms in the Hamiltonian resulting from this type of interaction. These terms can categorized according to the number of state indices that are identical. The most general term has four different excited state indices.

The corresponding terms in Eq. (D.1) are

$$\langle fg|V_{ij}|f'g'\rangle \left(\hat{b}_{if}^\dagger \hat{b}_{jg}^\dagger \hat{b}_{if'} \hat{b}_{jg'} + \text{h.c.} \right) + \langle gf|V_{ij}|g'f'\rangle \left(\hat{b}_{ig}^\dagger \hat{b}_{jf}^\dagger \hat{b}_{ig'} \hat{b}_{jf'} + \text{h.c.} \right). \quad (\text{D.11})$$

If the four state indices are identical in the matrix element ($f = g = f' = g'$), there is a single contribution to the Hamiltonian in Eq. (D.1) given by

$$\langle ff|V_{ij}|ff\rangle \hat{b}_{if}^\dagger \hat{b}_{if} \hat{b}_{jf}^\dagger \hat{b}_{jf}. \quad (\text{D.12})$$

This term represents the electrostatic interaction between two molecules in the same excited state. If only two excited state indices are identical ($f = f'$ and $g = g'$) we have contributions representing electrostatic interaction between two molecules in different excited states

$$\langle fg|V_{ij}|fg\rangle \hat{b}_{if}^\dagger \hat{b}_{jg}^\dagger \hat{b}_{if} \hat{b}_{jg} + \langle gf|V_{ij}|gf\rangle \hat{b}_{ig}^\dagger \hat{b}_{jf}^\dagger \hat{b}_{ig} \hat{b}_{jf}. \quad (\text{D.13})$$

and contributions representing energy exchange processes between excited states

$$\langle fg|V_{ij}|gf\rangle \left(\hat{b}_{if}^\dagger \hat{b}_{jg}^\dagger \hat{b}_{ig} \hat{b}_{jf} + \text{h.c.} \right) + \langle gf|V_{ij}|fg\rangle \left(\hat{b}_{ig}^\dagger \hat{b}_{jf}^\dagger \hat{b}_{if} \hat{b}_{jg} + \text{h.c.} \right). \quad (\text{D.14})$$

Additional terms are possible if three excited state indices are equal, but we do not consider such terms in this work.

D.3 Transformation to exciton operators

We define exciton creation operator $\hat{B}_{if}^\dagger = \hat{b}_{if}^\dagger \hat{b}_{i0}$ and its hermitian conjugate $\hat{B}_{if} = \hat{b}_{i0}^\dagger \hat{b}_{if}$. Using $\hat{b}_{if}^\dagger \hat{b}_{ig}^\dagger = 0 = \hat{b}_{if} \hat{b}_{ig}$, it is straightforward to show that number operator \hat{n}_{if} is given by the product

$$\hat{B}_{if}^\dagger \hat{B}_{if} = \hat{b}_{if}^\dagger \hat{b}_{i0} \hat{b}_{i0}^\dagger \hat{b}_{if} = \hat{b}_{if}^\dagger \hat{b}_{if} \left(1 - \sum_g \hat{b}_{ig}^\dagger \hat{b}_{ig} \right) = \hat{b}_{if}^\dagger \hat{b}_{if} \equiv \hat{n}_{if}, \quad (\text{D.15})$$

and the related identity $\hat{b}_{if}^\dagger \hat{b}_{ig} = \hat{B}_{if}^\dagger \hat{B}_{ig}$. The Hamiltonian in Eq. (D.1) can be separated into terms containing different powers of exciton operators by collecting

the results from Eqs. (D.6)-(D.12). If we omit the summations over molecule and state indices the resulting partition is

(a) *Order zero*

$$\langle 00|V_{ij}|00\rangle \quad (\text{D.16})$$

(b) *Order one*

$$\langle f0|V_{ij}|00\rangle \left(\hat{B}_{if}^\dagger + \hat{B}_{if} \right) + \langle 0f|V_{ij}|00\rangle \left(\hat{B}_{jf}^\dagger + \hat{B}_{jf} \right) \quad (\text{D.17})$$

(c) *Order two* ($f \neq g$)

$$\begin{aligned} & (\langle f0|V_{ij}|f0\rangle - \langle 00|V_{ij}|00\rangle) \hat{B}_{if}^\dagger \hat{B}_{if} + (\langle 0f|V_{ij}|0f\rangle - \langle 00|V_{ij}|00\rangle) \hat{B}_{jf}^\dagger \hat{B}_{jf} \\ & + \langle f0|V_{ij}|0f\rangle \left(\hat{B}_{if}^\dagger \hat{B}_{jf} + \text{h.c.} \right) + \langle 0f|V_{ij}|f0\rangle \left(\hat{B}_{jf}^\dagger \hat{B}_{if} + \text{h.c.} \right) \\ & + \langle ff|V_{ij}|00\rangle \left(\hat{B}_{if}^\dagger \hat{B}_{jf}^\dagger + \text{h.c.} \right) \end{aligned} \quad (\text{D.18})$$

$$\begin{aligned} & \langle f0|V_{ij}|g0\rangle \left(\hat{B}_{if}^\dagger \hat{B}_{ig} + \text{h.c.} \right) + \langle 0f|V_{ij}|0g\rangle \left(\hat{B}_{jf}^\dagger \hat{B}_{jg} + \text{h.c.} \right) \\ & + \langle f0|V_{ij}|0g\rangle \left(\hat{B}_{if}^\dagger \hat{B}_{jg} + \text{h.c.} \right) + \langle 0f|V_{ij}|g0\rangle \left(\hat{B}_{ig} \hat{B}_{jf}^\dagger + \text{h.c.} \right) \\ & + \langle fg|V_{ij}|00\rangle \left(\hat{B}_{if}^\dagger \hat{B}_{jg}^\dagger + \text{h.c.} \right) + \langle gf|V_{ij}|00\rangle \left(\hat{B}_{ig} \hat{B}_{jf}^\dagger + \text{h.c.} \right) \end{aligned} \quad (\text{D.19})$$

(d) *Order three* ($f \neq g \neq f'$)

$$\begin{aligned} & (\langle ff|V_{ij}|f0\rangle - \langle 0f|V_{ij}|00\rangle) \hat{B}_{if}^\dagger \hat{B}_{if} \left(\hat{B}_{jf}^\dagger + \hat{B}_{jf} \right) \\ & + (\langle ff|V_{ij}|0f\rangle - \langle f0|V_{ij}|00\rangle) \left(\hat{B}_{if}^\dagger + \hat{B}_{if} \right) \hat{B}_{jf}^\dagger \hat{B}_{jf} \end{aligned} \quad (\text{D.20})$$

$$\begin{aligned} & (\langle fg|V_{ij}|f0\rangle - \langle 0g|V_{ij}|00\rangle) \hat{B}_{if}^\dagger \hat{B}_{if} \left(\hat{B}_{jg}^\dagger + \hat{B}_{jg} \right) \\ & + (\langle gf|V_{ij}|0f\rangle - \langle g0|V_{ij}|00\rangle) \left(\hat{B}_{ig}^\dagger + \hat{B}_{ig} \right) \hat{B}_{jf}^\dagger \hat{B}_{jf} \end{aligned} \quad (\text{D.21})$$

$$\langle fg|V_{ij}|f'0\rangle \left(\hat{B}_{if}^\dagger \hat{B}_{jg}^\dagger \hat{B}_{if'} + \text{h.c.} \right) + \langle gf|V_{ij}|0f'\rangle \left(\hat{B}_{ig}^\dagger \hat{B}_{jf}^\dagger \hat{B}_{jf'} + \text{h.c.} \right) \quad (\text{D.22})$$

(e) *Order four*

$$(\langle ff|V_{ij}|ff\rangle + \langle 00|V_{ij}|00\rangle - \langle f0|V_{ij}|f0\rangle - \langle 0f|V_{ij}|0f\rangle) \hat{B}_{if}^\dagger \hat{B}_{if} \hat{B}_{jf}^\dagger \hat{B}_{if} \quad (\text{D.23})$$

D.4 Many-level model Hamiltonian

The next step in the derivation consists in summing over molecular indices, using the invariance of the interaction operator \hat{V}_{ij} under the exchange $i \leftrightarrow j$. For example, the summation of the terms in Eq. (D.17) reads

$$\begin{aligned} \frac{1}{2} \sum_{i,j \neq i} \left\{ \langle f0|V_{ij}|00\rangle (\hat{B}_{if}^\dagger + \hat{B}_{if}) + \langle 0f|V_{ij}|00\rangle (\hat{B}_{jf}^\dagger + \hat{B}_{jf}) \right\} \\ = \sum_{i,j \neq i} \langle f0|V_{ij}|00\rangle (\hat{B}_{if}^\dagger + \hat{B}_{if}), \end{aligned} \quad (\text{D.24})$$

as can be easily verified for the case of two molecules. Similar expressions can be obtained for the remaining terms of the interaction Hamiltonian. For simplicity, quartic terms in exciton operators that involve more than one excited state are neglected in this work. The truncated form of the original Hamiltonian in Eq. (D.1) for N interacting molecules can be written as

$$\mathcal{H} = U_0 + \sum_f \hat{H}_1(f) + \sum_{f,g} \hat{H}_2(f,g) + \sum_{f,g,f'} \hat{H}_3(f,g,f'). \quad (\text{D.25})$$

The first term is an energy term that is constant for molecules at fixed positions. It is given by

$$U_0 = \varepsilon_0 N + \frac{1}{2} \sum_{i,j \neq i} \langle 00|V_{ij}|00\rangle, \quad (\text{D.26})$$

where ϵ_0 is the energy of the ground state. The second term in Eq. (D.25) has contributions from a single excited state. It can be written as

$$\begin{aligned}\hat{H}_1(f) = & \sum_i A_i^f \left(\hat{B}_{if}^\dagger + \hat{B}_{if} \right) + \sum_i \left(\epsilon_{f0} + D_i^f \right) \hat{B}_{if}^\dagger \hat{B}_{if} \\ & + \frac{1}{2} \sum_{i,j \neq i} J_{ij}^f \left(\hat{B}_{if}^\dagger + \hat{B}_{if} \right) \left(\hat{B}_{jf}^\dagger + \hat{B}_{jf} \right) + \sum_{i,j \neq i} C_{ij}^f \left(\hat{B}_{if}^\dagger + \hat{B}_{if} \right) \hat{B}_{jf}^\dagger \hat{B}_{jf} \\ & + \frac{1}{2} \sum_{i,j \neq i} U_{ij}^f \hat{B}_{if}^\dagger \hat{B}_{if} \hat{B}_{jf}^\dagger \hat{B}_{jf}.\end{aligned}\quad (\text{D.27})$$

In this expression we have defined the single particle energies

$$A_i^f = \sum_{j \neq i} \langle f0 | V_{ij} | 00 \rangle,$$

and

$$D_i^f = \sum_{j \neq i} \left\{ \langle f0 | V_{ij} | f0 \rangle - \langle 00 | V_{ij} | 00 \rangle \right\},$$

as well as the interaction energies

$$C_{ij}^f = \langle ff | V_{ij} | f0 \rangle - \langle f0 | V_{ij} | 00 \rangle$$

$$J_{ij}^f = \langle f0 | V_{ij} | 0f \rangle = \langle ff | V_{ij} | 00 \rangle,$$

and

$$U_{ij}^f = \langle ff | V_{ij} | ff \rangle + \langle 00 | V_{ij} | 00 \rangle - 2\langle f0 | V_{ij} | f0 \rangle.$$

The third term in Eq. (D.25) contains contributions from two different excited states. It is composed of several terms (see Eq. (D.19)). For simplicity, we consider a single term of the form ($f \neq g$)

$$\hat{H}_2(f, g) = \frac{1}{2} \sum_{f, g} J_{ij}^{fg} \left(\hat{B}_{if}^\dagger \hat{B}_{jg} + \hat{B}_{if} \hat{B}_{jg}^\dagger \right). \quad (\text{D.28})$$

This term describes the direct coupling between different eigenstates of $\hat{H}(f)$ corresponding to different molecular excited states.

The final term in Eq. (D.25) contains contributions from three different excited states. For simplicity, we only consider cubic terms corresponding to fission and fusion process given in Eq. (D.22). The interaction Hamiltonian is ($f \neq g \neq f'$)

$$\hat{H}_3(f, g, f') = \sum_{f, g, f'} F_{ij}^{fgf'} \left(\hat{B}_{if}^\dagger \hat{B}_{jg}^\dagger \hat{B}_{if'} + \hat{B}_{if'}^\dagger \hat{B}_{if} \hat{B}_{jg} \right). \quad (\text{D.29})$$

where the interaction energy is given by

$$F_{ij}^{f,g,f'} = \langle fg | V_{ij} | f' 0 \rangle.$$

Appendix E

Simple methods for the polaron problem

In this appendix perturbative results for the Fröhlich, Holstein and Su-Schrieffer-Heeger (SSH) polaron models are established. These are standard results in polaron theory. Perturbative expressions in the weak and strong coupling regimes are useful when comparing with more sophisticated analytical approaches or numerical results. The perturbative calculations follow closely Refs. [84, 205] and the numerical algorithm is original.

The polaron Hamiltonian can be written as

$$\hat{H} = \hat{H}_p + \hat{H}_{ph} + \hat{H}_{int} \quad (\text{E.1})$$

where \hat{H}_p is the Hamiltonian describing the free particle or quasi-particle, \hat{H}_{ph} is the phonon Hamiltonian and \hat{H}_{int} describes the exciton-phonon interaction. Different polaron models assume different forms for the interaction Hamiltonian \hat{H}_{int} .

E.1 Fröhlich polaron

Weak coupling perturbation theory

The particle-phonon interaction Hamiltonian \hat{H}_{int} in the Fröhlich polaron model is given in Eq. (6.3). If the dimensionless coupling α is less than unity, the polaron

energy can be evaluated accurately using Rayleigh-Schrödinger (RS) perturbation theory to second order [84]. The first order contribution vanishes because \hat{H}_{int} couples phonon states where the total phonon number changes by one unit. The second order correction to the energy of state $|n\rangle$ is given by

$$E_n^{(2)} = \sum_k \frac{|\langle k^{(0)} | \hat{H}_{\text{int}} | n^{(0)} \rangle|^2}{E_n^{(0)} - E_k^{(0)}} \quad (\text{E.2})$$

The zero-th order state of interest describes a particle with momentum \mathbf{p} and the phonon vacuum (zero temperature), i.e., $|n^{(0)}\rangle = |\mathbf{p}\rangle|0\rangle$. Virtual transitions (off-resonant) to one-phonon states $|k^{(0)}\rangle = |\mathbf{p} + \mathbf{q}\rangle|n_{\mathbf{q}} = 1\rangle$ contribute to the energy.

Replacing the \hat{H}_{int} from Eq. (6.3) into Eq. (E.2) gives (using $\hbar = 1$)

$$E_{\mathbf{p}}^{(2)} = -\frac{1}{V} \sum_{\mathbf{q}} \frac{|M_0|^2}{q^2} \frac{1}{\omega_0 - \mathbf{p}^2/2m + (1/2m)(\mathbf{p}^2 - \mathbf{q}^2)}. \quad (\text{E.3})$$

Assuming a three-dimensional geometry, the wavevector summation is replaced by integration as $\sum_{\mathbf{q}} = V \int d^3q / (2\pi)^3$. The $1/q^2$ factor cancels out with the q^2 factor in the volume element. Integration over the azimuthal angle gives a factor of 2π . The resulting expression is $E_{\mathbf{p}}^{(2)} = -\frac{|M_0|^2}{4\pi^2} \times I$, where

$$I = \int_0^\infty dq \int_0^\pi \sin\theta d\theta \frac{1}{(1/2m)(\omega_0 + q^2 - 2pq\cos\theta)}. \quad (\text{E.4})$$

The integral can be solved using the change of variables $v = \cos\theta$, followed by $x = (q - pv)/(2m)^{1/2}$. In terms of these variables I can be written as

$$I = \frac{(2m)^{1/2}}{2} \int_{-1}^1 dv \int_{-\infty}^\infty dx \frac{1}{\omega_0 - E(p)v^2 + x^2} \quad (\text{E.5})$$

$$= \frac{(2m)^{1/2}}{2} \int_{-1}^1 dv \frac{\pi}{A^{1/2}}, \quad (\text{E.6})$$

where $A = \omega_0 - E(p)v^2$. This result is valid for $A > 0$. In the first line we have use the fact that the integrand is an even function of q to extend the lower integration limit to $x = -\infty$. The integral in the second line gives an arcsin function. The final

result is thus

$$E_{\mathbf{p}}^{(2)} = -\alpha \left(\frac{\omega_0^{3/2}}{E(p)^{1/2}} \right) \arcsin \left(\frac{E(p)^{1/2}}{\omega_0^{1/2}} \right) \quad (\text{E.7})$$

where $E(p) = p^2/2m$. For small momentum $p \rightarrow 0$, we can use the Taylor expansion $\sin^{-1}x = x + x^3/6 + O(x^5)$ to write the energy of the low-momentum states as

$$E_{\mathbf{p}} = \frac{\mathbf{p}^2}{2m} \left(1 - \frac{\alpha}{6} \right) - \alpha\omega_0. \quad (\text{E.8})$$

From this expression the effective mass near the band minimum is $m^* = m/(1 - \alpha/6)$ and the polaron ground state energy ($p = 0$) is $E_g = -\alpha\omega_0$.

E.2 Holstein polaron

Canonical transformation in the strong coupling regime

The particle-phonon interaction Hamiltonian \hat{H}_{int} in the Holstein model is given by Eq. (6.11), with interaction energy $M_{\mathbf{q}} = g/\sqrt{N}$. In the strong coupling regime where $g^2/2J\omega_0 \gg 1$, the Hamiltonian is best solved by transforming the particle operators from the momentum to the site representation using the unitary transformation $\hat{c}_{\mathbf{k}} = N^{-1/2} \sum_i \hat{c}_i \exp[i\mathbf{k} \cdot \mathbf{R}_i]$ and the relation $\sum_{\mathbf{k}} \exp[i\mathbf{k} \cdot (\mathbf{R}_i - \mathbf{R}_j)] = \delta_{i,j}N$. The resulting Hamiltonian can be partitioned as $\hat{H} = \hat{H}_0 + \hat{V}$, where

$$\hat{H}_0 = \varepsilon \hat{c}_i^\dagger \hat{c}_i + \sum_{\mathbf{q}} \omega_{\mathbf{q}} \hat{a}_{\mathbf{q}}^\dagger \hat{a}_{\mathbf{q}} + \frac{g}{\sqrt{N}} \sum_{i\mathbf{q}} \hat{c}_i^\dagger \hat{c}_i e^{i\mathbf{q} \cdot \mathbf{R}_i} (\hat{a}_{\mathbf{q}} + \hat{a}_{-\mathbf{q}}^\dagger), \quad (\text{E.9})$$

where ε is the rest energy of the particle. The perturbation term corresponds to the hopping of the particle

$$\hat{V} = -t \sum_{i,j} \hat{c}_i^\dagger \hat{c}_j. \quad (\text{E.10})$$

The Hamiltonian \hat{H}_0 contains the particle-phonon interaction. Its eigenstates are polaron states corresponding to an immobile particle dressed by a phonon cloud. This Hamiltonian can be diagonalized using the canonical transformation $\hat{U} = e^{\hat{S}}$, where

$$\hat{S} = \sum_{j\mathbf{q}} \hat{c}_j^\dagger \hat{c}_j e^{i\mathbf{q} \cdot \mathbf{R}_j} \frac{M_{\mathbf{q}}}{\omega_{\mathbf{q}}} (\hat{a}_{-\mathbf{q}}^\dagger - \hat{a}_{\mathbf{q}}), \quad (\text{E.11})$$

is a displacement operator. Transformed operators are obtained as $\bar{A} = UAU^\dagger$. We need to consider only the transformation on each operator separately since $\bar{A}\bar{B} = UABU^\dagger = UAU^\dagger UBU^\dagger = \bar{A}\bar{B}$. The explicit form of the operator \bar{A} is obtained using the identity

$$\bar{A} = e^S A e^{-S} = A + [S, A] + \frac{1}{2!} [S, [S, A]] + \dots \quad (\text{E.12})$$

Assuming the particle operators have bosonic commutation relations, the transformed annihilation operator \bar{c}_i can be written as

$$\bar{c}_i = \hat{c}_i \left[1 - D_{i,\mathbf{q}} + \frac{1}{2!} D_{i,\mathbf{q}}^2 + \dots \right] = \hat{c}_i e^{-D_{i,\mathbf{q}}}, \quad (\text{E.13})$$

where

$$D_{i,\mathbf{q}} = \left[\sum_{\mathbf{q}} e^{i\mathbf{q} \cdot \mathbf{R}_i} \frac{M_{\mathbf{q}}}{\omega_{\mathbf{q}}} \left(\hat{a}_{-\mathbf{q}}^\dagger - \hat{a}_{\mathbf{q}} \right) \right]. \quad (\text{E.14})$$

This result is normally written as $\bar{c}_i = \hat{c}_i \hat{X}_i$ or $\bar{c}^\dagger = \hat{c}_i^\dagger \hat{X}_i^\dagger$, where $\hat{X}_i = e^{-D_{i,\mathbf{q}}}$ is an operator that acts on the phonon degrees of freedom.

The transformed phonon operators can also be obtained using Eq. (E.12). Using the fact that the second order commutator vanishes we obtain

$$\bar{a}_{\mathbf{q}} = \hat{a}_{\mathbf{q}} - \frac{M_{\mathbf{q}}}{\omega_{\mathbf{q}}} \sum_i \hat{c}_i^\dagger \hat{c}_i e^{-i\mathbf{q} \cdot \mathbf{R}_i}. \quad (\text{E.15})$$

Using this expression and its hermitian conjugate $\bar{a}_{\mathbf{q}}^\dagger$, the transformed phonon Hamiltonian $U \hat{H}_{\text{ph}} U^\dagger = \omega_{\mathbf{q}} \bar{a}_{\mathbf{q}}^\dagger \bar{a}_{\mathbf{q}}$ for each phonon mode \mathbf{q} gives

$$\bar{H}_{\text{ph}}(\mathbf{q}) = \omega_{\mathbf{q}} \bar{a}_{\mathbf{q}}^\dagger \bar{a}_{\mathbf{q}} = \omega_{\mathbf{q}} \hat{a}_{\mathbf{q}}^\dagger \hat{a}_{\mathbf{q}} - \left(\hat{a}_{-\mathbf{q}}^\dagger + \hat{a}_{\mathbf{q}} \right) M_{\mathbf{q}} \sum_i \hat{c}_i^\dagger \hat{c}_i e^{i\mathbf{q} \cdot \mathbf{R}_i} + \frac{M_{\mathbf{q}}^2}{\omega_{\mathbf{q}}} \sum_{i,j} \hat{c}_i^\dagger \hat{c}_i \hat{c}_j^\dagger \hat{c}_j e^{i\mathbf{q} \cdot (\mathbf{R}_i - \mathbf{R}_j)}. \quad (\text{E.16})$$

Similarly, the particle-phonon interaction for each phonon mode gives

$$\begin{aligned} \bar{H}_{\text{int}}(\mathbf{q}) &= \sum_i \bar{c}_i^\dagger \bar{c}_i e^{i\hat{\mathbf{R}} \cdot \mathbf{R}_i} M_{\mathbf{q}} \left(\bar{a}_{\mathbf{q}} + \bar{a}_{-\mathbf{q}}^\dagger \right) \\ &= \left(\hat{a}_{\mathbf{q}} + \hat{a}_{-\mathbf{q}}^\dagger \right) M_{\mathbf{q}} \sum_i \hat{c}_i^\dagger \hat{c}_i e^{i\mathbf{q} \cdot \mathbf{R}_i} - 2 \frac{M_{\mathbf{q}}^2}{\omega_{\mathbf{q}}} \sum_{i,j} e^{i\mathbf{q} \cdot (\mathbf{R}_i - \mathbf{R}_j)} \hat{c}_i^\dagger \hat{c}_i \hat{c}_j^\dagger \hat{c}_j, \end{aligned} \quad (\text{E.17})$$

where the identities $M_{-\mathbf{q}} = M_{\mathbf{q}}$ and $\omega_{\mathbf{q}} = \omega_{-\mathbf{q}}$ have been used. The transformed particle number operators at the same site is given by $\bar{n}_i = \bar{c}_i^\dagger \bar{c}_i = \hat{c}_i^\dagger \hat{X}_i^\dagger \hat{c}_i \hat{X}_i = \hat{c}_i^\dagger \hat{c}_i \hat{X}_i^\dagger \hat{X}_i = \hat{n}_i$. The quartic term in particle operators corresponds to a phonon-mediated interaction between particles. This interaction is irrelevant in a single particle problem. For a single particle, the only non-zero contribution is given by the diagonal term in the summation ($i = j$), which reduces to $\hat{n}_i \hat{n}_i = \hat{n}_i$.

Using the transformed operators in Eqs. (E.16) and (E.18), and the Holstein form of the interaction energy $M_{\mathbf{q}} = g/\sqrt{N}$, the Hamiltonian \hat{H}_0 can be written in diagonal form

$$\bar{H}_0 \equiv \hat{U} \hat{H}_0 \hat{U}^\dagger = \hat{c}_i^\dagger \hat{c}_i (\varepsilon - \Delta E_g) + \sum_{\mathbf{q}} \omega_{\mathbf{q}} \hat{a}_{\mathbf{q}}^\dagger \hat{a}_{\mathbf{q}}, \quad (\text{E.18})$$

where $\Delta E_g = N^{-1} \sum_{\mathbf{q}} g^2 / \omega_{\mathbf{q}}$ is the polaron shift from the single particle energy ε .

The transformed particle hopping interaction \bar{V} contains the product of particle operators at different sites

$$\bar{c}_i^\dagger \bar{c}_i = \hat{c}_i^\dagger \hat{c}_j \hat{X}_i^\dagger \hat{X}_j = \hat{c}_i^\dagger \hat{c}_j e^{D_{i,\mathbf{q}} - D_{j,\mathbf{q}}},$$

where $D_{i,\mathbf{q}}$ is given in Eq. (E.14). Strong coupling perturbation theory can be studied using the transformed Hamiltonian $\hat{H} = \bar{H}_0 + \bar{V}$, where $\bar{V} = -\bar{t} \sum_{ij} \bar{c}_i^\dagger \bar{c}_j$ is a small term describing the hopping of a polaron between lattice sites. The phonon-dressed hopping amplitude is given by

$$\bar{t} = t e^{-S_T}, \quad (\text{E.19})$$

where $e^{-S_T} = \langle i | \hat{X}_i^\dagger \hat{X}_j | i \rangle$ is the expectation value over the thermal phonon state. An analysis of strong coupling perturbation theory for the Holstein polaron can be found in Ref. [215] and references therein.

E.3 SSH polaron

Sharp transition in the non-adiabatic limit

The particle-phonon interaction Hamiltonian \hat{H}_{int} in the SSH polaron model is given in Eq. (6.20). For Einstein phonons, the interaction energy is proportional to $\alpha = \tilde{\alpha}t/\sqrt{2m\omega_0}$, where ω_0 is the phonon frequency, m is the mass of the lattice oscillators, t is the particle hopping amplitude and $\tilde{\alpha}$ is a numerical constant of order unity. For large phonon frequencies such that $\omega_0 > 4t$ (non-adiabatic limit), Rayleigh-Schrödinger perturbation theory gives an accurate value for the polaron energy. For a one-dimensional array with optical phonons and nearest-neighbour hopping, the polaron energy to second order in \hat{H}_{int} is

$$E_k^{(2)} = -2t \cos(k) + \frac{16\alpha^2}{N} \sum_q \frac{\sin^2(q/2) \cos^2(k-q/2)}{2t \cos(k) - \omega_0 - 2t \cos(k-q)}. \quad (\text{E.20})$$

In the extreme non-adiabatic limit $\omega_0 \gg 2t$, the wavevector dependence of the energy denominator can be ignored. The integral is elementary and gives the energy

$$\begin{aligned} E_k &= -2t \cos(k) - \frac{16\alpha^2}{\omega_0} \int_{-\pi}^{\pi} \frac{dq}{(2\pi)} \sin^2(q/2) \cos^2(k-q/2) \\ &= -2t \cos(k) - \frac{2\alpha^2}{\omega_0} [2 - \cos(2k)]. \end{aligned} \quad (\text{E.21})$$

In addition to an overall energy shift $\Delta = -4\alpha^2/\omega_0$, the polaron band consists of a term associated with nearest-neighbour hopping $-2t \cos(k)$ and a term arising from second-order next-nearest-neighbour hopping $-t_2 \cos(2k)$, where $t_2 = -\lambda t$. The relative contribution of these two terms can be represented by the dimensionless coupling constant

$$\lambda = \frac{2\alpha^2}{t\omega_0}. \quad (\text{E.22})$$

At the critical coupling λ_c , the polaron effective mass m^* at the origin of the Brillouin zone $k = 0$ vanishes. At this coupling, the polaron dispersion has an

inflection point at $k = 0$, i.e.,

$$\left. \frac{d^2 E_k}{dk^2} \right|_{k=0} = 2t(1 - 2\lambda_c) = 0, \quad (\text{E.23})$$

which gives $\lambda_c = 1/2$. The minimum of the polaron dispersion at any value of λ occurs at the wavevector k_0 that satisfies

$$\frac{dE_k}{dk} = 2t \sin(k_0) [1 - 2\lambda \cos(k_0)] = 0. \quad (\text{E.24})$$

For $\lambda \leq 1/2$, the minimum occurs at $k_0 = 0$. For $\lambda > 1/2$, we have $k_0 = \cos^{-1}(1/2\lambda)$, i.e., the minimum shifts towards the middle of the Brillouin zone at $k_0 = \pi/2$ when $\lambda \gg 1/2$.

E.4 Exciton-phonon coupling constant $M(\mathbf{k}, \mathbf{q})$

In order to derive the system Hamiltonian in wavevector space, the starting point is the generalized polaron Hamiltonian in the site representation

$$\hat{H}_{\text{int}} = \frac{1}{2} \sum_{i,j \neq i} (\mathbf{x}_i - \mathbf{x}_j) \times \left(\nabla D_{ij} [\hat{B}_i^\dagger \hat{B}_i + \hat{B}_j^\dagger \hat{B}_j] + \nabla J_{ij} [\hat{B}_i^\dagger \hat{B}_j + \hat{B}_j^\dagger \hat{B}_i] \right), \quad (\text{E.25})$$

and expand the displacement operators in Fourier modes as

$$\mathbf{x}_i = \frac{1}{\sqrt{N}} \sum_{\mathbf{q}\lambda} \sqrt{\frac{\hbar}{2m\omega_0}} \hat{e}_{\mathbf{q}\lambda} \left(\hat{a}_{\mathbf{q},\lambda} + \hat{a}_{-\mathbf{q},\lambda}^\dagger \right) e^{i\mathbf{q} \cdot \mathbf{R}_i}, \quad (\text{E.26})$$

where \mathbf{q} is the phonon wavevector, and $\hat{e}_{\mathbf{q},\lambda}$ is the unit vector in the direction of the displacement with polarization λ . As noted before, the phonon spectrum is discrete with excitation energy $\hbar\omega_0$, as is the case of optical phonons in a solid. We also expand the exciton operators in Fourier modes as explained in Chapter 5:

$$\hat{B}_i = \frac{1}{\sqrt{N}} \sum_{\mathbf{k}} \hat{B}_{\mathbf{k}} e^{i\mathbf{k} \cdot \mathbf{R}_i}. \quad (\text{E.27})$$

Inserting these definitions in Eq. (E.25), we obtain

$$\begin{aligned}
\hat{H}_{\text{int}} = & \frac{1}{2N^{3/2}} \sum_i \sum_{j \neq i} \sum_{\mathbf{q}, \lambda} \sum_{\mathbf{k}, \mathbf{p}} \left(\frac{\hbar}{2m\omega_0} \right)^{\frac{1}{2}} \left(\hat{a}_{\mathbf{q}, \lambda} + \hat{a}_{-\mathbf{q}, \lambda}^\dagger \right) \hat{B}_{\mathbf{k}}^\dagger \hat{B}_{\mathbf{p}} \left(e^{i\mathbf{q} \cdot \mathbf{R}_i} - e^{i\mathbf{q} \cdot \mathbf{R}_j} \right) \\
& \left[\hat{\epsilon}_{\mathbf{q}, \lambda} \cdot \nabla D_{ij} \left(e^{i(\mathbf{p}-\mathbf{k}) \cdot \mathbf{R}_i} + e^{i(\mathbf{p}-\mathbf{k}) \cdot \mathbf{R}_j} \right) \right. \\
& \left. + \hat{\epsilon}_{\mathbf{q}, \lambda} \cdot \nabla J_{ij} \left(e^{-i\mathbf{k} \cdot \mathbf{R}_i + i\mathbf{p} \cdot \mathbf{R}_j} + e^{-i\mathbf{k} \cdot \mathbf{R}_j + i\mathbf{p} \cdot \mathbf{R}_i} \right) \right], \tag{E.28}
\end{aligned}$$

which can be simplified by collecting the exponentials associated with the same site position, and perform the summation \sum_i using the orthogonality of the discrete wavevector states to eliminate the sum over \mathbf{k} . We define the intermolecular separation vector as $\mathbf{R}_m = \mathbf{R}_i - \mathbf{R}_j$ to relabel the summation over lattice sites, which gives the hermitian exciton-phonon interaction Hamiltonian

$$\begin{aligned}
\hat{H}_{\text{int}} = & \frac{1}{2} \left(\frac{\hbar}{2Nm\omega_0} \right)^{\frac{1}{2}} \sum_{m \neq 0} \sum_{\mathbf{q}, \lambda} \sum_{\mathbf{p}} \left(\hat{a}_{\mathbf{q}, \lambda} + \hat{a}_{-\mathbf{q}, \lambda}^\dagger \right) \hat{B}_{\mathbf{p}+\mathbf{q}}^\dagger \hat{B}_{\mathbf{p}} \\
& \left(1 - e^{-i\mathbf{q} \cdot \mathbf{R}_m} \right) \left[\hat{\epsilon}_{\mathbf{q}, \lambda} \cdot \nabla D(\mathbf{R}_m) \left(1 + e^{i\mathbf{q} \cdot \mathbf{R}_m} \right) \right. \\
& \left. + \hat{\epsilon}_{\mathbf{q}, \lambda} \cdot \nabla J(\mathbf{R}_m) \left(e^{-i\mathbf{p} \cdot \mathbf{R}_m} + e^{i(\mathbf{p}+\mathbf{q}) \cdot \mathbf{R}_m} \right) \right], \tag{E.29}
\end{aligned}$$

or written in a more standard form as

$$\hat{H}_{\text{int}} = \frac{1}{\sqrt{N}} \sum_{\mathbf{q}, \lambda} \sum_{\mathbf{k}} M_{\lambda}(\mathbf{k}, \mathbf{q}) \left(\hat{a}_{\mathbf{q}, \lambda} + \hat{a}_{-\mathbf{q}, \lambda}^\dagger \right) \hat{B}_{\mathbf{p}+\mathbf{q}}^\dagger \hat{B}_{\mathbf{p}}, \tag{E.30}$$

where the exciton-phonon coupling constant is given by

$$\begin{aligned}
M_{\lambda}(\mathbf{k}, \mathbf{q}) = & 2i \left(\frac{\hbar}{2m\omega_0} \right)^{\frac{1}{2}} \sum_{m > 0} \left(\hat{\epsilon}_{\mathbf{q}, \lambda} \cdot \nabla D(\mathbf{R}_m) \right) \sin(\mathbf{q} \cdot \mathbf{R}_m) \\
& + \left(\hat{\epsilon}_{\mathbf{q}, \lambda} \cdot \nabla J(\mathbf{R}_m) \right) \left[\sin((\mathbf{k} + \mathbf{q}) \cdot \mathbf{R}_m) - \sin(\mathbf{k} \cdot \mathbf{R}_m) \right]. \tag{E.31}
\end{aligned}$$

The gradient of the dipole-dipole coupling $J(\mathbf{R}_i - \mathbf{R}_j)$, for example, can be written as

$$\nabla J(\mathbf{R}_m) = -3\tilde{J} \frac{\mathbf{R}_m}{|\mathbf{R}_m|^5},$$

where \tilde{f} is the factor of the dipole-dipole matrix element that depends only on the internal degrees of freedom of the molecules. This separation is in general possible, as explained in Chapter 2. This form of the exciton-phonon coupling is general for any lattice geometry, but in an optical lattice one can consider a simple cubic array, such that $\mathbf{R}_m = a\mathbf{m}$, where $\mathbf{m} = m_x\hat{\mathbf{x}} + m_y\hat{\mathbf{y}} + m_z\hat{\mathbf{z}}$, and a is the lattice constant. In this case

$$\nabla\Lambda(\mathbf{R}_m) = -3\frac{\Lambda_{12}}{a}\frac{\hat{\mathbf{m}}}{|\mathbf{m}|^4},$$

where Λ_{12} denotes D_{12} and J_{12} , the nearest-neighbour couplings. This definitions leave the coupling constant $M_\lambda(\mathbf{k}, \mathbf{q})$ as

$$M_\lambda(\mathbf{k}, \mathbf{q}) = -6i\sqrt{\frac{\hbar}{2m\omega_0a^2}} [D_{12}g_\lambda(\mathbf{q}) + J_{12}(g_\lambda(\mathbf{k} + \mathbf{q}) - g_\lambda(\mathbf{k}))], \quad (\text{E.32})$$

where the mode-coupling function $g_\lambda(\mathbf{k})$ is given by

$$g_\lambda(\mathbf{k}) = \sum_{m>0} (\hat{e}_{\mathbf{q},\lambda} \cdot \hat{\mathbf{m}}) \frac{\sin(a\mathbf{k} \cdot \mathbf{m})}{|\mathbf{m}|^4}. \quad (\text{E.33})$$

Appendix F

Bell's inequality for angular and time correlations

In the first part of this appendix a simplified derivation of Bell's inequality is presented. The derivation follows closely Refs. [169, 236] which are based on orientation measurements in spin-1/2 systems. The second part of the appendix demonstrates the equivalence between the Bell-type inequalities based on spin orientations and the time-evolution of rotational states.

F.1 Proof of Bell's inequality

A pair of spin-half particles is prepared in some distant past. One particle is sent to observer A and the other to observer B. Each observer measured a spin component. The vectors \vec{a} and \vec{b} denote the directions chosen for observation by observers A and B, respectively. We assume that λ represents all “elements of reality” associated with the spins. The variable λ (possibly multidimensional) contains all the information concerning the results of possible measurements performed on the spins. This information is determined at the particle source and is described by the probability density $\rho(\lambda)$. The results of the measurements made by observers A and B are denoted as A and B . Both of these results may depend on the unknown variable λ , but locality implies that the results obtained by observer A cannot de-

pend on the choice of orientation direction \vec{b} made by observer B. We therefore write $A(\vec{a}, \lambda)$ and $B(\vec{b}, \lambda)$ for the results obtained by each observer.

Correlations between measurements performed by observers A and B will be revealed in the joint probabilities for their measurement outcomes. This classical correlation is given by

$$E(\vec{a}, \vec{b}) = \int d\lambda \rho(\lambda) A(\vec{a}, \lambda) B(\vec{b}, \lambda). \quad (\text{F.1})$$

If we consider only two possible directions for each separate measurement, after performing a large number of measurements on each particle both observers can join their results to obtain the quantity

$$\begin{aligned} S &= E(\vec{a}, \vec{b}) + E(\vec{a}, \vec{b}') + E(\vec{a}', \vec{b}) - E(\vec{a}', \vec{b}') \\ &= \int d\lambda \rho(\lambda) \left\{ A(\vec{a}, \lambda) [B(\vec{b}, \lambda) + B(\vec{b}', \lambda)] + A(\vec{a}', \lambda) [B(\vec{b}, \lambda) - B(\vec{b}', \lambda)] \right\}. \end{aligned} \quad (\text{F.2})$$

Let us assume that the possible values of projection measured by observer A satisfy $-\lambda_{\max} \leq A \leq \lambda_{\max}$, and that an analogous inequality holds for the results obtained by observer B. For spin-half particles, there are only two possible projections that can be measured, i.e., $\lambda_{\max} = +1$. Therefore extrema for the value of the integral in Eq. (F.2) are achieved when the integrand in curly brackets is a maximum or minimum. This occurs only when A and B have the values $\pm\lambda_{\max}$. Ignoring the dependence on λ , it is easy to see that the product

$$A(\vec{a}) [B(\vec{b}) + B(\vec{b}')] + A(\vec{a}') [B(\vec{b}) - B(\vec{b}')] \quad (\text{F.3})$$

is equal to either $-2\lambda_{\max}^2$ or to $2\lambda_{\max}^2$, when A and B assume their maximum or minimum values regardless of the choice of settings \vec{a} and \vec{b} . This is because one of the B brackets vanish while the other has the value $\pm 2\lambda_{\max}$. The remaining A factor in each term provides an additional λ_{\max} . This proves the Bell inequality in the form due to Clauser, Horne, Shimony and Holt [261]

$$|S| \leq 2\lambda_{\max}^2. \quad (\text{F.4})$$

For a pair of spin-1/2 particles in the singlet Bell state $|\Psi^-\rangle = \frac{1}{\sqrt{2}}(|01\rangle - |10\rangle)$, it is straightforward to show that this inequality is violated. The orientation measurement operator along the direction \vec{a} is given quantum mechanically by $\hat{O} = \vec{a} \cdot \vec{\sigma}$, where $\vec{\sigma}$ is the vector Pauli matrix. The eigenvalues of the orientation operator \hat{O} are $\lambda = \pm 1$. The quantum mechanical orientation correlation function is given by

$$E(\vec{a}, \vec{b}) \equiv \langle \Psi^- | \vec{a} \cdot \vec{\sigma} \otimes \vec{b} \cdot \vec{\sigma} | \Psi^- \rangle = -\vec{a} \cdot \vec{b}. \quad (\text{F.5})$$

Substituting this expression into Eq. (F.3) gives (ignoring an overall minus sign)

$$\vec{a} \cdot (\vec{b} + \vec{b}') + \vec{a}' \cdot (\vec{b} - \vec{b}').$$

This quantity is maximized when \vec{a} is parallel to $\vec{b} + \vec{b}'$ and \vec{a}' is parallel to $\vec{b} - \vec{b}'$. Since the orientation vectors have unit norm, the maximum value of this quantity is $2\sqrt{2}$, which is called the Cirel'son bound [243]. This bound is achieved by maximally entangled bipartite states of two-dimensional qubits.

F.2 Equivalence between spin orientations and rotational evolution

Let us consider two molecules each in a rotational state within the subspace $\mathcal{S} = \{|0\rangle \equiv |N=0, M_N=0\rangle, |1\rangle \equiv |N=1, M_N=0\rangle\}$. For each molecule the orientation of the rotating internuclear axis with respect the polarization of the a laser is measured by observers A and B. The measurement operator is $\hat{O} = \cos \theta$, where θ is the angle between the molecular axis and the space-fixed Z -axis (the polarization direction). In the two-dimensional rotational subspace \mathcal{S} the orientation operator is given by $\hat{O} = (1/\sqrt{3})\hat{\sigma}_x$. The rotational Hamiltonian can be written as $\hat{H}_R = B_e \hat{\sigma}_z$, where B_e is the rotational constant.

The two-time orientation correlation function $E(t_a, t_b) = \langle \hat{O}_a(t_a) \otimes \hat{O}_b(t_b) \rangle$ enters into the formulation of Bell-type tests using the rotational time-evolution Chapter 7. The single-molecule orientation operator $\hat{O}(t_a)$ in the Heisenberg picture can

be written as

$$\begin{aligned}
\hat{O}(\tau_a) &= \frac{1}{\sqrt{3}} \times e^{i\hat{\sigma}_z \tau_a/2} \hat{\sigma}_x e^{-i\hat{\sigma}_z \tau_a/2} \\
&= \frac{1}{\sqrt{3}} [\cos(\tau_a) \hat{\sigma}_x - \sin(\tau_a) \hat{\sigma}_y] \\
&= \vec{a} \cdot \vec{\sigma}
\end{aligned} \tag{F.6}$$

where $\tau_a = 2B_e t_a / \hbar$ is a dimensionless time and $\vec{a} = (\cos(\tau_a)/\sqrt{3}, -\sin(\tau_a)/\sqrt{3}, 0)$. The operator $R(\phi_a) = \exp[-i\hat{\sigma}_z \phi_a/2]$ corresponds to an (active) rotation around the space-fixed Z -axis by an angle ϕ_a . The time evolution of the orientation operator $\hat{O}(t_a)$ thus corresponds to a counterclockwise rotation of the orientation direction from $\vec{a} = (1/\sqrt{3})\hat{a}$ from the positive X axis by an angle $\phi_a = \tau_a$ in the XY plane. Therefore, choosing a different time t_a to perform the molecular orientation measurement is equivalent to changing the orientation of the Stern-Gerlach apparatus for the case of spin-1/2 particles in a plane. The two-time orientation correlator can thus be written as $E(t_a, t_b) = \langle \vec{a} \cdot \vec{\sigma} \otimes \vec{b} \cdot \vec{\sigma} \rangle$, which is equivalent to the spin orientation correlator in Eq. F.5. In other words, the analogy is exact between Bell-type inequalities based on the rotational time-evolution with the original results based on spin orientations.